DAMAGE ASSESSMENT IN COMPLEX STRUCTURES USING ACOUSTIC EMISSION

PhD Thesis

May 2016

Safaa Khairry Jeaaz Al-jumaili

B.Sc., M.Sc.

Cardiff School of Engineering

Cardiff University

Cardiff

UK

Declaration

This work has not previously been accepted in substance for any degree and is not currently submitted in candidature for any degree.

Signed……....(candidate) Date……

Statement 1

This thesis is being submitted in partial fulfilment of the requirements for the degree of PhD

Signed……....(candidate) Date……

Statement 2

This thesis is the result of my own independent work/investigation, except where otherwise stated. Other sources are acknowledged by explicit references.

Signed……....(candidate) Date……

Statement 3

I hereby give consent for my thesis, if accepted, to be available for photocopying and for inter-library loan, and for the title and summary to be made available to outside organisations.

Signed……....(candidate) Date……

Prifysgol Caerdydd **SUMMARY OF THESIS** **Cardiff University**

Candidate's Surname: Al-jumaili **Institute at which study pursued:**

Candidate's Forenames: Safaa Khairry Jeaaz Cardiff University

Candidate for Degree of: PhD

Full Title of Thesis: Damage Assessment in Complex Structures Using Acoustic Emission

Summary:

This thesis investigates the behaviour and failure of simple and complex structures using the structural health monitoring system (SHM). The work focuses on Acoustic Emission (AE) to detect, characterise and locate damage within metallic and composites structures under a fatigue loading regime. The work was divided into two main areas of research:

1. Damage Characterisation

Damage detection utilising AE was conducted through an extensive experimental programme in large-scale carbon fibre composite structures. Different assessment techniques were used to assess different damage mechanisms within the structure under fatigue failure. The source mechanisms characterisation in a large scale fatigue specimen was performed using a novel parameter correction technique (PCT). This is a significant advance, offering (in large scale structures) more reliable source characterisation.

2. Damage Localisation

Experimental investigations were undertaken to assess the novel AE location technique proposed in this work in a variety of structures. The new technique, known as Automatic Delta T mapping technique (Automatic DTM), provides an accurate, easy to use, fast and reliable damage localisation technique.

Key words: Acoustic emission, fatigue, structural health monitoring, damage detection, damage localisation, damage characterisation.

Acknowledgements

I would like to take this opportunity to express a great debt of gratitude to my academic supervisors Prof. Karen Holford, Dr. Rhys Pullin and Dr. Mark Eaton for their guidance, immense support and patience throughout my work. I would also thank Dr. Matthew Pearson for his advice, help and endless answering of questions. My thanks also to the technical staff at Cardiff School of Engineering especially Ian King, Steffan Jones, Garry Shipley, Richard Rogers and Harry Lane for their help, support and technical advice throughout my experimental investigations.

I would also thank my parents, my brothers and my sister and the rest of my family for supporting me though out the years, I thank my friends who have often reminded to keep smiling and to have fun.

Finally I extend my deepest thanks to my dearest wife Lamiaa and my lovely sons Fahad and Zakaria for their patience and support throughout my study.

Glossary

Terms relating to the physical phenomenon of AE (ASTM 1982):

Hit – the term of hit used to indicate that a given AE channel has detected and processed an acoustic emission transient.

Event – A group of AE hits that was received from a single source.

Source - A mechanical mechanism that produces AE signals.

Terms relating to the detection of the signal:

Acoustic emission signal - The electrical signal obtained through the detection of acoustic emission.

Noise – Signals produced by causes other than acoustic emission, or by acoustic emission sources that are not relevant to the purpose of the test.

Couplant - Substance providing an acoustic coupling between the propagation medium and the sensor.

Sensor - Device that converts the physical parameters of the wave into an electrical signal.

Terms relating to the processing of the signal:

Threshold - A preset voltage level, which has to be exceeded before an AE signal is detected, and processed. The following terms are made with reference to the threshold (Figure i).

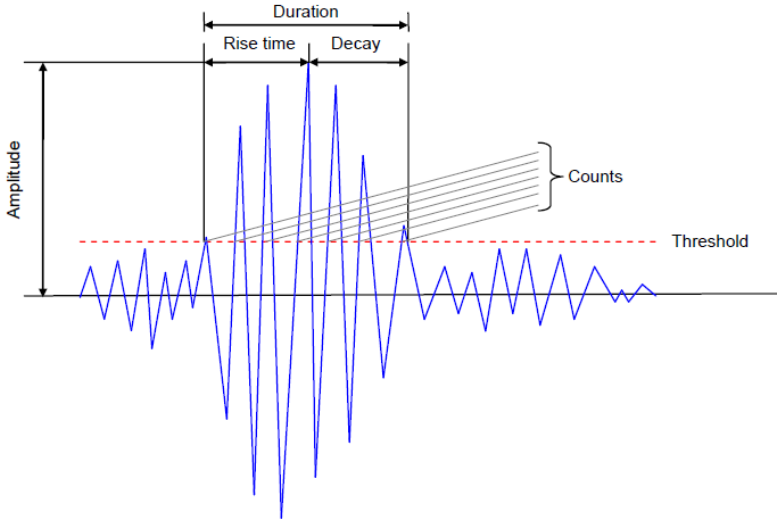

Figure i. AE waveform features

Duration - The interval between the first and last time the threshold was exceeded by the signal.

Peak Amplitude - Maximum signal amplitude within the duration of the signal.

Counts - Number of times the signal amplitude exceeds the threshold.

Rise Time - The interval between the first threshold crossing and the maximum amplitude of the signal.

Initiation Frequency - The average frequency of the waveform from the initial threshold crossing to the peak of the AE waveform.

Energy (Absolute) - The integral of the squared voltage signal divided by the reference resistance (10kOhm) over the duration of the AE waveform packet.

Time driven data – Values recorded periodically with time.

Hit driven data – Values recorded at the time of each AE hit.

Terms relating to wave propagation:

Dispersion - The phenomenon whereby wave velocity varies with frequency.

Group wave velocity - The perceived velocity at which a packet of energy (or wave packet) travels.

Phase wave velocity - Velocity of individual waves within a packet of energy (or wave packet), each wave may travel at a different velocity (see dispersion). Phase velocity does not have to equal group velocity.

Attenuation - The rate at which signal amplitude is reduces with distance of propagation.

S_0 mode – Symmetrical or extensional fundamental Lamb wave mode that propagates in plate like materials and are sensitive to in-plane damage.

A_0 mode - Asymmetric or flexural fundamental Lamb wave mode that propagates in plate like materials and are sensitive to out-of-plane damage.

Hsu-Nielson (H-N) Source – An artificial source of AE (Hsu and Breckenridge 1981).

Time of Arrival (TOA) – Traditional AE source location algorithm used to located AE sources in structures. Using the difference in arrival times between transducers and a known wave velocity to estimate the location of an AE event by minimising the error between the measured and calculated different in arrival times.

Delta T mapping technique – Advanced AE location technique, an area of interest is identified on a structure. Artificial AE source is used at node positions

within the interest area and resulting time of arrival recorded at the transducers. This enables the generation of different in arrival time contour maps for each transducer pairing. These are used to identify contours when trying to locate actual AE events, the maps are overlaid at the intersection of the contours corresponding to an estimate source location (Baxter et al. 2007).

AIC Delta T mapping technique – Uses the same technique as above but uses the Akiakie Information Criteria (AIC) (Maeda 1985) to determine the onset of an AE wave. The AIC uses the entropy of the signal to determine between when the wave has structure and when it has not i.e. between signal and noise.

Wavestream – Raw AE activity recorded for a set time period irrespective of the threshold used.

Wavelet Transform – Signal processing technique which decomposes a transient signal in order to release a time frequency representation of a wave.

Ultrasonic C-scanner – An ultrasonic technique which is used to detect, measure and characterise a range of manufacturing and in-service defects in composite materials.

STA/LTA – Short Term Averaging / Long Term Averaging.

CFRP – Carbon Fibre Reinforced Polymer

HFRP – Hybrid Fibre Reinforced Polymer

GFRP – Glass Fibre Reinforced Polymer

Nomenclature

C	Wave velocity in the medium	($m.s^{-1}$)
C_{AE}	Calculated wave speed	($m.s^{-1}$)
$C_{(S/A)}$	Velocity of the s_0 or a_0 wave mode	($m.s^{-1}$)
C_A	Flexural (asymmetric) group velocity (a_0)	($m.s^{-1}$)
C_S	Extensional (symmetric) group velocity (s_0)	($m.s^{-1}$)
D	Distance between transducers	(m)
d	Distance between sensor pair	(m)
d_1	Distance from source to first hit transducer	(m)
d_2	Distance from source to second hit transducer	(m)
N	Number of items in the sample	
r	Distance of propagation	(m)
t	Current sample point	
Δt	Difference in arrival times between transducer pairs	(s)
Δt^1	Difference in arrival times of s_0 and a_0 modes	(s)
T	Final sample point	
T_1	Time of travel from source to sensor 1	(s)
T_2	Time of travel from source to sensor 2	(s)
$T_{S/A}$	Difference in time of arrival of s_0 or a_0 wave mode	(s)
T source	Time difference of the source	(s)
T training map	Time difference of the training map	(s)
Var	Variance	(V^2)
V_{ref}	Reference voltage at sensor	(V)
V_s	Signal voltage at sensor	(V)
(X_s,Y_s)	X and Y positions of the source	(m)
(X_i, Y_i)	X location and Y location of transducer i	(m)
Z	Perpendicular distance from neutral axis between two sensors to source	(m)
θ_{TOA}	Angle	(radian)

Table of contents

List of Figures

List of Tables

1 Introduction

1.1 Novelty Statement

This thesis investigates the ability to detect, locate and characterise damage mechanisms within large-scale metallic and composite material specimens using Structural Health Monitoring (SHM) systems for aerospace applications. The work focuses on the use of Acoustic Emission (AE) advanced techniques and their application to monitoring large-scale structures under fatigue failure. The novelty in the work is highlighted below:

- A study of AE wave propagation effects on damage characterisation in complex large-scale structures in order to extract meaningful results.
- A novel Parameter Correction Technique (PCT) was developed to correct the traditional AE parameters and used for the first time to achieve successful artificial AE source discrimination in large-scale composite specimen.
- Successful real AE source discrimination in large-scale composite specimen under fatigue load was achieved using the PCT.
- Development of a selecting tool, based on a clustering approach, to select the valid events at each grid point of the Delta T technique, which now provides a considerable improvement in the Delta T mapping by greatly decreasing the process time and improving the reliability of location calculation, through the elimination of human error.
- Development of the AIC Delta T AE source location calculation by using a new approach, known as the Minimum Difference Approach (MDA), to eliminate any human manipulation of the data.
- A novel fully Automatic Delta T Mapping (Automatic DTM) technique was developed and applied to artificial AE source location in a simple structure for the first time and a significant improvement was observed over the traditional time of arrival location method and the AIC Delta T mapping technique.
- Robustness testing of the full automatic Delta T technique in complex aerospace grade aluminium specimens with comparison between the Automatic Delta T mapping with the AIC Delta T and time of arrival (TOA) methodologies.

1.2 Background

SHM systems allow structures, such those found in aerospace, to be continuously monitored by the use of permanently mounted or embedded transducers utilising Non-Destructive Testing (NDT) techniques. This monitoring enables the early detection of the deterioration of a structure. Different systems are available and selecting the appropriate one depends on many factors such as the application type, system capabilities and operation environment limitations.

An effective SHM technique would offer operators the potential to make significant cost saving whilst maintaining or improving safety. These systems will reduce or stop the scheduled inspections on the structure which put the structure out of service. Furthermore, the maintenance will be conducted only when it is required and not dependent on the number of operational hours.

For example, in the aerospace industry, use of SHM systems will enable the development of optimised and efficient structures in agreement with environmental legislation. At the design stage, safety factors in critical areas could be reduced if these systems are implemented. This will lead to reduced component weight, with the benefit that lighter aircraft consume less fuel and have lower harmful emissions.

Composite materials offer many advantages as an aerospace structural material and in other essential industries; not least is the potential for weight saving. For this reason their adoption by aircraft manufacturers has become extensive, in response to pressure to reduce both environmental impact and running costs of commercial aircraft (Eaton et al. 2012a). Recently, due to the high resistance to oxidation composite materials are used increasingly for primary structural components in ground and marine transportation. Nowadays the reinforced composite structure has become widely used in large-scale safety critical structures for infrastructure and transport, (in space, air, ground, energy and marine sectors), at a rapid rate. Such structures can have very high costs of ownership resulting from downtime and inspection to ensure safe operation. These structures require SHM for continuous and global monitoring of the structure in order to increase safety and reduce the amount of inspection required.

AE has great potential for use in SHM systems. It can be usefully exploited for real time monitoring of the entire structure and enables the provision of feedback about the structural integrity, damage evolution and hence can increase the time periods between inspections, which is particularly useful in order to reduce cost of inspection especially on hard to access structures such as off-shore wind turbines. Moreover, AE is capable of detecting the damage location within the structure. This will reduce and limit the inspection area and hence reduce the inspection cost. Also, AE has the ability to identify damage phenomena by correlating the detected AE signals with a particular failure mechanism which is considered as an efficient feature to provide a valuable tool to investigate the integrity of the structures (Sause et al. 2012).

Although AE has the potential to provide in-service SHM of structures, the damage characterisation and localisation in complex large-scale components still has some limitations. Development of more advanced analysis techniques is required to provide more reliable and quantitative damage characterisation. Furthermore, an easy to use, fast to apply, cost-effective, and very accurate for damage localisation technique in complex structures is key for the uptake of SHM systems using AE. This thesis investigates the development of key technological areas for the reliable damage characterisation and localisation in large-scale complex structures.

1.3 Aims and objectives

This work focuses on the development of advanced AE techniques for improved quantitative analysis in complex aerospace metallic and composite structures. The main objectives of this thesis are:

- A thorough investigation of the effect of the wave propagation in large-scale composite materials on the recorded AE data.
- The discrimination between different composite damage mechanisms AE signals generated at different positions from the AE sensor.
- Overcome issues related to using different sensors data in damage discrimination analysis.
- Overcome problems of losing AE data in the damage discrimination analysis due to using one sensor data.

- To further develop the Delta T mapping technique for improved damage location.
- To carry out experimental investigations into damage detection and location of different damage mechanisms in both metallic and composite structures.

1.4 Thesis organisation

Chapter one contains an introduction to the thesis including the novelty contained, background, aims and objectives, an outline of SHM and the scope of the research.

Chapter two presents background theory and reference work in the areas of wave propagation, source location and source characterisation of AE signals in composite structures.

Chapter three contains details of the instrumentation and experimental techniques commonly used throughout this work.

Chapter four discusses damage characterisation in composite materials and includes an experimental investigation on the effect of AE wave propagation in inhomogeneous composite materials on the recorded AE data. Furthermore this chapter provide a full description of the novel correction technique, the PCT. Additionally, artificial source characterisation and real source characterisation with the comparison with the traditional approaches are presented.

Chapter five discusses damage location in a simple and complex metallic structure using a novel AE location technique. Full description of the novel full automatic Delta T mapping technique is provided. Results comparing the automatic Delta T, the AIC Delta T and time of arrival (TOA) methodologies are provided.

Chapter six summarises the overall discussion of the results of this thesis.

Chapter seven summarises the finding of this thesis and discusses potential directions for further work.

1.5 Published outputs

A total of four journal papers and two conference papers have been published through direct and associated research activities which are either directly related to or associated with this thesis. These are:

Journal Publications

Al-Jumaili, S. K., Eaton, M. J., Holford, K. M., Pearson, M. R., Crivelli, D. and Pullin, R. (2016a) “Characterisation of Fatigue Damage in Composites Using an Acoustic Emission Parameter Correction Technique” Composites Part B: Engineering (under review).

Al-Jumaili, S. K., Pearson, M. R., Holford, K. M., Eaton, M. J. and Pullin, R. (2016c) “Acoustic emission source location in complex structures using full automatic delta T mapping technique” Mechanical Systems and Signal Processing 72–73, pp. 513-524.

Al-Jumaili, S. K., Holford, K. M., Eaton, M. J. and Pullin, R. (2015) “Parameter Correction Technique (PCT): A novel method for acoustic emission characterisation in large-scale composites” Composites Part B: Engineering 75, pp. 336-344.

Crivelli, D., Guagliano, M., Eaton, M., Pearson, M., Al-Jumaili, S., Holford, K. and Pullin, R. (2015) “Localisation and identification of fatigue matrix cracking and delamination in a carbon fibre panel by acoustic emission” Composites Part B: Engineering 74, pp. 1-12.

Conference Publications

Al-Jumaili, S. K., Pearson, M., Holford, K. M., Eaton, M. J. and Pullin, R. (2016b) “Fast and Reliable Acoustic Emission Source Location Technique in Complex Structures” 24th UK Conference of the Association for Computational Mechanics in Engineering (ACME-UK). Cardiff, UK.

Al-Jumaili, S. K., Holford, K. M., Pullin, R. and Eaton, M. J. (2014) “A Parameter Correction Technique (PCT) for Acoustic Emission Characterisation in Large-Scale Composites” 31st Conference of the European Working Group on Acoustic Emission (EWGAE). Dresden, Germany.

2 Theory

2.1 Acoustic Emission

2.1.1 Background

AE is a physical phenomenon whereby elastic energy is released from a mechanical source mechanism, such as an advancing crack, in the form of transient elastic waves which propagate within the material and reach the surface, causing surface deformations which can be detected using piezoelectric transducers. AE is considered to be a NDT technique concerned with the passive monitoring of ultrasound in a structure (Miller and Hill 2005), and it is able to detect, record and interpret the high-frequency emissions due to initiation and growth of damage (Rippengill et al. 2003). The identification of an electrical signal, captured by a piezoelectric transducer, as the result of damage offers great advantages in the health monitoring process of structures (Pappas et al. 2004).

The frequency range of AE signals is approximately 10 kHz to 1 MHz, however it is more common for signals to be within the range of 100kHz to 300kHz (Miller and Hill 2005). A typical AE test setup is illustrated in Figure 2-1 where the displacement of the surface is detected using AE sensors mounted on the structure which convert this to an electrical signal by using a piezoelectric crystal. After sensing and pre-amplification, the signal is transmitted to the main instrument, where it is amplified and filtered. Modern AE technology began in 1950 with the work of Josef Kaiser who demonstrated the AE behaviour of irreversible plastic strain. Nowadays using modern computing (high processing power and huge storage ability) AE acquisition and processing rates have been increased. Acquisition of high data rates during AE testing with capture of full waveforms lead to a much deeper understanding of AE wave propagation.

Traditional NDT methods, such as ultrasound and x-ray, require a known input source and are defined as active techniques. On the contrary, AE is classed as a passive technique because it detects elastic waves released from the structure itself during deformation. Unstressed or non-active defects will not normally emit AE and will therefore not be detected.

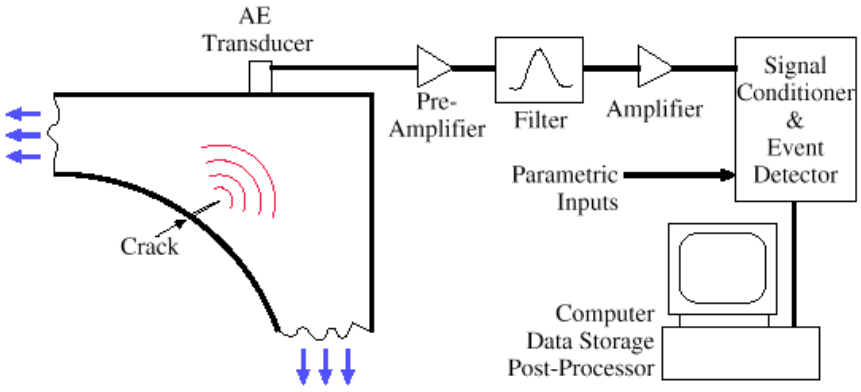

Figure 2-1. A typical AE test set-up (Huang et al. 1998)

2.1.2 AE source mechanisms

Emission from AE sources (for example in structures made of metal, concrete or composites) can be categorised as either transient or continuous. According to Vallen (2002) the two types of emission can be defined as follows; Continuous AE signals contain fluctuation amplitude and frequency but the signal does not end. Sources generating continuous AE include machine vibrations, friction and flow or leakage noise. Figure 2-2a shows an example of a continuous AE signal. Transient waves are burst type signals originating from sources such as abrupt and permanent changes in material such as fractures, crack growth, corrosion and defect related deformation processes. Transient signals have an obvious start and end point. Figure 2-2b shows an example of a transient wave.

Many different events can provide sources of AE in a structure, including internal events such as crack formation and external events such as impact of the structure by a foreign object. In this work the focus is on AE sources that are emitted in composite material structures only.

According to Wevers (1997), Huguet et al. (2002), Miller and Hill (2005), Loutas and Kostopoulos (2009) and Boominathan et al. (2014) the common sources of AE in continuous fibre composite materials are; fibre failure, fibre pullout, fibre / matrix debonding, matrix micro cracking, transverse matrix cracking, splitting parallel to fibres and delamination. Also, complex combinations of source mechanism can occur, i.e. fibre failure with fibre pullout or simultaneous fibre and matrix failure.

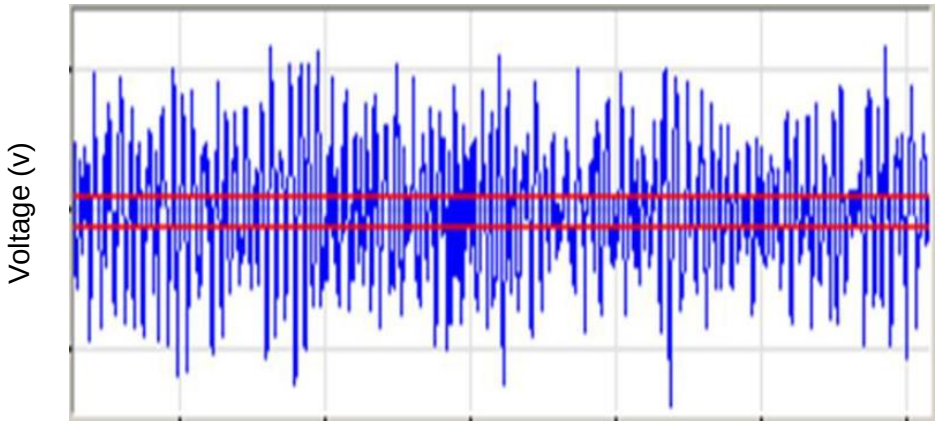

(a)

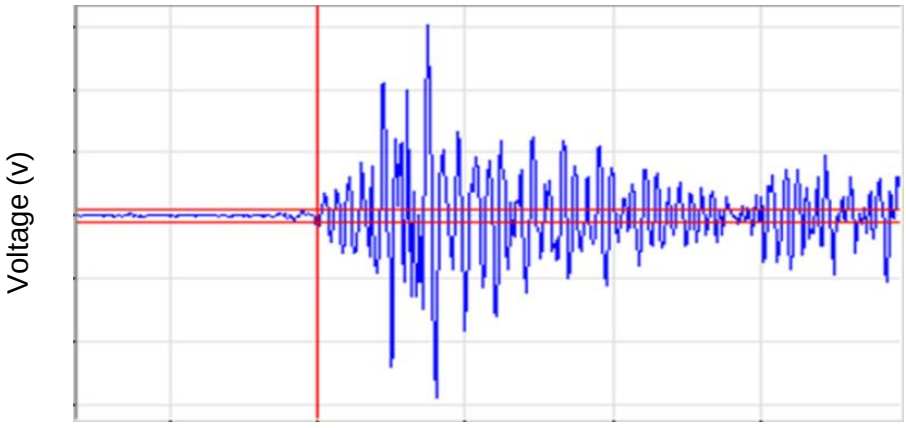

(b)

Figure 2-2. Types of AE signal (a) continuous wave (b) transient wave (Mohd 2013)

2.1.3 Signal measurement parameters

In AE signal analysis, the most commonly used signal measurement parameters are amplitude, counts, rise time, duration, and the measured area under the rectified signal envelope which is also called relative energy. Figure 2-3 shows the definition of simple waveform parameters. Other parameters which may be used include absolute energy, count-to-peak, average frequency, or spectral moment. However, the five principal parameters have become well standardised (Miller and Hill 2005).

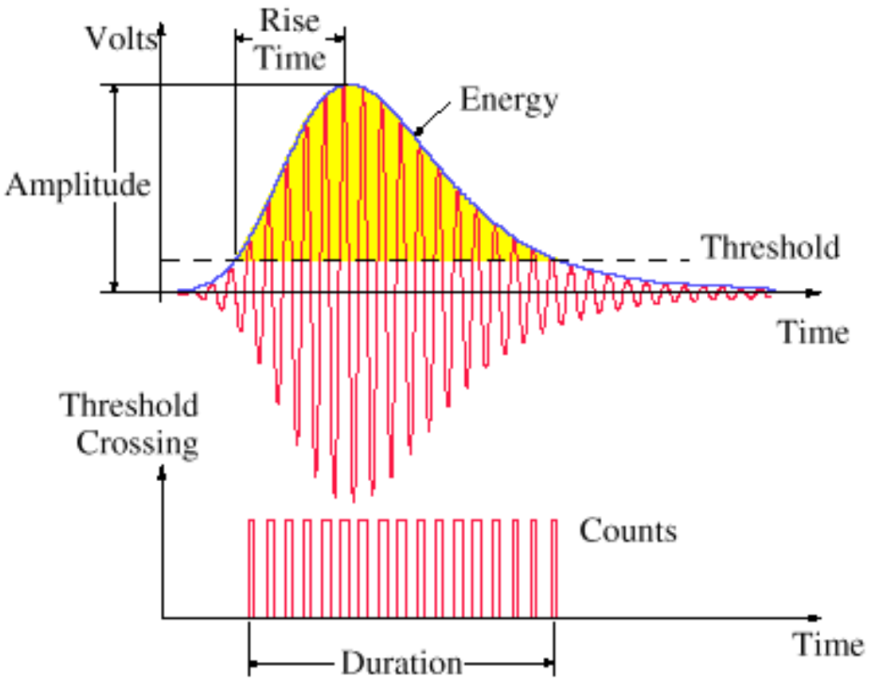

Figure 2-3. Definition of simple waveform parameters (Huang et al. 1998)

2.1.4 AE wave propagation

Acoustic emission propagates initially from the source point as a bulk wave. In an infinite medium these elastic waves propagate in two basic forms. longitudinal and transverse waves (Rindorf 1981). In the transverse mode the particle motion is perpendicular to propagation direction while in the longitudinal mode the particle motion consists of localised compression and rarefaction parallel to the propagation direction. Figure 2-4 shows the two wave forms.

If a solid media boundary is introduced, such as a surface, the two wave modes combine in a region close to the surface and a further wave mode may exist and is known as a surface wave or Raleigh wave (Figure 2-5).

In a plate-like structure (a medium bounded by two surfaces), two surface wave modes produced from the bulk waves couple at the surfaces (Rindorf 1981). These modes are the symmetric or extensional (s_0) mode and the asymmetric or flexural (a_0) mode shown in Figure 2-6. The waves that propagate in this type of structure are called Lamb waves. This type of wave is presented in many acoustic emission studies such as Holland et al. (2000), Aggelis et al. (2011), Grondel et al. (2002), Sause et al. (2013) and Asamene et al. (2015).

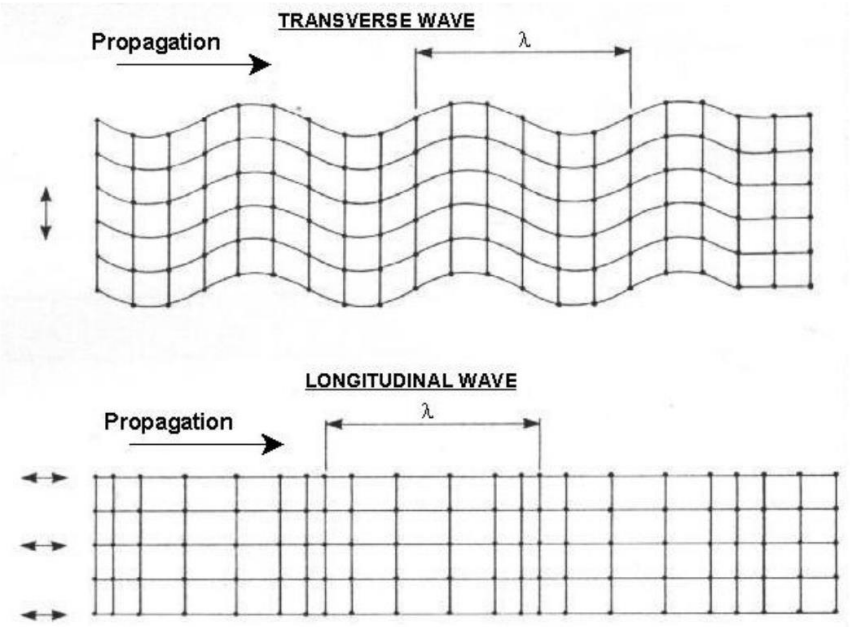

Figure 2-4. Basic wave propagation modes in a solid (Rindorf 1981)

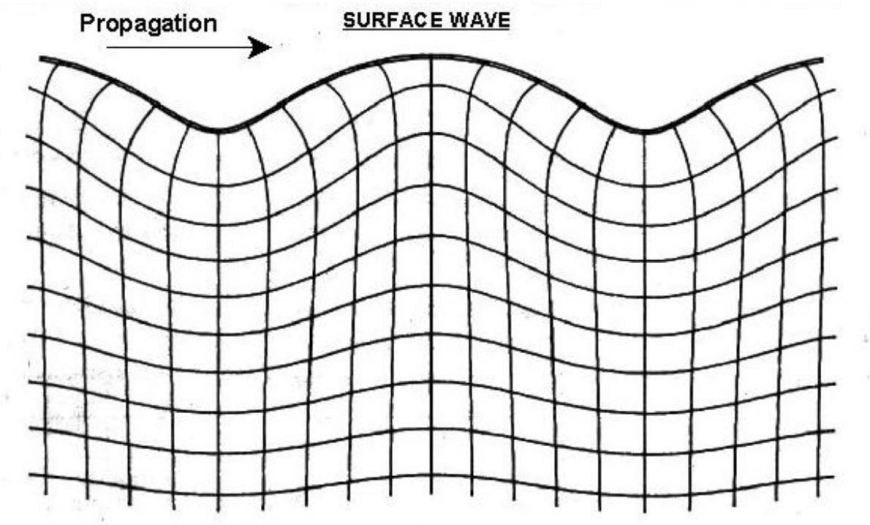

Figure 2-5. Surface wave particle motion (Rindorf 1981)

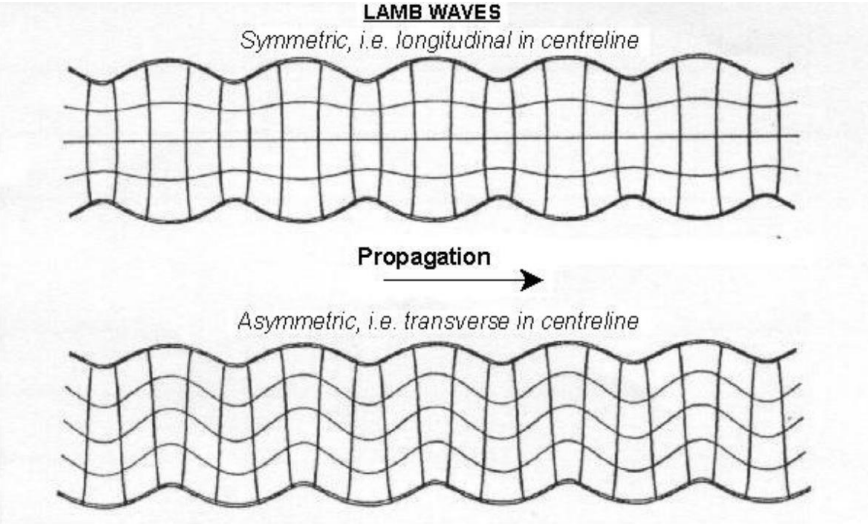

Figure 2-6. Two principal plate wave modes (Rindorf 1981)

The larger displacement component in the extensional mode is in the plane of the plate. For the flexural mode, the larger displacement component is perpendicular to the plane of the plate. The limits that Lamb waves occur are that the plate thickness is much smaller than the two other dimensions and the wavelength is much larger than the plate thickness (Ziola and Gorman 1991).

The plate like structure is widely used in industry for pipes and pressure vessels or aircraft wings and fuselages therefore the source characterisation and location analysis carried out in this study will focus on Lamb wave theory.

2.1.5 Velocity and dispersion

Lamb wave characteristics are discussed thoroughly by Rindorf (1981), Pollock (1986) and Gorman and Prosser (1991); the following is a brief summation of the relevant points.

Dispersion curves can describe the propagation of Lamb wave modes as the velocity varies with frequency. Figure 2-7 shows an example of the dispersion curves displayed as a function of velocity on the vertical axis and frequency (or thickness-frequency) on the horizontal axis (generated using commercially available, DISPERSE software).

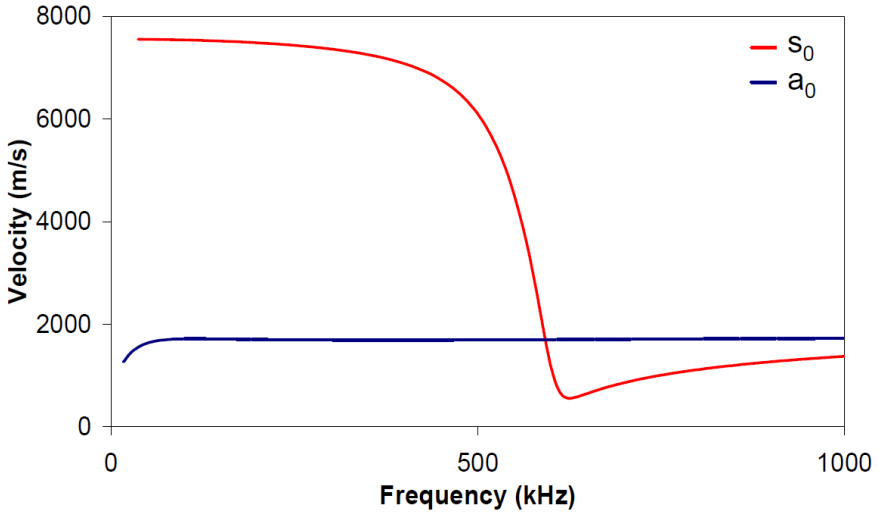

Figure 2-7. Typical dispersion curves for a 2.15mm thick cross-ply laminate (Eaton 2007a)

The dispersion curves show how, for a fixed plate thickness, different frequency components of Lamb waves travel at different velocities.

From the figure it is clear that the s_0 mode travels at a high velocity at low frequencies. This velocity is determined by the in-plane stiffness of the plate. On the other hand, the a_0 mode is slow and highly dispersive, because the velocity is determined by the flexural stiffness of the plate (which is low) and strongly on thickness.

A full understanding of the effects of propagation on the AE signals is essential for AE analysis. This becomes very important when considering wave propagation in anisotropic materials such as composites, because the material properties and therefore the propagation characteristics vary with direction.

2.1.6 Wave attenuation

AE signals lose energy as they propagate within the medium. Signal amplitude loss with propagation distance is known as attenuation (Miller and Hill 2005) and is another important part of wave propagation that must be understood before undertaking any AE signal analysis. The four main causes of attenuation as discussed by Pollock (1986) are detailed below.

- ***Geometric spreading***

The major contributor to attenuation is geometric spreading which causes considerable amplitude decrease. The wave energy is redistributed within the material as the wave propagates away from the source. This causes an amplitude decrease correspondingly. The amplitude decrease for a bulk wave can be determined as proportion of 1/r where r is distance of propagation. For wave propagation in two dimensions, such as Lamb waves, the amplitude of the signal decrease is in proportion to $1/r^{1/2}$ (Miller and Hill 2005).

- ***Internal friction***

Attenuation occurs due to degradation of elastic wave energy into heat through a variety of material-dependant mechanisms. Internal friction converts the acoustic energy into thermal energy within the material. In non-metals (such as composite materials) the effects of internal friction are typically much greater than that in metals. Internal friction in composite materials can be related to viscoelastic material behaviour, friction between surfaces that slip and incompletely bonded fibres. The absorption mechanism is usually frequency dependent and greater losses usually occur as AE waves propagate at a higher frequency.

- ***Wave dispersion***

The short pulse is spread out as it propagates due to the dispersion. This will result in reduced amplitude. The wave dispersion attenuation is dependent on the bandwidth and gradient of the dispersion curve for a given scenario.

- ***Dissipation into adjacent media***

The fourth attenuation mechanism is dissipation of acoustic energy into adjacent media. It is however of little relevance to this work and so is not discussed in any detail.

2.2 Source location

The purpose of the literature review is to identify the fundamental research methodologies for SHM systems used to locate the AE sources for both metal and composite structures.

Much of the AE propagation and location fundamentals were studied and presented by Pollock (1986) and Rindorf (1981). A detailed explanation and discussion of these works has been presented in detail by Baxter (2007) and Eaton (2007a).

One of the most attractive features of AE is the capability of source location and it is considered an important step for SHM (Kundu 2014). For large scale structures it is very costly and time consuming to inspect every part of the structure using the traditional inspection techniques, such as X-ray and ultrasonic techniques. If the damage location is known in advance it would enable maintenance teams to focus on a particular areas of concern when using other NDT techniques. In addition, knowledge of the damage location can improve damage characterisation, because damage mechanisms are often dependent upon particular geometric features and loading conditions.

The conventional AE source location technique, known as the time-of-arrival or TOA technique, is discussed in detail in the NDT handbook (Miller and Hill 2005). It has been widely used to locate AE sources in isotropic and homogenous structures and is based on detecting the arrival time of an AE signal at each of the sensors for the fastest propagating mode, which enables the source to be located using a simple triangulation technique. The TOA technique relies on the assumptions of a constant wave speed in all directions from the source to sensor and an uninterrupted propagation path between the source and the sensor. In realistic structures the wave speed is rarely constant due to thickness changes and anisotropy in composite materials, where the wave velocity is dependent on the propagation direction with the wave velocity of the fastest propagating mode being considerably higher in the fibre direction. Geometric features such as holes, lugs and structural discontinuities will also considerably affect the propagation path and velocity (Pullin et al. 2007a; Hensman et al. 2010).

These factors mean that the assumptions relied upon by the TOA technique are not valid and hence will introduce errors in the source location calculation. In addition, any errors in the determination of signal arrival times will result in a further loss of accuracy in the estimated source locations. The threshold crossing approach, used commercially to pick the time of arrival of the AE signal is not satisfactory, because using a high threshold level will lead to inaccurate time of arrival measurement, while a lower threshold value will increase the ability to pick

the accurate waveform onset but also increases the risk of a false trigger. In order to improve arrival time estimation a number of approaches have been investigated. The STA/LTA method compares the average energy in a short term window (STA) with the average energy in a long term window (LTA) prior to a point *i* in a signal (Earle and Shearer 1994). The change in ratio indicates the signal arrival, however, despite good performance in noisy data the use of averages makes accurate determination difficult and a threshold is still needed to detect the change. The cross-correlation technique (Ziola and Gorman 1991) has been used to find the arrival of a particular frequency within a signal by cross-correlating a short, single frequency, Gaussian windowed pulse with the recorded signal. An expansion of this is the use of wavelet transforms which identify energy arrival across a range of frequency. However it has been shown that the accuracy of this approach is poor in complex structures where multiple reflections are present (Hamstad et al. 2002). Lokajicek and Klima (2006) took the sixth order statistical moment of a sliding short time window which changes with the presence of structured data points associated to the signal. Although the moment is sensitive the detection of the change still relies upon a threshold. The use of neural networks has been investigated by Wang et al. (1995) however, its computational complexity limits its application in practice. A more reliable approach for arrival time estimation of seismic and ultrasonic signals adopts the Akiake Information Criteria (AIC) (Akaike 1974). The AIC was first adapted for use directly on transient seismic data by Maeda (1985). However, more recently it has been demonstrated for accurate determination of arrival time of AE and ultrasonic transient signals (Sleeman and van Eck 1999; Kurz et al. 2005; Sedlak et al. 2009; Hensman et al. 2010). The AIC function compares the signal entropy before and after each point *i* in a signal and returns a minimum at the signal onset where the greatest difference is seen between the high entropy random noise seen prior to signal onset and the low entropy structured signal after onset.

Attempts to improve upon the triangulation approach used in the TOA algorithm have been widely reported. AE source location in isotropic materials without prior knowledge of the wave speed has been reported by many researchers as an improvement over the simple TOA approach. Examples include the beamforming method (McLaskey et al. 2010; He et al. 2012) which is based on the delay-and-sum algorithm from small sensors array, the strain rosette technique (Matt and Di Scalea 2007) where the source location is predicted from the principal strain

directions using rosette arranged macro-fibre composite (MFC) transducers and the modal acoustic emission method, where the dispersion characteristics can be predicted of the AE wave modes in thin isotropic plates. Wavelet transform theory has been utilised to determine the arrival times of the different modes for one-dimensional location (Jiao et al. 2004) and two-dimensional location (Toyama et al. 2001).

AE location in anisotropic materials is very challenging due to variations in propagation velocities. A number of interesting approaches have been taken to solve this problem (Kundu et al. 2012; Niri et al. 2014; Kundu et al. 2015) and improvements in accuracy have been shown in simple laminated plates. Ciampa (2010) utilised a specific layout of sensors to locate impact events in anisotropic materials without knowing the plate properties. Solution of a system of nonlinear equations is required in this technique. Kundu et al. (2012) successfully developed a technique based on a cluster of sensors for application in anisotropic plates which avoids the need to solve a system of nonlinear equations. Niri et al. (2014) used the nonlinear Kalman Filtering algorithms (Extended Kalman Filter (EKF) and Unscented Kalman Filter (UKF)) as expansion of probabilistic localization algorithms to estimate the location of AE sources in anisotropic panels. Kundu et al. (2015) presents a two–step hybrid technique to locate sources in anisotropic plates. Wave propagation in a straight line is assumed in the first step to find the initial source location, while solving an optimisation problem provides the second step to improve the initial location accuracy.

However, none of these approaches account for structural complexities that may alter the wave propagation path and velocity, such as holes and thickness changes that may be present in reality. The DTM technique accounts for these sources of error. This technique is a mapping approach whereby artificial sources are used to map a structure and thus allow high location accuracy on realistic complex structures. Originally developed for complex geometry metallic structures (Baxter et al. 2007), the technique has also been shown to perform very well in anisotropic materials such as composites (Eaton et al. 2012b).

Although the DTM technique demonstrates the ability to locate with a high level of accuracy in complex structures, the collection and processing of training data can be very time consuming. It requires an operator with a background in AE to select

the optimal data to ensure the greatest possible accuracy. Furthermore, for locating AE sources an operators experience is used to determine a suitable cluster diameter (only the convergence points inside a specific cluster diameter are used to calculate the probable AE source location). Overcoming these problems will lead to a fully automatic process which would remove any human error and experience whilst still maintaining or improving the accuracy of source location.

One of the objectives of this work is to extend the previous work on the DTM technique presented by Baxter et al. (2007), Eaton et al. (2012b) and Pearson (2013) and create a fully automatic technique which reduces human input and increases accuracy and reliability whilst increasing the speed of the whole process.

2.2.1 Source location techniques

The most commonly used method for the AE source localisation is the TOA technique. This technique is integrated in all commercially available AE systems. Other techniques for AE source localisation are the “Single Sensor Modal Analysis Location” (SSMAL) and the last two modern versions of the recently developed “Delta T mapping technique”.

2.2.2 Time of Arrival (TOA)

The TOA location methodology can be explained simply by considering the propagation of the signal from an AE source traveling in one dimension as shown in Figure 2-8. The zonal location is the most basic way to locate the source in the beam and depends on the order in which the signal reaches each sensor (i.e. the hit order.) For example if the first sensor hit is sensor 2 then the expected source location will be in the range from the midpoint between sensor 1 and 2 to the midpoint between sensor 2 and 3 as presented in Figure 2-8a. This expectation relies on constant speed of the signal. By counting the second sensor hit, the source location area is further refined. If sensor 1 is the second hit, the source location area can be reduced to the range between the midpoint between sensor 1 and 2 to sensor 2 (Figure 2-8b).

If the hit sequence and the arrival time difference between the hits are known, more accurate source location can be determined (Figure 2-8c). The time

difference between the hits can be determine using Equation (2.1), for a hit sequence of sensor 2 first followed by sensor 1.

$$\Delta t = \frac{d_2 - d_1}{C_{AE}} \tag{2.1}$$

Where

C_{AE} = Calculated wave speed

Δt = Hits time difference

d_1 = Distance from source to first hit sensor

d_2 = Distance from source to second hit sensor

A more common expression in terms of d_1 is presented in Equation (2.2)

$$d_1 = \frac{D - \Delta t . C_{AE}}{2} \tag{2.2}$$

where *D* is the distance between sensors. If the event occurs outside the area between the two sensors as shown in Figure 2-8d, the time difference of the hits will be constant and equal to the time of flight between the two sensors.

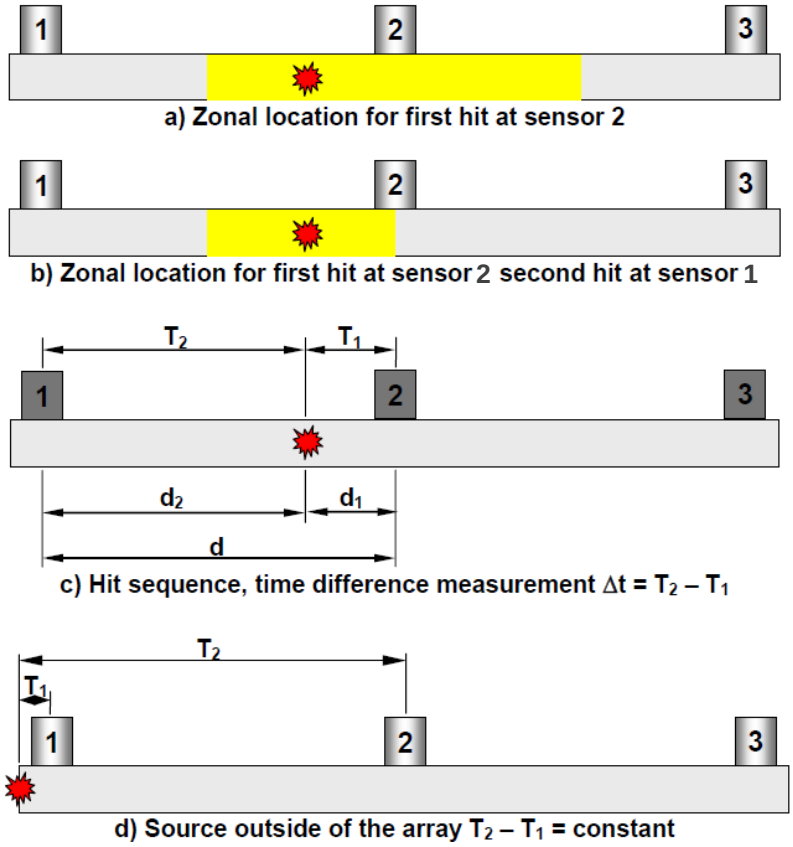

Figure 2-8. Linear source location (Miller and Hill 2005)

In two-dimensions the same methodology can be expanded. Two sensors at distance *d* apart on an infinite plate are presented in Figure 2-9. By assuming constant wave speed propagation from the source to all direction, then it can be shown that

$$\Delta t C_{AE} = d_2 - d_1 \tag{2.3}$$

and

$$Z = d_1 sin\theta_{TOA} \tag{2.4}$$

$$Z^2 = d_2^2 - (d - d_1 cos\theta_{TOA})^2 \tag{2.5}$$

then combining Equations (2.4) and (2.5) gives Equation (2.6)

$$d_1^2 sin^2\theta_{TOA} = d_2^2 - (d - d_1 cos\theta_{TOA})^2 \tag{2.6}$$

$$d_1{}^2 = d_2^2 - d^2 + 2d.d_1 \cos\theta_{TOA} \tag{2.7}$$

Substituting $d_2 = \Delta t\, C_{AE} + d_1$ from Equation 2.3 into Equation 2.7 gives Equation (2.8)

$$d_1 = \left(\frac{1}{2}\right)\left(\frac{(d^2 - \Delta t^2 C_{AE}^2)}{(\Delta t C_{AE} + d\cos\theta_{TOA})}\right) \tag{2.8}$$

For a known hit sequence and arrival time difference the source location can be determined by this curve equation. It is impossible to reach high accuracy source location in two dimensions with two sensors. A third sensor will improve the source location accuracy as presented in Figure 2-10. More accurate location will result from the intersection point of the three curves. Furthermore, increased location accuracy can be achieved by adding further sensors which increases the number of curves.

Errors in location accuracy can be caused by:

- Material inhomogeneity and the structure complexity; resulting in indirect path from the source to the sensor.
- Non-constant signal velocity; particularly in complex structures and complex materials such as composite materials.

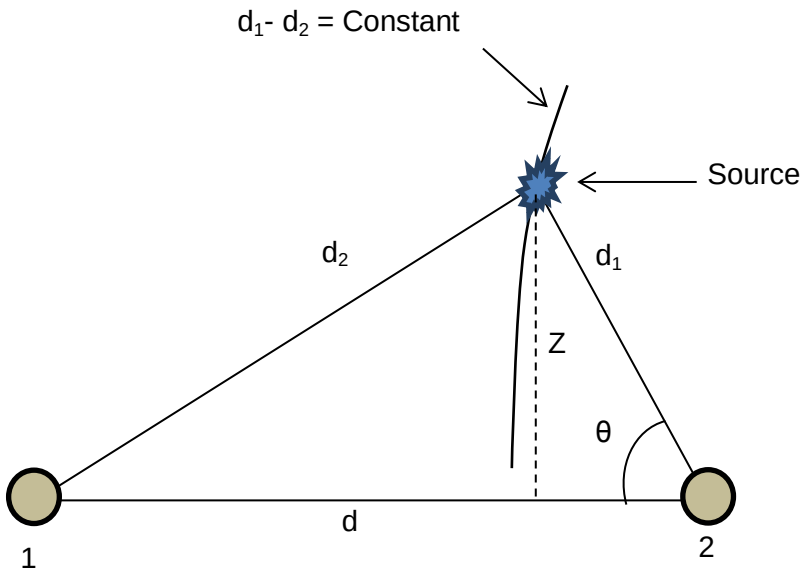

Figure 2-9. Two dimensional location with two sensors (Miller and Hill 2005)

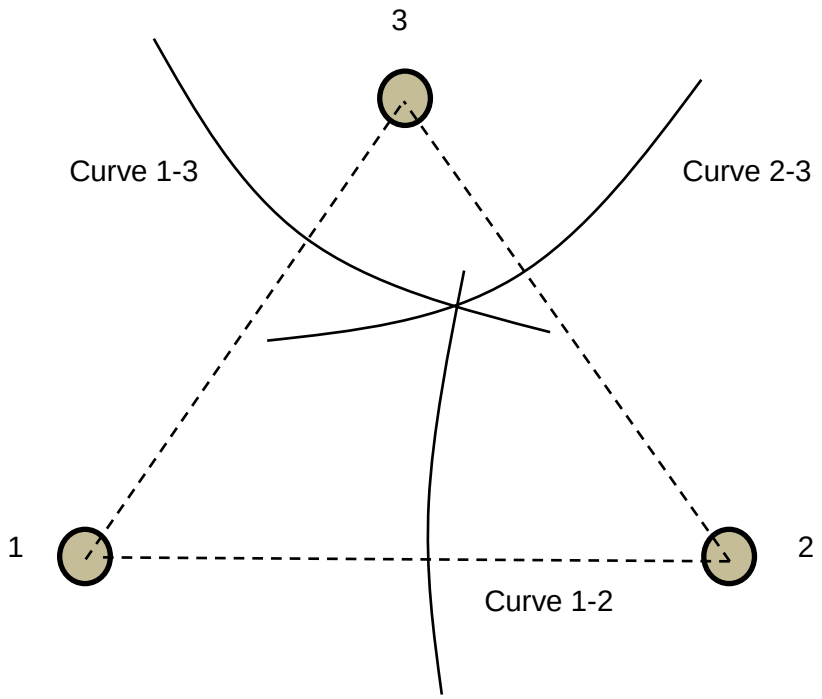

Figure 2-10. Two dimensional location with three sensors (Miller and Hill 2005)

2.2.3 Single Sensor Modal Analysis Location (SSMAL)

This technique exploits the dispersive nature of Lamb waves usefully and presents an alternative method to the traditional TOA technique. This technique is valid only if used to locate sources in plate-like structure and over sufficient propagation distance to allow the signal modes development. If a suitable broadband sensor is used to detect the wave in an appropriate manner, the separation of the different signal modes can be observed as presented in Figure 2-11. If the arrival time of each mode is determined, the source to sensor distance can be calculated using the temporal separation (Holford and Carter 1999) by Equation 2.9.

$$d_1 = \Delta t^1 \left(\frac{C_S C_A}{C_S - C_A} \right) \tag{2.9}$$

where

d_1 = source to sensor distance

C_S = extensional (symmetric) group velocity (s_0)

C_A = flexural (asymmetric) group velocity (a_0)

Δt^1 = difference in arrival times of s_0 and a_0 modes

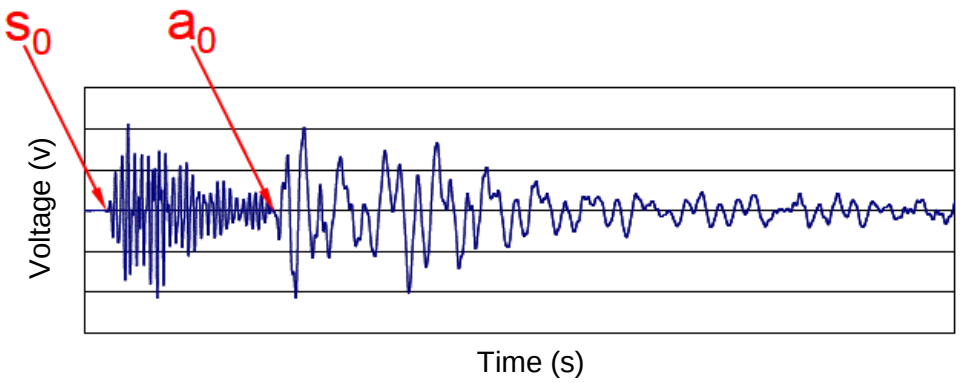

Figure 2-11. AE signal modes separation (an example)

2.2.4 Traditional Delta T Mapping location

As stated earlier, the main assumptions of the two traditional source location techniques, TOA and SSMAL, are the constant wave speed of the signal and straight path between the source and the sensor. In complex materials such as composite materials the wave velocities exhibit a directional dependency. Furthermore, in real structures it is rare to have a direct path between the source and the sensor.

In order to overcome these difficulties in complex structures and inhomogeneous materials, a novel method of source location known as DTM technique was developed. A through description with details of this technique can be found in (Baxter 2007), who showed over 50% location error improvement over the traditional TOA method in complex structure. Location improvement using the DTM technique has also been presented by Pullin et al. (2007a) and Pullin et al. (2007b). The technique has also been shown to perform very well in anisotropic materials such as composites (Eaton et al. 2012b). According to Baxter et al. (2007) the main steps for the implementation of the DTM technique are outlined briefly below:

Determine an area of interest and construct a grid system: The DTM technique offers the ability for complete coverage of structure or a part of the structure, which may have specific interest due to geometric features or stress concentrations. A grid is constructed on the area of interest within which AE events will be located. A source which creates a broadband artificial source is preferable and different sensor types can be used for the area of interest.

Sensors can also be placed within the area of interest, as long as most area of interest is within the sensor array.

Apply an artificial source to obtain TOA data: H-N source events (Hsu and Breckenridge 1981) are generated at each node position within the grid. The H-N source creates an artificial AE source which enables the determination of the TOA from source to sensors to be calculated for each sensor pair. Averaging the recorded TOAs of several events at each node of the grid is used to reduce source errors in the training data. Missing nodes data as a result of holes for example can be interpolated from surrounding nodes.

Calculate ΔT maps: Once the TOA data for each node position has been collected the difference in arrival time (Delta T) for each sensor pair can be calculated, for example four sensors would results in six sensor pairs. Knowing the co-ordinates of node results in the generation of average Delta T maps for each sensor pair. Contours of constant Delta T relative to all sensor pairs can be visualised as a resulting map.

Real AE data location: Once real AE data has been collected, the Delta T for each sensor pair from a real AE event can be calculated. The resulting Delta Ts for each sensor pair can be represented by a line of constant Delta T which indicates possible source location. By overlaying these identified contours for each sensor pair a convergence point is identified, indicating the source location. As with the TOA technique, at least three sensors are required to provide a 2D source location. The confidence in source location estimation can be improved using additional sensors. Theoretically all lines should intersect at one location; however in reality, not all lines will cross at the same point. Therefore, to estimate the source location all convergence points are identified and a cluster analysis provides the most probable source location.

The technique has been successfully used to determine the source location in aerospace grade and composite materials. However there some limitations as listed below:

- The arrival time estimation at each sensor is determined using the traditional threshold crossing approach which is not reliable. Other methods applied to increase the arrival time calculation reliability, such as

lowering threshold and using filtering, are explained in detail by Pearson (2013).

- Removing erroneous data and selecting the correct events for each node is conducted manually. As a result of that the training grid reliability highly depends on the operator.
- The manually process make the Delta T a high cost technique, resulting in a lengthy process depending on the size of the grid.
- Source location calculation is highly dependent on the optimum cluster diameter as determined by the operator. As a result of that, the final location accuracy is mainly depending on the operator decision.

These limitations have a direct effect on the performance of the technique and result in less accurate source locations.

2.2.5 AIC Delta T Mapping Location

The AIC DTM technique is an improvement used to supplement the traditional technique developed by Pearson (2013) in order to overcome the limitation of arrival time calculation. Although the traditional Delta T locates successfully AE source location in different structural materials and complexity, the major disadvantage is that the first threshold crossing approach is used to determine the time of the source at the sensors. Attenuation or dispersion of the signal leads to erroneous Delta T data. This will occur when the actual signal onset is lower than the setup threshold level. Pearson (2013) presents a solution of this problem by exploiting the Akiake information criteria (AIC) (Maeda 1985) to determine the actual signal onset for both the training and the actual event data. The same technique stated earlier by Baxter (2007) was followed, however a re-calculation of the arrival time steps is added. Flowchart steps of the AIC DTM as a comparison with the traditional technique are presented in Figure 2-12.

The form of the AIC was developed by (Maeda 1985) and is the following form:

$$AIC(t) = \mathrm{t}\log_{10}\big(var(x[1;t])\big) + (T - t - 1)\log_{10}\big(var(x[t;T])\big) \qquad (2.10)$$

where

var(x) = the variance of x, i.e. $\sum_i (x_i - \bar{x})^2 / N$

x[1;t] = section of x from 1 to t

The signal x(t) is broken into two parts; first part starts from the time (0) to time (t) and the second part from time (t) to the time (T) at the end of the signal. Equation (2.10) explains the variance similarity between two parts of the signal for every time (t). When the applied time becomes the same time of the signal onset, minimum similarity is observed. At this time the similarity is between the high entropy noise before the signal onset and the low entropy of the waveform. The actual arrival time of each waveform, training data or the actual test data, is determined using the minimum value of the AIC function. This algorithm was successfully used to determine the arrival time of AE waveforms by Kurz et al. (2005) and Sedlak et al. (2009).

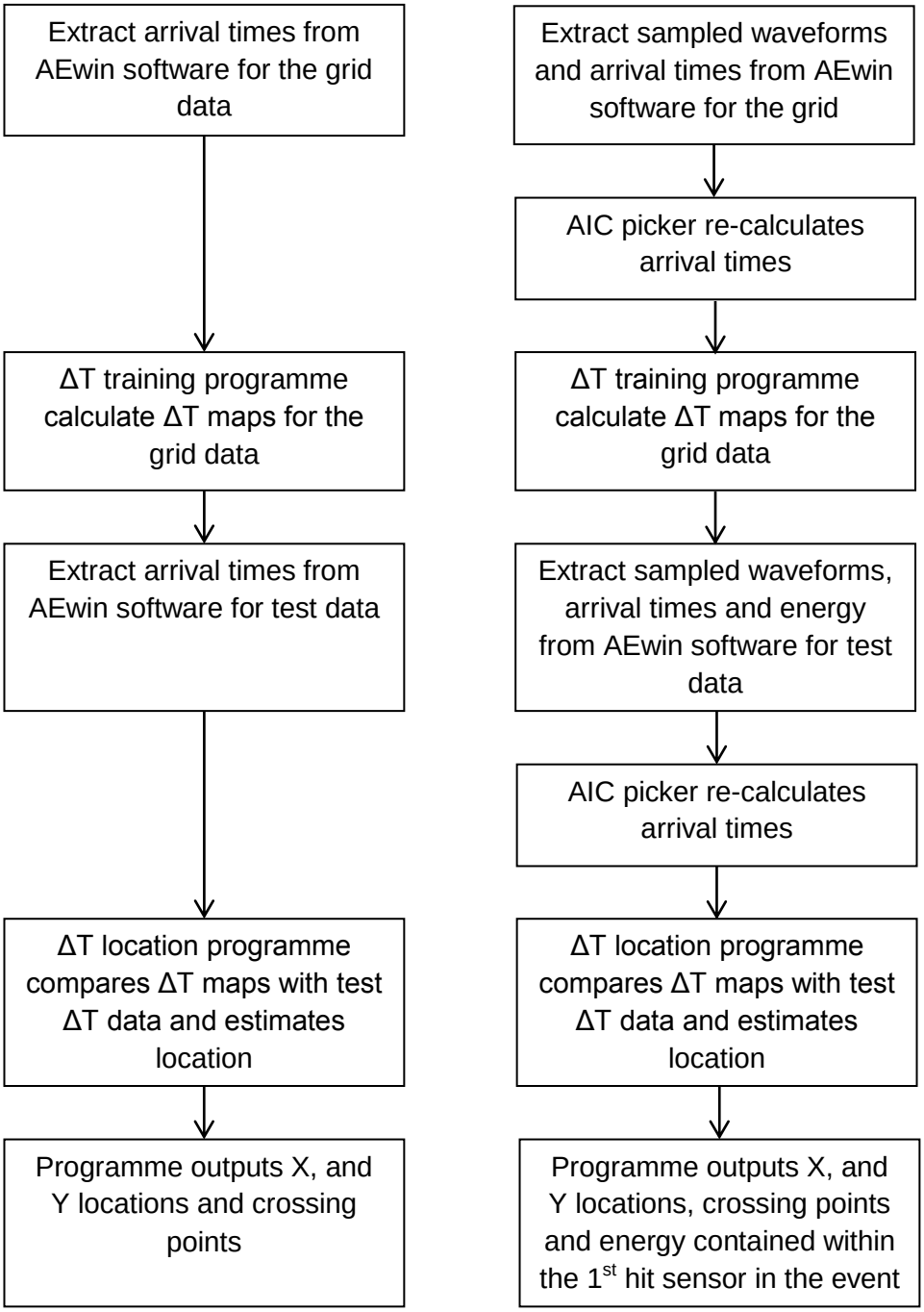

Figure 2-12. Flow diagram representation of the (a) Delta T mapping technique and (b) AIC Delta T mapping technique (Pearson 2013)

Figure 2-13 and Figure 2-14 show the arrival time determination using the threshold crossing and the AIC methods for two waveforms, high amplitude and low amplitude respectively. In the case of high amplitude signals the two techniques refer to the same arrival time. However in the low amplitude signal

case the obvious difference and clear separation between the two techniques to determine the arrival time hence the threshold crossing approach would generate errors as detect incorrect arrival time. It should be noted that these examples shows the two extremes of the scale. A good improvement was achieved using the AIC DTM over traditional DTM technique when used in complex structures and complex materials.

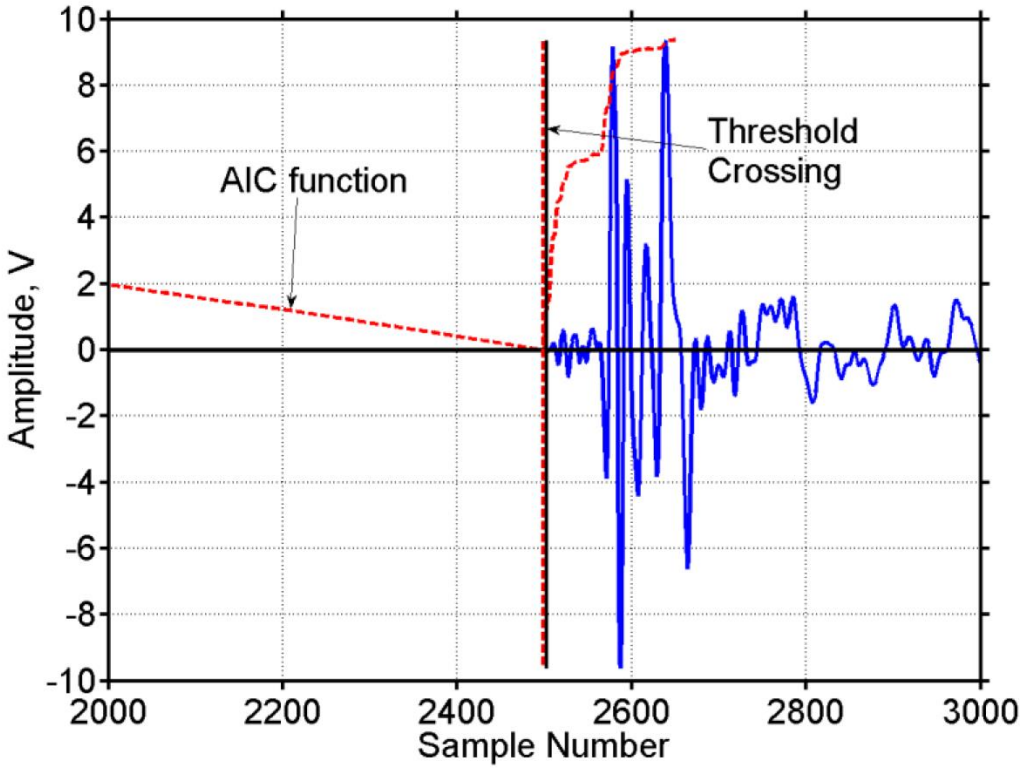

Figure 2-13. Arrival time comparison for a high amplitude AE waveform (Pearson 2013)

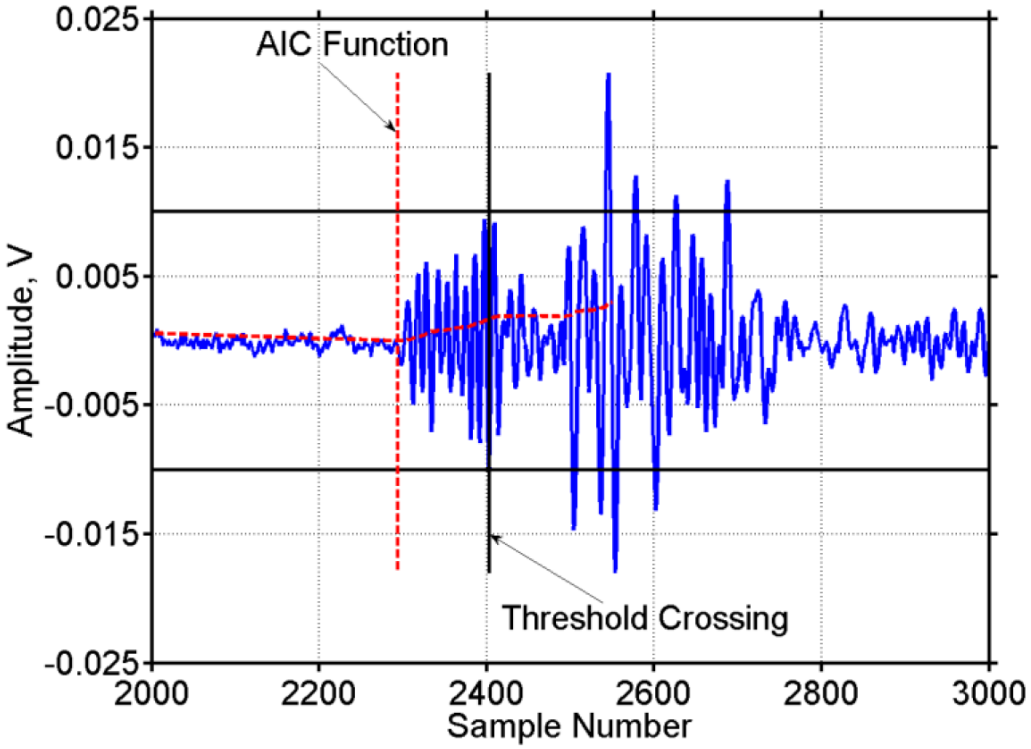

Figure 2-14. Arrival time comparison for a low amplitude AE waveform (Pearson 2013)

Although a successful result was achieved using this technique to locate AE events within complex structures of composite and metallic materials, there are still some limitations which affect the performance of the whole technique. Firstly, as mentioned above several events are required to be generated at each node in the grid. Selection of the correct events and removing erroneous data is essential to constructing the training maps. Nominally this is conducted by recording times at which erroneous data occurred and by visual inspection by the operator, resulting in a lengthy process depending on the size of the grid. Secondly, only the convergence points inside a specific cluster diameter are used to calculate the probable AE source location (step (4) Section 2.2.4). The optimum cluster diameter is determined by the operator by collecting data from known random node positions and comparing the error between actual and estimated source locations before testing commences.

These limitations have a direct effect on the performance of the technique and result in less accurate source locations. The inclusion of incorrect events in each grid point will affect the training map accuracy and/or selecting non-optimum cluster diameters will affect source location accuracy. Furthermore, the process

of manual selection of optimum training data is time consuming. Filtering the recorded data for the training map can be an expensive process. For example, the pie chart in Figure 2-15 shows the percentage of the time consumption of each step of constructing the training map; map drawing, generating H-N sources and manually filtering of the events. From the figure, it is clear that the most time consuming part is the events filtering (more than 75% of the time expensive). Practically, for training a map of 20 x 20 cm grid dimensions and 2.5 cm mesh resolution, the events filtering consumes about 8 hours by a skilled operator.

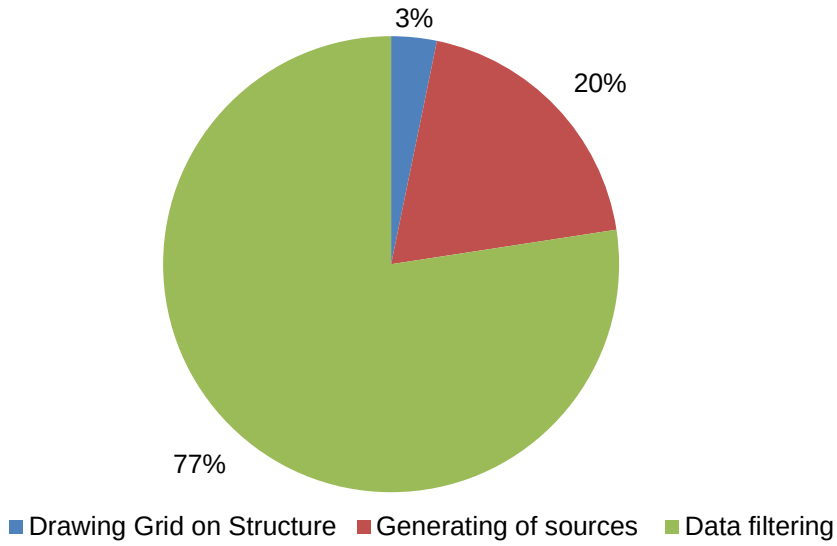

Figure 2-15.Time consumed for generating Δt grids

In Chapter 5 a new fully automatic DTM technique is presented which overcomes these limitations.

2.3 Source characterisation

The AE technique is also useful for studying real-time damage evolution and identifying the different types of damage because it is sensitive to various damage modes (Dzenis 2003; Maillet et al. 2014). In general, damage phenomena identification is carried out by correlating the detected AE signals with a particular failure mechanism (Sause et al. 2012).

To date, most studies carried out to discriminate damage mechanisms in composite materials under different loading regimes have been based on conventional AE analysis in which AE signal features are recorded directly using

the AE acquisition systems. The features are then used to cluster signals exhibiting similarities in groups depending on their values. The traditional AE features extracted directly from the signal waveform include amplitude, count, duration, etc. (Miller and Hill 2005) and additional features are extracted from the waveform using special transformations such as frequency (Qi 2000; Lu et al. 2011). These analyses usually use the AE activity diagrams versus load or number of cycles, the correlation between two or more of AE descriptors and also using unsupervised and supervised classification techniques.

The detection of damage mechanisms using AE and the ability to automatically classify these damage mechanisms and monitor their evolution is very desirable. However this requires the challenging interpretation of AE transients that contain information resulting from the source mechanism, but also from the propagation path, the medium and the sensor transfer function. Hence careful consideration of AE data is required in order to maximise subtle differences and increase classification accuracy between the composite damage mechanisms. It is understood that even in a similar test with permanent test conditions each sensor can record different signals due to sensor type, sensor location, signal attenuation and superposition as a result of signal reflections from specimen edges (Prosser et al. 1995; Johnson 2002; Moevus et al. 2008; Lopresto et al. 2009). Nevertheless the AE signal still contains useful information on the damage mechanism.

Composite fatigue damage evolution has been extensively investigated using different techniques (Talreja 1989; Gathercole et al. 1994; Mao and Mahadevan 2002). But in respect of using AE for damage evolution in composites, a conventional AE approach was applied by Dzenis (2003) to analysis fatigue damage development in un-notched composite laminate specimens. Furthermore, under a static fatigue loading regime, AE-based methods were used for Ceramic-Matrix-Composites (CMCs) lifetime prediction (Momon et al. 2010; Maillet et al. 2012). A number of these studies used traditional AE parameters such as amplitude, energy, duration, counts and counts to peak to describe the material fracture behaviour such as crack initiation and propagation (Zhuang and Yan 2006; Woo and Choi 2007).

In general the characterisation of AE signals is approached in one of two ways. The first is to examine changes in the signal parameters values using single

parameter, correlation plots and multi parameter analysis. These changes are then related to expected or observed damage during the test. The second approach is the consideration of digitally stored AE waveforms.

2.3.1 Traditional characterisation

The first researcher to correlate a damage mechanism in composite materials with an acoustic signature was Mehan (1971) who showed that each mechanism has a characteristic acoustic signature. The authors highlighted the correlation between frequency spectra with specific failure mechanisms. After more than four decades, to discriminate between different damage mechanisms, some authors correlate between each damage type and one traditional parameter such as amplitudes of AE signals (Kim and Lee 1997; Kotsikos et al. 1999) while others depend on the signal waveform frequency range (Kinjo et al. 1997; Mäder et al. 2001).

- ***Using amplitude distribution***

Correlation of the damage mechanism type with one traditional parameter such as amplitude is extensively used (Kim and Lee 1997; Kotsikos et al. 1999; Morscher 1999; Liu et al. 2012; Li et al. 2015). In self-reinforced polyethylene composite, damage mechanisms were investigated using AE amplitude distribution and the result were reported as; fibre matrix interfacial debonding, matrix plastic deformation and cracking, fibre pull-out, fibre breakage and interlaminar delamination are associated with acoustic emission events amplitude range 30-45 dB, 30-60 dB, 60-80 dB, 80-97 dB and 60-85 dB, respectively (Zhuang and Yan 2006). Furthermore, the acoustic signal amplitude varies with the corresponding damage mode during testing glass fibre reinforced polypropylene samples in tensile, tensile fatigue and crack propagation tests to be: (from 40 to 55 dB) corresponds to matrix cracking, (from 60 to 65 dB) to debonding, (from 65 to 85 dB) to pull-out and (from 85 to 95 dB) to fibre fracture (Barré and Benzeggagh 1994). Other researchers found when monitoring of damage in graphite/epoxy laminates the signals from matrix cracking and fibre bundle fractures are high in amplitude and frequency (Kim and Lee 1997).

Liu (2012) studied the damage evolution failure mechanisms of different lay-up patterns and hole sizes carbon fiber/epoxy composite laminates during tensile experiments via the acoustic emission by using a combination of information from

acoustic signal features (amplitude, cumulative counts and energy) to discern the different failure mechanisms. The author summarised the amplitude range for each failure mode. The amplitudes of the matrix cracking, fiber/matrix interface debonding, delamination, and fiber pull-out and fibre breakage are about 40–60 dB, 50–70 dB, 60–80 dB and 80–100 dB, respectively.

On the other hand, some researchers report that using the amplitude distribution to discriminate specific composite materials failure modes is very poor for a reliable damage mode identification (Pappas et al. 1998). Furthermore, using burst amplitude for damage classification in complex materials can be inaccurate (Bravo et al. 2013).

In general, there are other limitations with using the conventional AE parameters, such as amplitude, energy, duration and counts (Miller and Hill 2005), for damage characterisation. Many of these parameters can be dependent on one another, for example amplitude and energy, making classification less accurate. Furthermore, only the measured amplitude refers to the actual signal amplitude because it is measured in real time using the acquisition system. The rest of the signal features are calculated from the signal waveform and they are very dependent on the setup threshold value.

- ***Using frequency distribution***

As an effective method for damage characterisation, the frequency content of the recorded AE waveforms has been used. Some researchers have utilised the frequencies extracted from the signal waveform using Fast Fourier Transformation (FFT) whilst others have used the time–frequency domain via Wavelet Transforms (WT) (Qi 2000; Ni and Iwamoto 2002; Loutas et al. 2006; Marec et al. 2008; Arumugam et al. 2013). The Wavelet transform (WT) was used to overcome many drawbacks of the windowed fast Fourier transform (FFT).

For discrimination between different damage mechanisms, some authors correlate between each damage type and one frequency range, time-frequency or frequency-intensity domain of AE signals, (de Groot et al. 1995; Kinjo et al. 1997; Morscher 1999; Qi 2000; Mäder et al. 2001; Ni and Iwamoto 2002; Ramirez-Jimenez et al. 2004; Loutas et al. 2006; Woo et al. 2008; Oskouei et al. 2009; Li et al. 2015).

Giordano et al. (1998) investigated the fibre breakage in single-carbon-fibre composite based on a polyester matrix under tensile loading using the Fast Fourier transforms (FFTs) to obtain the frequency content of the signals. The author reported that a clear acoustic fingerprint could be characterized in terms of frequency content. Qi (2000) noted that the 90% of AE activates are released in a frequency range between 10 and 550 kHz and these frequencies are useful to ‘‘distinguish different AE signals from various possible failure modes in fibre reinforced composites’’.

De Groot et al. (1995) concluded that matrix cracking released frequencies between 90 and 180 kHz, fibre failure frequencies above 300 kHz, debonding frequencies between 240 and 310 kHz and pull-out frequencies between 180 and 240 kHz when loaded unidirectional carbon/epoxy material under different conditions fail under well-defined modes.

Bohse (2000) showed that matrix cracking releases the majority of signals with peak frequency lower than 350 kHz and the majority of fibre failure higher than 350 kHz. The investigation was done on pure epoxy and single fibre tensile specimens.

Ni and Iwamoto (2002) investigated the fundamental characteristics of AE signals, such as the attenuation and the frequency dependency of AE signals, using artificial sources at different frequencies before the fracture process of a single fibre composite. The authors showed that the frequencies of AE signals are almost unchanged while the amplitudes attenuate greatly with the increment of the propagation distance between the AE source and the AE sensors. The authors believed that the frequency analysis is an effective way in processing AE signals to identify the failure modes in composite materials. In order to understand which failure mode is prior to the other or how long a failure at a microscale remains, the time-frequency information was obtained using the wavelet transform (WT). The relationship between failure mode and peak frequency stated as matrix cracking is <100 kHz, debonding 200–300 kHz and carbon fiber break 400–450 kHz.

Ramirez-Jimenez et al. (2004) reported that the primary frequency extracted from the power spectrum using the Fast Fourier Transformation (FFT) for each AE signal can be used as the fingerprint of each event. The author showed in tensile

tests of different fibre orientation of glass/polypropylene specimens the AE signals with frequency range of 100 kHz refers to fibre/matrix debonding, 200 and 300 kHz are associated to be generated from fibre slippage and fibre pullout while the higher frequencies refer to the fibre breaking signals.

Damage characterisation of Mode I Delamination in Glass/Polyester composites show that events of low frequency (100–190 kHz) are related to matrix cracking, matrix/fiber debonding release from events of frequency range 200–320 kHz and sources of high frequency (380–430 kHz) are associated with fiber breakage failure mechanism (Oskouei and Ahmadi 2010). The same frequency ranges were noted by the authors in a previous study using E-glass fibers under tensile tests (Oskouei and Ahmadi 2009).

Li et al. (2012) monitored the fatigue damage and failure of carbon fiber-reinforced plastic (CFRP) bridge cables using AE to show that the failure models exhibiting matrix and fiber-matrix interface failures modes occur at the initial stage of fatigue testing, followed by delamination and fiber rupture. The investigations were done using the b value, Kurtosis index, and the (rise time/amplitude) ratio to describe the different damage stage while the damage types were identified using wavelet transformation applied on the recorded waveforms.

On other hand, the correlation between damage type and frequency ranges is not similar in all the studies (as summarised in Table 2.1) and this is considered to be a limitation to using frequency of AE waveforms as a discriminating factor between different damage types. The signal frequencies depend on many factors such as geometry, sensor response, propagation characterisation and source frequency (Eaton 2007a; Eaton 2007b) which make the damage mechanisms differentiation more difficult.

It would appear that using any single parameter analysis (such as amplitude distribution or the frequency distribution) to distinguish between different failure types has many limitations and is too weak to provide reliable damage characterisation.

Table 2.1 - Summation of Frequency Results

	Material	Matrix	Fibre	Debond	Pull-out
de Groot et al.	Carbon / Epoxy	90-180 kHz	above 350 kHz	240-310 kHz	180-240 kHz
Bohse	Glass / Polyprop	below 350 kHz	above 350 kHz		
Ni and Iwamoto	Carbon fiber strand	below 100 kHz	400–450 kHz	200–300 kHz	
Ramirez-Jimenez et al.	glass/polypropylene		420-500 kHz	~100 kHz	200-300 kHz
Oskouei and Ahmadi	E-glass fibers	100–190 kHz	380–430 kHz	200–320 kHz	

2.3.2 Correlation plots

In order to characterise AE signals into different damage mechanisms, signal parameter correlation plots have also been used. AE parameters such as amplitude, count, energy and duration can be plotted versus each other. However, due to using the same signal parameters previously discussed the same limitation still exists. Despite this obvious limitation correlation plots are still used for detection of damage initiation, high amplitude plus long duration hits refer to damage initiation, and they are limited to identify the damage severity, the future performance, damage characterisation and quantitative SHM (Eaton 2007a) .

2.3.3 Multi-parameter characterisation

An increase in the numbers of descriptors for each AE signal leads to a demand for the use of multidimensional analysis, where different damage mechanisms are identified from dividing AE data set into clusters according to their descriptors. Unsupervised and supervised classification techniques have been performed in many studies. If supervised pattern recognition is used, the number of damage mechanisms must be known in advance. The term unsupervised pattern recognition is used to describe the complete methodology consisting of

procedures for descriptors selection, cluster analysis and cluster validity (Huguet et al. 2002). The number of descriptors used in the analysis in general depends on operator decision. The majority of the multidimensional classification studies have been conducted with the intention of taking a large number of the signal descriptors in order to provide more powerful correlation between different damage mechanisms and the AE data classes.

Many multivariate classification approaches have been performed, individually or combined, by different means of several algorithms for composite material damage characterisation using real test data. These include *k*-means (Godin et al. 2004; Godin et al. 2005; de Oliveira and Marques 2008; Wang et al. 2011; Momon et al. 2012; Li et al. 2014; Masmoudi et al. 2015; Sawan et al. 2015), Maxmin Distance, Cluster Seeking, Forgy, *k*-means, Isodata (Kostopoulos et al. 2003; Kostopoulos et al. 2007), k-Nearest Neighbours (k-NN)(Godin et al. 2004), Fuzzy C-means (Marec et al. 2008; Oskouei et al. 2012; Arumugam et al. 2013), Principal Components Analysis (PCA) (Oskouei et al. 2012; Li et al. 2014), Gaussian mixture distribution (GMD) (Sawan et al. 2015), Artificial Neural Network (ANN) (such as the Self-Organising Map (SOM) (Godin et al. 2004; Godin et al. 2005; de Oliveira and Marques 2008; Gutkin et al. 2011; Albouy and Vieille 2014; Crivelli et al. 2014; Sawan et al. 2015) and Competitive Neural Networks (CNN) (Sawan et al. 2015)). Others works were performed using artificial AE sources using Support Vector Machine (SVM) (Zhao et al. 2010), Artificial Bee Colony (Omkar and Senthilnath 2009), Ant Colony Optimization (Omkar and Karanth U 2008).

Ben Ammar et al. (2013) investigated the mechanical behaviour of cross-ply laminates, different cross-ply (CFRP, HFRP and GFRP) laminates, under static tensile and buckling loading. The classification of damage in the materials is achieved by Fuzzy C-means using the several temporal descriptors of each burst of AE. The author finally correlates the clustering result to the main damage mechanism types (matrix cracking and fibre breakage) using the signal amplitude distribution of each class.

Masmoudi et al. (2014a) investigated sandwich composites using embedded piezoelectric AE sensors under static and fatigue loading in three-point bending test. Five selected traditional signal descriptors (energy, amplitude, rise time, counts and duration) were classified using the *k*-means classification technique

as an unsupervised classifier and the PCA was then utilised to provide simple visualization of the results. The classification was applied to a “four classes” problem and these classes were correlated to four damage mechanisms (core damage, resin cracking, fibres breaking and interfacial (skin/core) debonding) using the amplitude distribution of the classes signals.

Masmoudi et al. (2014b) applied an unsupervised clustering process using the *k*-means technique, associated with the PCA to visualize the result, on AE data recorded using embedded piezoelectric (PZT) sensors from E-glass/epoxy composites specimens under three-point bending static and creep loading. The classification input is five selected descriptors (energy, amplitude, rise time, counts and duration) and the results showed AE signals grouped into three classes. The final classes correlated to three damage modes (matrix cracking, fibre/matrix debonding and fibre breaking) using the signal amplitude distribution of each class signals.

Biocomposite material failure mechanisms were characterised using a classification procedure with a neural network based on a Kohonen non-supervised self-organizing map (KSOM), on the AE data recorded during monotonic and load-unload tensile tests on dog-bone specimens. Classification was conducted using three AE parameters (amplitude, count and duration). For mode identification, the amplitude distribution and the correlation plot of counts versus duration of AE events in each class are used to describe the failure modes (matrix micro-cracking, matrix/ matrix friction, decohesion and matrix/ fiber friction) (Bravo et al. 2013).

AE testing was used to investigate the damage evolution in natural polyethylene (NPE) composites under tensile and 3-point flexural tests. Traditional AE cumulative energy was used for damage evolution during the test while the fuzzy logic algorithm was used for the classification. The input data from each AE signal is the amplitude, counts and duration which was then used for the damage-mode identification. All data was grouped into matrix micro-cracking, matrix/matrix friction, decohesion and matrix/fiber friction (Bravo et al. 2015).

CFRP failure was investigated from various test configurations: tension, Compact Tension (CT), Compact Compression (CC), Double Cantilever Beam (DCB) and four-point bend End Notched Flexure (4-ENF). The AE data was analysed using

different pattern recognition algorithms: *k*-means, Self-Organising Map (SOM) combined with *k*-means and Competitive Neural Network (CNN). The three clustering techniques result were correlated with different damages types using the peak frequencies distribution (Sawan et al. 2015).

Various efforts have been found in literature to improve the multi-variable classification of the AE data and their accuracy. For example, Marec et al. (2008) reported that the unsupervised pattern recognition associated with principal component analysis can assist in identifying the most critical damage mechanisms associated with AE signals, leading to reliable classification of AE signals into specific damage modes. Many publications have reported on AE clustering using the PCA performed as dimensional reduction or as unsupervised clustering method. PCA has been also used with good effect as a dimension reduction technique and to provide simple visualisation of the high order AE data (Manson et al. 2001; Rippengill et al. 2003). The PCA technique was used successfully by Eaton et al. (2011b) to separate fatigue cracking signals from noise signals in a complex landing gear component under fatigue load. Furthermore, the PCA was used to distinguish between AE sources (crack growth and friction) generated in a box girder from a bridge (Manson et al. 2001).

The PCA is employed to transform interdependent coordinates, traditional parameters, into significant and un-correlated ones. The PCA finds combinations of variables or factors that describe major trends in a data set (Wise et al. 1999) and presents these on the principal components. The un-correlated principal components which have the majority of the original data information are used in the further analysis instead of the traditional features.

For composite material damage characterisation, Marec et al. (2008) classified AE data, collected from monitoring unidirectional fiber–matrix composites subjected to creep tensile tests and three-point bending tests, using unsupervised pattern recognition analyses (Fuzzy C-means clustering method) associated with a PCA to provide simple visualization of the classification results. The classification procedure was conducted twice, using time-based descriptors (amplitude, energy, duration, rise time and counts) and using time-frequency descriptors which were extracted from the stored waveforms using wavelet transforms. The main four damage mechanisms (matrix cracking, fiber-matrix debonding, fiber failure and delamination) were correlated with the classes in the

first round using the amplitude distribution while in the second round the frequency ranges were used. The author reported that using the time-frequency descriptors provided a better discrimination of damage mechanisms than using time-based descriptors.

Oskouei et al. (2012) used Fuzzy C-mean clustering as an unsupervised pattern recognition analysis to classify AE signals generated from composite Double Cantilever Beam (DCB) test specimens to produce preferential damage mechanisms. The classification analysis applied used six AE parameters (energy, amplitude, rise time, counts, peak frequency and duration). PCA was applied to provide simple visualisation of the clustering. The AE signals were clustered in three different classes and correlated to three different damage mechanisms (matrix cracking, fiber bundle breakage and debonding between fiber and matrix interfaces) using the signals frequency distribution.

Ben Ammar et al. (2014) investigated two types of sandwich composite materials under static and cyclic fatigue loadings (four-point bending test). The AE data was clustered into different damage types using automatic classification by the Fuzzy C-means technique. The descriptors used as input data to the classifier are amplitude, energy, duration, rise time and counts. The simple visualization of the clustering result into a two-dimension subspace was conducted by the PCA. The main damage mechanisms (core damage, resin cracking, fiber rupture, debonding of interface and delamination) were correlated to the classification classes using the amplitude, rise time, duration, decay time of signal and energy distributions of the signals.

Arumugam et al. (2013) proposed a procedure to discriminate between failure mechanisms in glass fiber reinforced polymer laminates subjected to tension load using the Fuzzy C-mean as clustering method. The dominant AE parameters (rise time, counts, energy, duration and amplitude) were used for clustering as input. Here the PCA was carried out only to visualise the results in a two-dimensional subspace. The amplitude, the duration and the frequency distributions of the signals were used for class labelling and found to correspond to fibre failure, matrix cracking and delamination. Finally the wavelet transform was used to extract the time-frequency of the fibre failure and delamination signals to highlight the frequency range difference in these classes. The Short-

Time Fast Fourier Transforms (STFFT) was used to sequence the of failure events.

In order to increase the input information of each AE signal to the clustering analysis and to reduce the attenuation effects on the recorded traditional AE parameters, parameter ratios have been used with the traditional parameters as input to a classifier. Many studies used these ratios (for example, the duration/amplitude and the amplitude/rise time ratios) to maintain the same signal signature and improve the clustering accuracy.

Moevus et al. (2008) applied the unsupervised multivariable clustering analysis using the *k*-means method on the AE data recorded from the tensile test on SiC_f/[Si–B–C] composite specimens. The traditional AE parameters and their ratios were used as input vector to the analysis. The PCA was used to provide new uncorrelated features and to reduce the dimensionality of the data before classification. After classification, traditional AE parameters (amplitude, rise time, energy distributions) were used to label the resulting clusters to different damage mechanisms such as the matrix cracking and debonding at the fibre–matrix interfaces.

The same procedure was used by Momon et al. (2012) on AE data collected during the static and cyclic fatigue of C_f/SiC composites. Unsupervised and supervised was applied using the *k*-means and K-nearest-neighbour classifier (K-NN), respectively. The PCA was used to provide new uncorrelated features and reduce the dimensionality of the input data vector. The parameters distributions of the energy, rise time, and amplitude were used to correlate the classes with different damage mechanisms (fibre breaks, matrix cracking, fibre/matrix debonding, yarn/yarn debonding and sliding at fibre/matrix interfaces or matrix cracks closing after unloading).

Defining the optimal features of the AE signals for use as input data to the clustering process is a very important step for the analysis of the data. It is well known that if too few features are selected, a poor classification result will be obtained due to neglect of important signal information with the unselected descriptors. On the other hand, too many features will lead to an over-parameterised model and will increase noise. In order to address this, hierarchical clustering has been utilised to eliminate the redundant signal features

and select the less-correlated or the uncorrelated AE features only. This selection is based upon the use of the correlation matrix of the data as presented by previous studies (Kostopoulos et al. 2003; Moevus et al. 2008; Kontsos et al. 2011; Wang et al. 2011; Momon et al. 2012).

In summary, multidimensional classification analysis can analyse many AE descriptors simultaneously and the number of the used descriptors mainly depends on the operator decision. Each class contains signals generated from one damage mechanism or more. Normally the classes are correlated with the main damage mechanises using single signal parameters such as the peak frequency distribution or amplitude distribution. In general, this correlation is validated using the signals location, the expected damage within test life and other NDT methods (for example, using the scanning electron microscope and the ultrasonic C-scan) conducted after the end of the test. Furthermore, most of these studies were conducted data from a single sensor.

2.3.4 Modal analysis

Damage discrimination analysis using AE descriptors has many limitations, as previously discussed. Amplitude is direct measurement; however other descriptors are highly dependent on acquisition threshold. Further to this many of these descriptors can be dependent on one another, for example amplitude and energy, making discrimination less accurate. These limitations make using the traditional signal descriptors for damage characterization inadequate. Some studies used the modal analysis of AE signals as damage characterisation. AE modal analysis uses the stored waveform to characterise damage by interpretation of the s_0 and a_0 plate wave modes.

Identification of the wave modes in 35mm thickness large spherical tanks was observed by Pollock (1986). More in depth studies showed that the amplitude of each wave mode is dependent on the source excitation direction as reported by Gorman (1991). The larger a_0 and s_0 produced when the H-N sources (Hsu and Breckenridge 1981) were generated on the surface and end of the plates, respectively, this study was conducted using thin aluminium and composite plates. Further to this, tests were conducted by Gorman and Prosser (1991) and Prosser (1991) by generating H-N sources (Hsu and Breckenridge 1981) on a slot of different angles on thin aluminium plates and showed that the s_0 mode

amplitude reduced and the a_0 amplitude increased as the source ordination changed from 0^o to 30^o, 60^o and 90^o, with respect to the plane of the plate.

There are several studies which use the wave modes amplitudes to distinguish between different damage mechanisms. For example in composite materials, the in-plane damage mechanisms such as matrix cracking in tensile specimens of carbon fibre / epoxy generate AE signals with dominate s_0 mode (Gorman and Ziola 1991; Prosser et al. 1995; Prosser 1996).

The (s_0/a_0) ratio known as the Measured Amplitude Ratio (MAR) was used successfully to discrimination between H-N sources generated at different orientations in a steel I-beam (Carter 2000). Pullin et al. (2005) investigated the orientation of fatigue crack sources in aerospace grade steel using the MAR value of the signals.

For damage characterisation in composite, Surgeon and Wevers (1999) used the amplitude ratio between the signal modes, the extensional and flexural modes, using modal acoustic emission in CFRP laminate under tensile and 3-point bending tests loading to identify the in-plane and out-of-plane failure modes. They showed that the (s_0/a_0) = 2.5 for matrix cracking signals under tension and the (s_0/a_0) = 0.51 for fiber failure signals under bending.

Mal (2002) observed that the wave motion due to fibre break and matrix cracking damage generated mostly extensional waves of higher frequency, while the motion due to the delamination is dominated by flexural waves of lower frequency.

The MAR was used successfully to distinguish between out-of-plane and in-plane damage sources using the AE data collected from tests of large-scale carbon fibre panels under buckling load (Featherston et al. 2009). The same technique, MAR, was performed by Eaton et al. (Eaton et al. 2011a) to distinguish between matrix cracking and delamination in small tensile test composite specimens.

Martínez-Jequier et al. (2015) used the modal analysis to distinguish between the delamination signals and the in-plane source signals during 3-point bending tests on carbon fiber-reinforced polymer (CFRP) composite plates. Splitting the a_0 and s_0 was done using frequency filters (high and low frequency filters) then

comparing the Root Mean Squared (RMS) of the AE signals in both frequency bands to distinguish between out-of-plane and in-plane damage sources.

As an improvement on the traditional MAR approach, the Measured Amplitude Ratio (MAR) with wave attenuation correction was presented and used successfully to distinguish between out-of-plane and in-plane damage sources using the AE data collected from testes of large-scale carbon fibre panels under buckling load (Eaton 2007a). Furthermore, McCrory et al. (2014) presents the corrected MAR approach in automatic way to discriminate between in-plane and out-of-plane damage mechanisms arising from large-scale carbon fibre panel subject to buckling. The s_0 and a_0 amplitudes of located signals are separated from one another using the time of flight information and band pass filters.

Although good results were achieved by using the modal analysis as damage characteriser, there are still some limitations such as: it is applicable to plate-like structures only and for the sources generated at enough distance from the sensor to enable the propagation modes to develop. Sources close to the sensor may not have identifiable plate wave modes. There can also be some difficulty to distinguish between the two signal modes. In specimens of small dimensions, signal reflections from boundaries are high and can therefore interfere with the signal which means that the two modes cannot be clearly identified. Increased structure complexity, due to cracks, holes and thickness change, will increase this difficulty. Furthermore, the modal analysis is unable to distinguish between damage mechanisms which occurs in-plane such as between fiber breakage and matrix cracking.

2.3.5 Summary of damage characterisation

The recorded AE signals have been utilised in different ways for the damage characterisation. Until now many researchers work with the multidimensional analysis and consider it as a reliable and sufficient solution to classify the AE signals into different classes depend on their descriptors values. However, most of these signal descriptors are affected by many factors such as the attenuation effect, superposition with reflected signals, homogeneity changing with angle, material properties changing with distance and the complex geometric structures. As a result of that the AE analysis can be compromised due to “incorrect” values being recorded. In general, using correct input data in the analysis leads to reliable output results and vice versa. If the input data is incorrect, increasing the

amount of input data or using more complicated analysis methods will not improve the result.

The main conclusions can be listed below:

- The AE waveforms have useful information and can be used to distinguish between different types of damage mechanisms.
- There is no universal signature for a given damage source. However, under permanent test set-up conditions, similar damage sources should generate AE signals with high similarities.
- Until now, to associate every AE signature to a specific failure type has been considered as a non-trivial challenge even in small-scale homogenous material specimens in a controlled environment. While using AE to characterise the failure mechanisms types in large-scale components is still limited.
- Each damage mechanism releases signals with different energies depending on many factors such as the load conditions.
- Damage characterised by classifying the AE data into classes depends on the signal similarities using single descriptor distribution, correlation plots and the multidimensional analysis.
- Single descriptor and the correlation plots have been proven to be limited to distinguish between different damage types. However, the multidimensional classification analysis is considered to be a reliable solution to classify AE signals into different clusters which refer different damage mechanisms.
- Selection of the input data to the multidimensional classification mainly depends on the operator decision.
- The number of classes equals the number of damage mechanisms or less.
- Classes attributed to different damage mechanisms normally depend on single descriptor distribution or the correlation plot. The expected damage evolution during the test and other NDT results at end of the test are normally used as evidence to support the class labelling and validate the clustering approach.

- Source locations are used as support to the labelling classes. Usually the location is calculated using traditional location techniques which are limited in complex material or complex geometry structures.
- If the classification is conducted using the AE data recorded directly using the acquisition system without removing the propagation effects, the reliability of the characterisation result will be affected.
- In composite materials, wave propagation and scattering phenomenon are complex, and this complexity increases further when AE propagation paths are interrupted by obstacles such as cracks, holes and thickness change. This will have a large impact on the recorded AE data.
- Using more complicated classification procedures on poor data will not improve the output reliability.
- Modal analysis is limited to plate like structures and for signals generated at enough distance from the used sensor. Furthermore, this approach unable to distinguish between in-plane sources.
- There are some limitations to use the signal modal analysis in small-scale, large-scale and/or complex geometry components.
- In most experimental work, numerous sensors are used during the test to record the AE activity. Usually these sensors are distributed in different locations on the specimen to cover all the specimen area. However, the damage characterisation was performed using only data from one sensor. So a huge amount of information related to the mechanical damage sources recorded using the other sensors is lost.

Most of the previous investigations into signal discrimination have been performed on small specimens and the propagation effect has not been considered. The propagation effects on the recorded signal parameters and the impact on the classification results was selected for further investigation using large scale composite structure. In Chapter 4 a novel correction technique known as PCT is presented which corrects the recorded parameter values.

3 Experimental Instrumentation and Techniques

3.1 Instrumentation

The AE equipment, software and techniques utilised throughout this research are described in this section.

3.1.1 AE data acquisition and storage

In this study two AE systems (Vallen and MISTRAS) have been used. These systems are manufactured by Vallen Systeme GmbH and Mistras Group Limited (MGL), respectively.

The Vallen AMSY-5 (**A**coustic Emission **M**easurement **Sy**stem) system utilises the ASIPP board (**A**coustic **Si**gnal **P**re-**P**rocessor) board located in the system case. The system provides eight AE channels and each one combines an analogue measurement section and digital processing. By using a dynamic range of 16 bit and sampling rate of 10 MHz, the signal is digitalized using an analogue to digital convertor. After performing the feature extraction (such as AE features and parametric data), the data is transferred via the ASIPP bus to the PCI-interface board (**A**E **Sy**stem **C**ontroller (ASyC)) to an external computer. The Vallen AMSY-5 block diagram is provided by Vallen (2006).

The MGL PCI2 acquisition system utilises the PCI-2 board, each board has two low noise AE channels. The number of boards can be expanded to four to provide a maximum of 8 channels. The specifications of each channel are an acquisition rate of 40MHz and 18bit A/D conversion. The PCI-2 board block diagram is provided by PAC (2004).

3.1.2 Transducers

In order to detect the surface displacement resulting from an AE event, suitable piezoelectric transducers are used. A typical piezoelectric transducer construction is presented in Figure 3-1. When stress wave fronts arrive at the specimen surface, small displacements will occur. Piezoelectric transducers are used to detect this mechanical movement and convert it into an electrical signal. This electrical signal will pass through a preamplifier. The preamplifier is either connected very close to the sensor or it is integrated into it, the electrical signal will provide with gain (typically 40dB). Through the preamplifier the unwanted

mechanical noise is removed using low frequency filtering. Generally, AE sensors are categorised into two types; wideband and resonant.

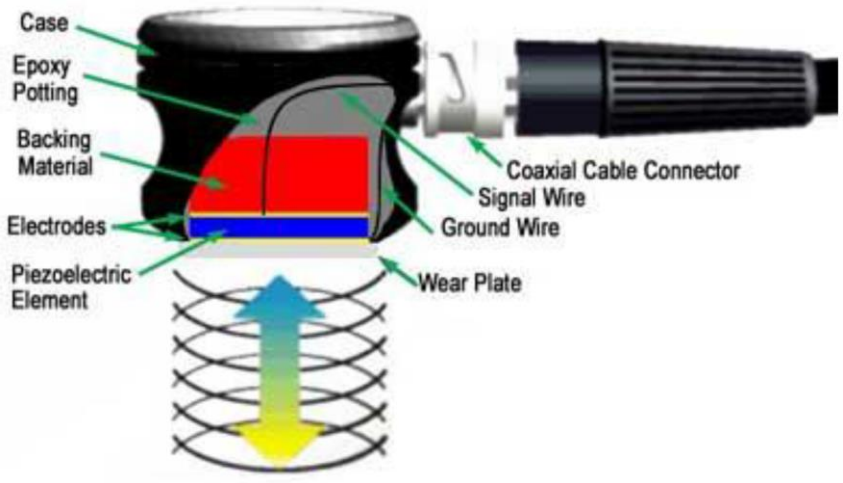

Figure 3-1. PCI-2 board block diagram

Resonant sensors are biased towards particular frequencies, where the piezoelectric materials of these sensors oscillate at greater amplitude than the other frequency. The working range of a typical resonant sensors is presented in Figure 3-2. This behaviour will improve the detection sensitivity, if the expected frequency of the desired signals is matching the resonant frequency of the transducer.

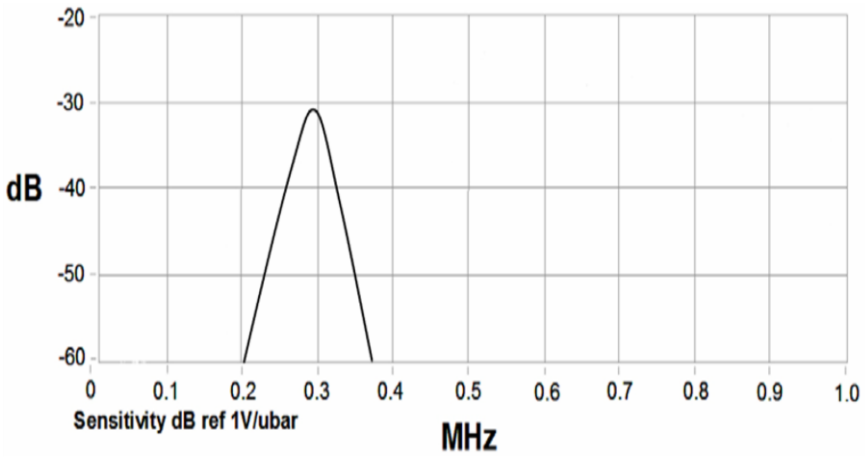

Figure 3-2. Theoretical resonant frequency transducer response (Baxter 2007)

Wideband sensors have flatter frequency response and work across a much larger frequency range than that of a resonant sensor but still maintain a good

level of sensitivity. The relatively flat frequency response of wideband sensors across their working range is presented in Figure 3-3. Wideband sensors are usually used in research applications, especially when frequency analysis or identification of wave modes is required.

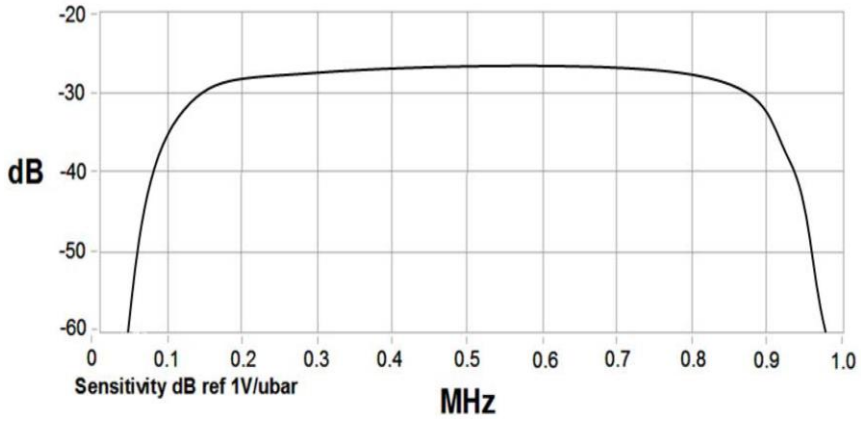

Figure 3-3. Theoretical frequency response of wideband sensor (Baxter 2007)

Three types of AE sensors were used in this investigation. Two of them are manufactured by Physical Acoustics and the third type is a broadband conical transducer manufactured by the National Physical Laboratory (NPL). The first two sensors are WD (wideband sensor) and Nano-30 (resonant sensor). Their working frequency, resonant frequency and dimension are shown in Table 3-1. An example of the typical calibration certificate for each of the Physical Acoustics sensors is shown in Figure 3-4. The transmitted sensitivity for the NPL transducer can be seen in Figure 3-5.

Table 3-1 Manufacturers Specifications of AE sensors used in throughout this work (ASTM 1986)

Sensor Type	Dimension Dia x Ht (mm)	Operating Frequency Range (kHz)	Resonant Frequency (kHz)
WD (wideband)	18 x 17	100-1000	650
Nano-30 (resonant)	8 x 8	125-750	300

From the calibration certificate for the WD sensor it can be seen that the frequency response is flat and without any dominant peaks. However, there is still

a number of small peaks observed on the calibration certificate. With the resonant sensor, Nano-30, there is clear peak frequency at approximately 300kHz. The conical transducer manufactured by NPL was developed in order to create an alternative to the H-N source (Theobald 2004). The transducer geometry is broadband piezoelectric element of conical shape of 3 mm thick with a 10 mm base and 1 mm tip. The conical transducer is used in this work to generate artificial sources in conjunction with a pulse wave generator.

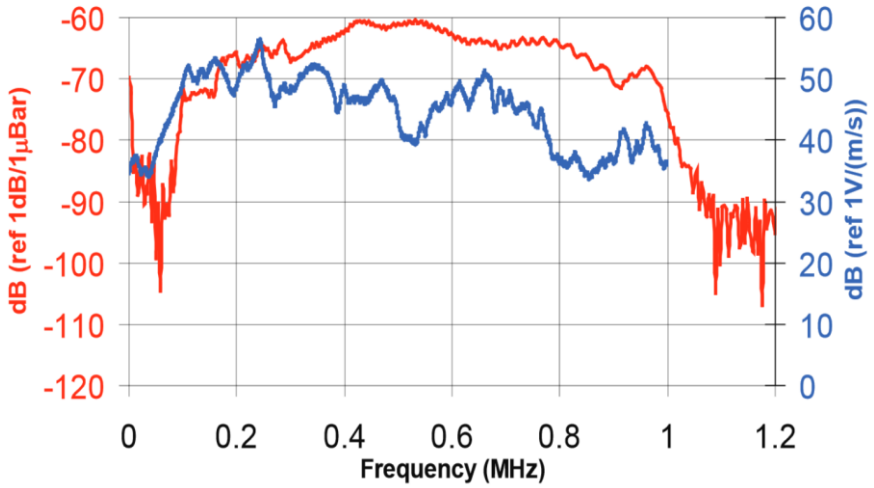

(a) WD

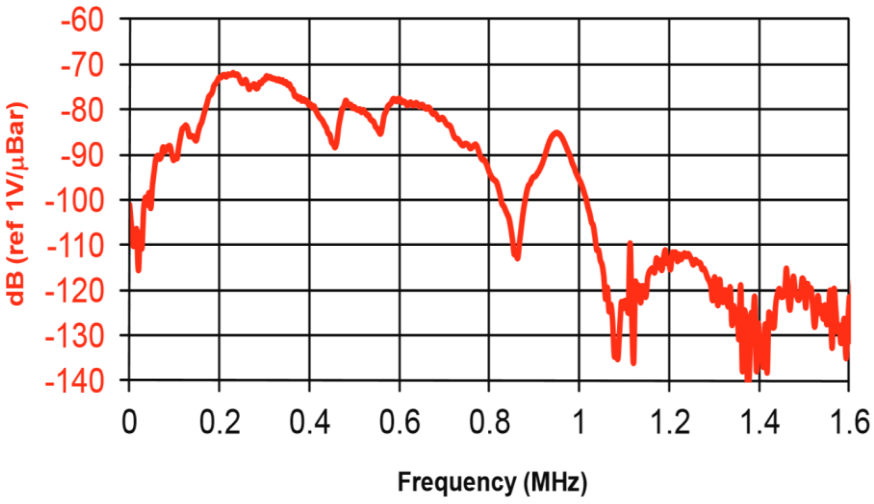

(b) Nano 30

Figure 3-4. Calibration certificates for (a) WD and (b) Nano30 sensors (Sensitivity dB ref 1V/µbar)

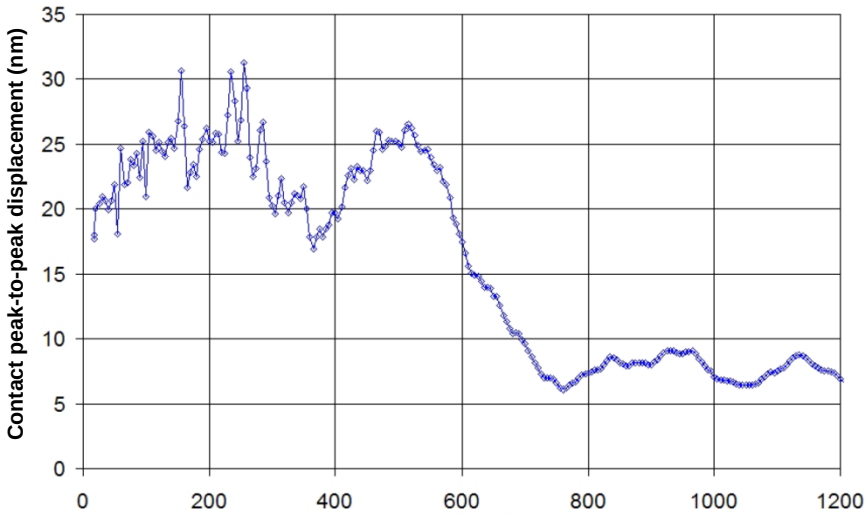

Figure 3-5. Conical transducer transmit sensitivity

3.1.3 AE preamplifier

The piezoelectric element in the sensor generates a small voltage and in order to amplify it to a more useable voltage a preamplifier is used. This step occurs before this signal is transmitted to the measurement circuitry. In order to minimise the pickup of electromagnetic interference the preamplifier is placed close to the sensors. The integral sensors have the preamplifiers built in.

The main benefit of using the preamplifiers is to enable the signal to be transmitted along a length of cable. So, if necessary, the main AE hardware can then be placed hundreds of metres from the structure under test. In general, the preamplifier provides a gain of 40 dB and can eliminate the mechanical and background noise using the high-pass or band-pass filter.

In this investigation non-integral sensors were used. Two types of preamplifiers were placed close to the sensor to provide optimum sensor coupling, suitable gain and excellent cable drive capability. The first type is a Vallen AEP3 preamplifiers (Figure 3-6a), with the gain set to 34 dB. A band-pass filter between 95 kHz and 1000 kHz was used. The second type is MGL 0/2/4 preamplifiers (Figure 3-6b) which had a frequency filter of 20 kHz to 1MHz were used throughout this study.

(a)

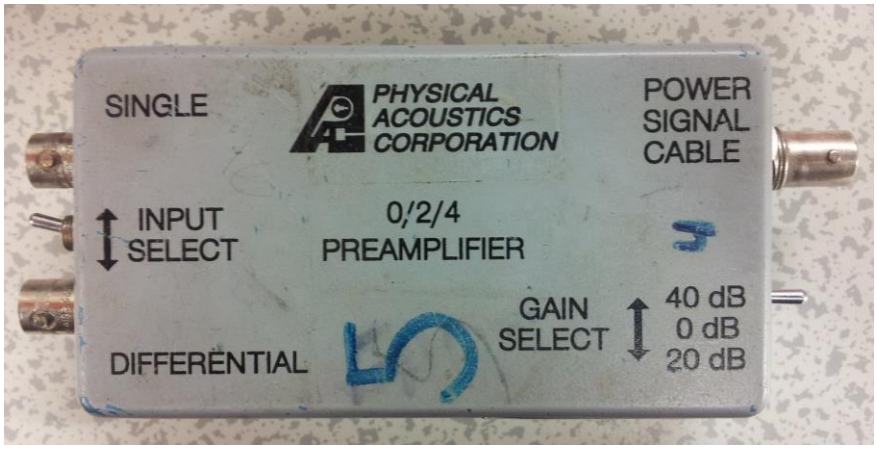

(b)

Figure 3-6. Preamplifiers (a) Vallen AEP3 (b) PAC's 0/2/4

3.1.4 Hsu-Nielson (H-N) source

Before starting each test, the sensor sensitivity was assessed after the sensor was installed and connected to the monitoring equipment. The sensitivity assessment was completed using the H-N pencil source (Nielsen 1980; Hsu and Breckenridge 1981) which is considered as an affordable, cost effective method. Several pencil lead breaks placed very close to the sensor are used to verify the response of an AE sensor (ASTM 1994).

Figure 3-7 shows the H-N pencil which uses a grade 2H lead with 0.3 mm or 0.5 mm diameter and has to be broken at a repeatable angle. The repeatable angle

can be achieved by using the PTFE guide ring 'Nielson Shoe' which is fixed to the end of the retractable pencil (Figure 3-8)

Figure 3-7. Hsu-Nielson pencil

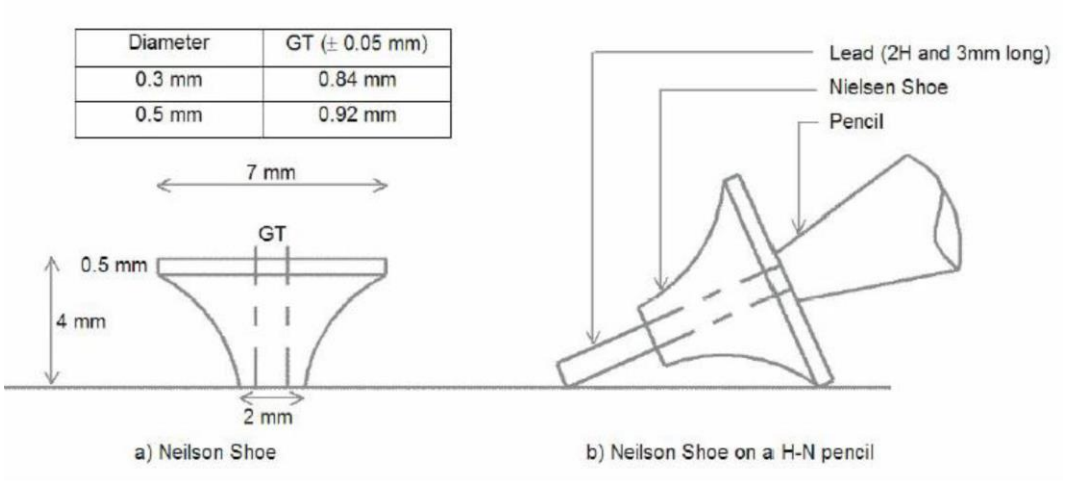

Figure 3-8. Nielson shoe (Rindorf 1981)

The recommended procedure for pencil lead break is as follows (ASTM 1994) ;

a) The lead feed button on the pencil is pressed repeatedly until the lead protrudes.

b) The end of the lead is levelled with the end of the guide tube by pressing the tip of the pencil perpendicularly towards an even surface while the feed button is pressed down.

c) The button is pressed a few times to cause the lead to protrude about 3 mm

d) The pencil is guided obliquely towards the test object until the guide ring rest on the surface.

e) The pencil is pivoted about the point of contact towards a steeper position to cause the lead to break.

In all tests during this investigation, a sensor properly mounted on a specimen surface responded to a H-N source with an amplitude of 98 to 100 dB when generated adjacent to the sensor.

3.1.5 Couplant

A couplant can be defined as any material which aids the acoustic wave transmission between sensor and specimen surface. If the sensor is directly placed on the specimen surface only a very weak signal is produced at the sensor. The situation is different if a couplant layer is placed between the specimen and the sensor as an improvement in signal is observed.

At the interference, an air gap (due to the microstructure of two contacting surfaces) causes energy transmission loss in the acoustic wave because the air acoustic impedance is much lower in comparison to that of the test specimen and sensor surface. The primary function of the couplant material is to fill the gaps and expel the air to increase the transmission of energy.

In order to achieve the optimal energy transmission between the sensor and the specimen surface, correct coupling selection is essential. There are many considerations when selecting the correct couplant for an AE test such as test duration, couplant stability, the frequency of sensors removal, condition of test environment and type of wave to be detected. According to (ASTM 1997) the selected couplant should;

a) Be appropriate to the test environment

b) Should not cause any damage to the structure or transducer

c) Be suitable for the type of motion detected.

A variety of couplants exist and are used for AE testing such as liquid, gel, grease and adhesive couplant.

Liquid couplant generally can be described as easy to use and easily removes the air gap between sensor and specimen. It can also provide better transmission for longitudinal waves. However, acoustic impedance is lower compared with

other types of couplant and due to low viscosity it tends to drip. So, they are inadequate for any vertical mounting application due to losing the couplant layer with time.

Grease based couplants have much higher viscosity than gels or liquids, so they are more suitable for rough surfaces. Brown grease is predominantly used in this investigation. Lateral sensor movement is allowed with this type of couplant which allows the trapped air to exit (Theobald et al. 2008). Furthermore, grease based couplants offer better long-term stability if well clamped in comparison with gels and liquids. In addition this type of couplant does not damage the surface. Furthermore, it is easy to apply and remove especially when transducers have to be moved to different places in a short time, such as the conical transducer in this work.

Adhesive agent can be used as a couplant and a mechanical fixture. Adhesive agents can provide better transmission for both longitudinal and shear waves if correctly applied. This type of couplant is suitable for applications where sensor stability is critical such as DTM source location. There are many types of adhesive agents and the most common used in AE testing are cyanoacrylate and silicon rubber compounds. In this work the silicone rubber compound has been used. This type has many features such as it can be applied as a fluid to produce a thin layer, it is bubble free and at the same time provides a permanent bond for the transducers during the test. This couplant can provide excellent sound transmission which is similar to the grease but provides a strong bond (Theobald et al. 2008). Furthermore, the silicone rubber compound is applicable to rough surfaces and is suitable for vertical mounting applications. Using this type of bond has lower risk of sensor damage compared with cyanoacrylate bond when sensors are removed.

3.1.6 Pulse generation

In order to drive the conical transducer and generate an artificial AE source, electronically generated pulses were used. In this work a pulse generator manufactured by MGL was used (ARB-1410 Arbitrary Waveform Generator Board or “wavegen” board). The ARB-1410 arbitrary waveform generator board block diagram is provided by PAC (2003). The “wavegen” board contains a standard PC’s PCI-bus and with its provided software is capable of producing analogue signals with frequencies of up to 15MHz and amplitudes of up to

±150V, using a 14bit, 100MHz Digital to Analogue Converter (DAC) (PAC 2003). The provided software allows a variety of output signals such as square wave, saw tooth, sine wave etc. Each one of these signals can be generated with different frequency and amplitude ranges, making it possible to generate a wide variety of signals. In this work the conical transducer and the pulse generator were used to provide an artificial source of varying frequency, amplitude and signal shapes in order to simulate different damage mechanisms.

3.1.7 Measurement of wave velocity

For the AE event location, calculated using both the TOA and SSMAL techniques, the wave velocity should be calculated in advance. In the SSMAL case, the velocities of both wave modes are required. As discussed in Section 2.2 in composites this is additionally complicated due to the velocity will be directional depending on fibre orientation.

Practically, the velocity of both wave modes can be determined by following these steps:

At a known distance apart on a structure, two sensors are placed. Adjacent to sensor 1 on the centre line of the sensor, an H-N source is performed, as shown in Figure 3-9, using a synchronous trigger, which makes channel 2 begin recording when the signal crosses the threshold at channel 1.

The arrival times of the wave modes can then be identified from the recorded waveform at channel 2 (Figure 3-10). In that specific material direction, the velocity can be determined using Equation 3.1.

$$C_{S/A} = \frac{T_{S/A}}{D} \tag{3.1}$$

Where:

$C_{S/A}$ = Velocity of the s_0 or a_0 wave mode

$T_{S/A}$ = Difference in time of arrival of s_0 or a_0 wave mode

D = Distance from source

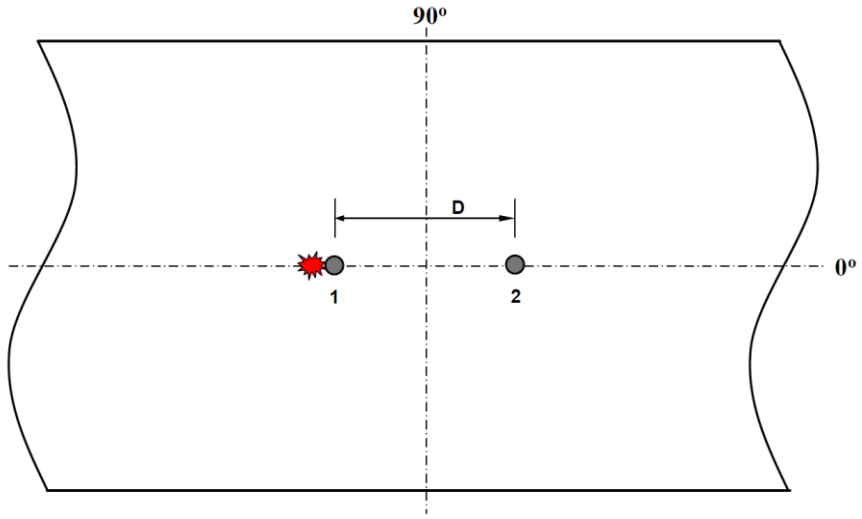

Figure 3-9. Velocity measurement (Eaton 2007a)

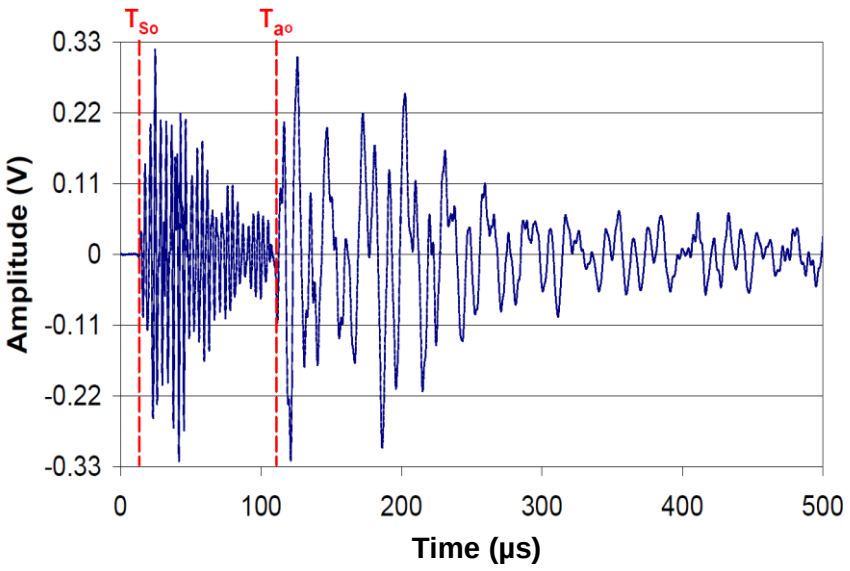

Figure 3-10. Wave mode arrival times (Eaton 2007a)

3.1.8 Graphical representation

The AE data and the investigation and analysis of results are commonly completed in a graphical format. There are many format of displays, the following is a description of the more common types.

Time-history plots: displays the feature evolution versus the time such as user-selected AE features or other parameters such as load against time. Cumulative plots or rate based plots of AE hits or events against time can also presented using this type of graph. The cumulative plots can be used to identify the damage

evolution during the test life. Figure 3-11 shows a typical time history plot of cumulative AE events.

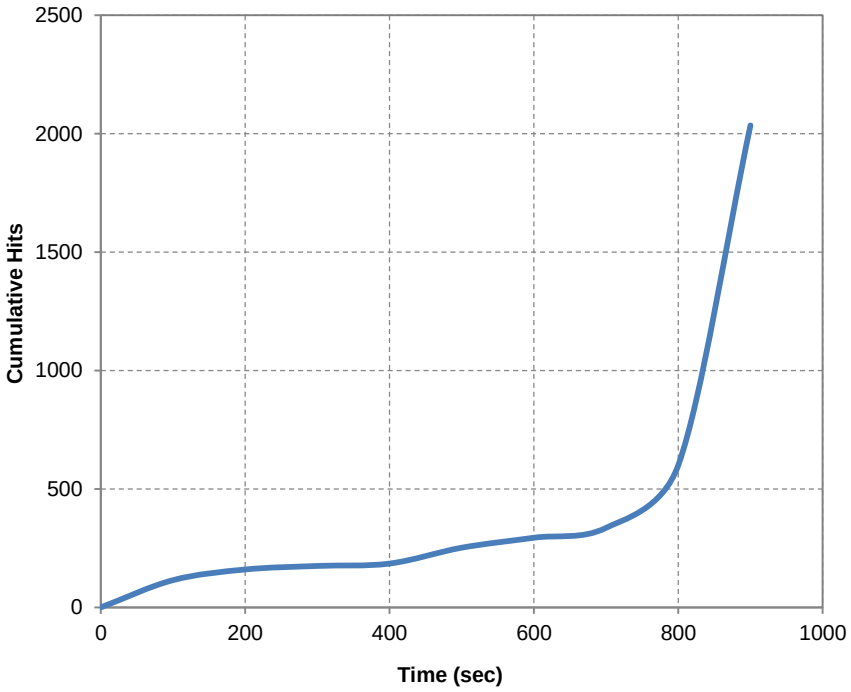

Figure 3-11. Typical time history plot of cumulative AE events

Location plots: Two techniques for AE source location were utilised during this work, Two-dimensional TOA location and DTM location techniques. The two-dimensional locations and the DTM locations are presented in two ways during this work. Using the scatter plots of x and y position as shown in Figure 3-12 and using spatial binning plots where points are coloured by the density of events in order to show high AE activity (Figure 3-13).

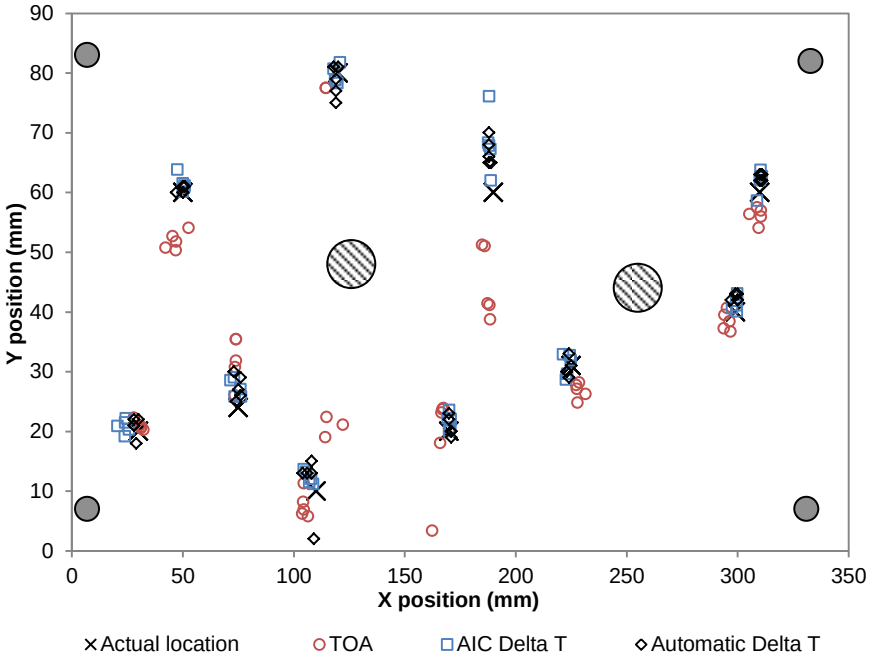

Figure 3-12. Typical planar location using an array of six sensors

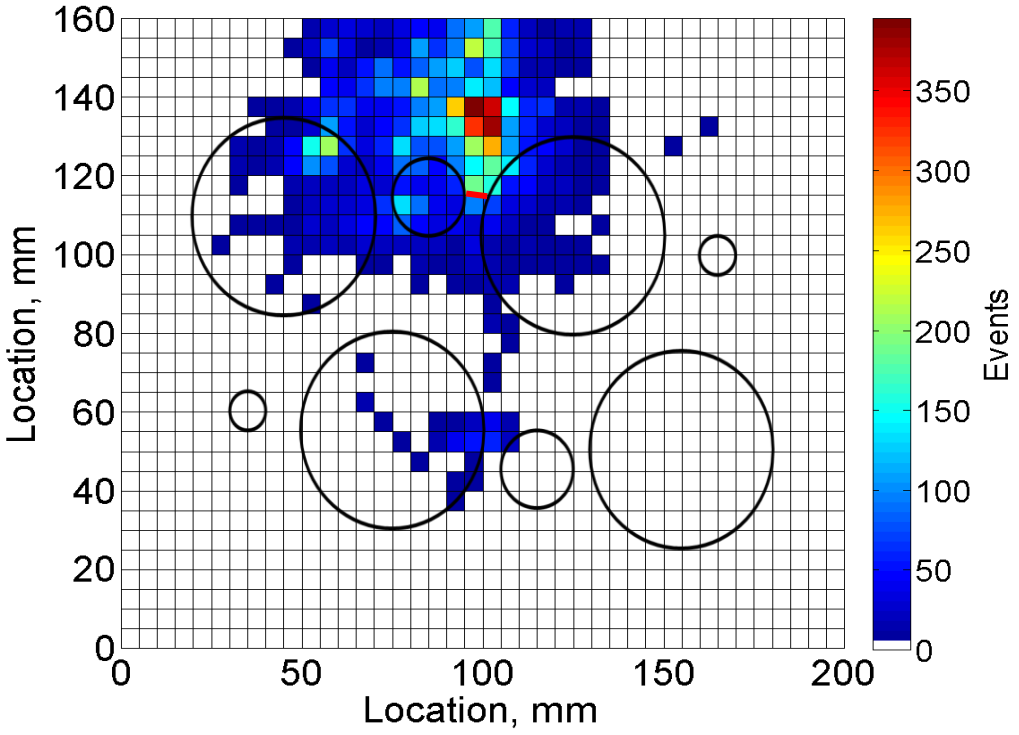

Figure 3-13. Two dimension location results as spatial binning plots

Correlation plots: The relationship between two AE parameters can be displayed using a correlation plot. These plots can be used for damage indication and/or identification. Figure 3-14 shows an example of the correlation plot where amplitude is compared with duration for a signal.

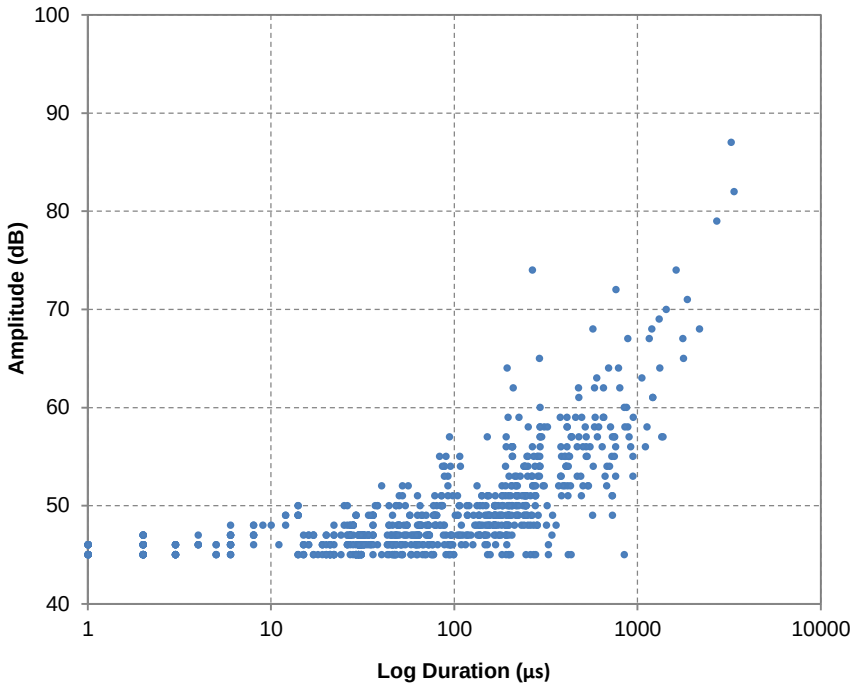

Figure 3-14. Correlation plot of amplitude versus log duration

Waveforms: A waveform is the AE signal time domain representation which is similar to a trace captured on an oscilloscope. The amplitude of a signal presented in the vertical axis in volts and the horizontal scale is the elapsed time from the trigger point. An example of a recorded AE waveform displayed in time domain is presented in Figure 3-15. In both systems (Vallen and MGL) the AE signal amplitude is calculated in dB_{AE} relative to a 1µV reference voltage at the transducer. The amplitude in dB is then given according to Equation 3.2.

$$Amplitude = 20\log_{10}\left(\frac{V_s}{V_{ref}}\right) \tag{3.2}$$

Where:

$Amplitude$ = Amplitude (dB)

V_s = Voltage of peak excursion

V_{ref} = The reference voltage

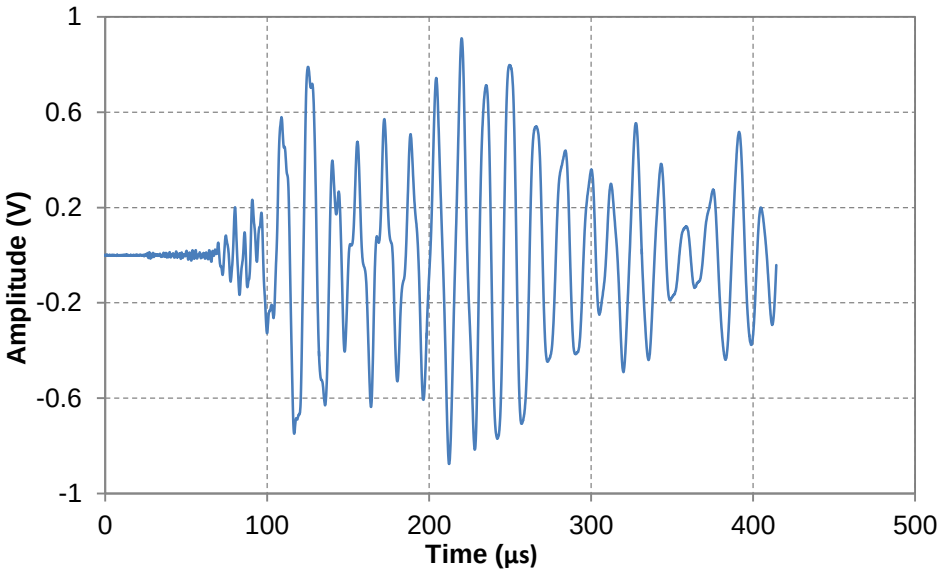

Figure 3-15. Typical AE waveform plot display

C-scan images: The C-scan result is presented in a colour image which is scaled relative to the amount of signal lost at that specific position in the scan area. A greater signal loss is caused due to diffraction and attenuation of the signal due to damage in an area. Comparing two images, pre-test and post-test, gives clear observation of damage. Figure 3-16 shows an example of the C-scan images.

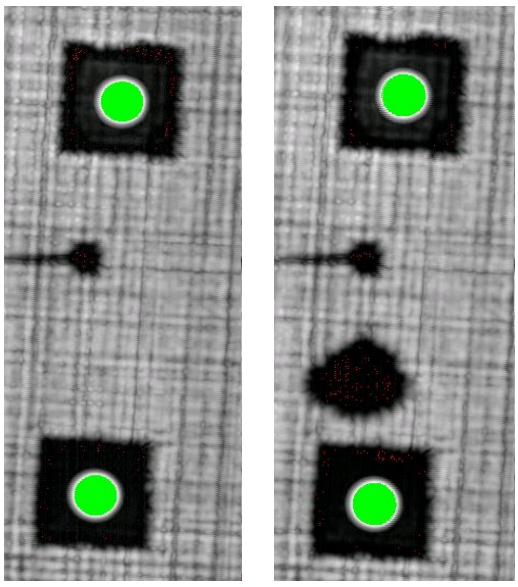

(a) post-test (b) pre-test

Figure 3-16. C-scan images

4 Source Characterisation

4.1 Introduction

In industry, accurate characterisation of damage using NDT techniques is vital in order to assist the operator of the structure in decisions regarding the integrity of the structure. In service, when SHM techniques with damage characterisation ability are used to provide continuous and global monitoring of the structure the result is increased safety, longer intervals between structure inspections and hence a reduction in maintenance cost.

SHM techniques which are well developed in homogeneous materials do not translate easily to complex structures (such as aircraft landing gear components which have many wall thickness changes, lugs, small radii and other geometric features) and/or complex materials (such as composites due to their complex and anisotropic properties). This is especially true in AE where propagation behaviour significantly affects the signal data and can lead to incorrect damage characterisation.

Firstly, this chapter will describe a novel solution to enable AE parameters to be “corrected” to account for the material properties and the geometry of the structure. The Parameter Correction Technique (PCT) derives an empirical relationship between signal parameters and varying source amplitude from a number of locations, across a structure. This method does not require knowledge of the sensor location or wave velocity. A five-step description of the process is provided and practical results from an initial trial are presented. Results from the initial trial demonstrate a considerable improvement over the use of conventional parameters.

Secondly, the PCT is used to correct the recorded AE event parameters and increase the damage identification reliability for real test data. The AIC DTM technique was used to locate damage signals with high accuracy in a large fatigue specimen, which generated different damage sources. The unsupervised clustering technique, *k*-means, was used with the main signal parameter as an input vector to identify and characterise the most critical damage mechanisms in the specimen.

A comparison between the traditional and the corrected parameters results is provided. The results show that there is a good agreement between the corrected parameters clustering classes and the ultrasonic C-scan investigation result. Based on the PCT results the main damage mechanisms of composite including matrix cracking and delamination are identified. This investigation can contribute towards on-site health monitoring of large-scale structures using the application of AE techniques.

4.2 Data Processing

4.2.1 Parameter Correction Technique (PCT) Methodology:

The novel technique in this thesis utilises an artificial source to record the relationship between acquired signal parameters and varying source amplitude from an array of locations, creating a multi-layer map of features for each sensor. Each layer represents one source amplitude and demonstrates the variation in parameters with source to sensor distance. Then for each position within the map, multiple layers (at different amplitudes) can be stacked up to construct the relationship between source amplitude and recorded parameters. Using these relationships, any previous, current or future AE data received from within the PCT map area can be corrected. This method does not require knowledge of the sensor location or wave velocity. The PCT methodology was first presented in Al-Jumaili et al. (2014) and a five-step description of the technique is provided below:

- **Determine area of interest:** The PCT method can provide a complete coverage of an entire structure or part of a structure for time-saving purposes. It can be used as an improvement method to correct parameter values of AE emitted from important areas, which are predicted to have high stress levels using analysis methods such as finite element.
- **Map system Construction:** A grid is constructed on the area of interest within which AE events will be generated. It is important that sources and not the sensor should be referenced within the grid. Placing the sensors within the grid is unnecessary (Figure 4-1a) and does not affect the result.
- **Apply artificial sources to obtain parameter value data set:** Artificial source with varying input amplitude are generated at each node of the grid to provide AE parameter readings at each sensor. An average result of the recorded AE data is achieved by repeating the same source amplitude several

times at each node, reducing the error. Interpolation between node points allows for greater spatial resolution and accounts for missing node data as a result of holes, for example. The resulting data can be presented as a contour map (Figure 4-1b) showing the parameter values recorded from each grid position using the same source amplitude.

- **Calculate PCT maps**: A contour map is generated for each source amplitude and then used to generate a multilayer map (Figure 4-1c) that allows more accurate correction of AE parameters from sources with varying amplitude. For any (x, y) coordinate within the grid a relationship can now be formed between the source amplitude (in volts) and the recorded parameter value, by taking the parameter value from each map level (Figure 4-1d).
- **Real AE data parameters re-calculation:** When real AE data are recorded from a test they can be corrected using the PCT maps in the following way:
    I. Calculate source location: signals are located using the DTM algorithm to give an accurate estimate of their source position. Knowledge of the source position is essential to the operation of the PCT process.
    II. Determine parameter vs source amplitude relationship: Using the estimated source position the relevant parameter vs source voltage relationship can be determined from the multi-layer map for each sensor. If the source position is not at a known grid position then data are interpolated to derive the required relationship.
    III. Correct parameters: Using the parameter vs source amplitude relationship, the correct source amplitude can be determined from the recorded parameter. If the recorded parameter falls between amplitude levels used when training the map, then interpolation is used to ensure accurate correction. Furthermore if the recorded parameter falls outside the range of training amplitudes then extrapolation is used to determine the correct source voltage. The average of the corrected source parameters from all sensors is then taken as the final corrected value.

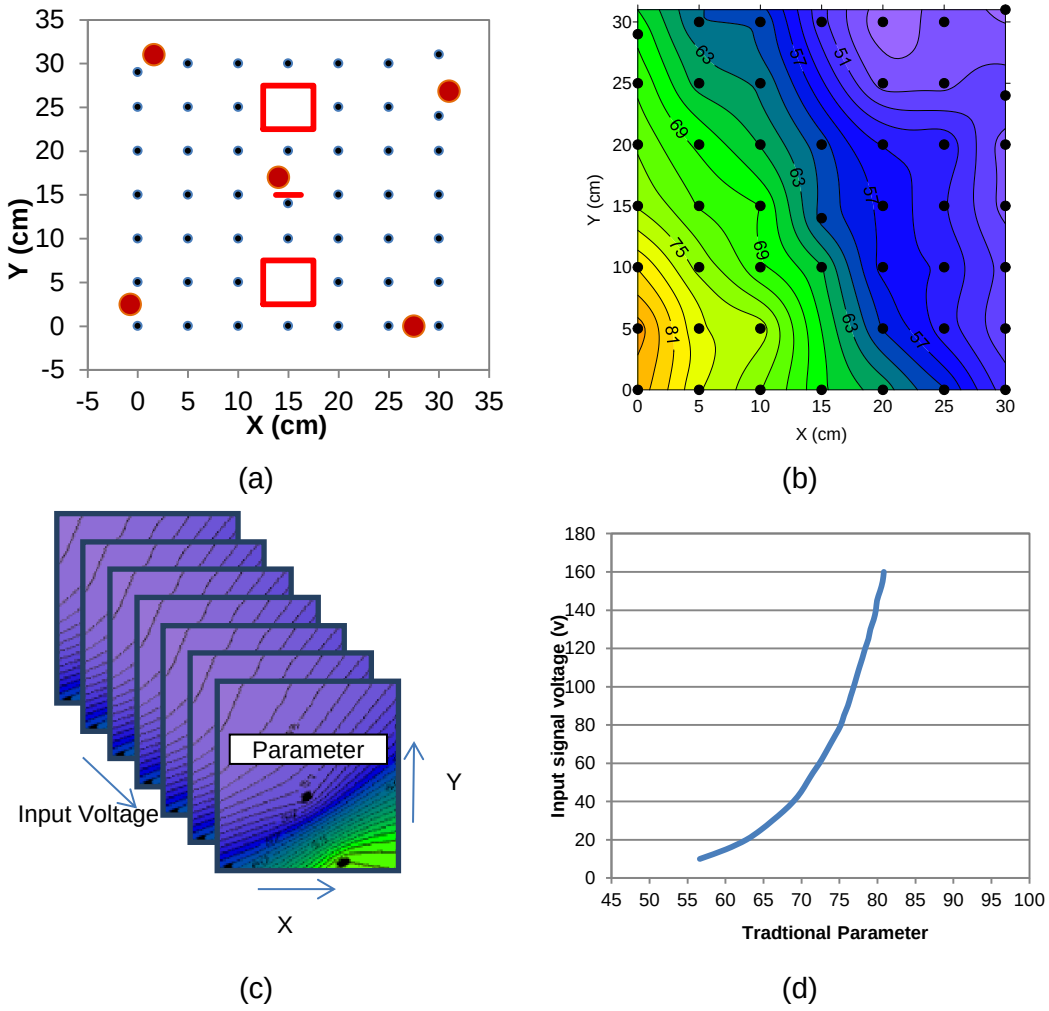

Figure 4-1 (a) the PCT grid (b) Traditional amplitude values within the PCT grid (c) the structure of the PCT map for each parameter of each sensor (d) Different locations parameter-voltage relationships

4.2.2 Validation Test Methodology:

The PCT's performance is assessed within a multi-parameter classification process to classify different artificial AE sources. This is achieved by using previously labelled signals as input vectors to the multi-dimensional process and then checking the correct assignment of the signals. Here, the AE signals are treated as a pattern vector described by a number of features. The same data is used twice as an input vector to the multivariate statistical techniques. In the first case the traditional signal parameters were used, while in the second case the same parameters are passed through an extra stage to correct them using PCT. The classification results from both cases are presented for comparison. The main idea here is that the accuracy of classification is used as a criterion of

classifier performance. Because the classifier is the same in both cases, the accuracy will reflect the PCT performance. The unsupervised clustering method and their performance were evaluated through two special mathematical criteria. The clustering pattern involves the steps presented in Figure 4-2.

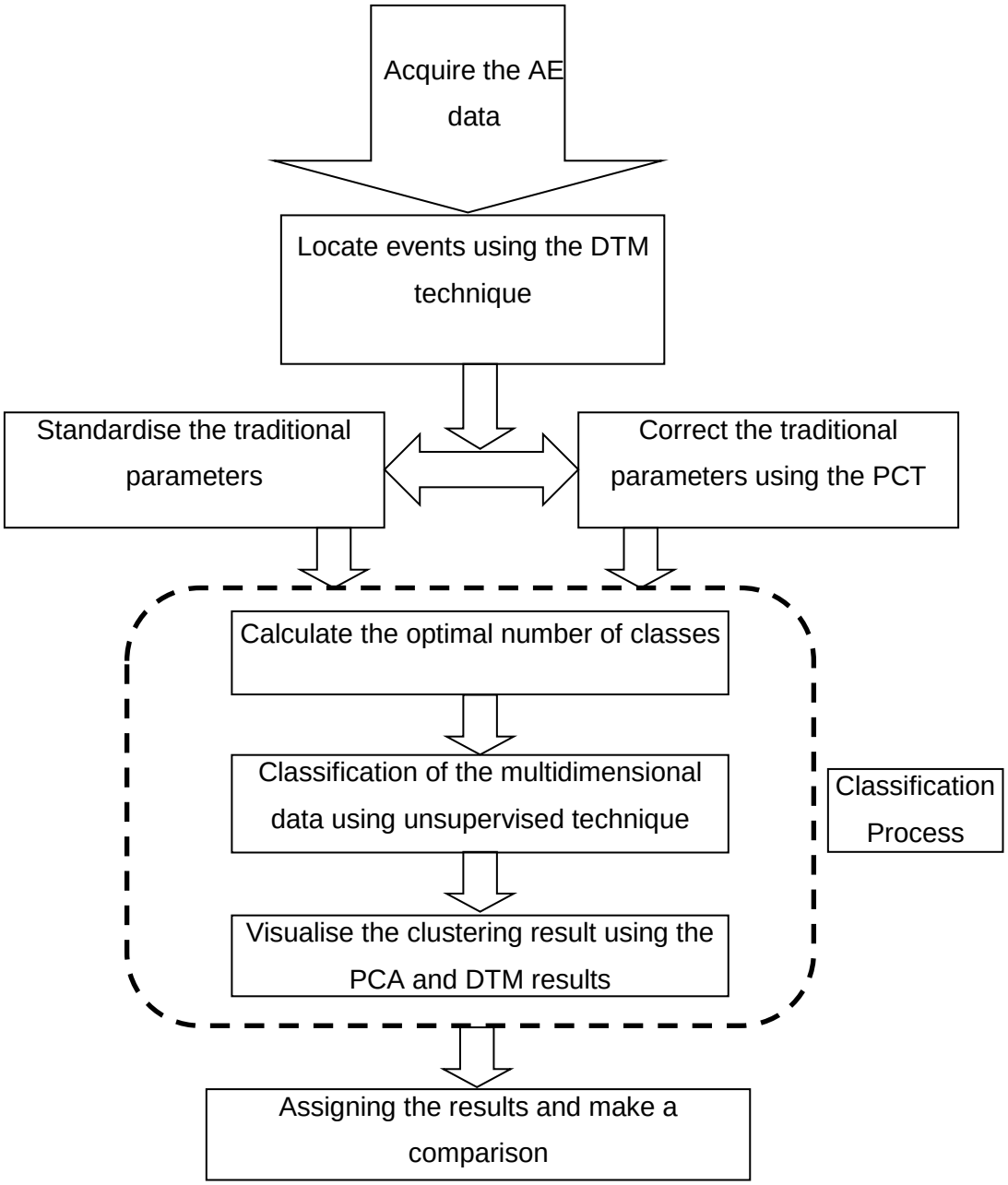

Figure 4-2. Flowchart of the PCT validation test

In both cases, each AE signal is identified using four basic features, namely, amplitude, counts, energy and duration. In order to avoid biasing the classification towards the feature exhibiting the highest physical dimensions, in the first case when traditional parameters are used, the AE data is standardised (Manson et al. 2001; Rippengill et al. 2003). In the second case the standardisation is not required because the corrected parameters have already received equal weighting from the PCT, which is considered an advantage that will reduce computing time.

The unsupervised clustering is performed using the *k*-means technique. The *k*-means clustering aims to partition *n* observations into *k* clusters, specified in advance, in which each observation belongs to a cluster (MacQueen 1967). Knowing in advance the number of desired classes is necessary to conduct the *k*-means process. The optimal number of classes is determined by evaluating the clustering results using validity criteria. Two widely-used clustering quality criteria, the Silhouette (Rousseeuw 1987) and Davies-Bouldin (David and Donald 1979) indexes, are used as an indication of the compactness and the separation among the resulting classes. Higher cluster quality results in a maximum value of the Silhouette criterion and minimum value of Davies-Bouldin criterion. Two-dimensional visualisation for the clustering results is achieved using PCA as a visualisation and dimension reduction method. The technique provides a two-dimensional projection of the *n-dimensional* space, where *n* is the number of selected descriptors, four in this work, and using PCA will provide visualization of the separation of the clusters. The PCA is known as a classical method of multivariate statistics and its theory and use are well documented in textbooks from that field Sharma (1995). In this work the more basic techniques for classification and visualisation are used, because the main objective of this study is not improving the multi-dimensional statistical techniques themselves but to improve the results by using reliable and correct input data. It is understood that using more complicated multi-dimensional algorithms with incorrect input data will definitely lead to greater processing time and will not improve the result accuracy. Also, it is important to bring to the attention of the reader that the simple techniques can be applied in the case of largely separable data and give accurate results if the correct input data is used.

4.2.3 Real AE characterisation Methodology:

An unsupervised clustering technique was used as a statistical tool to classify numerically the AE signals into different types of damage mechanisms released from a composite panel under fatigue load. It should be noted that it is the intention in this work to apply this classification procedure to signals from located AE events only. Only those AE sources that have high energy, are able to hit at least three sensors and are considered to be an event will be used in the analysis. That is because the PCT is only capable of working with located events as discussed in (4.2.1).

In this investigation the main four signal parameters, (amplitude, count, duration and energy), will be used as input data in the clustering process. The classification procedure is performed twice, using traditional parameters (Case1) and using the re-calculated parameters using the PCT (Case 2). The same procedure as presented in Figure 4-2 is used in this analysis (without the PCA visualisation step).

After location of the AE events, using the DTM technique (Baxter et al. 2007), the located events parameters are corrected using the PCT to use them in Case 1. While, the traditional parameters are standardised in order to have equal weighting and to use them as input to Case 2. The optimal number of classes should be known in advance. Two common clustering quality criterions, Silhouette (Rousseeuw 1987) and Calinski-Harabasz (Dudoit and Fridlyand 2002) indexes, were used to determine the optimal number of classes which correspond to the maximum value of the two criteria.

4.3 Assessment using Artificial Source

4.3.1 Experimental Procedure:

- ***Test specimen***

The carbon fibre specimen used in this investigation is shown in Figure 4-3. The specimen was manufactured in an autoclave from Hexcel Corporation M21/35%/UD268/T800S uni-directional pre-preg material. Hand lay-up using 8 layers from unidirectional pre-preg (laid up as $[0/90]_{2s}$) was used to produce 500 x 500 mm and the nominal thickness of the final product is 2.1 mm.

The central area of interest of 300mm x 300mm was used in this work and all locations in the rest of this study will be measured in respect to this area. During the fabrication procedure an artificial matrix crack was initiated at the centre of the panel by cutting the inner layer's (3^{rd} and 6^{th}) fibre in 0^{o} direction by 25mm using a fresh sharp razor (Figure 4-3c). The artificial crack end points are (137.5, 150) and (162.5, 150) mm. This action was done in order to weaken this region and make the matrix only transfer the load and make the matrix cracking more likely to occur here where the material is no more supported by longitudinal fibres (same load direction). In this stage high attention was made to ensure that the two cracked layers were aligned. After the layup process the panel was cured in an autoclave and vacuum bag. Before curing the panel was prepared on an aluminium plate which was covered with polytetrafluoroethylene (PTFE). The panel has full vacuum and moulding pressure applied before using the recommended curing cycle by the material supplier. Figure 4-4 shows the curing cycle, which consists of a heat up rate from room temperature of 2.96 ^{o}C/minute to 175 ^{o}C and held for two hours, the panel was then cooled at 3.62 ^{o}C/minute. The whole curing cycle was applied under full vacuum.

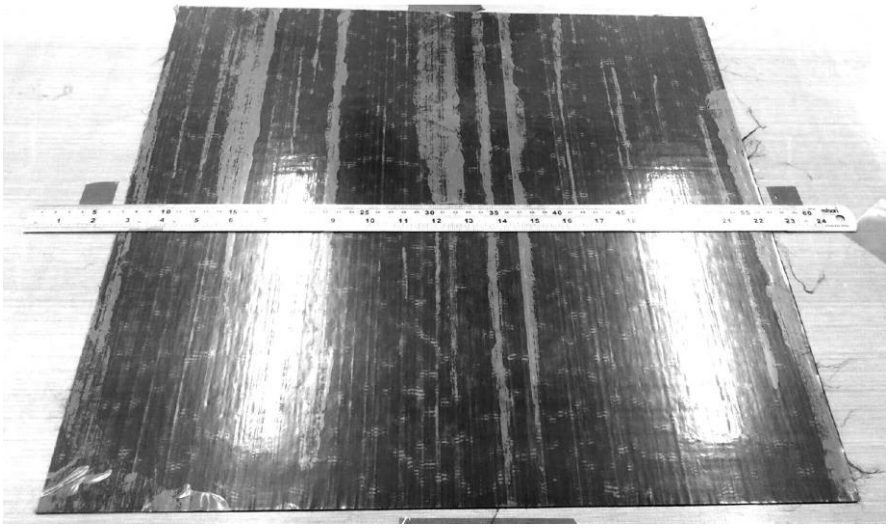

(a)

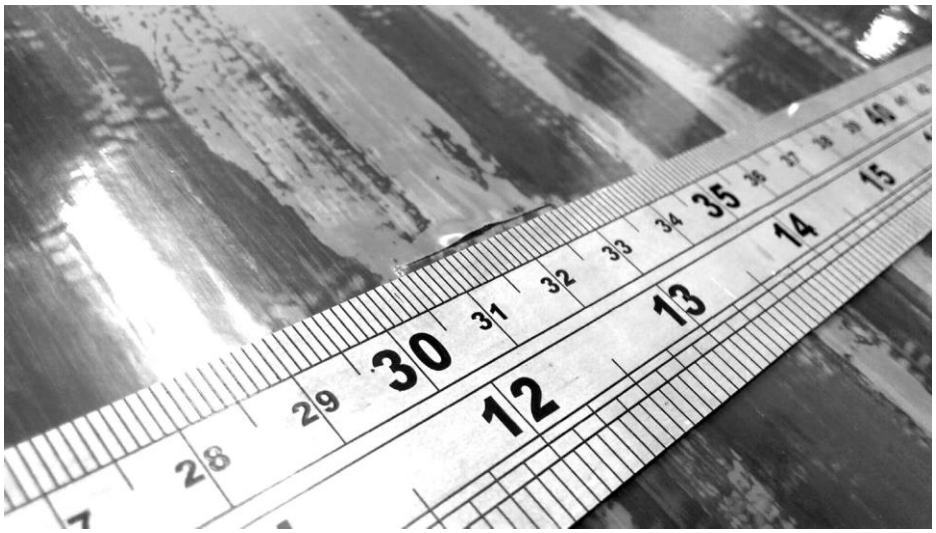

(b)

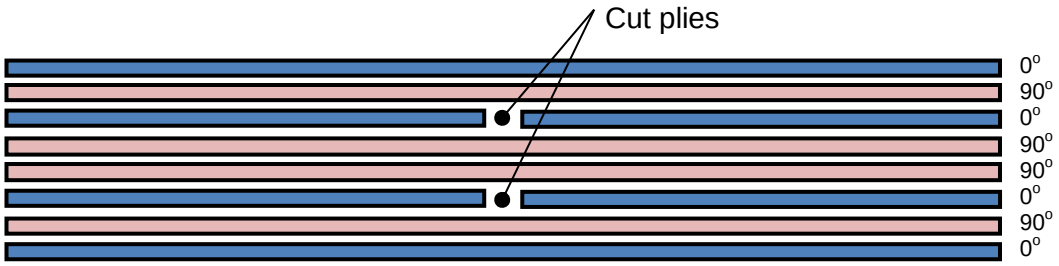

(c)

Figure 4-3. The test specimen. a) manufacturing panel b) artificial cut c) schematic of cut plies

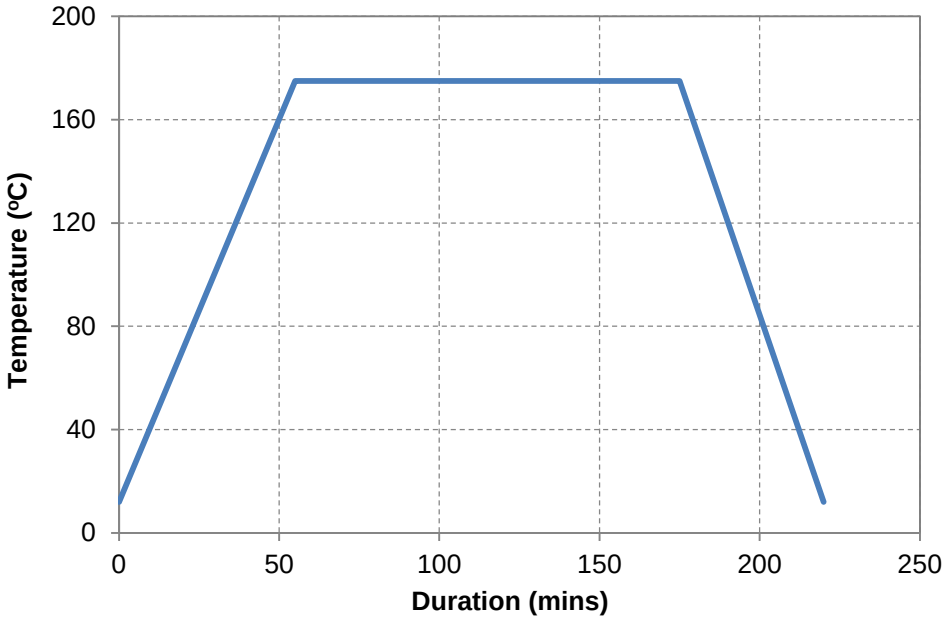

Figure 4-4. Cure cycle for the composite panel

In order to identify any induced damage after manufacturing, the tested panel was inspected prior to the test using ultrasonic C-scanning.

In order to transfer the tension load to the test specimen, four 5mm thick aluminium tabs with 50mm x 50mm dimensions were glued onto both sides of the panel along the 0^o material direction using the resin ARALDITE 420 A/B (2 Component Epoxy Adhesive). To accelerate the gluing process the specimen and tabs were cured at 50 centigrade for 4 hours. The specimen was drilled through the tabs to produce a 20mm hole. The test specimen configuration is presented in Figure 4-5. After the drilling the specimen was C-scanned again in order to be sure there was no internal damage.

After applying several fatigue cycles to the panel with different load levels, local delamination was produced by impacting the specimen using a low velocity impact by a polished hemispherical tup of 20mm diameter, between the tabs. Nine repeated low velocity impacts were used, from 5J to 14J with various intervals (5, 5, 6, 7, 8, 10, 12, 12 and 14 J). Following the final impact event, C-scan inspection of the panel was conducted in order to assess the delamination area. Figure 4-6 shows the C-scan result of the specimen before and after impact.

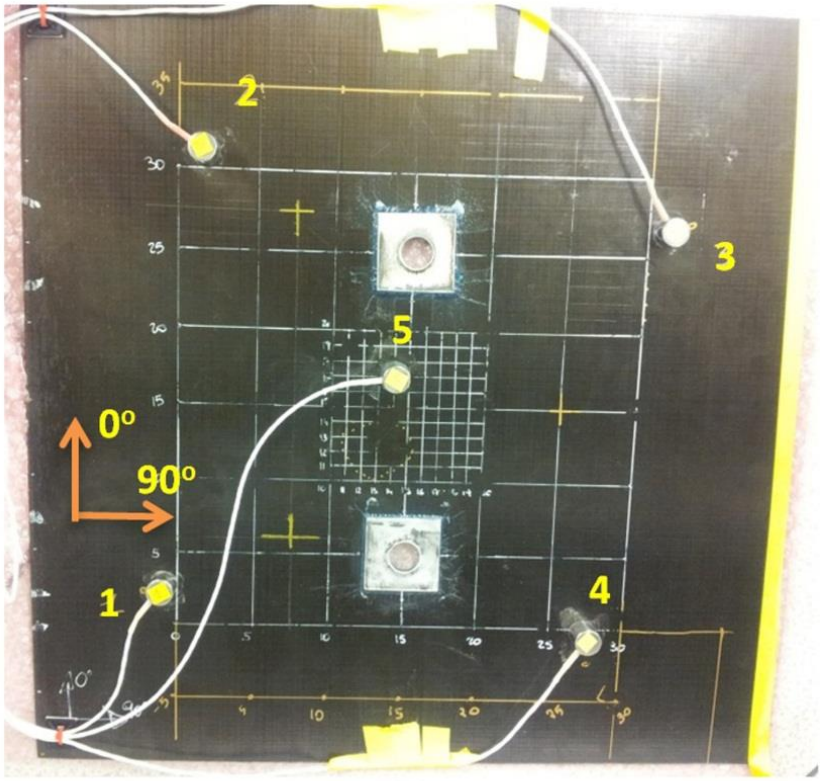

(a)

Figure 4-5. Test specimen configuration

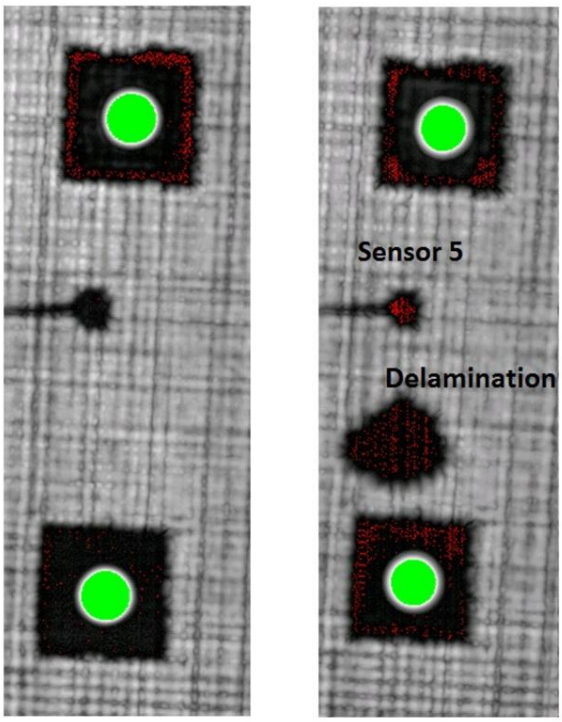

(a) (b)

Figure 4-6. C-scan images (a) before impact (b) after impact

- ***AE acquisition:***

AE was continually monitored during the tests (using the artificial sources test and during the fatigue test) using Vallen AMSY-4 data acquisition system, with 5 MHz sample rate and 34 dB pre-amplification using the Vallen AEP3 pre-amplifiers. The AE signals were monitored using five PAC WD wideband transducers with bandwidth of 100-1000 kHz and a resonant frequency at 650 kHz. Ambient noise was filtered using 44.9 dB threshold. The sensors were coupled on the specimen using Silicon adhesive (Loctite 595) to provide an acoustic couplant agent and a mechanical fixture and the sensors relative positions are shown in Figure 4-7. The sensors positions are provided in Table 4-1. Mounted sensor sensitivity testing was performed using a Hsu-Nielson (H-N) source (Hsu and Breckenridge 1981).

Before starting the test the Delta-T grid was created on the same side as the sensors. A square grid was drawn with two resolution grids. The smaller grid (100mmx100mm) with 10mm resolution was used at the centre of the panel near the artificial crack location and the second grid is 300mmx300mm with 50 mm resolution. The finer grid resolution was selected near to the artificial crack location in order to locate AE signals with higher accuracy by taking into account local discontinuities. Figure 4-7 shows the Delta T grids. The mapping training data were collected before the test by generating five pencil lead breaks on each grid node. Then the Delta T maps were calculated using the time difference between sensors pairs (for 5 sensors we have 10 maps). Figure 4-8 shows an example of the Delta T training maps. It is interesting to see how the specimen geometry, such as tabs, affects and disturbs the wave propagation. It is also interesting to observe the effect of the material inhomogeneity on the wave velocity of the material.

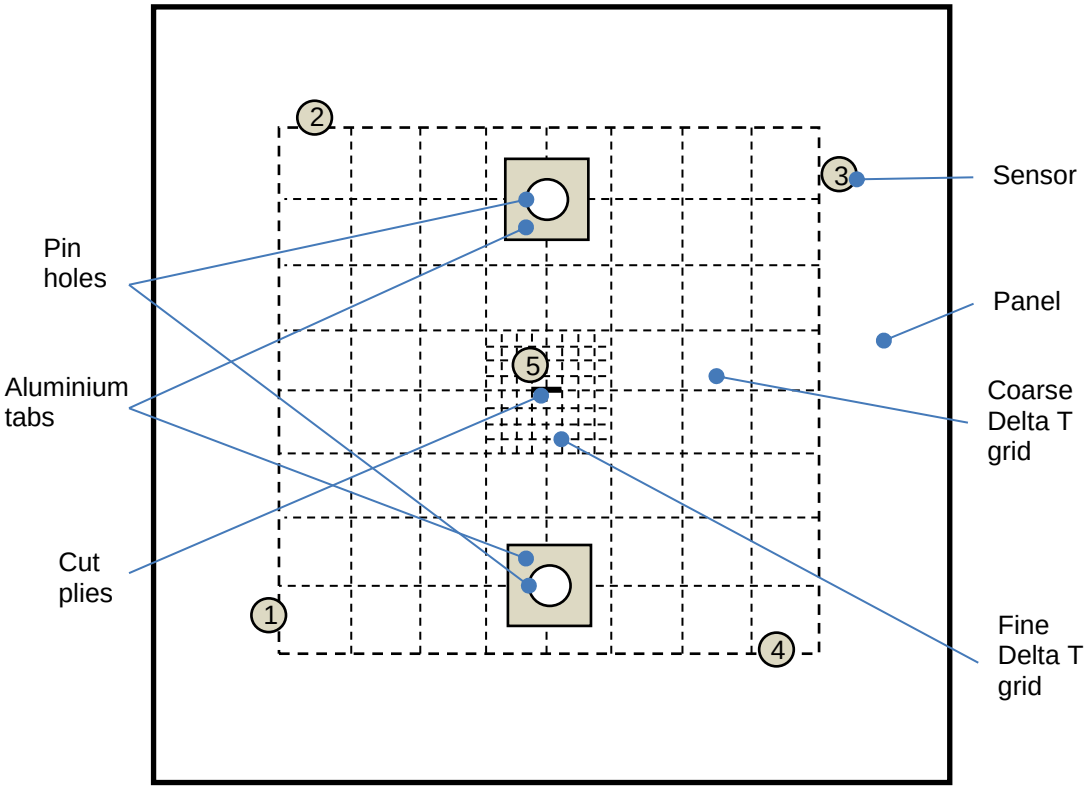

Figure 4-7. Geometry of the test specimen

Table 4-1. Location of the sensors on the panel from the reference corner

	X location mm	Y location mm
Sensor 1	-7.5	25
Sensor 2	16	310
Sensor 3	310	268.5
Sensor 4	275	0
Sensor 5	140	170

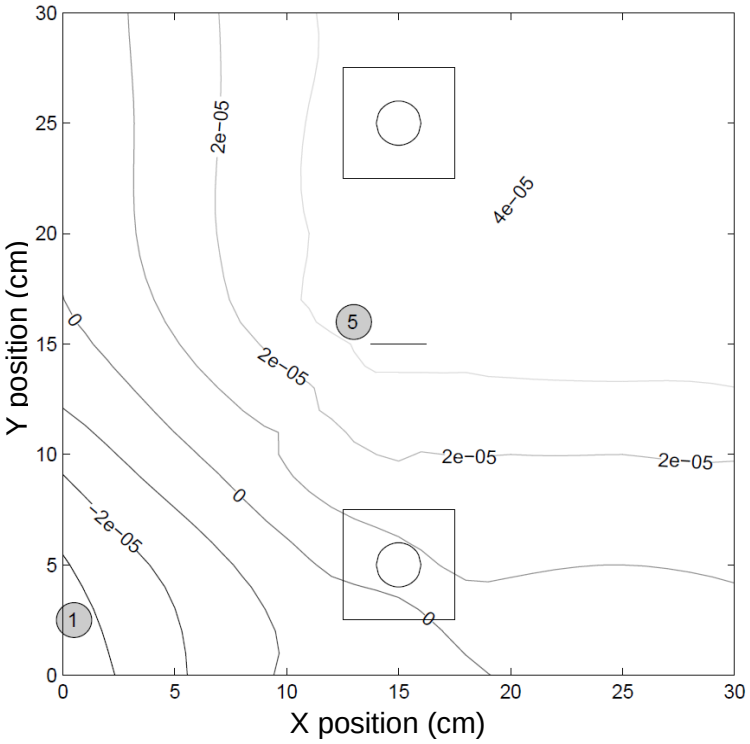

(a)

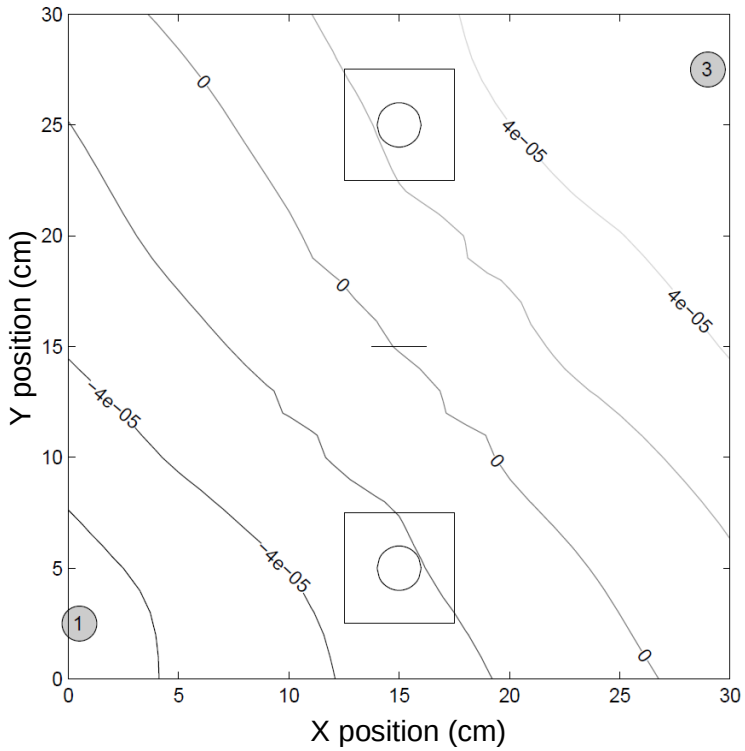

(b)

Figure 4-8. Delta T training maps a) ch1-ch5 b) ch1-ch3

The PCT grid was created on the specimen on the side of the sensors. Grid area was selected to be on the same Delta T area (300mmx300mm) with 50mm resolution (Figure 4-9). An artificial AE source was used to generate grid signals for the training map (Al-Jumaili et al. 2015). This was achieved using a MGL arbitrary waveform generator (WaveGen1410) and an in-house manufactured broadband conical transducer provided by the NPL, UK. Multi-purpose grease was used as a couplant to provide good contact between the conical transducer and the specimen surface.

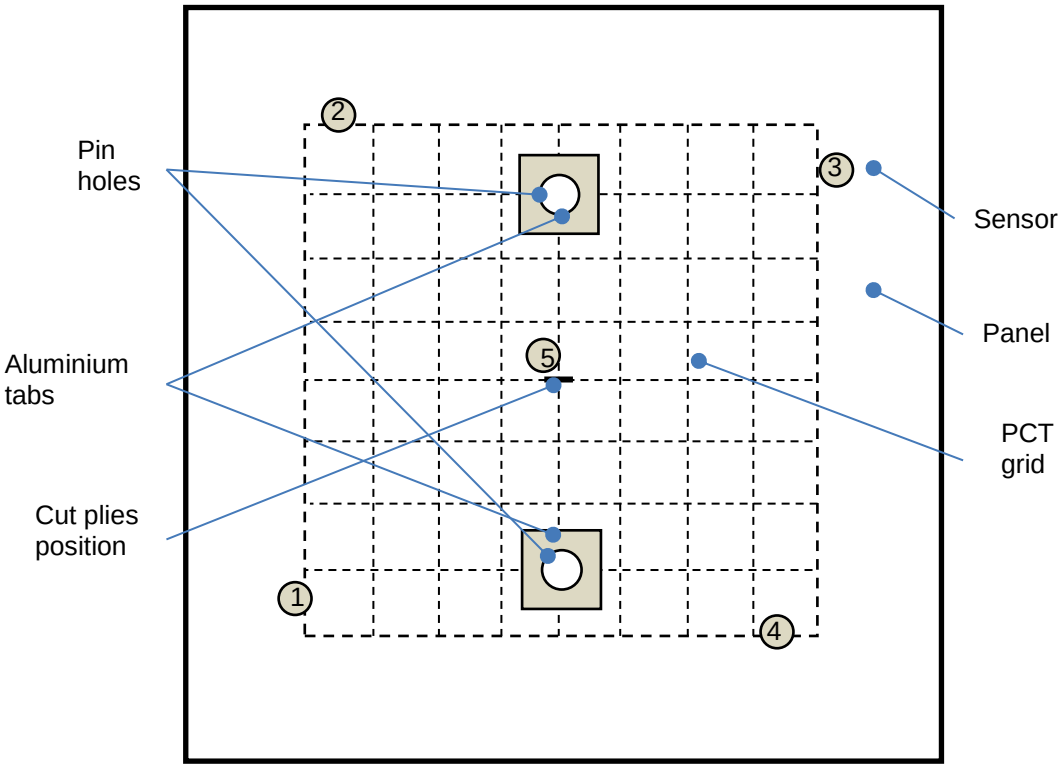

Figure 4-9. The PCT grid

4.3.2 Results and discussion:

- **Initial PCT practical calculations:**

In this work, the training data for the PCT mapping was collected from an area of 300 x 300 mm, identical to the Delta-T map area, because having accurate events location is essential to apply the parameters correction. This area contains several components of geometry features such as holes, thickness change, fibre discontinuity and delamination. A PCT grid density of 50 mm was used, creating 47 nodes on the PCT mapping area as shown in Figure 4-10. Two nodes were not available to collect due to their location within the tabs holes (node (50,150)

mm and node (250,150) mm). Because there is no restriction on the use of irregular nodes distribution, the nodes very close to the sensors positions were shifted by approximately 10 to 20 mm from the proposed node location to enable a signal to be generated by the broadband conical transducer. The shifted points are (150, 150), (300, 250), (0, 300) and (300, 300) mm. The training map of the PCT grid is shown in Figure 4-10 with the shifted nodes.

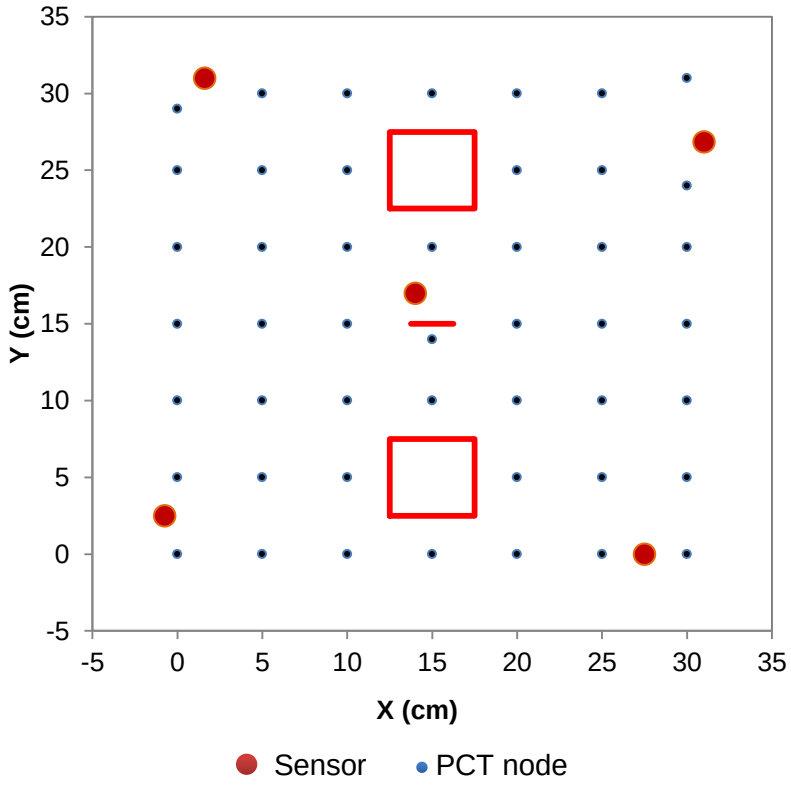

Figure 4-10. The training map of the PCT grid

In order to excite the AE system an artificial excitation pulse (rectangular shape pulse of 10 µs width) was generated at each node via the wave generator with the conical transducer, with an amplitude from 10 volts to 160 volts, increasing at 5 volt increments. At each position and increment the pulse was repeated 5 times to provide an average and avoid any erroneous results. AE signal parameters were recorded in real time using the five sensors. For each input pulse voltage, each parameter value from each sensor data was interpolated to cover all of the area between the nodes. So each input pulse voltage will create five counters, one for each sensor for only one parameter. Figure 4-11 shows the four traditional parameters values within the PCT grid recorded using sensor 1 at

the 160 volt source amplitude, as an example. The other four sensors exhibited similar behaviour to that presented in this figure.

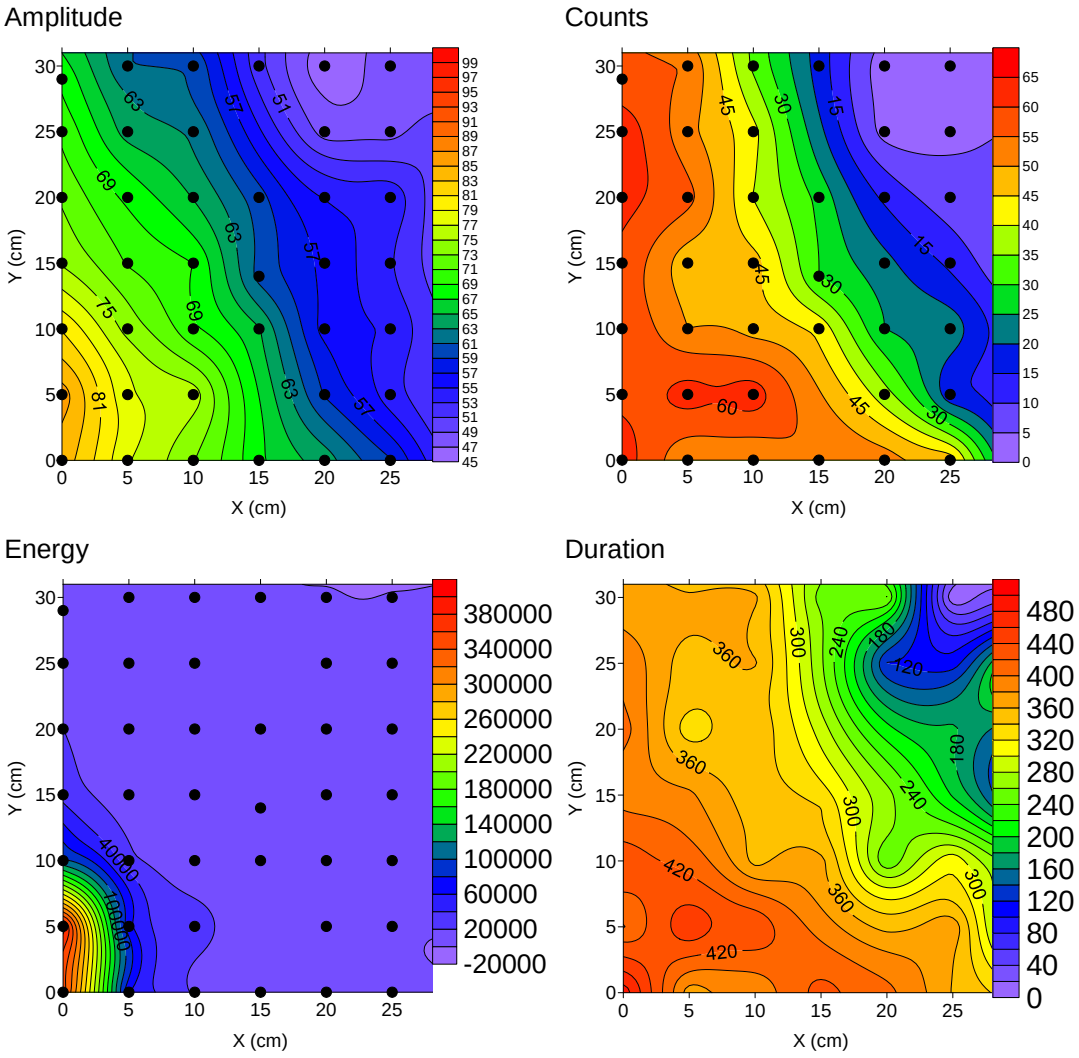

Figure 4-11. Traditional parameters recorded by sensor 1 generated from same source (160v).

The PCT training maps highlight the problems related to using AE for classification in large-scale composite components and provide important information about the real signal attenuation within the structure. Figure 4-11 shows how the recorded AE parameter values vary greatly with the propagation direction, Euclidian distance between the source and recording sensor and with propagation path features such as holes and thickness changes. This highlights the difficulty of AE sources identification in anisotropic materials and large components.

The AE features show interesting behaviour to the propagation path. For example, the signal amplitude value is essentially affected by propagation distance, i.e., attenuation. However, this relationship between the attenuation rate and the distance is not constant. Attenuation shows different behaviours depending on the propagation direction. It can be seen clearly that at the vertical line at x=0 mm that is 0^o propagation line (along the fibre direction) the attenuation is less than that at the 45^o propagation line (off of the fibre direction). Also, it is clear to note how the obstacles and geometry change will affect the attenuation value and thus the recorded parameter values. The amplitude attenuates along the fibre direction at 0^o (with x =0 mm) and 90^o (y = 50mm) at different rates. This is due to the tab locations and the hole on the 90^o propagation path. In real structures this problem will be exacerbated due to the large scale and presence of more complex features (holes, boundaries, thickness changes, etc.).

Most previous studies have been conducted using small-scale specimens without consideration of the effects of signal propagation direction or structural features on the recorded data, which is not the case here. The effect that the observed variation can have on the accuracy of any analytical solution is significant and as a result it is difficult to characterise AE signals generated from different locations within large-scale complex structures using AE data directly.

Clearly, if one could correct each recorded parameter according to the parameter distribution contours, as shown in Figure 4-11, then many of these problems would be negated. Unfortunately, in practice, there are many limitations. This is because each damage mechanism generates signals with different levels of energy, while the presented contour was generated from one energy level source. Furthermore, the final assessment relies mainly on the inspector's own experience and subjective decision-making, because the correction process will depend on the chosen sensor data and the specific correction distance from that sensor. Moreover, the difficulty will increase if the AE data was collected using more than one sensor, as is the situation in large-scale structures, because it will be difficult to find a comparable scale between the corrected data from different sensors. The proposed PCT overcomes the dependency on the operator choice and obtaining the corrected results by using a comparable scale. This is considered to be a significant improvement in the field of AE. It makes it possible

to compare with more confidence the AE collected from different source locations, different specimens, different materials and from different sensor types.

The relationship between the recorded parameter values and the input pulse voltage at each position within the PCT grid can be obtained for each sensor. For example, Figure 4-12 shows the relationship between the parameter values recorded by sensor 1 versus the pulse input voltage from three arbitrary source positions. The arbitrary positions are (30, 40), (220, 50), (107, 223) mm. The sensor 1 was selected arbitrarily and each one of the other sensors show different relationships. It was noted that the relationships for both the amplitude and energy are smoother than that of the count and duration. This is because amplitude and energy are less dependent on the acquisition threshold level in comparison with counts and duration. Furthermore, the two locations (220, 50) and (107, 223) mm are located at approximately the same distance from sensor 1 but they have different relationships. That is because the signal propagation path is different for these two points both in fibre direction and presence of obstacles. This further supports the fact that the material nature and structural geometry play an important role on the recorded AE data and that any solution that does not take these factors into account will be limited and unreliable. Also the use of a single relationship applied for whole the specimen area will give unacceptable results because every location has different parameter relationships for the same signal and for each sensor. The relationships extracted from the PCT maps are used to correct the recorded AE parameters and obtain the corresponding voltage values.

As a result, the structure of the PCT training map for each parameter is a data set of five dimensions and arranged by (sensor number, X axis location, Y axis location, input pulse voltage and the parameter value).

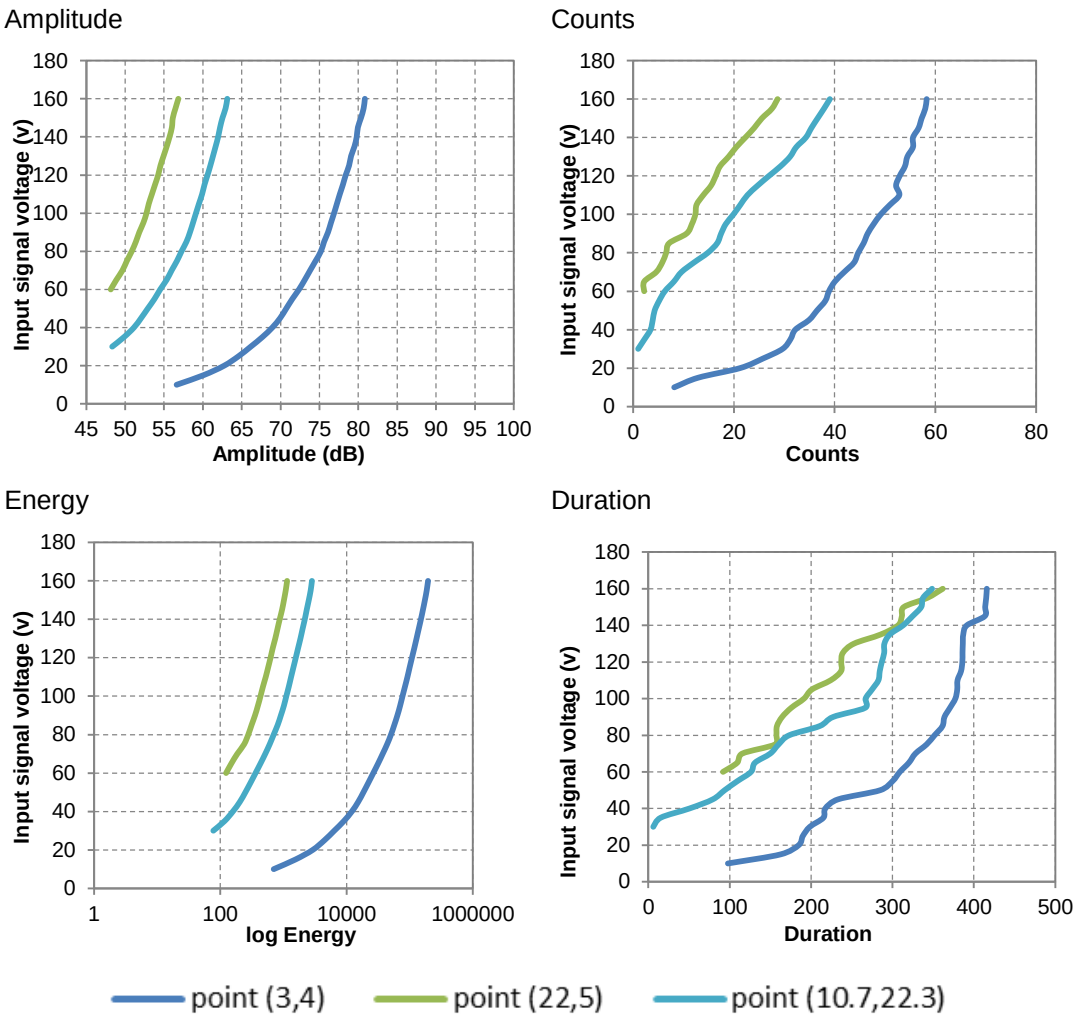

Figure 4-12. Different locations traditional parameters relationship with the input pulse voltage recorded by sensor 1 generated from same source

- ***Validation Approach:***

In order to validate and assess the performance of the parameter correction methodology, a validation test was performed on different types of artificial sources. This used artificial signals with varying width and shape to represent different source types. The sources were selected to make characterisation as follows; Firstly between signals with different source amplitudes but similar in waveform and signal width; Secondly, between two sources with different waveform signals but similar in input amplitude and frequency; Thirdly, between three similar waveform sources with similar amplitude but with different frequencies. The source details are shown in Table 4-2. Six arbitrary positions were chosen to conduct this investigation and at each position each source type

was repeated five times to reduce the error. The position of each testing point is labelled during the rest of this work according to the information provided in Table 4-3.

Table 4-2. Artificial sources details

The source code	001	002	003	007	009	010
Pulse name (waveform)	Sine wave	Sine wave	Sine wave	Saw tooth	Saw tooth	Saw tooth
Wave envelop	Sine curve	Sine curve	Sine curve	Sine curve	Sine curve	Sine curve
Frequency (kHz)	300	300	300	300	200	100
Cycle	1	1	1	1	1	1
Amplitude (V)	50	100	150	100	100	100

Table 4-3. The point number and its location on the specimen

Point number	**X (mm)**	**Y (mm)**
From 1 to 5	75	275
From 6 to 10	75	60
From 11 to 15	150	140
From 16 to 20	75	175
From 21 to 25	0	200
From 26 to 30	150	300

For each generated source the AE signal parameters were recorded by the sensors. Furthermore, the source locations were located using the DTM technique.

The actual and calculated location of each source is presented in Figure 4-13. In order to assess the DTM technique result accuracy, the average location error (the Euclidian distance between the actual source position and the calculated source position for the six arbitrary source locations) of all the signals was calculated to be 6.6mm and the standard deviation of the average location error was found to be 5.7mm. The average location error between the actual and calculated locations of each of signal sources is presented in Figure 4-14. The error bars in the figure represent 1 standard deviation above and below the average location error.

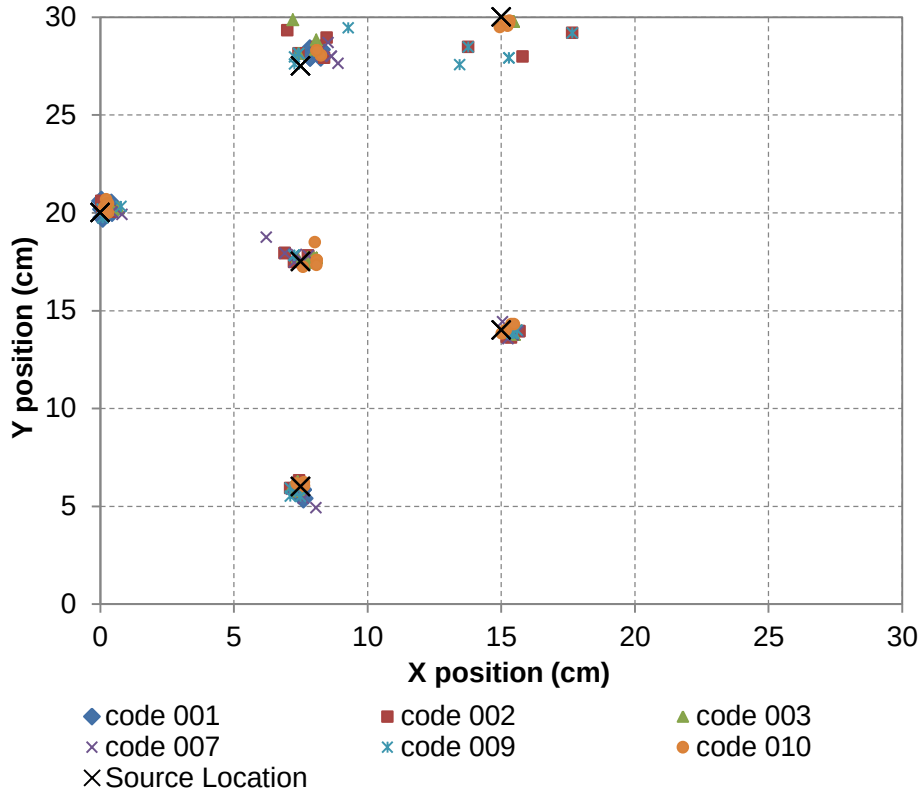

Figure 4-13. The actual and the calculated location using DTM technique

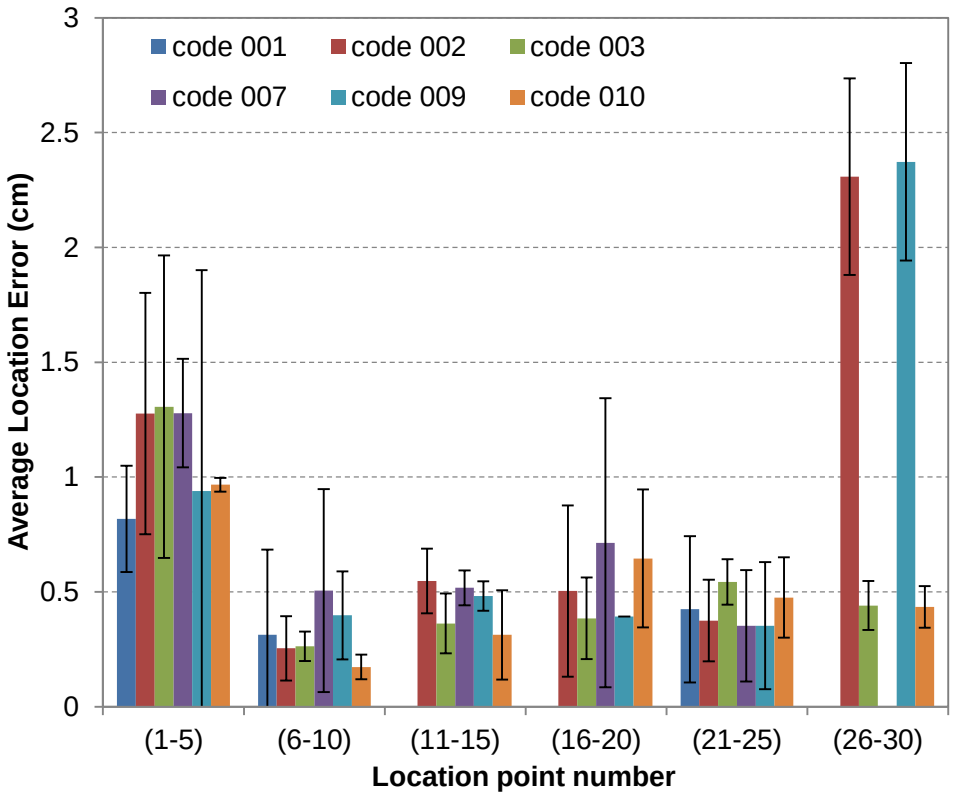

Figure 4-14 Average location error from different locations

For each located event, the traditional parameters relationships with the input pulse voltage in the PCT maps were identified. From these relationships the corrected parameter values for each event were calculated. To assess the performance of the PCT, a comparison was made between the traditional and the corrected parameters for the three tests. For the first test only, the comparison was made between the traditional parameters from the five sensors and the corrected parameters using the PCT results. The comparison is presented in Figures 4-15, Figure 4-16, Figure 4-17 and Figure 4-18 for the amplitude, count, energy and duration, respectively.

For the second and the third test, the same comparison was made between the traditional and the corrected parameters. In order to reduce the number of plots and the repetition, here sensor 1 data only was selected arbitrarily to use in the comparison with the PCT result, where similar results were achieved when the remaining sensors data is used. Figure 4-19 and Figure 4-20 show comparison between the four traditional parameters recoded via sensor 1 (plots on the left hand) versus the corrected parameters result from the PCT (plots on the right hand).

In all the figures the x-axis (Point Number) presents the source generation position on the specimen (Table 4-3). It is clear that the traditional parameters of the same source type are presented in different levels depend on the location of source generation. For example, in Figure 4-15 the source of type Code 003 was recorded at amplitude of 73.5 dB using sensor 1 when generated on the point (75, 60)mm, but the same source recorded using the same sensor at amplitude of 49.8 dB when generated on the point (150, 300)mm. The same behaviour can be noted for the rest of the positions for this source and for the other sources. It is clear that the propagation path features (signal attenuation, reflections, superposition, etc.) have a massive impact on the recorded signal parameters. Using these traditional parameters to identify the source type seems to be a very difficult challenge. Furthermore, it is clear that the same source from the same position is recorded at a different value depending on the used sensor. For example, in Figure 4-15 the source Code 003 recoded via sensor 2 at amplitude 73.8 dB and via sensor 4 at amplitude 49 dB when they generated from the same source position (75, 275) mm. The same behaviour is noted for the other traditional parameters (energy, count and duration) for all tests. This is expected

to be due the different transfer function for each sensor which makes source identification using more than one sensor data unacceptable.

If the figures Figure 4-15 to Figure 4-20 are presented using unlabelled data it will be more difficult to find common features between traditional parameters to identify each source separately. The corrected traditional parameters using the PCT are presented in the same figures. For example, in Figure 4-15 the corrected amplitude of each source is presented at almost the same level although they were generated at different positions on the specimen, demonstrating a significant improvement. The fluctuation in the PCT results is related to a number of sources of error. The largest error is considered to be due to the location accuracy and another potential source of error is that related to human manipulation (including accurate positioning of the artificial source and the level of coupling).

From these figures Figure 4-15 to Figure 4-20 it can be clearly concluded that using the signal parameter plots of the traditional parameters is completely misleading for source characterisation in large or complex structures. Each sensor records data with different levels depending on the source features and the signal propagation path features. As a result of that, using the traditional parameters for damage characterisation is a challenge. On the other hand the new technique, PCT, corrects the recorded parameters and provides an acceptable level for damage characterisation even by using single parameter plot. Here using the corrected parameters as an input in any simple or complicated analysis for identification between different sources will supply more confidence due to the significant improvement that observed from the PCT result. The figures presented demonstrate many significant and promising findings. Firstly, there is great discernible difference between the traditional parameter values from the different source locations. On the other hand, the traditional parameters were recorded with different values depending on the propagation path of each signal. Secondly, traditional parameters are limited and give unreliable results if they are used to distinguish between different source mechanisms in large-scale or complex geometry structures. Thirdly, it can be clearly seen that the PCT results provide a significant improvement in correcting the recorded parameter value. The corrected parameters eliminate all propagation effects on the recorded parameters.

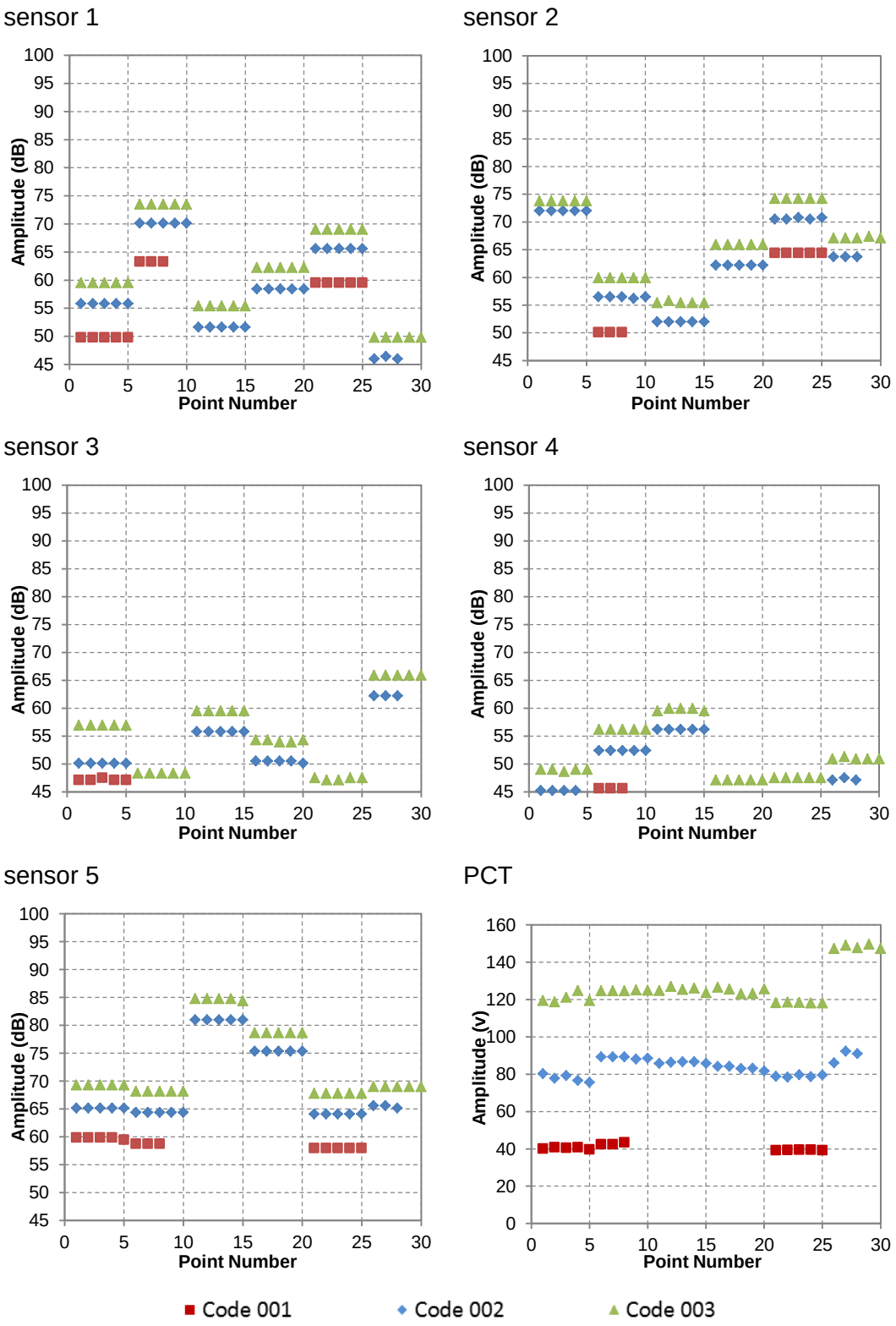

Figure 4-15. First test, comparison between the traditional amplitude values and the corrected amplitude using the PCT

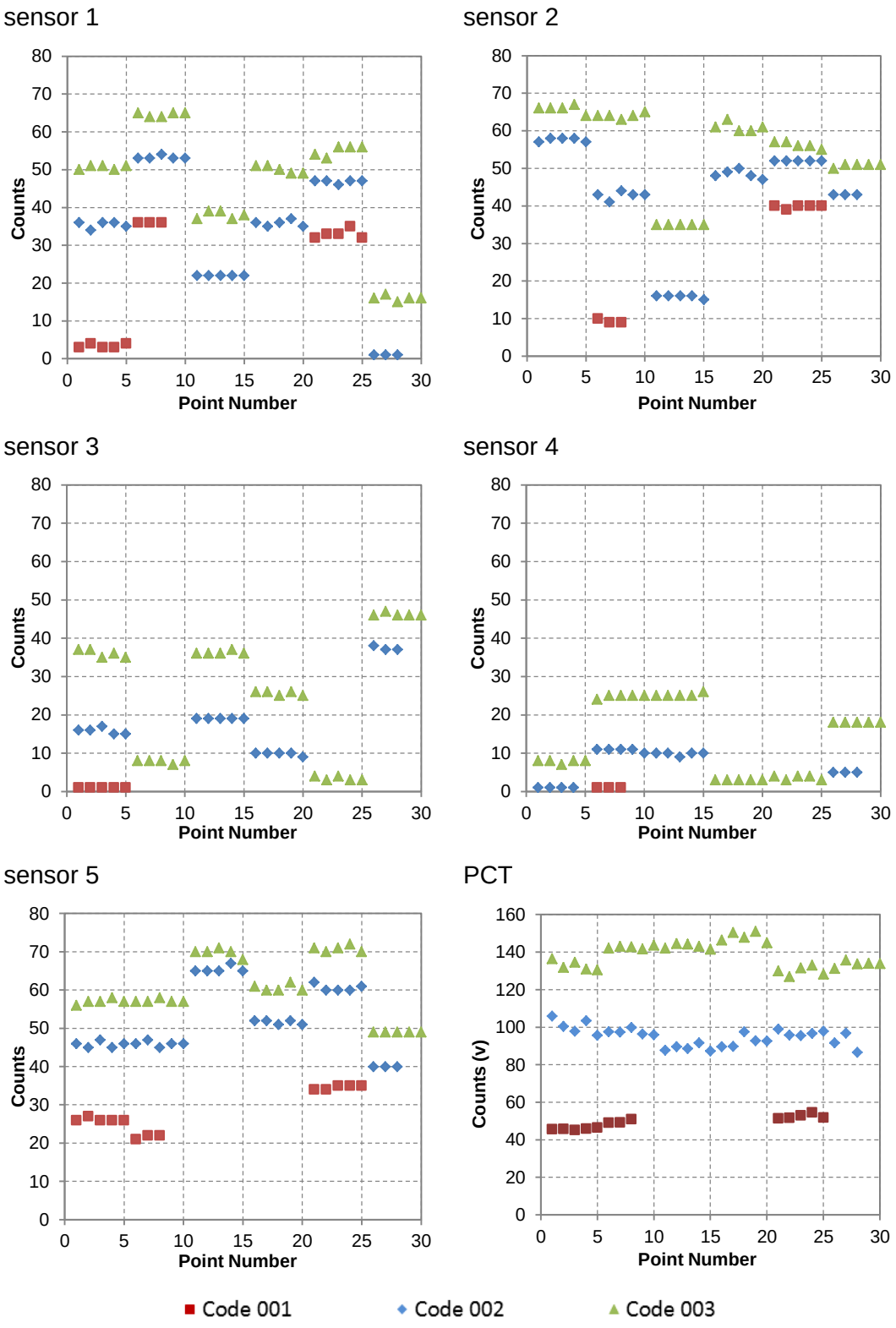

Figure 4-16. First test, comparison between the traditional count values and the corrected count values using the PCT

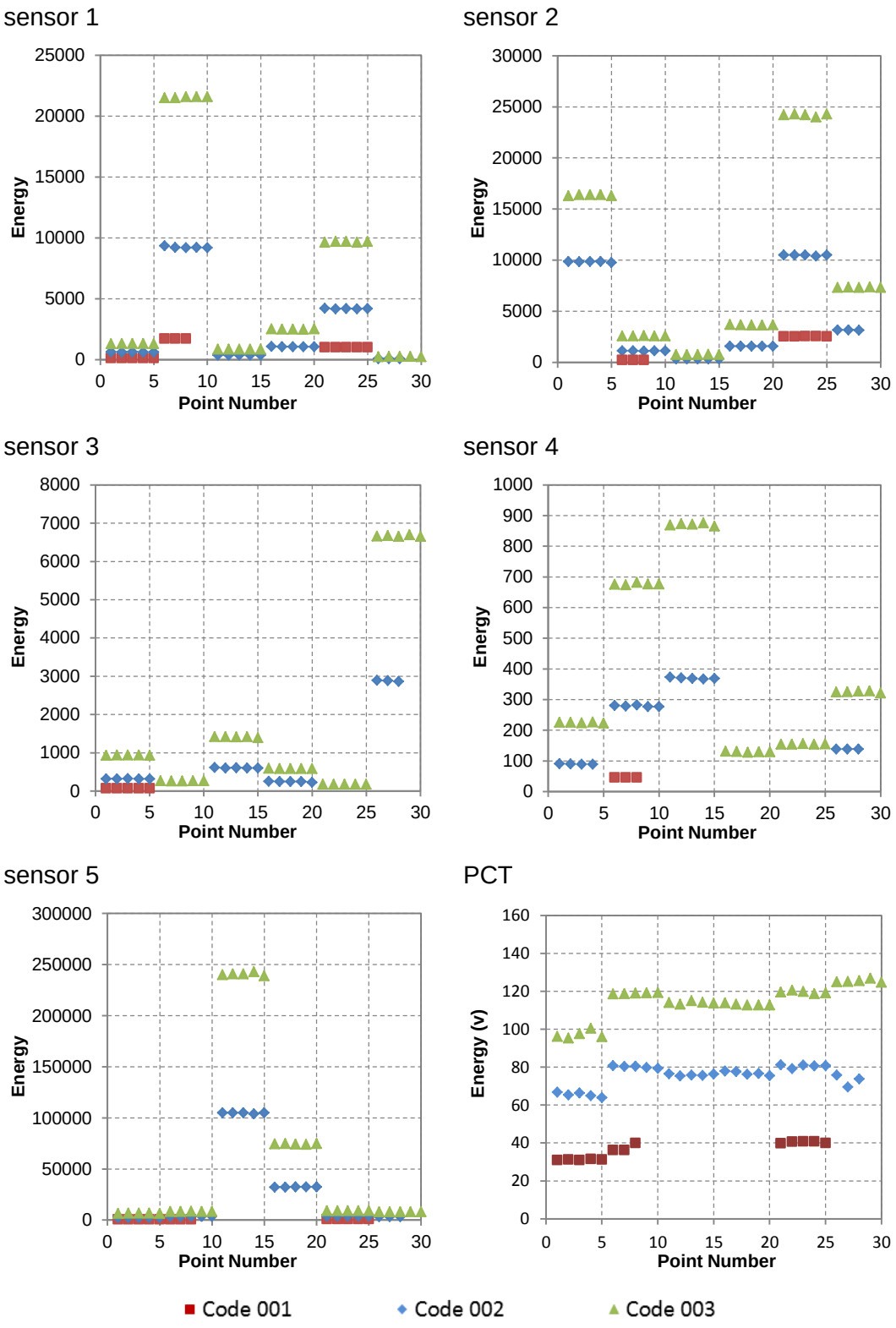

Figure 4-17. First test, comparison between the traditional energy values and the corrected energy values using the PCT

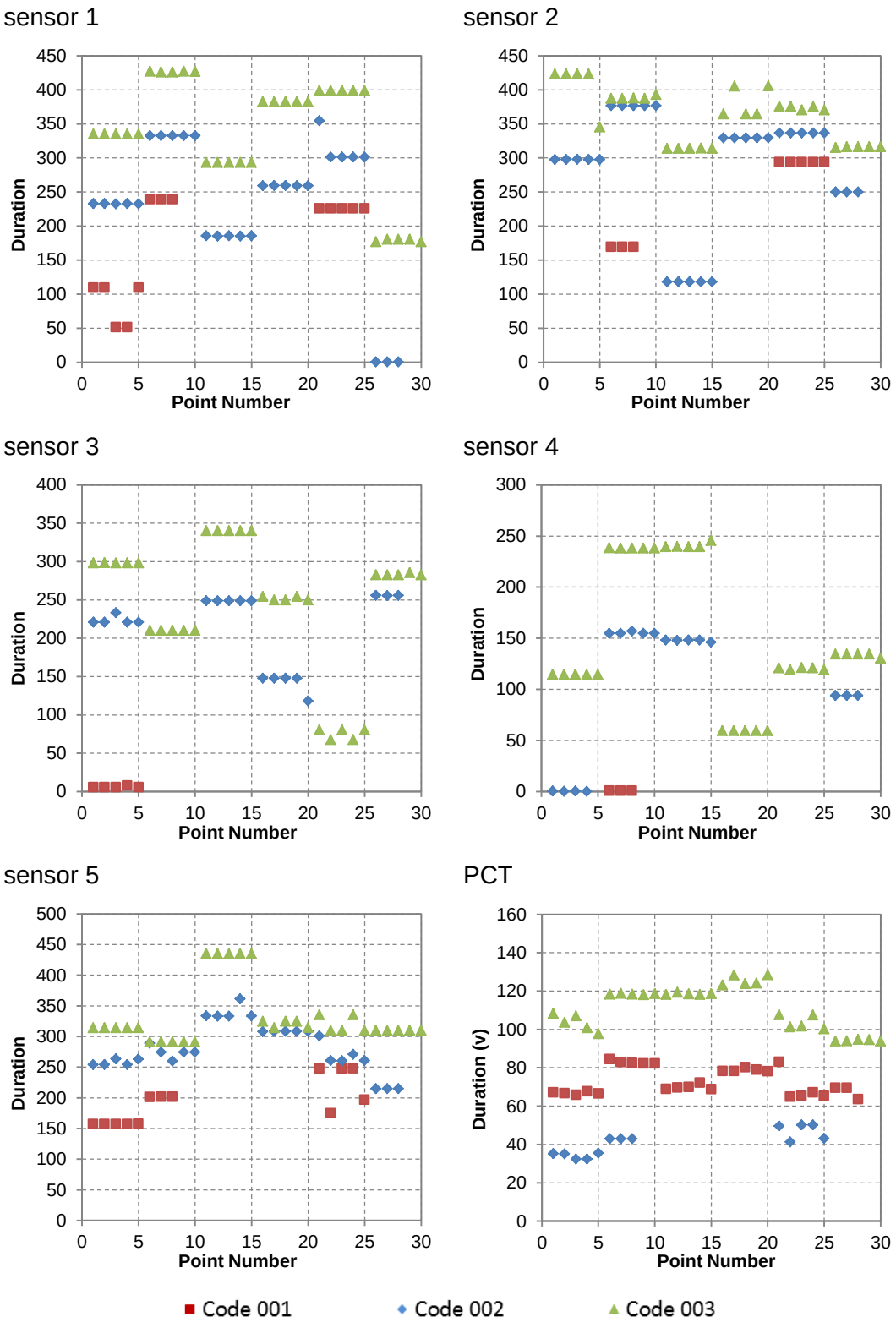

Figure 4-18. First test, comparison between the traditional duration values and the corrected duration values using the PCT

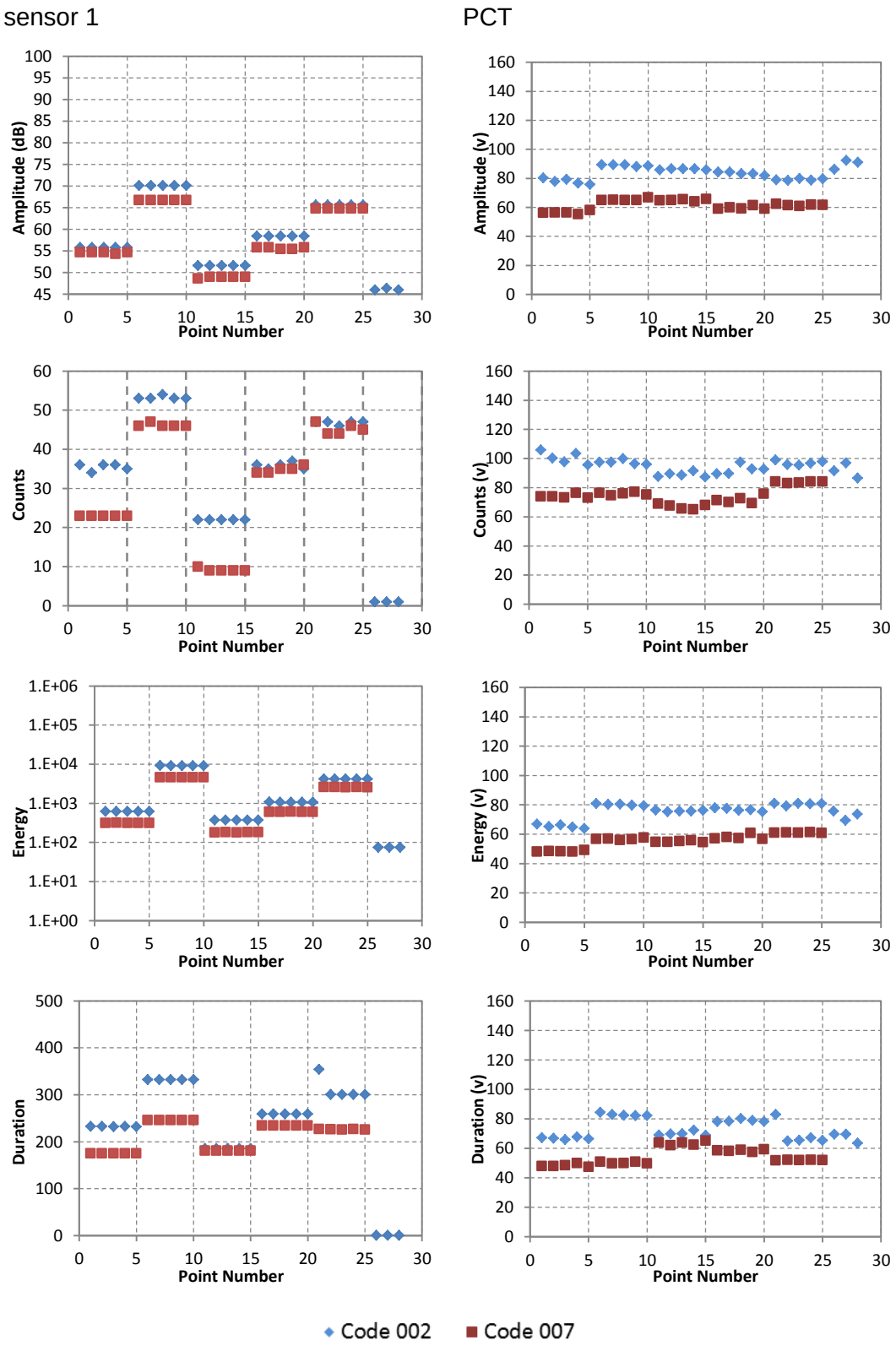

Figure 4-19. Test two: comparison between sensor 1 traditional parameters versus the corrected parameters

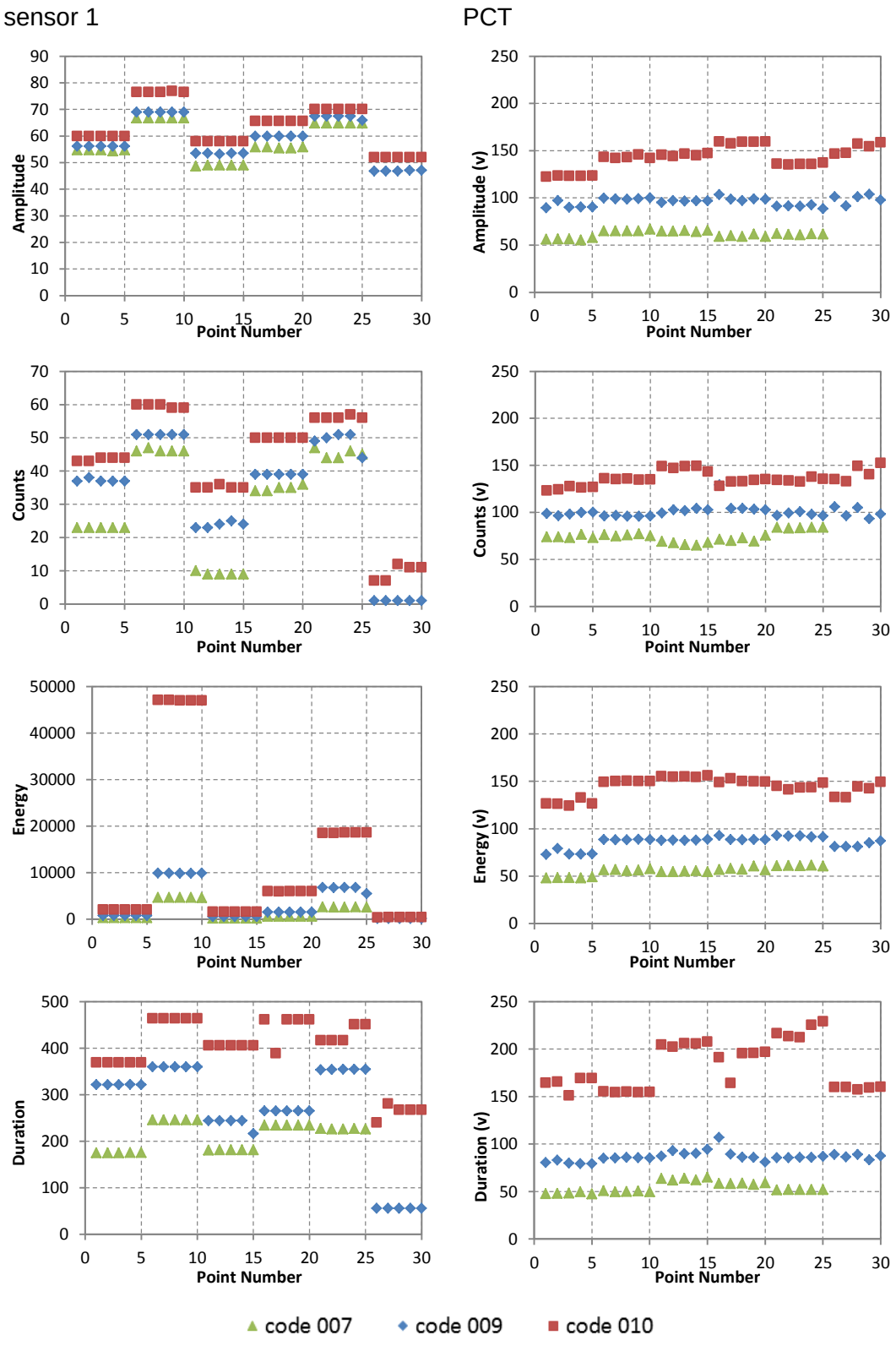

Figure 4-20. Test three: comparison between sensor 1 traditional parameters versus the corrected parameters

In addition to the substantial improvement achieved by correcting the AE parameters, it is worth highlighting another important advantage of the PCT. Due to use of data from all sensors, the PCT shows clear separation between different sources in the corrected parameters; this separation is not always clear when using traditional parameters recorded by one sensor. For example, in test two, the amplitude values of the two sources at location (75, 275) mm have approximately the same value (55.8 dB and 54.3 dB for sine wave and saw tooth sources, respectively) as presented in Figure 4-19. On the other hand, clear separation was accomplished in the PCT results in the same figure. The reason behind that, as noted earlier, is that the PCT calculates each event parameter value based on data from all sensors which recorded that event. Before this advance, source characterisation analysis has only been performed using only one sensor out of many sensors used in the experimental work. Researchers have not used data from multi sensors in analysis due to each sensor having a different transfer function and to prevent repeat or use of redundant data in the same analysis. The compelling reason to use many sensors in experimental work is to cover all of the specimen or structure area and to improve the AE events location calculations. In the PCT approach all sensors are exploited in a useful way. So, it can be concluded that using data from only one sensor is more challenging for source discrimination and damage identification. With the proposed technique, using data from many sensors makes it possible to improve the accuracy. Moreover, it is worthy of note that another important advantage of using the PCT is that all sensor data is used in the AE analysis. Using data from all sensors in the correction process leads to all the located events being used in the final results and there are no missing AE events. This is seen as a substantial advance over the traditional AE. Usually in medium and large-scale structures, it is difficult to collect all AE activity using one sensor and the operator will chose the sensor with the highest AE quantity to perform the analysis. This means that there is potential to miss AE events in the final analysis if they are located far away from the used sensor. Further investigation was undertaken to highlight this benefit. For example, the code007 source was repeated five times in each position of the six different locations, so ideally there would be 30 events recorded by all sensors. In reality the DTM locates only 25 events as shown in Figure 4-19 and Figure 4-20 because some signals hit less than three sensors

(Baxter et al. 2007). The number of signals hit at each sensor is provided in Table 4-4.

From Table 4-4 it can be seen that the variation in amount of AE data recorded by each sensor depends on the recorded sensor position from the source location. For example, if the traditional analysis was conducted using data from sensor 3 or sensor 4 that would mean losing 40% and 60% of the located AE activity, respectively. It can therefore be concluded that using the traditional parameters of data from one sensor to analyse AE data is limited in large-scale structures. In contrast, the PCT is able to use data from all sensors, as listed in Table 4-4 to correct the parameters, meaning there are no missing located AE events and that is considered as a significant improvement in this AE analytical approach.

Table 4-4. Sensors response of the Code007 source signals from six locations

Sensor No.	Number of signals detected	% of located data
1	25	100
2	25	100
3	15	60
4	10	40
5	25	100
The PCT	25	100

- ***Correlation Plots:***

For the detection and potentially the characterisation of damage, correlation plots are used extensively in classic AE testing. An assessment was performed using correlation plots between the parameters to distinguish between different sources. Ideally, the plots would group the AE data points based on their mutual similarity. Amplitude versus duration is a commonly used plot. For the traditional parameters, sensor 1 data was used in cases where the same behaviour was noted using the data from the remaining sensors. The comparison between correlation plots plotted using the traditional parameters recorded by sensor 1 and the PCT result is presented in Figure 4-21. From the figure it can be clearly seen that in the first case of using the traditional parameters plots the separation did not perform very well between the different source types and there is a

random distribution of the different signal sources. In contrast the PCT corrected parameter plots show significant improvement and separate the different sources types well from each other in separated clusters.

This demonstrates that in large or complex composite structures, the use of correlation plots of the traditional parameters to distinguish between different failures mechanisms is very difficult. On the other hand, corrected parameter correlation plots are sufficient to distinguish between different damage mechanisms.

sensor 1 PCT

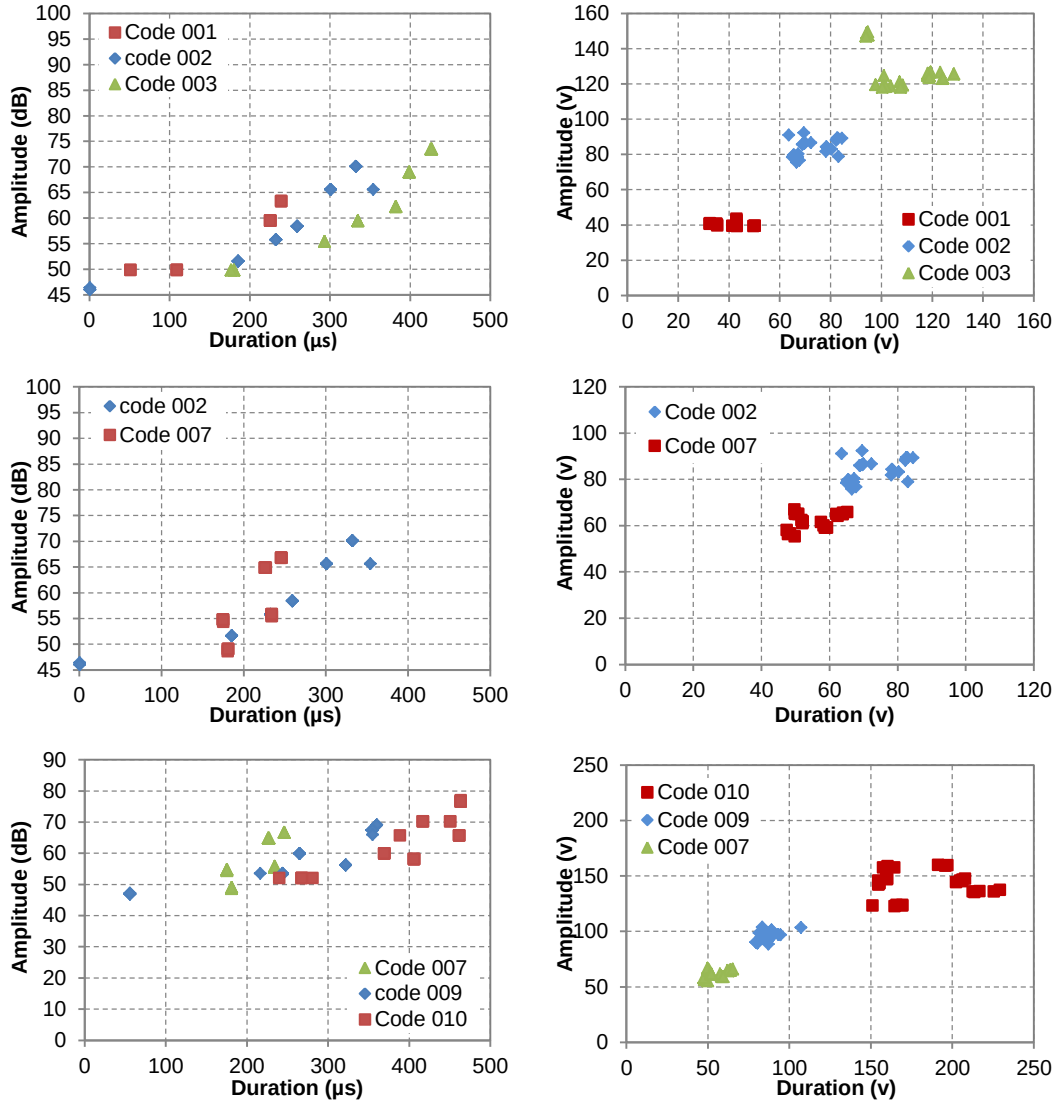

Figure 4-21. Correlation plots using traditional parameters (sensor 1) and the corrected parameters using the PCT

- ***Classification results:***

This part of the study investigates the performance of the PCT on the source identification process using multivariate statistical techniques for classification and visualisation. Two cases were performed. The first (Case-1) was performed using traditional parameters (recorded using sensor 1), while the second (Case-2) was performed using the corrected parameters. In each case, a data set of 71 labelled signals was used as an input vector and consisted of three different amplitude sources, namely, code001 (18.31% of signals), code002 (39.44% of signals) and code003 (42.25% of signals). These sources were previously detailed in Table 4-2.

The optimal classes number was calculated (using the procedure presented in 4.2.2), normalised to their maximum values and presented in Figure 4-22. According to the clustering quality criterion values, optimal classes number for the Case-1 was calculated to be six and ten using the Silhouette (Rousseeuw 1987) and Davies-Bouldin (David and Donald 1979) criteria, respectively, demonstrating poor accuracy when using traditional AE features. From the figure it can be clearly seen that the optimal classes number doesn't refer to the actual number of sources types and that misleads the clustering process in advance. For Case-2 the optimum classes number was calculated to be three using both criteria, highlighting the improvement when using corrected parameters. However, because the number of sources is known to be three, the unsupervised clustering procedure was performed with three classes in both cases to ensure fair comparison of their classification performance. The signals were then clustered into the three classes using the *k*-means algorithm and identified as Class-1, Class-2 and Class-3 for the next stage of analysis.

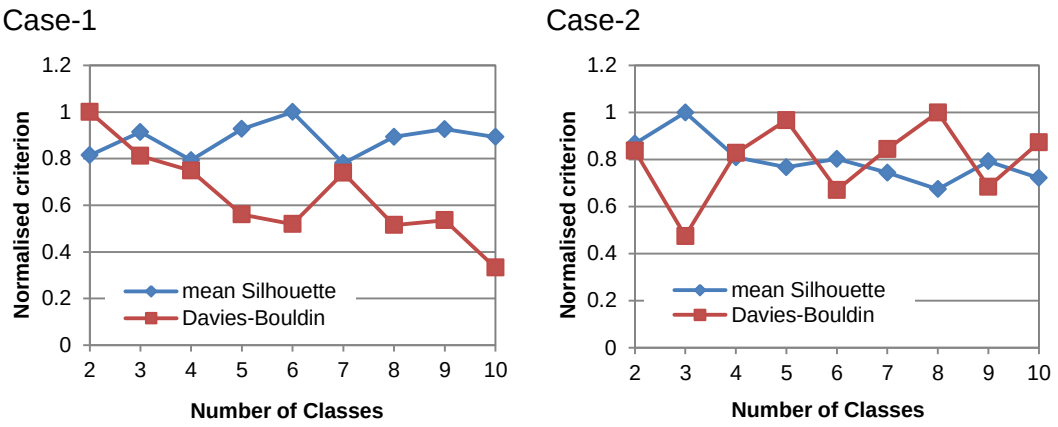

Figure 4-22. The clustering quality criterion values for the two cases.

In order to confirm this cluster classification, visualisation of class separation using the PCA was performed using the same input data set as used in the clustering process. Figure 4-23a and b presents the PCA visualisation of the clustering result projected in a score plot for PC1 versus PC2 for the both cases. Three sizeable clusters which are well separated with no overlap between them is the key point to note from this figure. Furthermore, the percentage indicates the variance in the principal component, showing that the variability of data in only the PC1 is roughly 86% and 96% for Case-1 and Case-2, respectively. That means the four dimensions of the original data are well separated already on one dimension and that results in a huge amount of variance of the original data being captured by the first component. This is strong evidence to show that the class elements (signals) have, with high confidence, four features which are different from the other classes' elements. This evidence is impalpable depending only on the clustering method without the simple visualization provided by the PCA. This will support the proposal that the classification result is highly likely to be generated from different sources and the clustering process is seemed to be successful.

It is understood that the successful classification of the AE data should be achieved only when the different source signals separate into different clusters and each class contains only one signal type. This means each one of the three separated classes elements of each case arose from one of the three used sources, Code001, Code002 and Code003. In the present work, the AE signals labels are known in advance. Therefore, the classification class elements were correlated to the original signal sources for validation purposes. It is worth to

point out that without prior knowledge about the signals labels, these three classes identified using the clustering method in each case will blindly relate to the different AE activities. For validation purposes, elements of each class are presented with the source type label in the two dimension PCA plot in Figure 4-23c and d. From the figure, the Case-1 results show the three sources signals are shared out amongst the three classes. Each class contains different source signals with varying percentages as presented in Table 4-5. On the other hand, the successful classification was achieved in Case-2 where each source type belongs to only one class. That mean the classifier, *k*-means technique, has accurately classified the AE data into its true classes. It also identified all observations in Class-1 as arising from Code001 source. All those in Class-2 were identified as from Code002 source and all those in Class-3 from Code003 events (Table 4-5).

These results show significant improvement over conventional techniques; the classifier can distinguish between the different AE sources with high accuracy and zero signals were misclassified, due to using the corrected parameters. This is a significant advance towards the goal of using AE as an identification technique between different damage mechanisms in large-scale composite materials components.

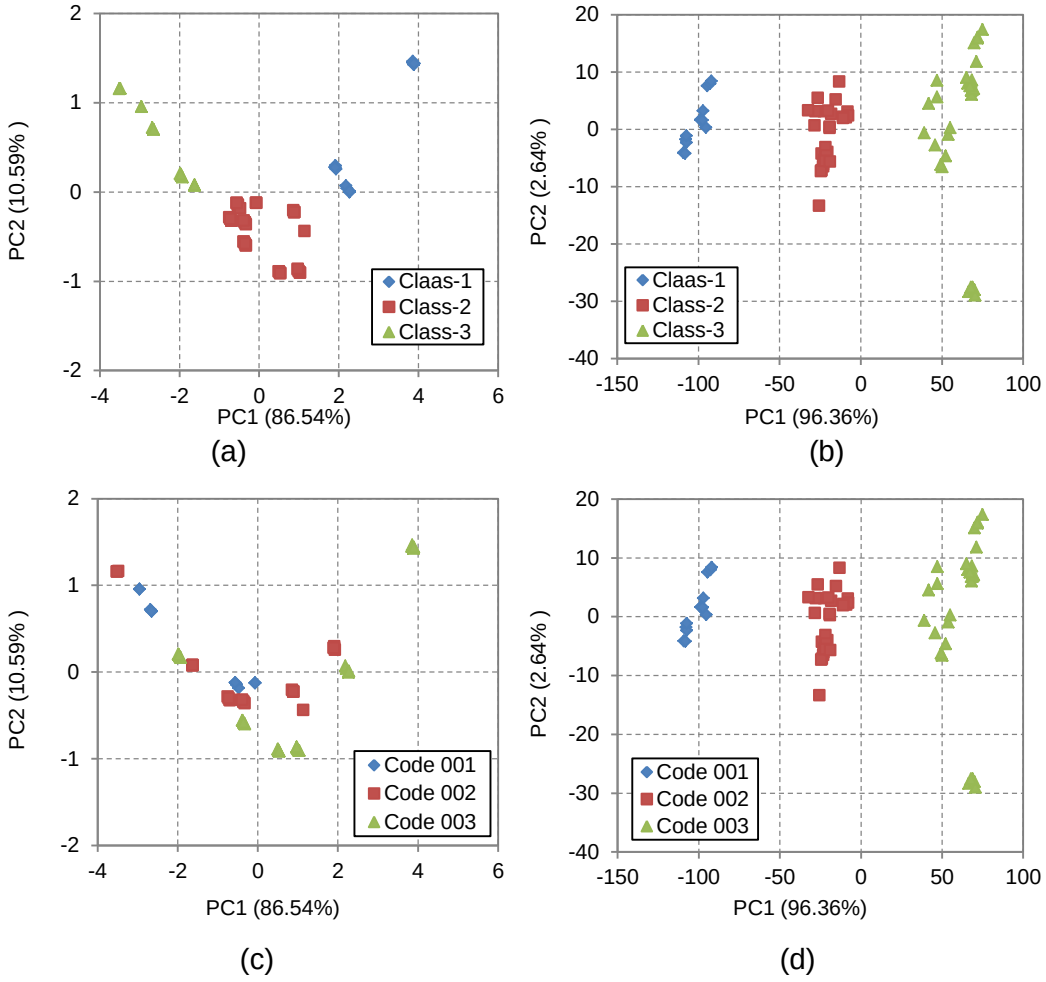

Figure 4-23. The *k*-means clustering results presented using PCA (a) traditional parameters clustering with the class number label (b) corrected parameters clustering with the class number label (c) traditional parameters clustering with the source type label (d) corrected parameters clustering with the source type label

Table 4-5. A summary of the clustering result with each class ingredients.

	Traditional parameters (Case-1)			Corrected parameters (Case-2)		
	Code 001 (%)	Code 002 (%)	Code 003 (%)	Code 001 (%)	Code 002 (%)	Code 003 (%)
class-1	0	33.33	66.67	100	0	0
class-2	21.06	39.47	39.47	0	100	0
class-3	27.78	44.44	27.78	0	0	100

From Figure 4-23c the Case-1 result appears to scatter randomly across the three classes. The important point for consideration is to find the main factor that causes this clustering error. In order to resolve this, the three classes of each case were laid over the DTM location, as presented in Figure 4-24a and b. This figure provides an additional and extremely useful piece of information. From the Case-1 result (Figure 4-24a) it can be concluded that there are two factors that play an important role on the clustering process; the signal propagation path and the source features. So, the three classes were distributed in the following manner. Class-1 corresponds to events recorded as high energy due to low attenuation propagation path or/and high or medium amplitude input sources. Class-2 corresponds to events recorded as medium energy due to medium attenuation propagation path and low/high/medium amplitude input sources. Finally, Class-3 corresponds to events recorded as low energy due to high attenuation propagation path and low/ medium /high amplitude input sources.

From the above, the clustering process using the traditional parameters in large-scale composite structure seems unable to provide correct source identification. This is because, as stated previously, the source signature which carries the signal features changes with path propagation complexity. This weak performance of the classification process is definitely enhanced by the propagation path influence on the signal features.

On the other hand, assignment of clustering results of Case-2, Figure 4-24b, shows that the Parameter Correction Technique (PCT) is able, with high performance, to eliminate all the signals features changes due to the propagation path influences which cause the clustering and identification AE source problems. Therefore, the PCT is a suitable and effective technique to correct the AE parameters and show the original source signature.

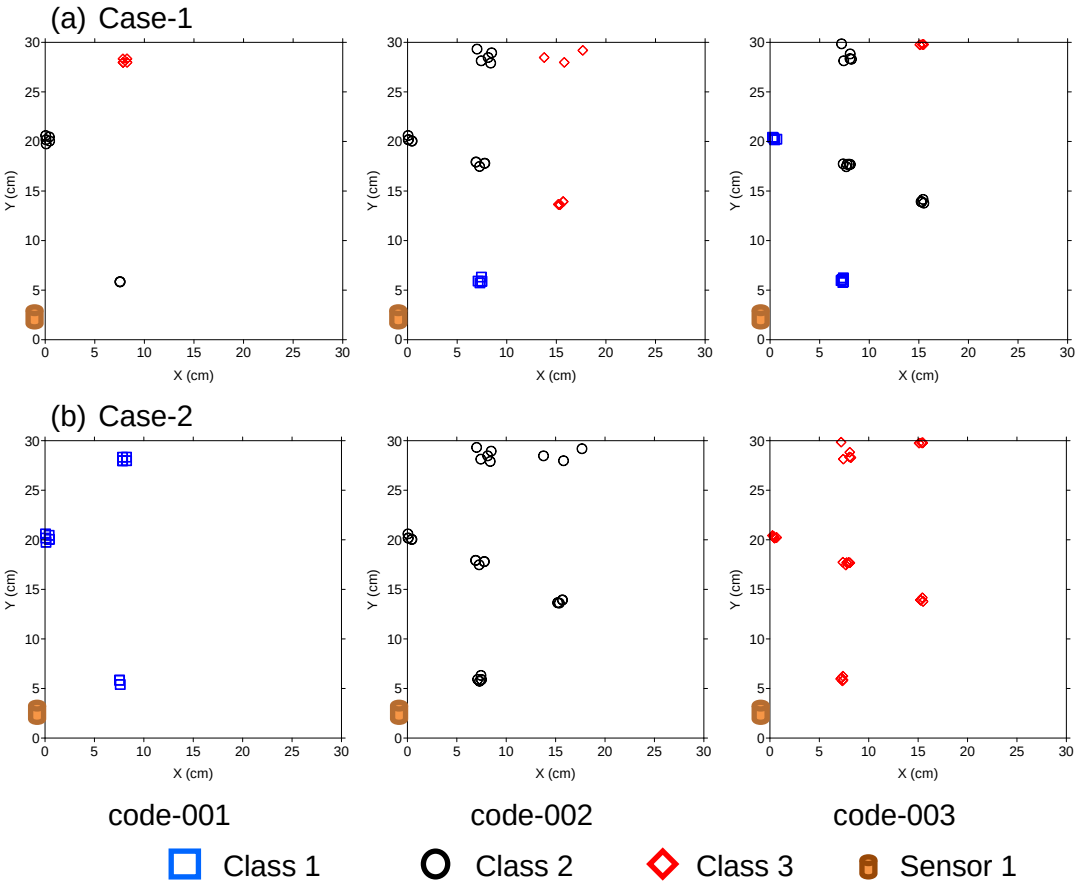

Figure 4-24. The DTM location of each source type with the clustering result label (a) Case-1 (b) Case-2

In summary, many observations are noted as a result of this work. It has been shown that clustering the AE sources depending on the recorded AE data is not an easy and trivial task. Furthermore, the results assist the hypothesis that the clustering process using the traditional parameters cannot provide accurate results in the case of large-scale composite components. That is because the input to the clustering process includes the influence of propagation path influences. On the other hand, the corrected parameters using the PCT improved the clustering process significantly thereby separating the different signal sources from different locations into separated classes. Therefore, the PCT is considered to be an effective tool to correct the traditional parameters values and overcome the modification of the parameters due to the propagation path influence.

4.3.3 Conclusions:

PCT provides a novel approach for overcoming the problems associated with AE parameters changing in large-scale composite components or complex geometry

structures due to signal propagation path effects. In the present investigation, the new technique was examined using a variety of artificial sources on different locations on a carbon fibre composite specimen. A continual and significant improvement in overall performance/efficiency was achieved in the corrected parameters generated from different amplitude, waveform and frequency sources at different locations. The performance of this technique was seen to be very good. Moreover, the robustness of the approach was assessed for commercial use.

A comparison with traditional parameters was conducted using single parameter analysis, correlation plots and multi-dimensional clustering analysis. The AE data was collected from different AE sources generated on different locations on a unidirectional carbon fibre specimen. Results reveal that the traditional parameters are completely misleading for damage identification in large-scale components. Moreover, an excellent corrected result was obtained using the corrected parameters. The PCT shows the ability to use all sensors data to improve accuracy and avoid losing data. On the basis of this investigation we can state that the PCT gives an important benefit to the identification between different damage mechanisms. These findings show great potential for the use of AE monitoring in SHM of large-scale composite structures as found in aerospace structures and wind turbines.

Including all these factors in one algorithm and correcting the recorded AE data was difficult to achieve in practice and in an automatic and robust fashion. The proposed PCT technique overcomes all detrimental factors and corrects the recorded parameters with a high performance by using the actual path propagation of each signal.

The PCT technique does have some limitations. Firstly, because the AE event location is essential to start the correction of its parameters, only located events can be corrected using the PCT. Secondly, this technique considers each structure as unique and thus it is necessary to generate a unique training map for each specimen or for each area of interest in the structure.

4.4 Validation in Fatigue Test

4.4.1 Experimental Procedure

- ***Test specimen:***

The same carbon fibre specimen as used in the previous test was used in this investigation. Here is some further information about the conducted fatigue test. The applied load is transfered from the testing machine through the specimen using a 20 mm diameter pin. A schematic drawing of the specimen fitting in the tensile machine is shown in Figure 4-25. Furthermore, the test was monitored continuously using the same previous acoustic emission setup, DTM and the PCT.

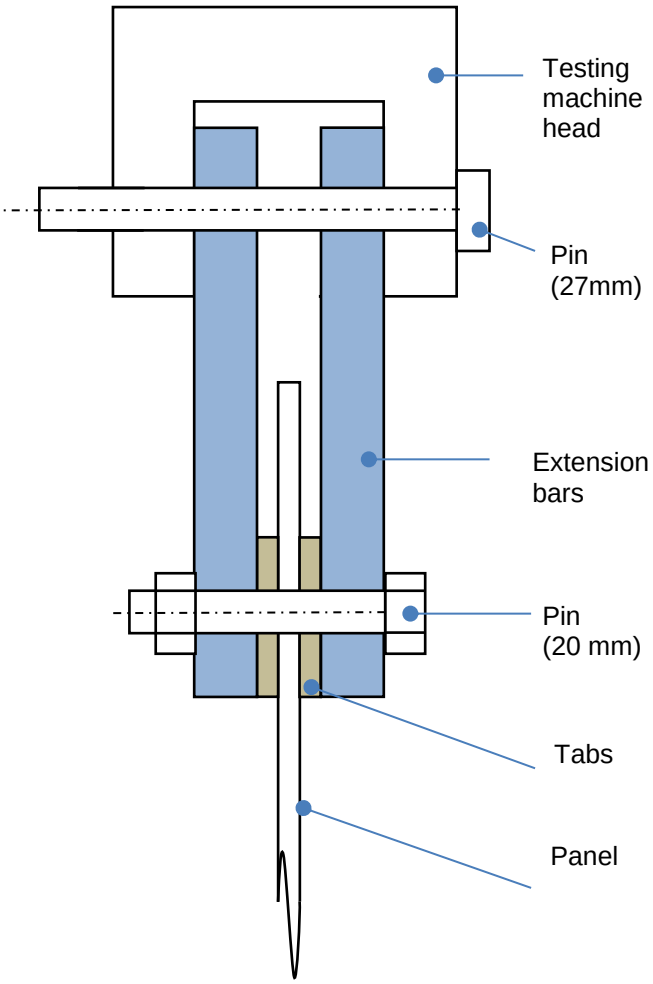

Figure 4-25. Testing panel fitted in the testing machine

- ***Test plan:***

After collecting data from the DTM and PCT grids, the panel was ready for testing. In order to fit the panel in the testing machine, four extension bars (230x60x15mm) were used between the machine and the panel (one pair at each end) (Figure 4-26). These extension bars were connected to the machine using a 27mm diameter pin and to the panel through the tabs hole with a 20mm pin. When the load increased a threaded pin with nut was used. The threaded pin was tightened before starting the test to ensure the friction between the bars and the tab surface was high to improve the load transfer between the machine and the panel. Before starting every part of the test particular care was used to ensure the extension bars are vertical (using a spirit level) at almost zero load and then the threaded pin was tightened again. The panel fitted on the testing machine is presented in Figure 4-26.

The panel was subjected to tension-tension fatigue loading regime with peak load starting at 8 kN at the start of the test until 31 kN at the end of the test. The test was performed in two stages, before impact and after impact, with the details as follow. The test was performed as batches and each one consisted of 5000 cycles at 1Hz each. The load amplitude at each batch was fixed. After each batch the panel was removed from the testing machine and tested using the C-scan in order to discover any new damage in the panel. The applied load for the next batch was dependent on the investigation result on the panel using the C-scan and the AE activity. If there was no or little AE activity observed with no damage evolution from the C-scan image the load was increased, otherwise another batch was made at the same load level. The first stage (before impact) was ended at 21 kN and subsequent C-scan inspection. Table 4-6 contains the batch numbers and the applied load.

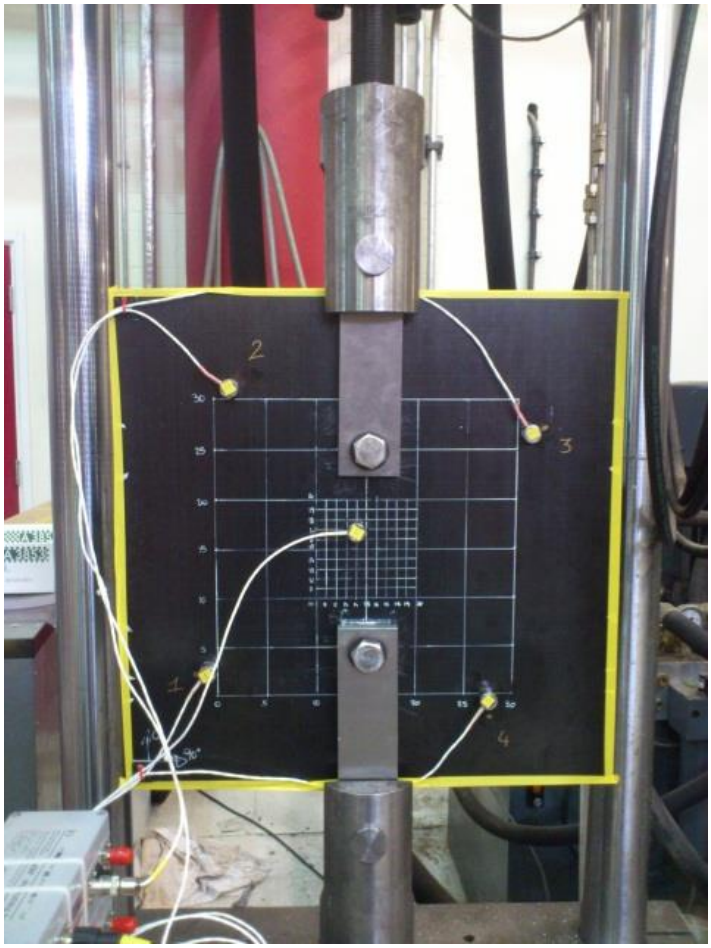

Figure 4-26. The specimen fitted in the tensile machine

Table 4-6 The batch numbers and the applied load for the first stage.

Batch No.	Load (kN)	Batch No.	Load (kN)	Batch No.	Load (kN)
1	8	9-11	12	19	17
2	8	12-13	13	20-21	18
3-5	9	14-16	14	22	19
6-7	10	17	15	23-25	20
8	11	18	16	26	21

The C-scan images after the manufacturing and at the end of the first stage of the test (without impact) are presented in Figure 4-27. It is obvious the dark regions in the images refer to the panel tabs and the sensor number 5 with its cable.

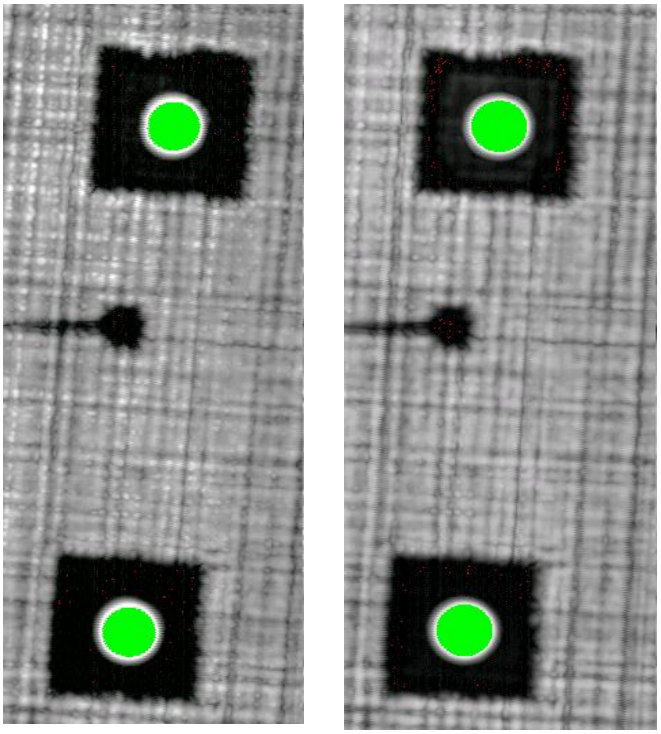

(a) After manufacturing. Before applying the load

(b) Before impact. After batch number 26.

Figure 4-27. C-scan images of the panel after manufacturing and the first stage

During the first stage of the test, AE activity around the artificial crack location was evident. The panel was then prepared to introduce another damage mechanism by impact using an Instron Dynatup 9250HV impact machine at different energy levels (from 5 to 14J). The impact position was selected to be in the loading path between the artificial crack and the lower tab. The panel was fitted in the impact test machine as seen in Figure 4-28. The main purpose was to impact the panel to generate AE activity from a delamination area simultaneously with signals generated from the artificial crack. The C-scan was performed after impact to investigate the delamination area and its result is presented in Figure 4-29. Then the panel was re-tested with the previous loading procedure. Table 4-7 shows the applied batches with the corresponding load of the second stage.

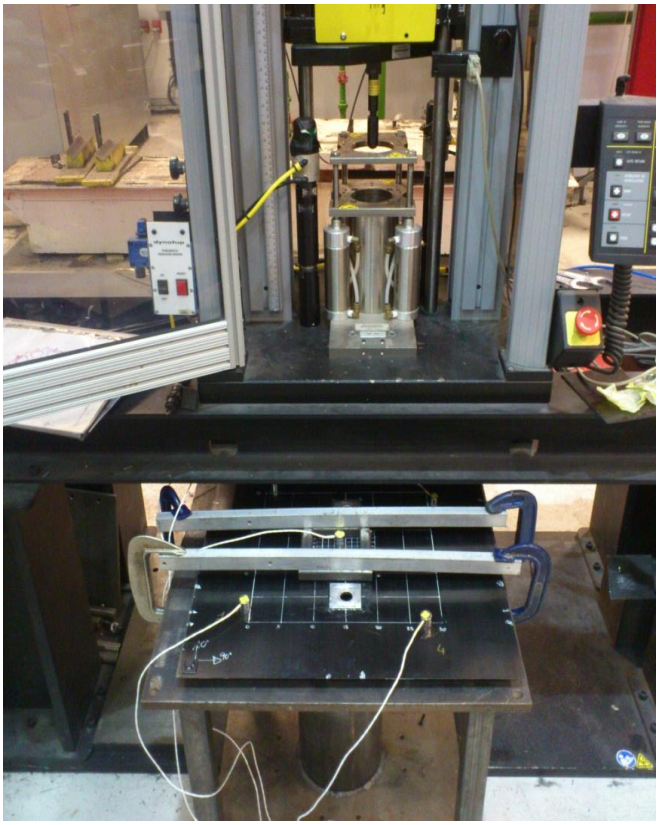

Figure 4-28. The specimen fitted in the impact machine

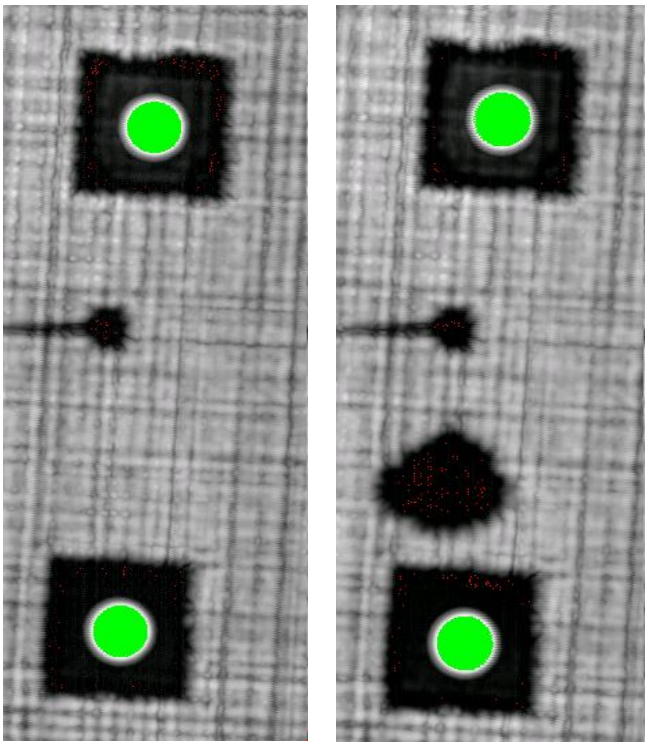

(a) Before impact (b) After impact

Figure 4-29. C-scan images of the panel before and after impact

Table 4-7. The batch numbers and the applied load after impact.

Batch No.	Load (kN)	Batch No.	Load (kN)
1	14	15	24
2	16	16-17	25
3	18	18	26
4-5	19	19-20	27
6	20	21-22	28
7-8	21	23-24	29
9-11	22	25-30	30
12-14	23	31	31

At the end of the second stage the C-scan inspection was performed to investigate any change in the delamination size. Figure 4-30 shows the C-scan images of the panel at the start and the end of the second stage.

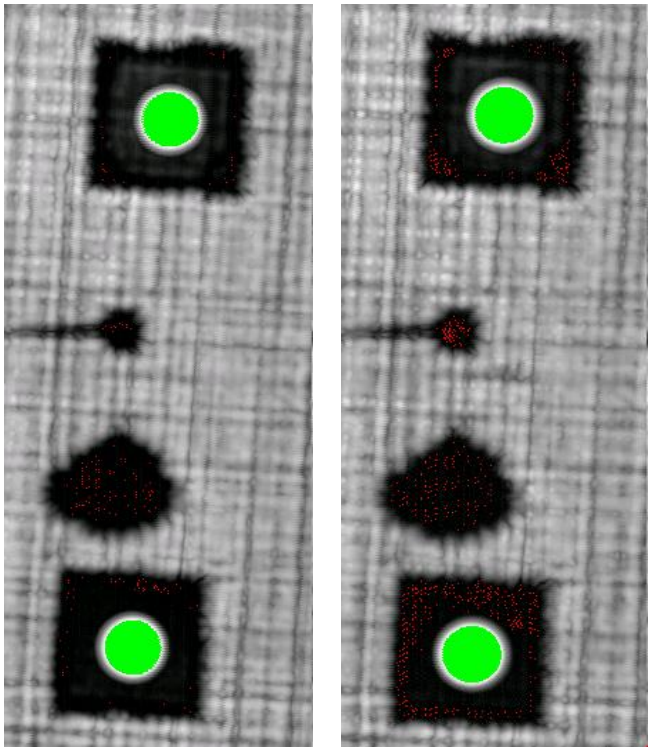

(a) At start of second stage (b) At end of second stage

Figure 4-30. C-scan images of the panel at the start and the end of second stage

4.4.2 Results and discussion

- ***Before impact:***

Visual inspection using naked eye was performed on the panel during the first stage of the test before and after each batch to discover any obvious damage. The inspection results refer to whether any obvious damage was detected.

From the C-scan images in the first stage, it is confirmed that no additional damage has been introduced during the test, no high attenuation (dark) areas are found in the C-scan images (Figure 4-27) which refer to the out of plane discontinuities like delamination. The in-plane crack area which refers to matrix cracking is slightly darker but it is difficult to confirm that using the ultrasonic C-scan.

It should be noted, that the identification of transverse defects, such as matrix cracking, is difficult using both visual and ultrasound C-scan inspection. C-scan inspection is more sensitive to out of plane damage.

AE activity during the first stage was filtered and all the AE signals which hit two sensors or less were removed. The result of the AE source location using the Delta T mapping technique for all AE activity during this stage is presented in Figure 4-31. It is clear that events are clustered quite closely at the tab area on the panel. There is a high intensity region of activity located at the artificial crack. The high AE activity released from the tabs corners a result of cracking in the tabs bond. This was expected during the test because the stress field induced by the fixture is likely to produce a concentration of stresses in these regions. During the test the bolt was used instead of the pin to reduce the amount of activity released from the tabs.

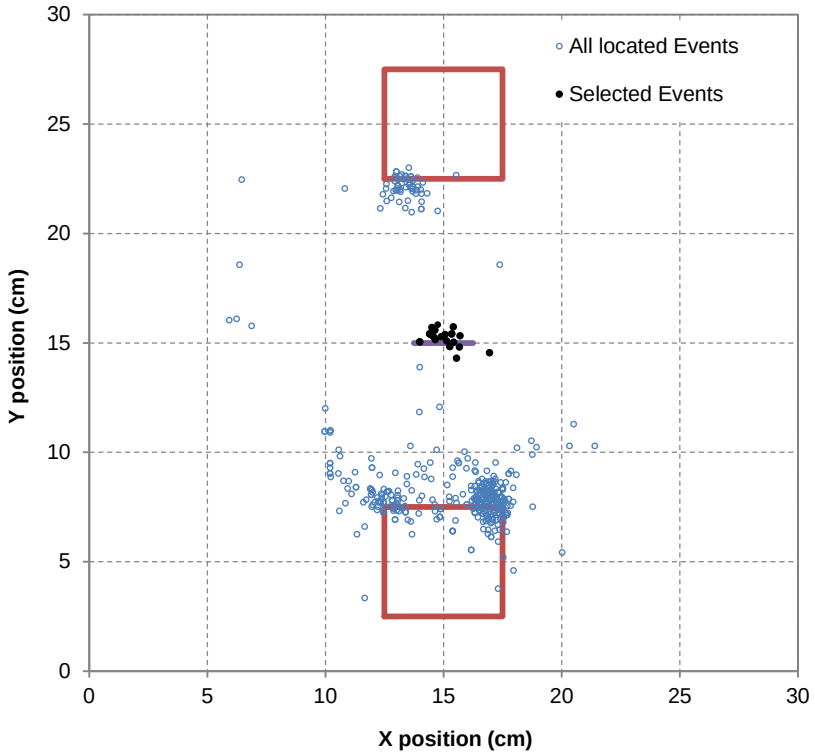

Figure 4-31. The DTM location of AE events before impact.

- ***Post impact:***

The visual inspection was performed during the second stage of the test on the panel to discover any obvious damage. No obvious damage was detected using the visual inspection on the panel. C-scan images at the start and end of the second stage show no obvious increase in the delamination size (Figure 4-30).

The AE activity during the second stage increased significantly in comparison with the first stage due to increasing the applied load and increasing the AE sources (the artificial crack, the delamination area and the tabs bound). The located AE events during the last batch (batch 31) of the second stage are presented in Figure 4-32. High AE activity was located at the upper tab location with very little activity at the lower tab and also in the location of the delamination area. The test was stopped after this batch due to significant AE activity in the delamination area. From the figure there are events separated in the unloaded area. The misallocated events form a low percentage of the total located events. Events located lower than x=100 mm are about 6.6% of the total located events in this set.

It has to be noted that the signals from the artificial crack are lower in number than in the first stage and moved towards the crack tip region. This is a consequence of the fact the stiffness of the crack region has reduced and the stress field increased at the crack sides. This may have led to the release of some AE signals from some damage mechanisms at the crack tip region. In the respect of using the AE as SHM tool, damage localisation and identification, the results highlight AE as a successful method for damage location for reliable SHM systems.

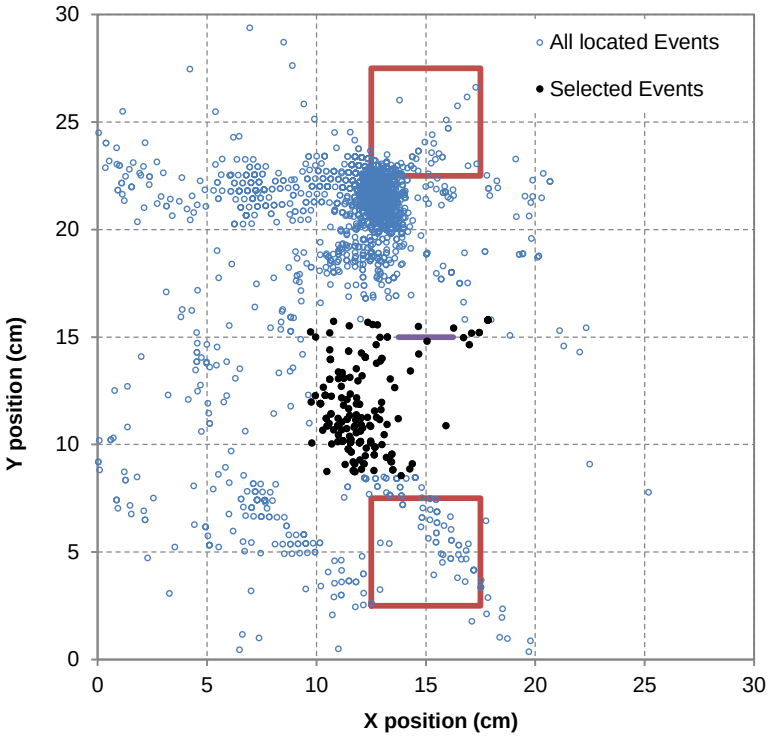

Figure 4-32. The DTM location of the recorded events after impact.

In order to work on damage identification, a focus on the signals from the artificial matrix cracking and the delamination area are considered. The main target of this study was to generate two different mechanisms. The located events before impact were selected for the clustering purpose focussing signals prior to impact and delamination area post impact (Figure 4-31, Figure 4-32).

From the selected located events, the number of events recorded by each sensor was investigated. In most cases of large scale components not all the located signals are recorded using all the used sensors due to the signal attenuation effect. In this case, some events were recorded and located using three or four

sensors. On the other hand, the PCT technique will use all the selected events in the correction process and all these events will appear in the final result of the technique. Figure 4-33 shows the missing located events percentage per sensor out of the total selected events. It can be seen clearly that the highest missing events was occurred with sensor number 5. So, if the sensor in position 5 data was used to perform any analysis that mean losing about 22.6% of the total selected events. This behaviour may be unexpected as sensor 5 is very close to the activity area. The reason may be because this sensor was saturated recording the high activity of AE from all sources in this region (the high and low signals energy) in comparison with the rest of sensors, which would record only the signals which have enough energy to reach them.

This figure highlights the problem of analysis of AE data when depending on only one sensor and how it will lead to a loss of AE activity. On the other hand, the PCT will use all sensors data to correct each located event. So, there is no loss of located events in the corrected data, which is considered as an important advantage for using AE as a damage identifier in large-scale components.

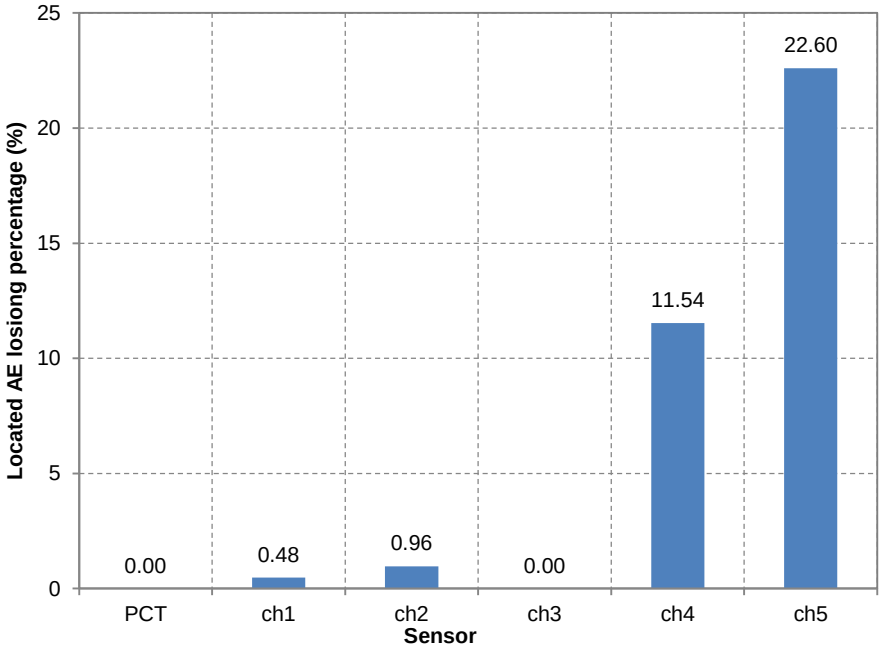

Figure 4-33. Located events losing depend on the used sensor

- ***AE data classification***

The classification analysis is performed in order to discriminate the damage mechanisms. The proposed classification approach was performed for two cases, using traditional AE parameters and using the corrected AE parameters. The input vector to the classifier in each case will be the main four signal features (Amplitude, Energy, Count and Duration). After normalising the traditional features recorded using each one of the five sensors and a recalculation of the AE parameters using the PCT the optimal number of classes was calculated for each case. The optimal number of each case was obtained according to two clustering quality criteria and the results are presented in Figure 4-34.

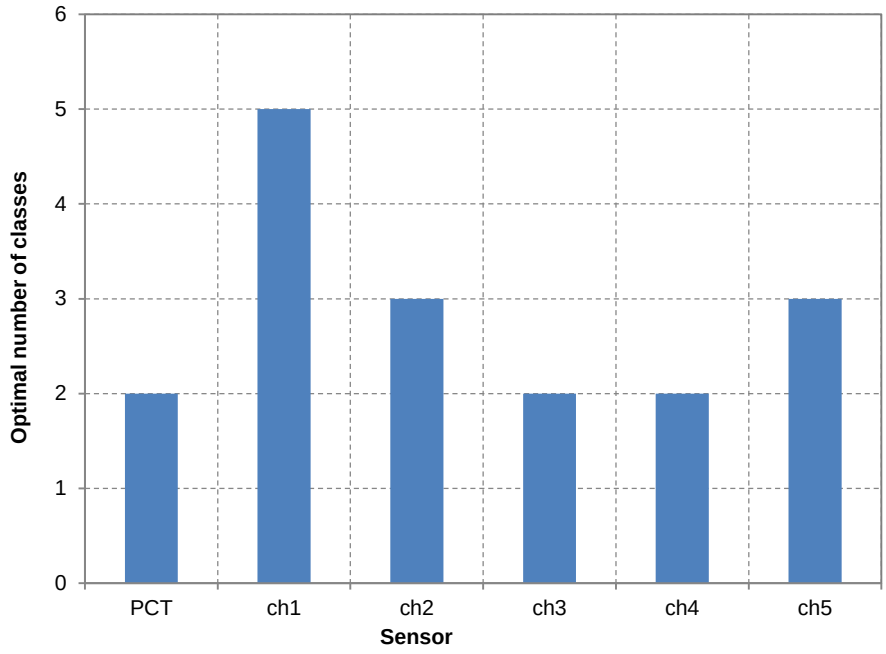

Figure 4-34. The optimal number of classes

The classification using each sensor data was performed. A similar analysis was performed using the corrected data. Figure 4-35 presents the classification result as a percentage of the number of events in each class to the actual numbers of events recorded by the used sensor. From this figure there are two points. Firstly, with using the traditional data it is clearly there is more than one solution depending on which sensor data was used as input to the classifier. One can conclude that, it is difficult to decide which result is correct. Normally the operator will select the sensor with the largest data quantity or the sensor result which corresponds to the expected damage to present the accurate solution.

Secondly, there is a unique solution from using the PCT data as input to the classifier. That will increase the classification result reliability and avoid the operator decision to take a part in the analysis.

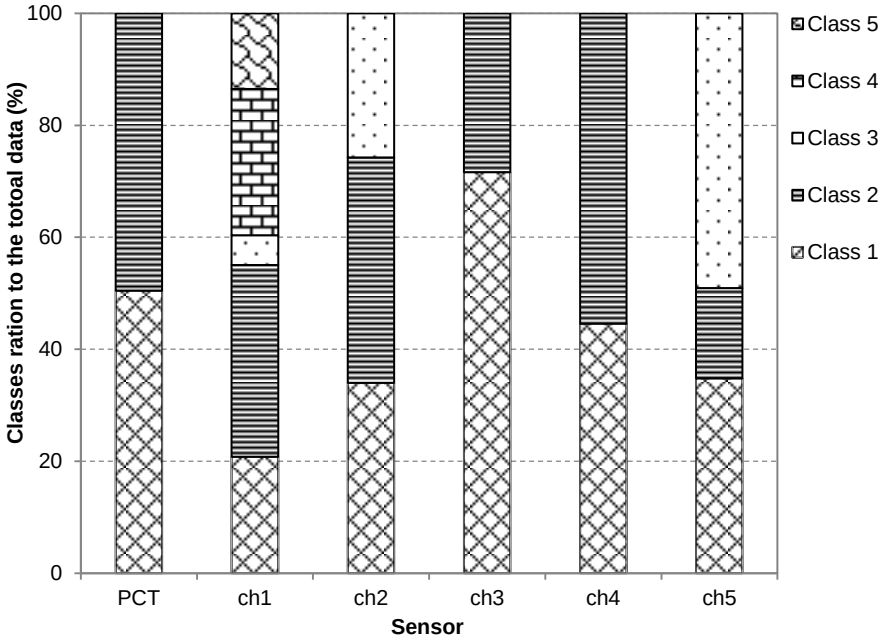

Figure 4-35. The Class percentage for each case

In order to allow a better visualization of the classification results, class location of each case is presented in Figure 4-36. It can be seen from the figure there are many final solutions and the classes location vary depend on the input data to the classifier.

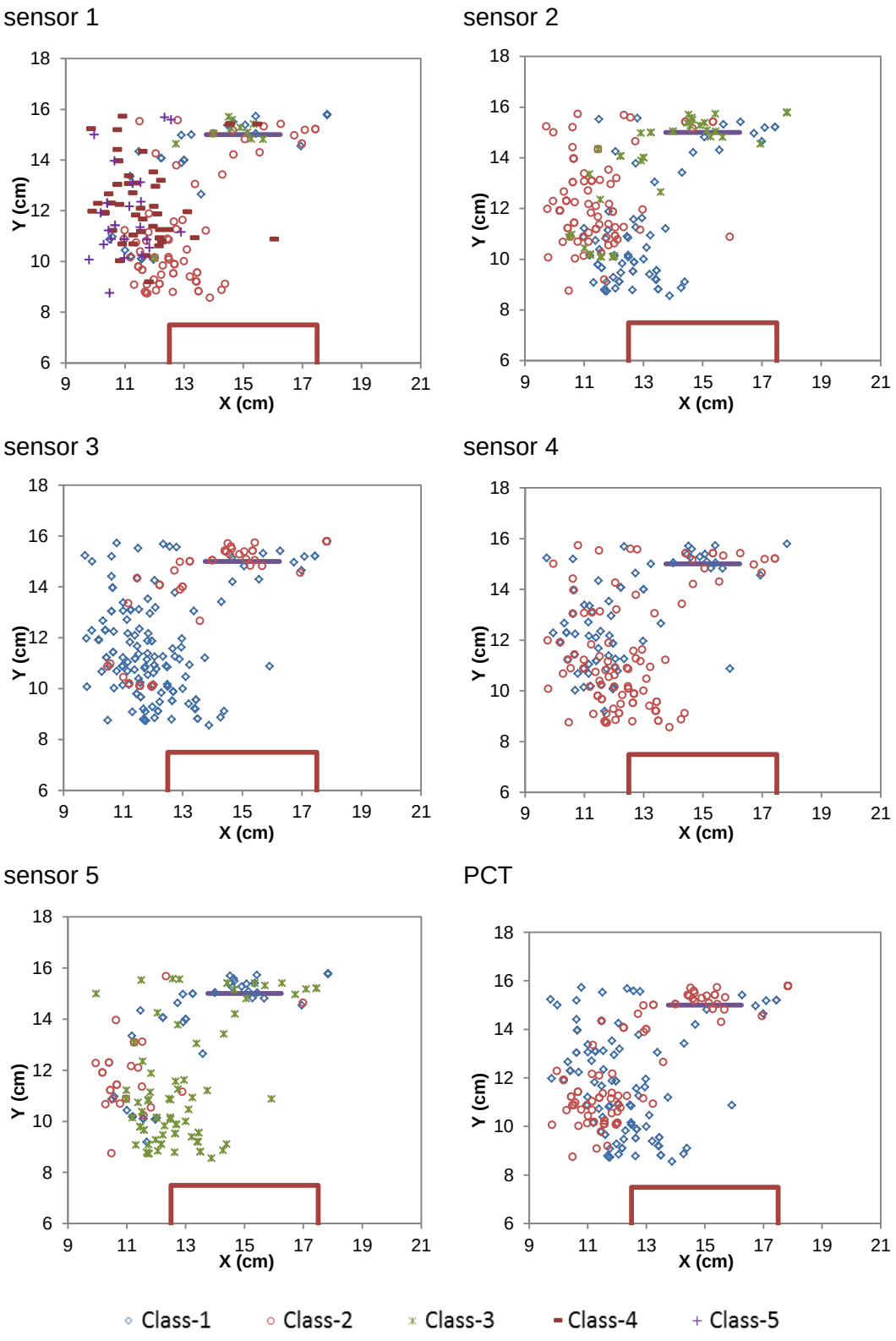

Figure 4-36. The Class location for each case

From reviewing the classification results, it is evident that it is difficult to rely on sensor data to achieve reliable damage classification when the data was collected from different distances from the sensor (Al-Jumaili et al. 2015). This is also supported from the fact that generally using one sensor data will lead to loss of some located AE data and that will reflect negatively on the final result. Furthermore, in the PCT data where the attenuation effect was overcome, it can be clearly seen that the most reliable result is achieved. As a result of that only the PCT result was adopted.

In order to characterise the possible different damage mechanisms which take place in this test, the AE response in this test is generally divided into two parts; the pre-impact stage which corresponds to the located AE activity at the artificial crack region and the post-impact stage which corresponding to the activity at both damage regions (artificial crack and delamination area).

In the pre-impact stage AE was generated from matrix cracking. After matrix cracking the crack is fully developed and a silent AE stage in the artificial crack region starts. Although there are stress concentrations on both crack tips, the pristine plies in the specimen support this area to prevent any further crack propagation and support the structure to prevent any more crack evolution. After locating the AE signals in this region, low energy AE sources, whose signals are unable to reach at least three of the sensors, were generated and recorded using the closest sensor. This situation remains until the end of the first stage. So the matrix cracking is the most dominant damage mechanism in this region as it begins from the weakened region of cutting plies.

The location of the PCT classes as two segments before impact is shown in Figure 4-37. It can be clearly seen that before impact the Class-2 is dominant. It is highly likely Class-2 elements generate from matrix cracking.

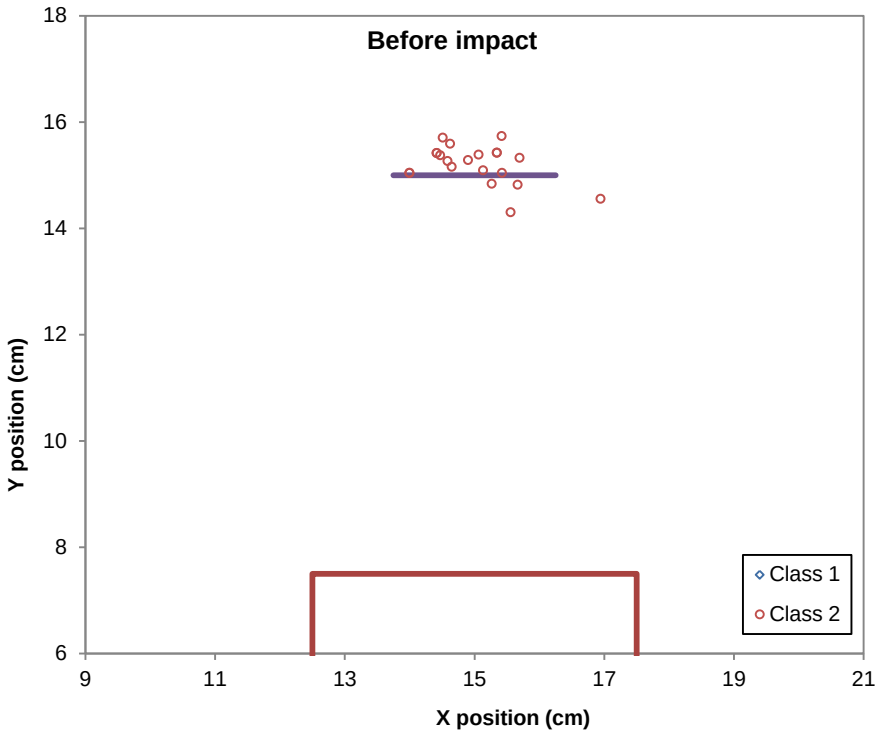

Figure 4-37. DTM locations of the classification results (PCT)

The post impact stage contains two regions of sources, the artificial crack and the delamination area, and the applied load during the fatigue cycles was increased until it reached 31 KN at the final batch. Here one can note that the located events at the crack region were located near the artificial crack tips. That may be due to the fact that when the load is increased the support plies around the crack will suffer from stress concentrations that lead to more damage mechanisms mostly from matrix cracking.

After impact the delamination region became active and there is high AE activity located in the delamination location although there is no clear sign that the delamination grew in size during the test from the c-scan images.

This AE activity is related to two sources. Impact will cause plastic deformation on the specimen surface. When the deformed surface becomes loaded, as in our case, the weakened matrix will crack and generate signals from matrix cracking. This is expected from the impacted area under tension load which generates matrix cracking signals because this area becomes weaker.

The second is due to internal friction generating emission in composites under fatigue. The friction or fretting between the delamination faces can produce substantial AE.

The location of the PCT classes of the after impact segment is shown in Figure 4-38. By matching between the PCT classification result and the located signals after impact, there are two sources of signals associated between the two classes. The signals in the centre of the delamination area belong to Class-2 which correlated to the matrix cracking. The Class-1 separated within the delamination area as expected due to the friction between the delamination surfaces.

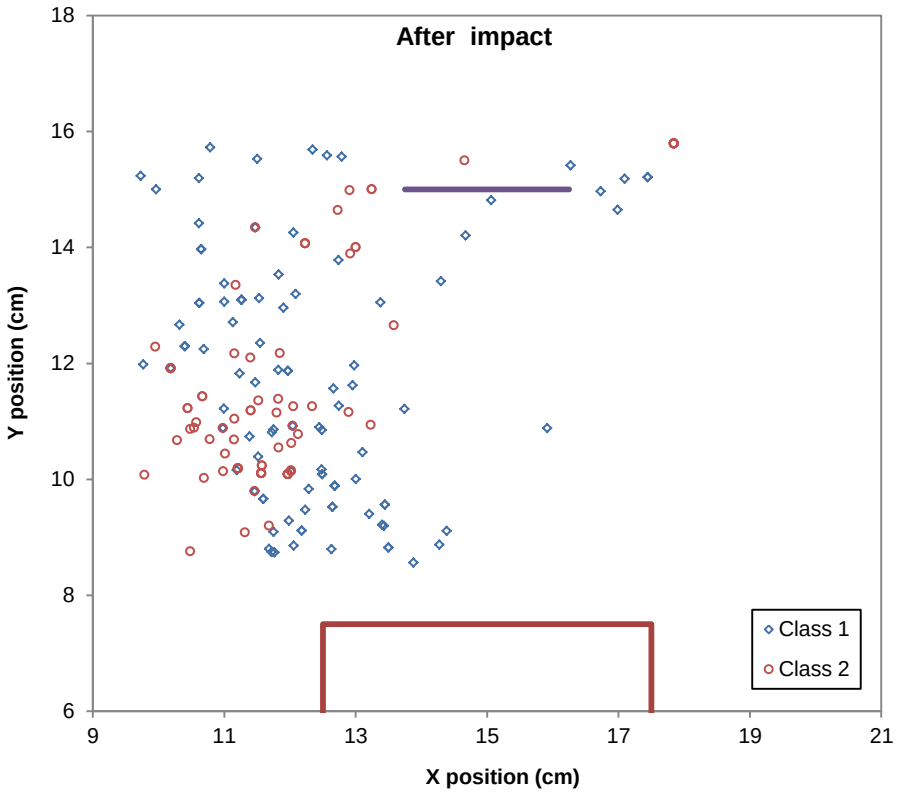

Figure 4-38. DTM locations of the classification results (PCT)

This work shows clearly that the developed methodology allows different source signals to be classified into different groups. The classification result using the corrected data using the PCT provides a more reliable solution. The two class problem leads to classification of the located AE signals into matrix cracking signals and friction signals from the delamination area.

The PCT technique offers great benefit of overcoming the challenge and the difficult task of dealing with the traditional signal parameters for damage identification by eliminating signal propagation from the source to the sensor effects. Furthermore, the PCT solution is unique, while using traditional features leads to many solutions depending on which sensor data is used. Also PCT overcomes the problem of using one sensor data in the analysis which will lead to loss some of the located events which are undetected using the used sensor. Indeed, using the PCT allows for a drastic enhancing of the interpretation of the measured data and it is suitable for large scale specimens. If this technique is used in real time it offers the possibility of tracing damage mechanism type development automatically at the same time as the location is determined.

4.4.3 Conclusions:

The main aim of the present work is to use the AE data recorded from the fatigue test of a composite material panel to identify different source mechanisms. In this experimental work generating two distinct artificial AE signal sources was achieved. The first source related to matrix cracking and the second related to impact induced in-plane delamination. This test was run in two segments, pre-impact and post-impact, and each segment contains different load batches. Subsequent visual inspection on the specimen shows only a barely visible indent at the impact site with no visible damage sign on the artificial crack location. Furthermore, subsequent ultrasonic C-scanning was conducted after each batch in order to track the internal damage evolution. The DTM was used to locate the AE events with high performance.

A fully automated classification technique was applied in order to identify these two different sources and to correctly separate them. The classification was conducted using the traditional AE features and using the corrected AE features using the PCT. The traditional feature classification result was unreliable, highly dependent on the operator decision which makes the classification process not fully automatic. Classification results using the corrected features resulted in clusters clearly identifying the most critical damage types. The C-scan results support the proposition that it can detect two different damage mechanisms and these are most likely to be matrix cracking and delamination.

These results highlight the limitation of using the traditional AE features for damage identification in large scale and complex materials; limitations that are

only likely to increase with the application of composite parts with more complex geometry, such as curvatures, holes and ply drops. So, using the recorded AE data from large-scale component for characterisation analysis is a challenging task and the difficulty increases if the structure geometry is complex such as the anisotropic materials.

The results also demonstrate how such limitations can be overcome through using accurate AE features using the advanced technique. The PCT technique is shown to be an effective tool to correct the AE data and compensate for the propagation path influence on the recorded AE data used for discrimination between damage mechanisms. Furthermore, using all sensors allows all the located events to be involved in the final analysis.

4.5 Overall Conclusions

PCT provides a novel approach for correction of traditional AE parameters by eliminating all propagation effects on the recorded parameter and presents each source at a stable level. As a result of that it overcomes particular problems associated with source characterisation in complex large scale structures with most current characterisation approaches.

Two tests conducted demonstrated the significant improvement in terms of correcting the traditional parameters over the traditional recorded parameters using the acquisition system. The initial validation test was conducted using artificial sources and was shown to correct the traditional parameters which were recorded from different locations on the specimen. This result has greatly improved on the source characterisation and increased the result reliability of using the characterisation by a single parameter, correlation plots and the clustering approach. The second test, a fatigue test conducted on composite specimen, demonstrated the ability to correct the real AE traditional parameters and improve the characterisation reliability.

A summary of the PCT:

Practicality

- A simple, practical approach to overcoming the problems associated with source characterisation in complex structures or/and materials, such as aerospace components.
- Only the area of interest need to be examined, this will reduce the PCT operation cost.
- There is no need to provide information about the sensor location or any information about the signal attenuation, reflection and/or superposition within the structure. All this information is defined with regards to a user defined PCT map.
- Key areas can be addressed during and post-test, only if there is no significant damage causing huge geometry change during the test and effect on the PCT maps information, allowing previous data to be replayed through the PCT software.
- The constraints with this method are; firstly, because the AE event location is essential to start the correction of its parameters, only located events can be corrected using the PCT. Secondly, this technique considers each structure as unique and thus it is necessary to generate a unique training map for each specimen or for each area of interest in the structure. Thirdly, the sensors cannot move once the PCT maps assessment has been conducted. In case one senor or more have been relocated, the PCT maps assessment must be repeated.

Performance

- The PCT provide a significant improvement in correcting the recorded traditional parameter value. The corrected parameter is deemed to be more than acceptable as it eliminates all propagation effects on the recorded parameter and presents each source at a stable level while these sources are emitted from different positons on the structure.
- The PCT is able to use data from all sensors to correct the parameters. So, there are no missing located AE events and that is considered as a significant improvement in this AE analytical approach.

- The PCT highlights the use of traditional parameters is limited in large scale or complex structures for damage identification and provides unreliable source characterisation results.
- Due to use of data from all sensors, the PCT shows clear separation between different sources in the corrected parameters; this separation is not always clear when using traditional parameters recorded by one sensor.
- The PCT provides only one unique characterisation solution while there are many final solutions when using the traditional parameters depending on the used sensor.

Future Developments

The PCT results from the validation test using the artificial sources show slight fluctuation which is related to a number of sources of error. The location accuracy is considered as the largest error source on the PCT results. Another potential source of error is that related to human manipulation (including accurate positioning of the artificial source and the level of coupling). Future work to overcome this problem may include:

- Develop a fully automatic process to generate the PCT maps sources which may prevent any human manipulation on the collected data and reduce the operation time cost as well.
- Improve the source location techniques to increase the location accuracy. Due to the PCT depending completely on the calculated event location to start the correction process, improvement in location accuracy will increase the PCT result reliability.

5 Acoustic Emission Source Location

5.1 Introduction

The time of arrival (TOA) technique is traditionally used to locate AE sources, and relies on the assumption of constant wave speed within the material and uninterrupted propagation path between the source and the sensor. In complex structural geometries and complex materials such as composites, this assumption is no longer valid. DTM was developed in Cardiff in order to overcome these limitations; this technique uses artificial sources on an area of interest to create training maps. These are used to locate subsequent AE sources. However operator expertise is required to select the best data from the training maps and to choose the correct parameter to locate the sources, which can be time consuming process. Full details of these techniques and their limitations is provided in section 2.2.

This chapter presents a new and fully automatic DTM technique where a clustering algorithm is used to identify and select the highly correlated events at each grid point automatically and the “Minimum Difference” approach is used to determine the source location. This removes the requirement for operator expertise, saving time and preventing human errors. A thorough assessment is conducted to assess the performance and the robustness of the new technique. In the initial test, the results showed excellent reduction in running time as well as improved accuracy of locating AE sources as a result of the automatic selection of the training data. Furthermore, because the process is performed automatically, this is now a very simple and reliable technique due to the prevention of the potential source of error related to manual manipulation.

5.2 Automatic Delta T mapping technique

In order to reduce the sources of error related to the existing AIC DTM technique, a new automatic approach is presented here. This approach selects the valid events at each grid point using an unsupervised clustering technique and calculates the AE source location using the MDA (Miller and Hill 2005) and (Scholey et al. 2009), this eliminates any human manipulation of the data. The main new features of the automatic DTM technique are presented in the flowchart (Figure 5-1). This section will describe each part of this approach.

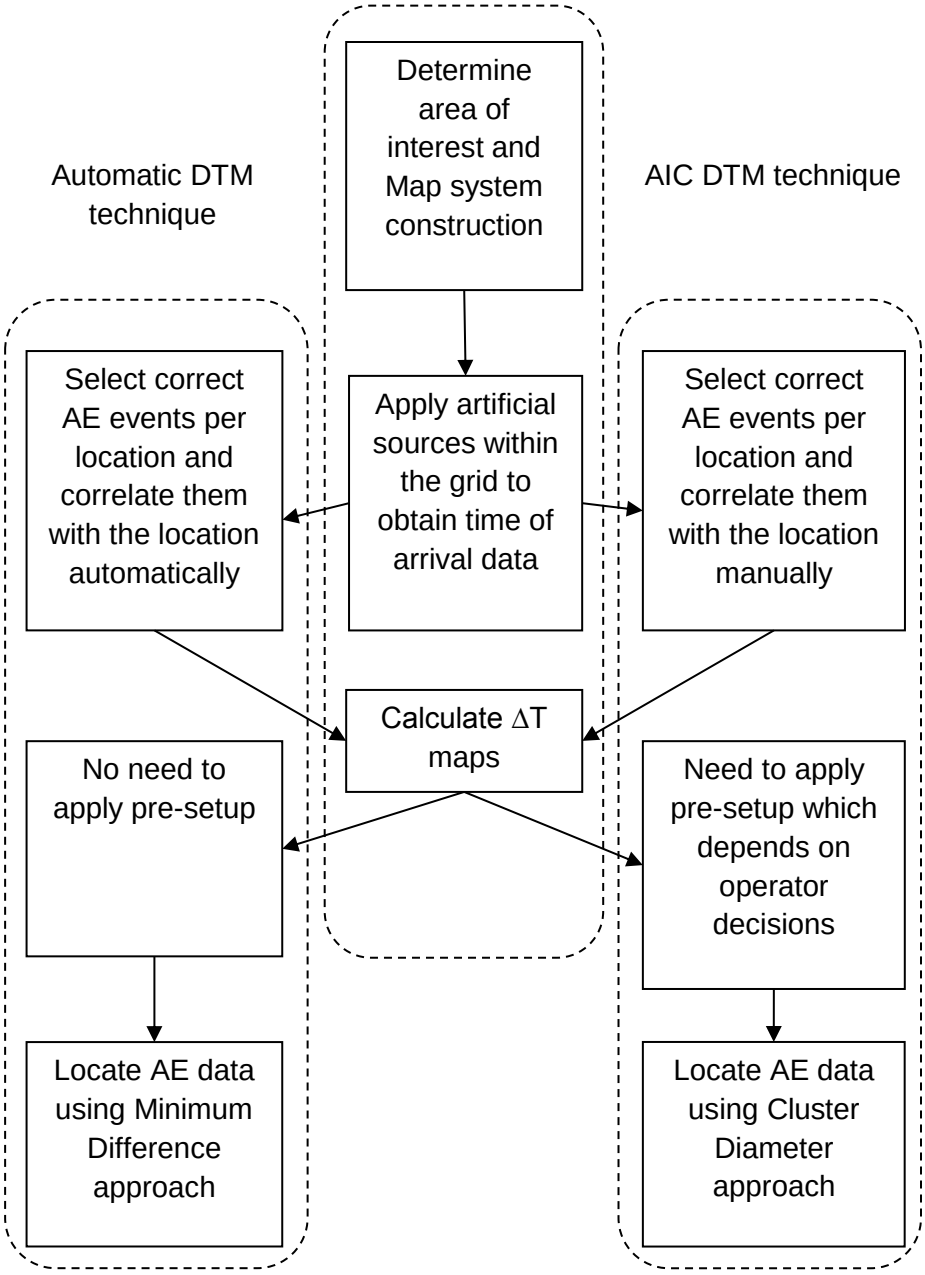

Figure 5-1. Automatic DTM technique steps and comparison with the AIC DTM technique

5.2.1 Automatic Grid Events Selection

After applying the artificial sources on each node of the grid (users do not have to generate a specific number of sources; five to ten H-N pencil lead fractures at each position is enough to allow arrival time repeatability, eliminate erroneous data and provide reliable data) the time of arrival to each sensor is obtained. The classification process is performed on each location event to select the highly

similar events, where the input data vector for the clustering process is the sensors pair's time difference and will be used for the similarity criteria. The events selection procedure to construct the ΔT maps follows these four steps:

1: Picking the correct waveform onset

Recording the correct signal arrival time from each waveform is vital in order to increase the location accuracy and to select the correct events at each position of the grid using the clustering algorithm. It is important to overcome the triggering abnormalities that are often observed, for instance when there is a very low amplitude first arrival mode, which can mean that the beginning of a waveform is missed by the AE acquisition software when using the traditional threshold crossing approach. In order to overcome this, the signal onset is determined using an Akaike Information Criterion (AIC) based approach (as discussed in Section 2.2.5). This process was reported previously by (Hensman et al. 2010) as an improvement to a version of DTM technique in order to determine the signal arrival time. (Eaton et al. 2012a) utilised this approach to determine the signal arrival time as improvement to the traditional DTM technique.

2: Prepare the data for clustering process

For each node within the Delta T grid, the recorded hits are separated as groups to create AE events automatically using a time based approach. Practically, in two dimensions, to consider and locate an event at least three different sensors must be hit (Section 2.2.2). In this work the specimens were relatively small so that using a high energy source (H-N) an event is very likely to hit at least three sensors. As a result of that any event recorded using all the used sensors was saved for the next step, while any event which does not record using all the used sensors was discarded). Simultaneously, the incorrect hits were filtered and removed automatically (e.g., set of hits at less than the number of used sensors using the actual used sensors as a filtering condition, hits were recorded without waveforms using the time matching approach between the extracted hits text file and the recorded waveforms files, hits from the second part of double pencil lead breaks and hits from reflected waveforms from the specimen edges which hit the same sensor more than once using a time window approach). Then, the AE hits from each point within the delta grid are correlated with the point coordinates (x, y) automatically, using time stamps placed by the operator within the collected data. The time stamps are placed in the data following acquisition from each grid

node and are then used to automatically identify which hits are associated with each grid node.

3: Apply the unsupervised clustering

For each grid node, unsupervised classification is performed to select correct events and to construct the training maps. All highly correlated events (similar to each other) are selected and the lower correlated are discarded. The selected events are treated as pattern vectors and used as an input to the unsupervised clustering. Each event is identified by the calculated difference in time of arrival for each sensor pair (for example, the case of four sensors creates six sensor pairs 1-2, 1-3, 1-4, 2-3, 2-4 and 3-4). The correlation between events refers to the similarity between the events arrival time difference of their sensor pairs. A complete link hierarchical clustering algorithm (Anderberg 1973) is then used to group events based on their similarity, or correlation coefficient.

The complete link hierarchical clustering algorithm for data of N events is described by the following four steps:

a. Assign each event to its own group (for N events we have N groups).
b. Compute the distances (similarities) between groups, where the distance is equal to the largest distance from any member of one group to any member of another group.
c. Reduce the number of groups by one through merging the most similar pair of groups.
d. Repeat steps 2 and 3 until all items form a single group.

At a higher level of correlation coefficient a greater number of groups will exist because the events in each group must be very highly correlated and vice versa, at a low correlation coefficient fewer groups will exist because each group can contain lesser correlated difference in time of arrival for each sensor pair. In this work the 0.99 correlation coefficient level from the largest group was selected and all events in this group were used (correlation coefficient of 1 means total correlation); each group at this level or above is deemed to contain highly correlated events and used for onward analysis. Conversely the groups are deemed to be suitably less correlated at a correlation level lower than the highest level. So, they are ignored and not used for onwards analysis. For example, the correlation between ten events generated on the same node is calculated using

the proposed approach and presented as the dendrogram plot presented in Figure 5-2. It is clear that the selected events with correlation level =>99% are (1, 2, 5, 4, 7, 8, 3 and 10) and all the remaining events (9 and 6) at this node were discarded.

After selection of the valid events at each node the training data is ready to calculate the ΔT map between each sensors pair.

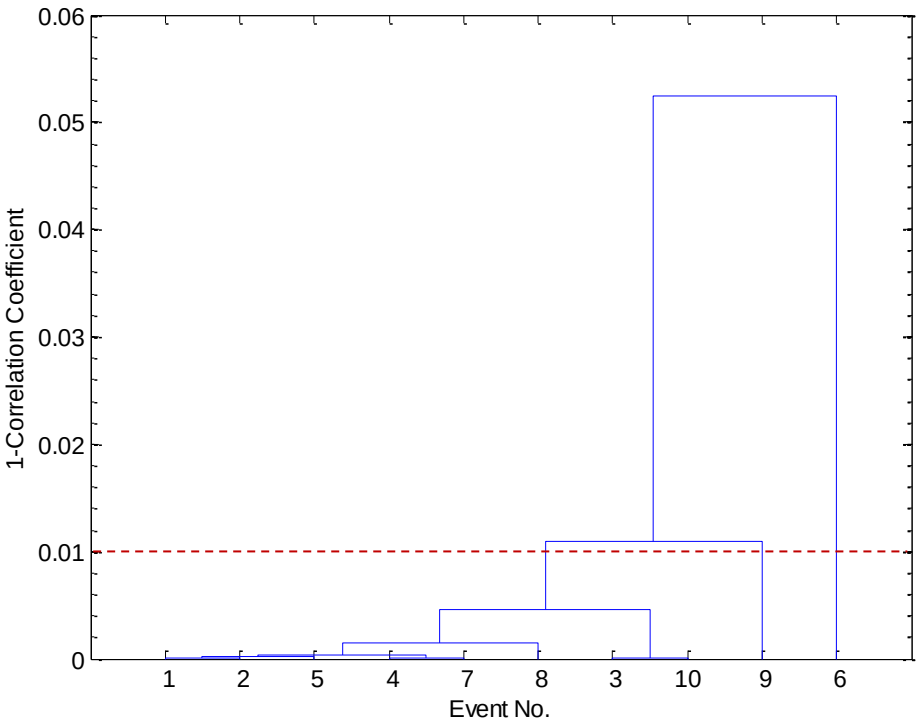

Figure 5-2. Example of the correlation level between 10 events in one node

4: Calculate ΔT maps

The average values of the difference in time of arrival for each sensor pair is calculated from the selected events at each grid point. In the case of 4 sensors, six Δt maps are created. Finer resolution grids are created using interpolating between training data points in order to provide high precision of the location calculation results. In this work the 0.5 mm resolution was selected to perform the calculations.

5.2.2 Calculate Location Using Minimum Difference Approach

In order to overcome the need to identify the cluster size for calculation of the real AE data location, a new approach is presented here; this will be known as the MDA. This is a numerical approach, which is dependent on finding lowest

different point between the source data and the training map data. This procedure of this approach can be divided into two parts; source events data preparation and determination of the source location.

1: Source events data preparation

Before determining the location of an event, the event data is prepared by the following steps.

a. Correct the arrival time at each sensor recording this event using the AIC approach.
b. Calculate the time difference between sensor pairs. If the event was recorded by three sensors, there will be three values of time difference.

2: Determination of the Source Location

After calculating the event sensor pairs time difference, the second part of the MDA is applied for each event by following these steps.

a. Subtract the event time difference of a specific sensor pair of the same sensors Δt map to generate a new matrix. Repeat the same process for the rest of the event sensor pairs. All Δt maps that do not match the event pairs will be discarded and will no longer be used in the calculations.
b. From the new matrices, sum the differences of all sensors pairs (n) to generate a sum matrix using the equation:

$$sum = \sum_{1}^{n} |T\ source - T\ training\ map| \tag{5.1}$$

where: T source: is the time difference of the source, T training map: the time difference of the training map (ΔT maps).

c. Find the point within the grid at which the minimum difference with the source time difference occurs. This point is taken to be the calculated source position. Figure 5-3 shows an example of the time differences matrix with the minimum difference point.

Using this approach will avoid any human interaction with the calculation process and therefore reduce the error source, increase the result reliability and reduce the running time of the whole process.

A comparison of the conventional TOA, AIC DTM and Automatic DTM for located AE events in a number of specimens and materials will be presented in the experimental section of this chapter.

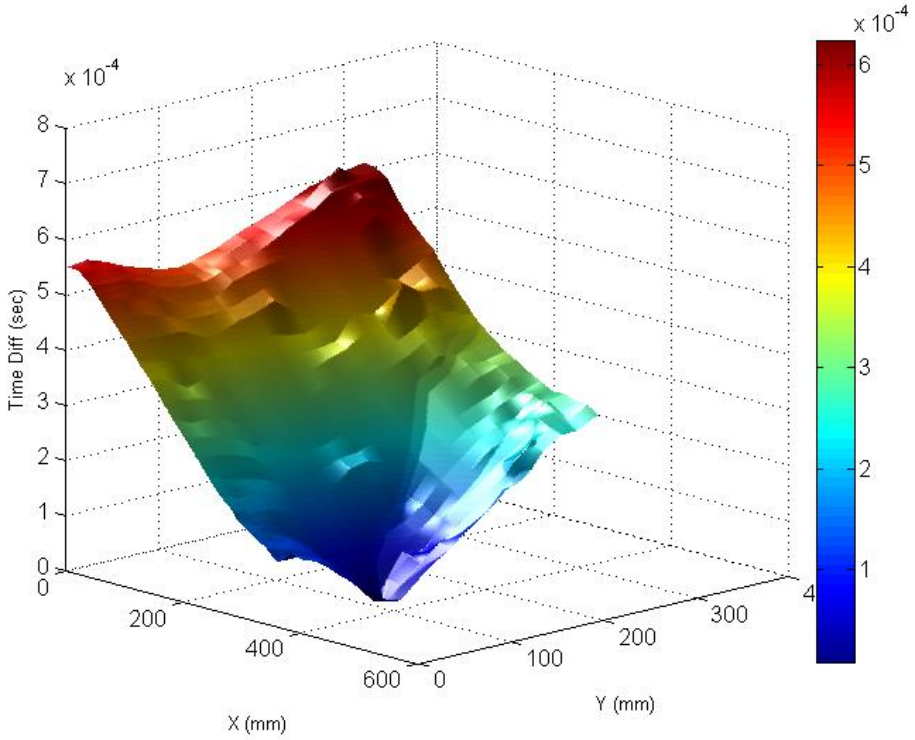

Figure 5-3. Example of the sum matrix with the location of minimum difference

5.3 Experimental Procedure

In order to evaluate the performance of the Automatic DTM technique against the traditional TOA and AIC DTM technique, three tests were conducted; one using simulated AE in a simple steel specimen, the second using simulated AE in a complex aluminium specimen and finally a validation test using AE from fatigue failure in a complex aluminium specimen.

The first test was conducted on a simple geometry specimen made from 20 mm thick ASTM 516 grade 70 steel with overall dimensions of 90 mm x 2m. At 17 mm from one end of the specimen a grid was constructed on the specimen with dimensions of 300 x 90 mm. Within this grid two geometric features were present; the first was 4.4 mm wide and 10 mm deep v-notch and the other was a 20mm diameter half circle cut out as shown in Figure 5-4. Six AE sensors were mounted to the specimen using silicone RTV adhesive (Loctite 595) to provide an acoustic

coupling and a mechanical fixture (Figure 5-5). The silicon was left to cure at least 24 hours before commencing the test. Four of the sensors are MGL Nano 30 (sensors 1-4) and two MGL WD sensors (sensors 5 and 6) were used and their relative positions are shown in Figure 5-5. Nano 30s have a physical size of 8mm diameter and 8mm height and a working frequency of 125 to 750 kHz. They are a resonant transducer but have a broad band response inside the working range of the transducer. The WD transducers are physical larger with a size of 18mm diameter and 17mm height and have a working frequency range 100 to 1000kHz; again these transducers are resonant however also have a flat frequency response outside the resonant frequency. Table 5-1 shows the location of the sensors with reference to the bottom left hand corner of the specimen.

AE Data was recorded using a MGL PCI-2 system with a 45dB threshold and a 5 MHz sample rate. Prior to testing, DTM training data was collected from the grid nodes at two resolutions, 10mm resolution near notch area (40 x 90 mm) and 20mm resolution for the rest of the grid (Figure 5-5). For the purpose of the training data ten H-N sources were generated at each node on the grid. In order to assess the correct events selection approach, an initial test was conducted on three arbitrary positions (details of positions provided in Table 5-2). Various cases of ten H-N sources were conducted at each position. Furthermore, ten arbitrary locations were selected within the grid and five H-N sources were performed at each position. The location of these positions is presented in Table 5-3. For the recorded signals, from all six sensors, locations were calculated using the TOA, AIC DTM and the Automatic DTM. Prior to the test, for the TOA technique an experimentally derived wave speed of 4600m/s was determined and the co-ordinates of the sensors were used as an input to the technique. Furthermore, when the AIC DTM technique was used, visual inspection was used to remove erroneous events from each position in the training data grid.

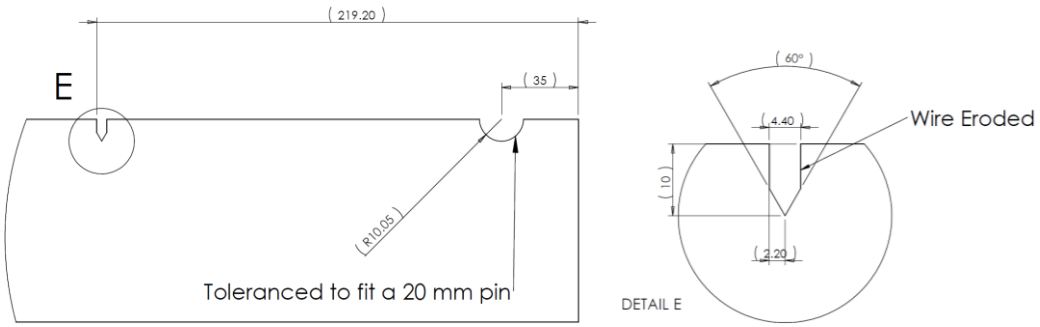

Figure 5-4. Location and dimension of the v-notch and the half circle cut

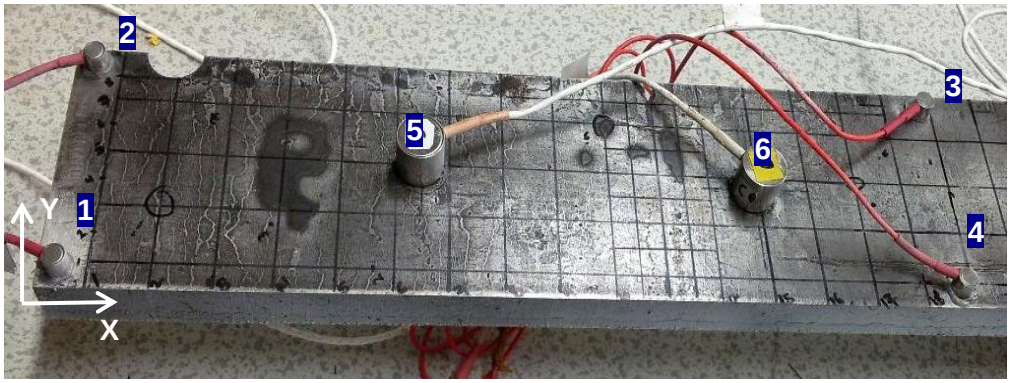

Figure 5-5. Steel specimen configuration

Table 5-1. Location of the sensors on the specimen from the reference left end corner

Sensor type / No.	X(mm)	Y(mm)
Nano 1	7	7
Nano 2	7	83
Nano 3	333	82
Nano 4	331	7
WD 5	126	48
WD 6	255	44

Table 5-2. Location of the initial test points position.

Point No.	X(mm)	Y(mm)
First point	37	20
Second point	197	70
Third point	297	50

Table 5-3. Location of the arbitrary source positions on the specimen

position No.	X(mm)	Y(mm)	position No.	X(mm)	Y(mm)
1	30	20	6	299	40
2	110	10	7	50	60
3	75	24	8	120	80
4	170	20	9	190	60
5	225	31	10	310	60

To assess the performance of the Automatic DTM on more complex geometry specimens, a further test was conducted on an aerospace grade 2024-T3 aluminium plate, with dimensions of 370x200mm with a thickness of 3.18mm. The specimen contained a series of differing diameter circular holes around the vertical and horizontal line of the specimen as shown in Figure 5-6. A MGL PCI-2 system was used to record all AE data at 40 dB threshold and 2MHz sampling rate. Four Nano-30s were adhered on the front face of the specimen (Figure 5-6) using silicon RTV (Loctite 595). All transducers were connected to MGL 0/2/4 pre-amps which had a frequency filter of 20 kHz to 1MHz. The DTM grid (with resolution of 10mm) on the specimen covered an area of interest of 200mm x160mm (Figure 5-7). Five H-N sources were used at each node position within the grid. Following the collection of training data, further H-N sources were collected from random positions within the grid, to assess the performance of the all the locations strategies used in this investigation. Care was taken to select random positions that were not concurrent with locations used in the collection of training data and three H-N sources were conducted at each position (Table 5-4). The average wavespeed was experimentally determined as 5400 m/s. Source locations were calculated using the four sensors data using the three techniques, TOA and the DTM techniques.

Further investigation was conducted on the aluminium specimen to generate real AE sources. A tension-tension fatigue test was applied on the specimen until the final failure. The load was transferred from the testing machine to the specimen using a 20 mm loading pin. In order to distribute the applied load on the specimen, 5mm steel plates either side were connected on the specimen end using seven M10 bolts on each end. The cyclic frequency was 2Hz with a minimum load of 0.25kN and a maximum load increasing from 5kN at the start of the test to 24kN at final failure. Full details of the load analysis and calculation is presented by (Pearson 2013).

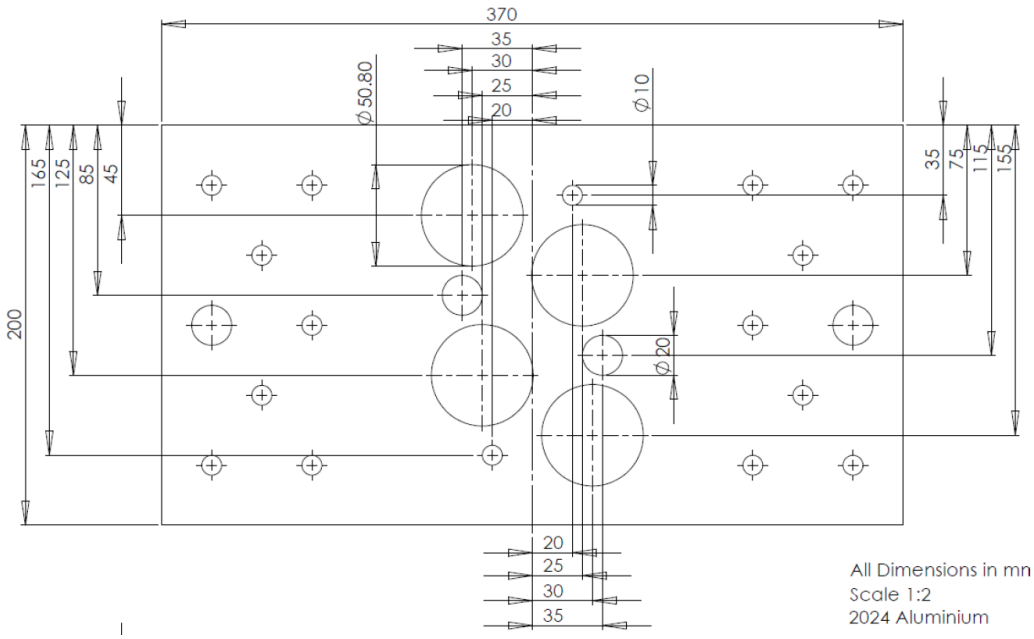

Figure 5-6. Location and dimension of the central machined holes (Pearson 2013)

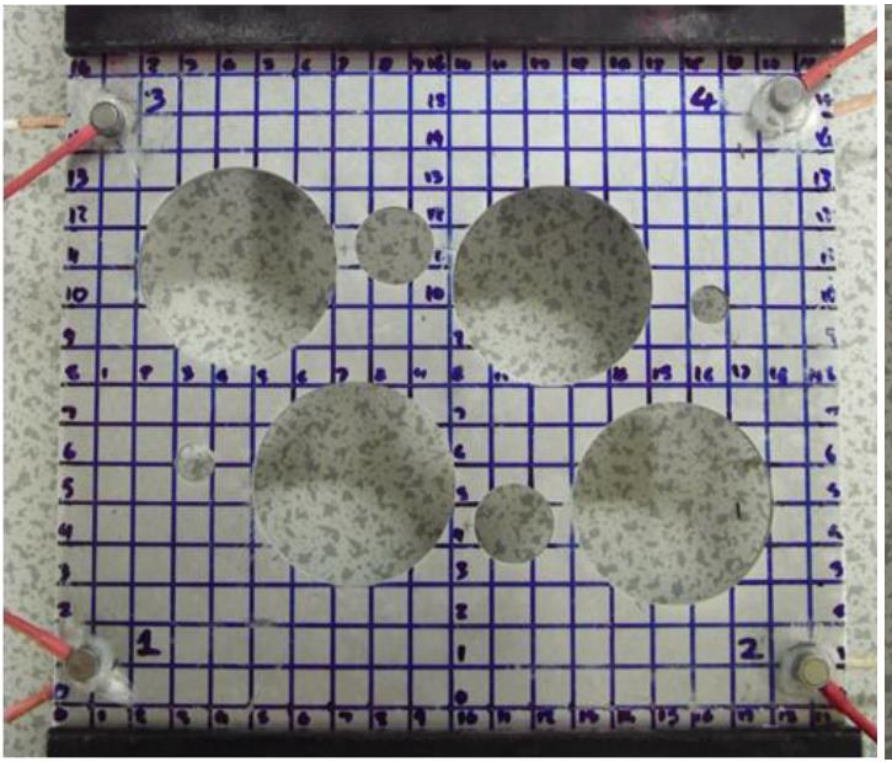

Figure 5-7. Aluminium specimen configuration

Table 5-4. Location of the arbitrary source positions on the specimen

Position No.	x, mm	y, mm
1	20	110
2	74	114
3	100	115
4	104	44
5	126	45
6	181	50

5.4 Results and Discussion

5.4.1 Initial Practical Validation Test

On each of three positions, the ten H-N sources were generated in twelve different styles. For each style, some of these sources were generated exactly on the point position and will be referred to by (On). Other sources were generated around the positions with different distances from about 10 to 20 mm and will be referred to by (Ar) and the rest were generated at far distance from the position

about 100 to 500 mm and will be referred to by (Far). For example, the first generated style has the first three sources of type (On) followed by five sources of the kind (Ar) and the rest of the sources of the kind (Far). Each generated style was repeated on the other positions. The order of source generation of the three positions is presented in Table 5-5. These sources were generated in two cases one with and one without amplitude filtering. The quantity of data recorded in the second case is much higher than the first case, 2199 hits and 15892 hits for the first case and the second case, respectively. The high quantity of hits makes the manual selection of the valid events more difficult and increases time consumption. Intuitively, if the amplitude filtering facility is used, the AIC DTM efficiency will improve. Practically, selection of the correct amplitude filtering level in the acquisition setup is manual and completely depends on the operator decision. Incorrect decision may lead to loss of important events. Furthermore, the level value needs to update continuously depending on the location of grid nodes from the sensors. This will increase the source of error and increase the time consumption during the recording of the training maps data. By using the new full automatic DTM technique all these limitations are overcome.

For the first case, the automatic selection approach was applied and the highest correlated events were selected correctly to be the (On) kind for all generating styles. The first position result of all styles is presented in Table 5-6(a). The same valid results were achieved for the rest of the positions. For the second case the same correct results was achieved as presented in Table 5-6(b). It can be seen that in both cases the proposed methodology selected the correct events. This will lead to more a reliable and automatic DTM approach.

Table 5-5. recorded events order at each location.

		Sources order									
Style No.	Position	1	2	3	4	5	6	7	8	9	10
Style 1	First Position	On	On	On	Ar	Ar	Ar	Ar	Ar	Far	Far
Style 1	Second Position	On	On	On	Ar	Ar	Ar	Ar	Ar	Far	Far
Style 1	Third Position	On	On	On	Ar	Ar	Ar	Ar	Ar	Far	Far

Table 5-6. The highest correlated events on the first position

(a) Case 1

Style No.	Sources Order										Clustering Program Result									
											1	2	3	4	5	6	7	8	9	10
1	On	On	On	Ar	Ar	Ar	Ar	Ar	Far	Far		o	o							
2	On	On	On	Ar	Ar	Ar	Ar	Ar	Ar	Ar	o	o								
3	On	On	On	On	Ar	Ar	Ar	Ar	Far	Far		o	o							
4	On	On	On	On	Ar	Ar	Ar	Ar	Ar	Ar			o	o						
5	On	On	On	On	On	Ar	Ar	Ar	Far	Far			o		o					
6	On	On	On	On	On	Ar	Ar	Ar	Ar	Ar			o	o						
7	On	On	On	On	On	On	Ar	Ar	Far	Far			o			o				
8	On	On	On	On	On	On	Ar	Ar	Ar	Ar	o			o						
9	On	On	On	On	On	On	On	On	Ar	Far	o							o		
10	On	On	On	On	On	On	On	On	Far	Far	o	o								
11	On	On	On	On	On	On	On	On	On	Far								o	o	
12	On	On	On	On	On	On	On	On	On	On					o		o			

(b) Case 2

Style No.	Sources Order										Clustering Program Result									
											1	2	3	4	5	6	7	8	9	10
1	On	On	On	Ar	Ar	Ar	Ar	Ar	Far	Far	o	o								
2	On	On	On	Ar	Ar	Ar	Ar	Ar	Ar	Ar	o		o							
3	On	On	On	On	Ar	Ar	Ar	Ar	Far	Far		o		o						
4	On	On	On	On	Ar	Ar	Ar	Ar	Ar	Ar	o	o								
5	On	On	On	On	On	Ar	Ar	Ar	Far	Far	o			o						
6	On	On	On	On	On	Ar	Ar	Ar	Ar	Ar	o	o								
7	On	On	On	On	On	On	Ar	Ar	Far	Far		o		o						
8	On	On	On	On	On	On	Ar	Ar	Ar	Ar	o				o					
9	On	On	On	On	On	On	On	On	Ar	Far		o			o					
10	On	On	On	On	On	On	On	On	Far	Far			o				o			
11	On	On	On	On	On	On	On	On	On	Far			o				o			
12	On	On	On	On	On	On	On	On	On	On			o					o		

5.4.2 Validation testing on the steel specimen

In order to determine the source location using the AIC DTM, the optimal cluster size was calculated firstly using the trial and error procedure of assessing the

accuracy of calculated position against the actual known positions at different values of cluster diameter. Figure 5-8 shows the average location error (the Euclidian distance between the actual source position and the calculated source position) for all the 50 sources versus the cluster diameter used in the AIC DTM algorithm. The optimal cluster size will refer to the lowest error value and here in this work it was selected to be 8mm. But practically, the lowest average error of all source locations does not mean it is the lowest error value for each source individually. Many sources have the lowest location error at a different cluster value. For example, the location error for the first six positions (position 1 to 6) is presented in Figure 5-9. In each position five events are presented and refer to the five generated N-H sources. The same behaviour has been noted for the rest of the positions. It therefore seems that cluster diameter selection is a tricky process and highly dependent on the operator decision. It is clear that the cluster diameter has a significant effect on the location accuracy with the error ranging from less than 4mm to over 12mm depending on the diameter used. Furthermore, the optimum cluster diameter calculation is a time consuming process because it is found using a trial and error process.

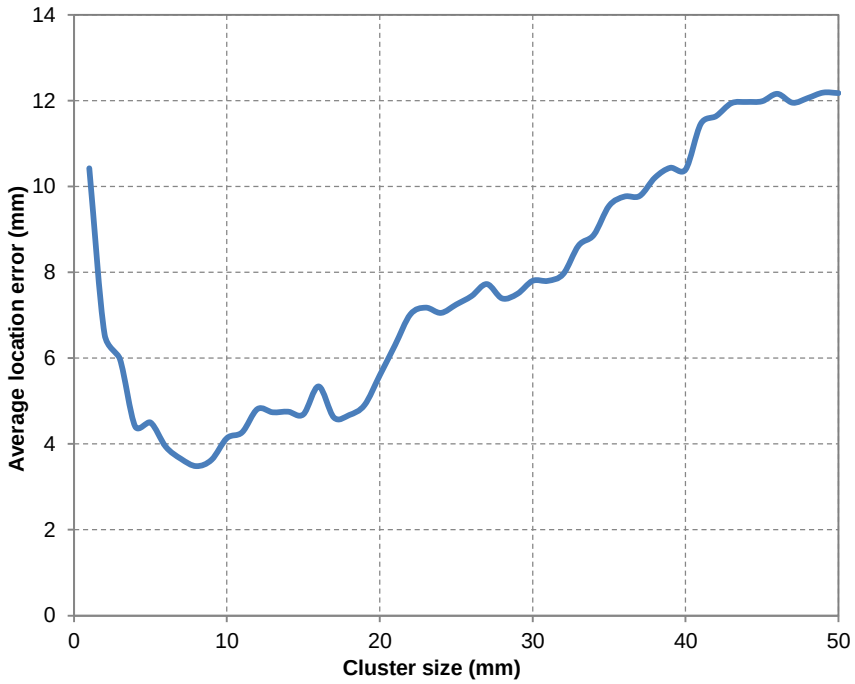

Figure 5-8. Cluster size effect on the AIC DTM accuracy

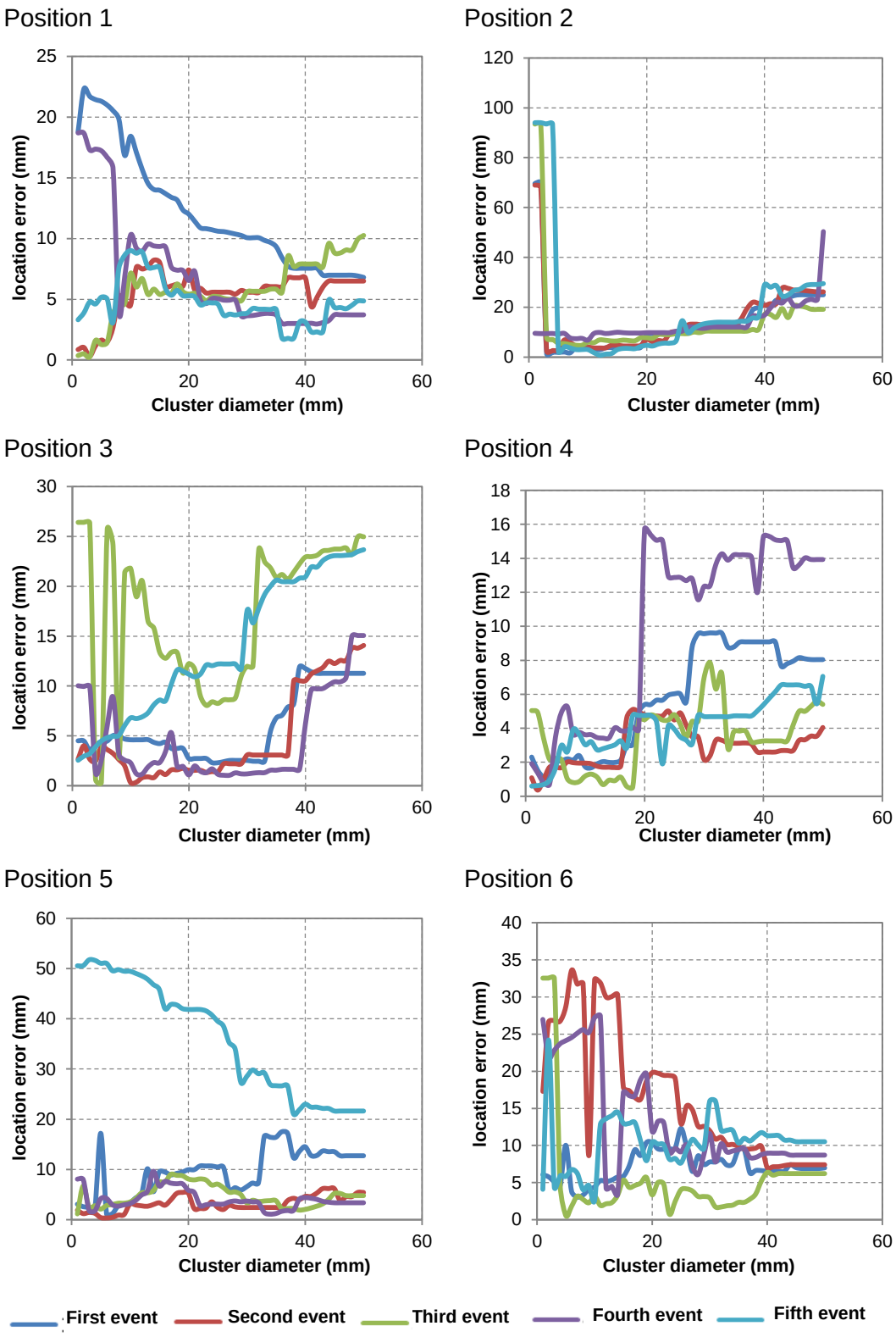

Figure 5-9. Location error for the first 30 sources (first 6 positions)

In the Automatic DTM, the erroneous events for each grid position are removed automatically using the unsupervised clustering procedure and only highly correlated events (>=99%) are selected and the source locations are calculated using the MDA. The locations results from H-N sources at the ten positions, calculated using the three location methods, graphically are presented in Figure 5-10. It can be seen that there is marked improvement in source location using the both DTM techniques over the traditional TOA technique due to the more accurate approach used for the arrival time determination. Furthermore, the improved Automatic DTM locations accuracy improved slightly over the AIC DTM due to using the new fully automatic approach for correct events selection to constructing the training data and overcame the need to use the cluster diameter which prevents any human manipulation.

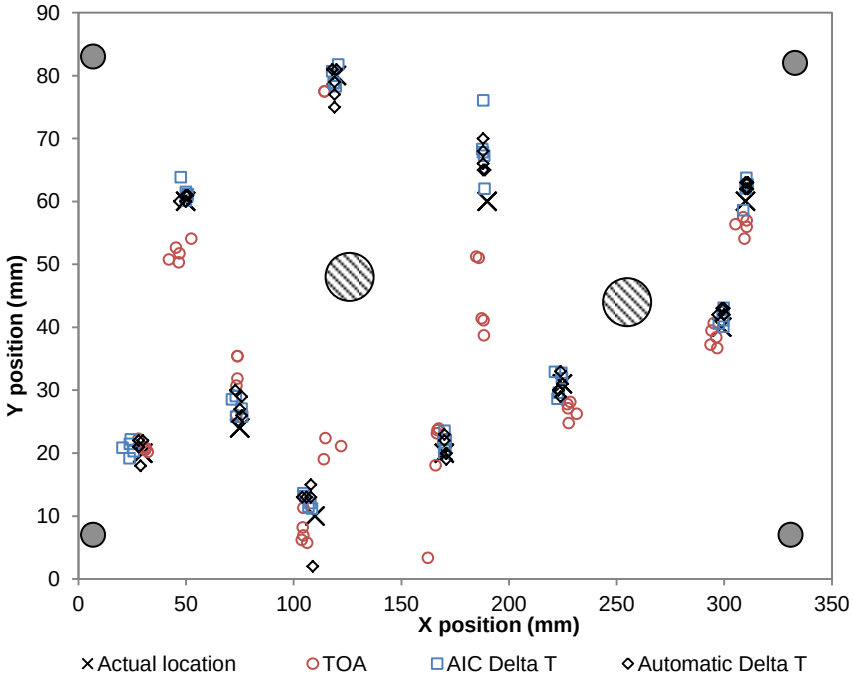

Figure 5-10. Calculated source location by three techniques

The average location error for the all 50 sources, calculated as the Euclidian distance between the actual source position and the calculated source position, using the three location methods is presented numerically in Figure 5-11. The error bars in the figure represent one standard deviation above and below the average location error. It can be clearly seen that the average error is reduced significantly to 3.48mm and 3.13mm using the AIC and Automatic DTM respectively compared with that of the TOA at 10.08mm. These results are

considered as promising because the error has been reduced by about 66% and 69% of the TOA error in a homogenous simple structure specimen. Furthermore the Automatic DTM reduces the error by approximately 10% over the AIC DTM because the data handling was completed automatically.

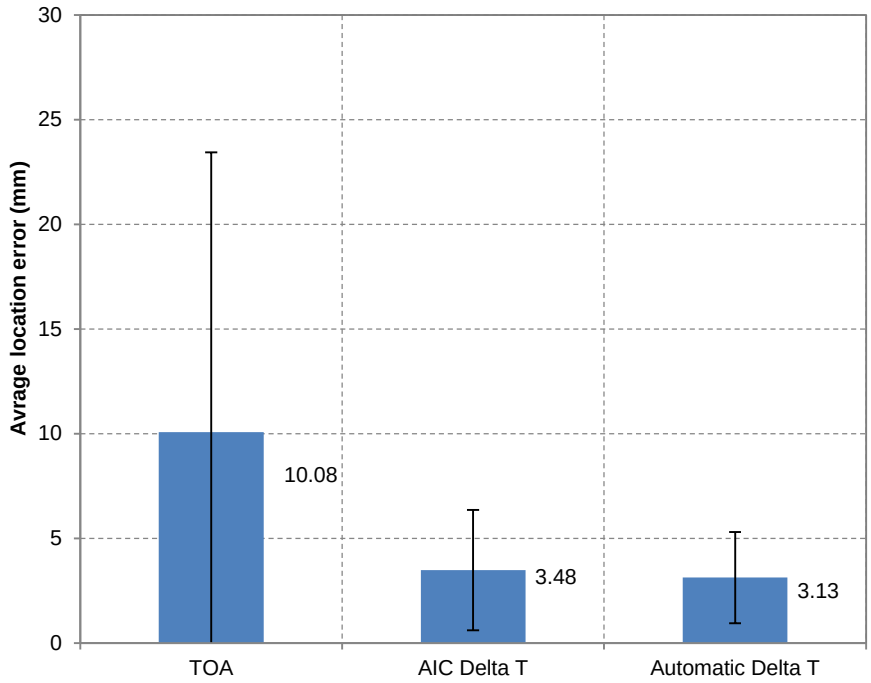

Figure 5-11. Average location error for the three techniques result.

Further benefit is achieved using the fully Automatic DTM technique. The results reveal that the new technique not only improves the location accuracy but also speeds up the whole process and make it a low time cost technique. A comparison between the AIC and the Automatic DTM based on the time resources of the operator is provided in Table 5-7. From the table, the most time consuming step in the traditional technique is the selection of data and preparing the training maps which cost about 8 hours (this refers to actual working hours by a highly skilled AE operator) for this grid (using finer resolution or a larger grid will cost more time). On the other hand, the Automatic DTM reduces the running time for constructing the training maps to only about 18 seconds which is a significant improvement. Moreover, the Automatic DTM does not need time for finding the optimal cluster diameter which cost about 3.6 hours running time in the AIC DTM.

Table 5-7 Running time comparison

Stage	AIC DTM (s)	Automatic DTM (s)
Prepare the AE data to construct the training maps	Approximately 28800 (operator)	18.2 (computational)
Calculate the optimal Cluster size (try from 1-50 mm)	13089 (computational)	0
Calculate the source location	262 (computational)	60.4 (computational)
Total time	42151	78.6

The initial testing results herald many significant and very promising findings. Firstly, the Automatic DTM technique presents fully automatic process which is a significant improvement to prevent any human manipulation on the results and reduces the technique cost (time sources and highly skilled operator needs) thus increasing the technique simplicity and result reliability. Secondly, it increases the result accuracy.

5.4.3 Validation testing on complex geometry aluminium specimen using artificial sources

For the AIC DTM calculations, the cluster diameter of 20mm was determined using the same previous procedure. The Automatic DTM was applied using 99% correlation per grid point and higher. Figure 5-12 displays a typical plot comparing the source location results which are listed in Table 5.4 calculated using the three techniques. The AIC and Automatic DTM results present as clusters close to the actual location position, while the TOA results show as clusters distributed far away from the position and outside the specimen boundary. The high accuracy of both the AIC and Automatic DTM over the traditional TOA approach to calculate source location in complex structure is clear and is a significant improvement. This is because the TOA relies on two assumptions, constant wavespeed through the structure and direct propagation line between the source and the sensor, which are difficult to achieve in real structures.

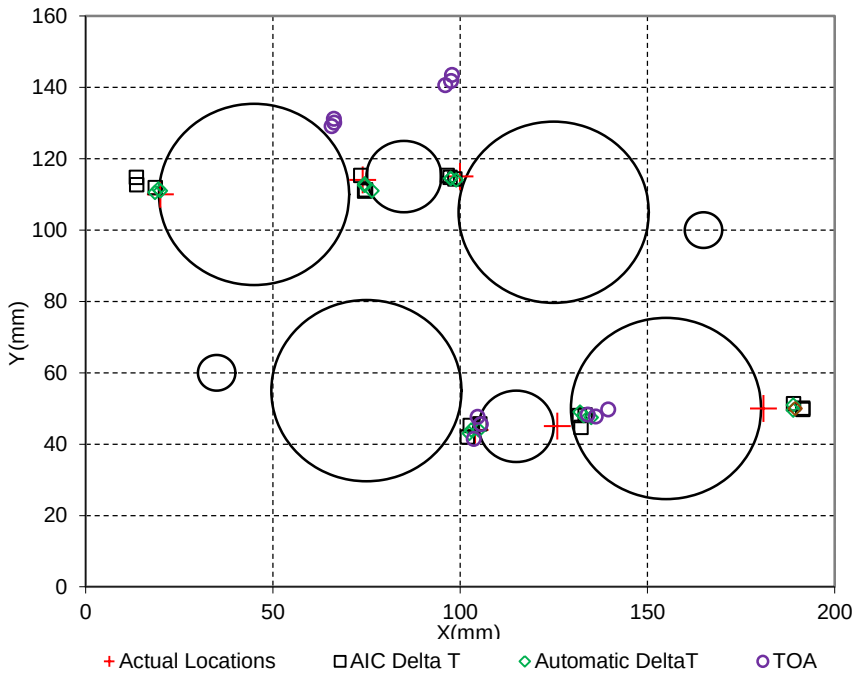

Figure 5-12. Source locations on a complex specimen using three techniques

The average location error for the 18 sources (the Euclidian distance between the actual source position and the calculated source position) is presented in Figure 5-13 as a comparison between the three techniques results, the error bars represent plus and minus one standard deviation about the average. Here the average error of both DTM techniques is much lower than the TOA and offer accuracy improvement about 44.7 times. This figure presents two important points. Firstly, it shows how the TOA is not well suited to dealing with source location in complex structure. This is because the assumptions used in this method, i.e. constant wave speed and straight propagation path are not valid in a complex structure. Secondly, the significant improvement is average location accuracy in the AIC DTM results (4.96 mm location error) over the TOA (222.18 mm location error) which was further improved using the new Automatic DTM (3.88 mm location error).

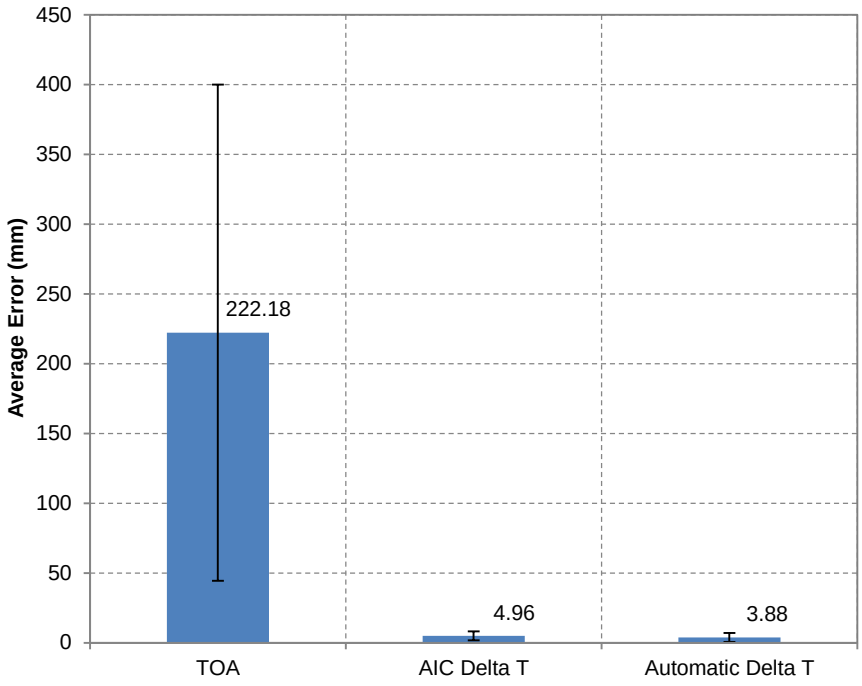

Figure 5-13. Sources location error

Comparing the Automatic DTM results with the TOA and the AIC DTM results highlights significant benefits such as the improvement of the accuracy and reliability of AE source location. Experimental investigations on simple and complex structure specimens have shown that the time consuming manual process is replaced with a highly reliable, automatic and less time consuming process.

So the Automatic DTM technique is a faster, easier to implement location technique which results in less testing downtime for set-up and operator skill making it more compatible with commercial needs. Having the automatic clustering technique for training data and MDA for the AE source estimation reduces the potential for human error, the need for a skilled operator and manual process of selecting the optimal location cluster diameter.

The results of this study highlight the potential for the use of AE monitoring as a tool of SHM for damage localisation task; a high simplicity, fast, reliable, cheap and accurate technique has been presented. If this technique is integrated with commercial AE monitoring systems, it will be a powerful tool to provide real time highly accurate source location within complex large-scale components.

5.4.4 Delta T results from fatigue test data on complex geometry aluminium specimen

The actual fatigue crack location is presented in Figure 5-14 and occurred as predicted in the high stress region around the thin webbed section between the holes. The AE source location from the test was calculated using the traditional and the Automatic DTM techniques using the same procedure as presented in section 5.4.3.

The AE location result is presented as spatial binning plots in order to provide an obvious comparison. The grid area was divided into 5x5mm sub-sections and the cumulative events per sub-section are present. The location of the actual crack is highlighted by the red line. Figure 5-15 and Figure 5-16 show the AE source location from the AIC and Automatic DTM technique, respectively. The figures show the significant cluster of events above the crack location. This cluster is located at around 15 mm from the location of the actual crack. These results show the high accuracy of the Delta-Ts to calculate the AE source location. With the presented new technique the same or higher location accuracy is achieved using less resources.

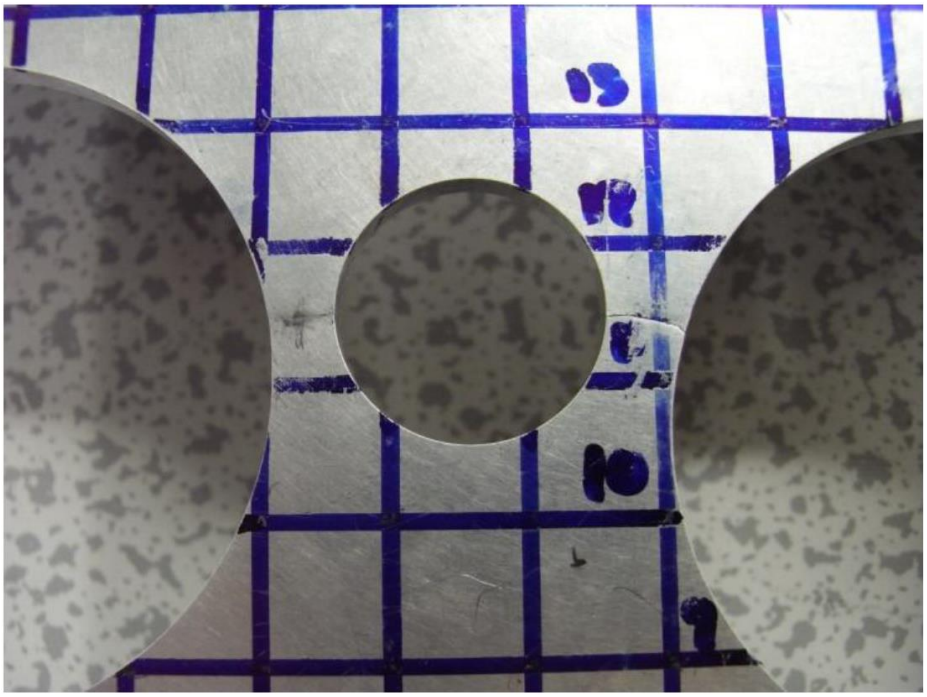

Figure 5-14. Crack location after the final failure (Pearson 2013)

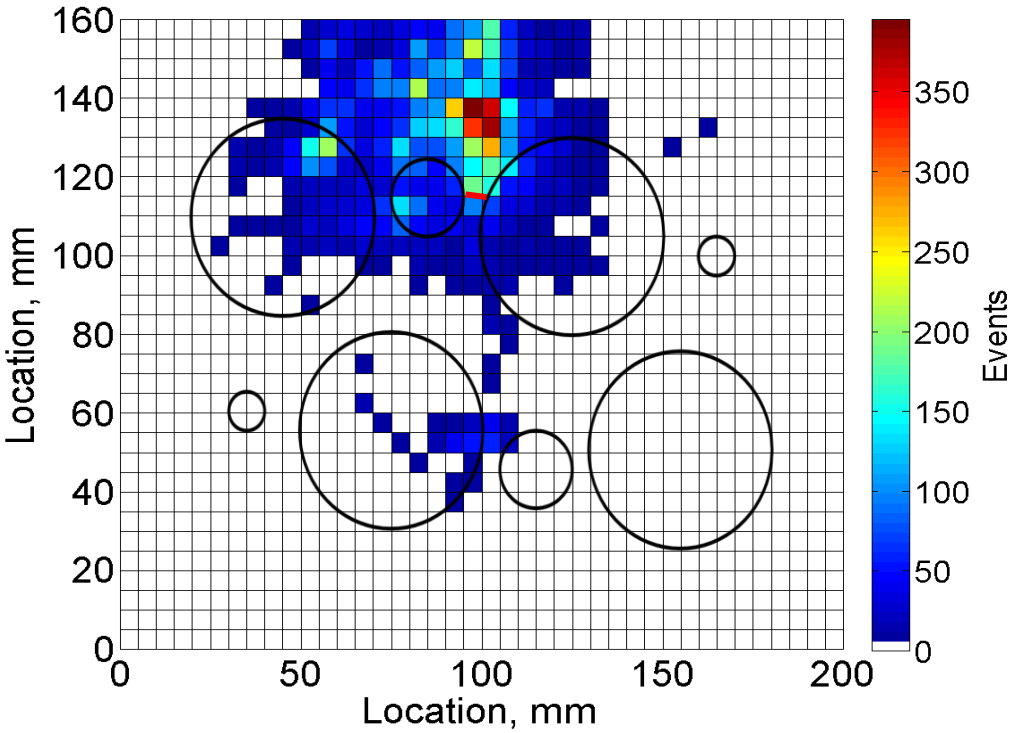

Figure 5-15. AIC DTM event location

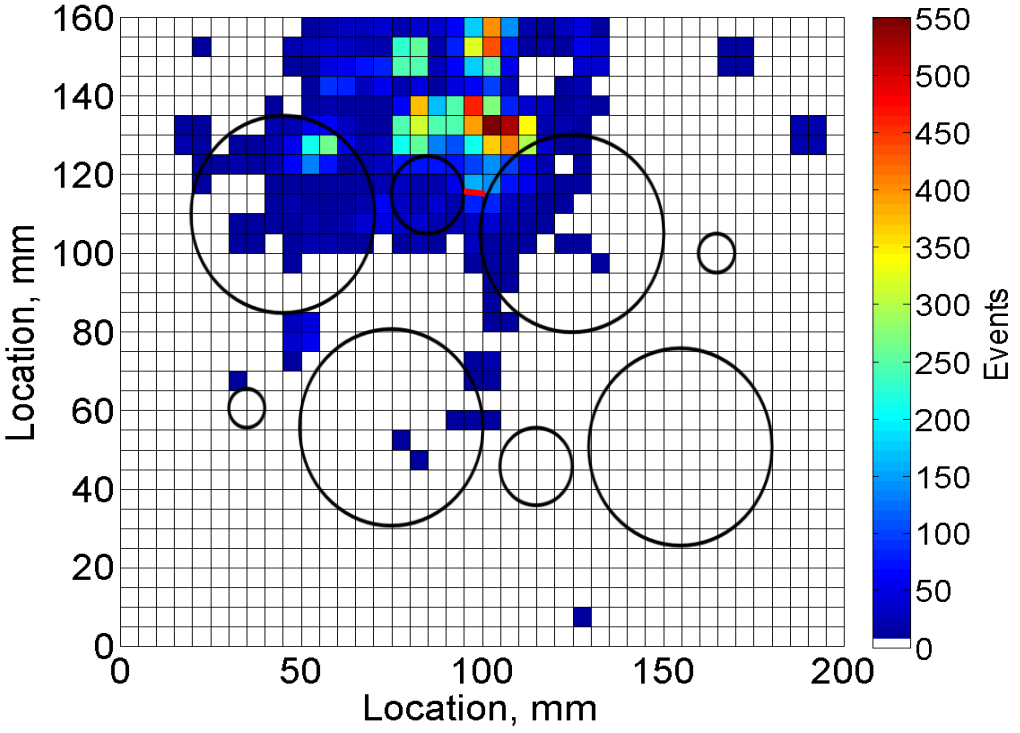

Figure 5-16. Automatic DTM event locations

5.5 Conclusions:

A new Automatic DTM technique was used in variety of tests on simple and complex structures. The results obtained here are excellent and demonstrate the success of the adopted methodology. The AIC DTM technique has been improved considerably as summarised below:

- Fast: The automatic selection and elimination of erroneous training data greatly decreases the process time from about 8 hours to just 18 seconds.
- Increased reliability: Making the process fully automatic increases the reliability of the result and eliminates human error.
- Efficient: The process requires less resources in terms of time and operator skill.
- More accurate: the technique results repeated and increased the excellent accuracy of the AIC DTM technique in an automated and efficient way. It shows an increase in the accuracy where it provides average location errors of 3.13mm and 3.88mm for simple and complex geometry specimen, respectively.
- Increased simplicity: No need for highly skilled operator to perform the whole process.
- More capability to apply in large scale structure.

The new approach robustness was assessed for its applicability to commercial use. Table 5-8, Table 5-9 and Table 5-10 show the main new features in the new technique over the traditional one.

Table 5-8. Full Automatic DTM and AIC DTM techniques comparison in the training grid construction

	AIC DTM technique	**Full Automatic DTM technique**
1	Generate source very slow to ensure there are no incorrect events	Very fast
2	Using the Front End Filters essential during the acquisition and need to update it for every reign on the specimen	No need for Front End Filters
3	Repeat acquisition lines on the grid if it has enormous error	No need for this step
4	Write notes about every step and the incorrect events time	No need for this step

Table 5-9. Full Automatic DTM and AIC DTM techniques comparison in the data filtering process

	AIC DTM technique	**Full Automatic DTM technique**
1	Remove manually hits that were recorded without waveforms.	Automatically
2	Remove manually double pencil lead breaks. (depend on the visual inspection)	Automatically (Remove only the incorrect part of the double PLB.)
3	Remove manually bouncing leads hit the specimen surface again at different location of the grid (the operator will depend on the written notes to find them)	Automatically
4	Remove manually accident sources from external sources (the operator will depend on the written notes to find them)	Automatically
5	Remove manually events having number of hits less than the number of the used sensors.	Automatically
6	Remove manually the event’s hits which recorded	Automatically

	twice using the same sensor.	
7	Remove manually the extra events were recorded at each point of the grid.	Automatically
8	Correlate each event with the location manually	Automatically
9	Generate the text (GridFileData.txt) manually	Automatically
10	Select the best events at each node within the grid completely depends on the skill of the operator. Who will make a decision about each event to consider it correct or incorrect.	Automatically (depend on correlation level between the events)
11	Use 5 PLBs as input to the training map and then the mean value will calculate	Can use lower number of PLB as input (reduce the running time).

Table 5-10. Full Automatic DTM and AIC DTM techniques comparison in calculating the real sources location

	AIC DTM technique	**Full Automatic DTM technique**
1	Need the extra step to calculate the optimal cluster size (costs time)	No need for this step
2	The process depends on the operator decision	Automatically
3	High accuracy	Maintain or increase the high accuracy of the AIC DTM
	Very Good Accuracy but Slow	**Very Good accuracy and fast**

6 Discussion

6.1 Discussion

The real-time health monitoring of complex structures, such as those found in many aerospace applications, is highly desirable due to the significant potential for cost saving through reduced down time and maintenance, whilst maintaining stringent safety requirements. Fatigue damage is considered to be one of the main causes of reduced structural integrity that can lead to catastrophic failure. The AE technique is often quoted as having the potential to globally detect, locate and characterise active damage sources using a distributed array of sensors. In practice the adoption of the AE technique has been limited due to its poor performance in complex geometries and materials, where the complex wave propagation behaviour makes interpretation of AE data highly challenging. This thesis has focused on addressing these limitations through the development of novel solutions for AE localisation and characterisation in complex structures. The following section discusses the significance of these presented works in the context of the current state of the art.

The characterisation of damage mechanisms using AE data has been the subject of a significant body of research work. Researchers have attempted to classify AE data into classes (damages) of similar signals using single descriptor distribution, correlation plots, multidimensional analysis and signal modal analysis. These approaches have been proven to be limited in term of their ability to distinguish between different damage types in large-scale complex structures (i.e. aerospace structures), because a number of factors affect the signal descriptors in addition to the source mechanism. These include signal attenuation, superposition with reflected signals, anisotropic material properties and complex geometric structures. If the classification is conducted using the AE data recorded directly from the acquisition system without consideration of these propagation effects, the reliability of the characterisation result will be reduced. Moreover, the requirement to compare data from a single sensor only (to avoid the effects of sensor transfer function) for these techniques restricts their use on large-scale structures where large numbers of sensors are required to provide full coverage. The result presented in this thesis show that damage characterisation

using AE becomes very limited or impossible in large-scale complex structures using these approaches.

The novel Parameter Correction Technique, PCT, presented in this thesis delivers a framework for the removal of propagation and sensor effects from recorded AE parameters. The presented results for the classification of artificial sources and real fatigue data using PCT showed a great improvement when compared with classification undertaken using traditional AE features. The results showed that using the PCT, AE sources could be correctly classified regardless of position in large complex geometry structures. This capability presents a solution to one of the most significant barriers to the introduction of the AE technique in industrial applications. Furthermore, the PCT classification considers data from multiple sensors, preventing the loss of located AE events in the characterisation analysis. As such, and unlike existing AE classification techniques, the PCT is scalable to large structure, such as those found in commercial aircraft and the multiple sensor data increases confidence and reliability of the classification results.

The source localisation capability of AE is one of the most attractive features and accurate location forms an important part of the PCT classification technique. However traditional localisation methodologies, such as TOA and SSMAL, rely on the assumption of a constant wave speed and uninterrupted propagation path between the source and sensor, which in complex structures are no longer valid; leading to poor performance.

Many attempts to improve upon traditional AE source localisation approaches have been previously presented demonstrating promising results. The ability to account for anisotropic wave speeds has been demonstrated by a number of researchers, including techniques that require no previous knowledge of wave speeds. However these approaches are still limited as they do not account for structural complexities that may alter the wave propagation path and velocity, such as holes and thickness changes that may be present in reality. The use of mapping techniques, such as the DTM technique presented here, has the potential to account for both variable wave speeds and geometric complexity. However the data processing requirements for the existing technique are very labour intensive and as such it is still considered an expensive technique and the final result is still highly dependent on operator decisions.

In this thesis a new fully automatic DTM technique has been presented, which consists of two main improvements. Firstly a clustering algorithm is used to identify and select highly correlated events at each grid point automatically; speeding up the process and ensuring only reliable data is selected. Secondly the “Minimum Difference” approach, is used to determine the source location, eliminating the requirement for the user defined cluster diameter, which often required a trial and error to define and can have varying optimum values across a location array.

The new technique offers the advantages of very fast and automatic selection of training data, increased reliability, elimination of human error, increased efficiency and reduced operator skill, whilst maintaining or exceeding the excellent accuracy of the previous DTM technique. These achievements make the DTM technique far more suited to application in large-scale structures, where previously the required operator time for data processing would have been prohibitive.

The presented techniques have been demonstrated to work effectively in large and complex structures. These techniques have made significant progress in overcoming the key barriers to the adoption of AE by industry (i.e. the ability to cope with structural complexity). This could have a significant impact in the aerospace industry as well as more broadly across the energy sector (wind turbines etc.) and transport/infrastructure. In these areas, significant cost savings can be made and safety standards improved, because reliable SHM system would allow a structure to operate for longer between planned, routine manual inspections resulting in less downtime and hence lowering the costs associated with maintenance over the course of the service life. Being aware of the integrity of a structure throughout the entirety of its use is also inherently safer than inspecting its condition at intervals. An AE system incorporating these techniques in a live, in situ testing scenario could be realised in the near future.

7 Conclusions and recommendations for future work

7.1 Conclusions

This thesis contributes to a practical improvement to the use of AE technique in SHM to locate and characterise damage signals. In this study the PCT, a novel approach, is presented and used for the first time to improve the accuracy and the reliability of damage characterisation in large-scale components. Furthermore, a new fully automatic DTM technique is presented and tested for the first time on simple and complex geometry specimens to provide, with fewer resources required, highly reliable and accurate source location. Illustrative results are shown for simple and complex structures, and comparison with traditional and recently developed approaches validates improvements.

The objective of this thesis has been achieved by introducing the two new techniques for damage assessment (characterisation and localisation). The thesis starts with an introduction of the research background of the area and then lists of the objective of this project in Chapter 1. A review of Lamb wave phenomena is introduced in Chapter 2 along with a brief review of traditional and advanced damage characterisation and localisation approaches in an isotropic and anisotropic plate. Chapter 3 contains details of the instrumentation and experimental techniques commonly used throughout this work.

In Chapter 4, the new PCT approach is been introduced and its implementation is described. A thorough investigation of the effect of wave propagation in large-scale composite materials on the recorded AE data and its effect on damage characterisation is carried out in this chapter. Furthermore, the new approach overcomes the difficulties associated with traditional damage discrimination analysis in large-scale complex structure due to wave propagation effects, the use of data from different sensors and the problem of losing information when using only data from one sensor. The illustrative characterisation results for an anisotropic square plate using both artificial sources and real AE data collected from conducting tension-tension fatigue test are shown. The results of the new approach are validated by comparing with the conventional AE analysis results which generally demonstrates the superiority of the new technique and the following conclusions were drawn:

- Traditional AE parameters are completely misleading for damage characterisation in large-scale complex components.
- The traditional feature characterisation results are shown to be unreliable, and highly dependent on the operator decision.
- PCT technique overcomes all detrimental factors and corrects the recorded parameters with a high performance by using the actual path propagation of each signal.
- The PCT shows the ability to use all sensors' data to improve characterisation accuracy and avoid losing data.
- The PCT offers the opportunity for a fully automatic system to be developed.

Chapter 5 starts to introduce the new approach 'automatic DTM' in details. To fully test the new approach, sources locations were calculated within simple and complex geometry isotropic specimens and show superior improvement over the traditional approaches. Implementation of the clustering analysis into the automatic DTM enables a more efficient procedure for damage localisation. The results obtained are excellent, in term of accuracy and reliability, and demonstrate the success of the newly adopted methodology. The following features were identified of the automatic DTM:

- Fast: The automatic selection and elimination of erroneous training data greatly decreases the process time.
- Increased reliability: Making the process fully automatic increases the reliability of the result and eliminates human error.
- Efficient: The process requires fewer resources in terms of time, operator skill and experience.
- More accurate: The technique was able to reproduce and even increase the accuracy of the already excellent accuracy of the AIC DTM technique, which was achieved in an automated and efficient way.
- Increased simplicity: No need for highly skilled operators to perform the process.
- More capability to apply in large scale structures.

An overall discussion of the results is presented in Chapter 6. Finally, the thesis is summarised and concluded in this chapter.

The improved damage characterisation and localisation analysis have been demonstrated to be able to provide more reliable and accurate results in complex materials and geometries structures than the traditional approaches. It is believed that further extension of the improved techniques and applications on SHM can provide additional efficient and accurate damage assessment in real time for the aircraft industry.

7.2 Recommendations for future work

Implementation of the new techniques provides additional capabilities of the AE technique in large-scale and complex structures. In particular, they provide correlation between the AE signals and the different types of damage and the localisation of these signals with high accuracy. Some recommendations for the future development based on the improved analysis are discussed below.

Further development of source characterisation is required. Because the AE event location is essential to start the parameters correction, only located events can be corrected using the PCT. Improving the location approaches will overcome this limitation by using one sensor approach or three sensors at each area on the structure. Moreover, the PCT technique considers each structure as unique and thus it is necessary to generate a unique training map for each specimen or for each area of interest in the structure. This will consume significant time. Developing an automatic method to generate the training maps will overcome this limitation and reduce the human error as well.

The automatic DTM source location has shown huge potential and can be refined in the following ways. Optimisation of number and location of calibration points will reduce the setup time. If this technique is integrated with commercial AE monitoring systems, it will be a powerful tool to provide real time highly accurate source location within complex large-scale components.

References

Aggelis, D. G., Kordatos, E. Z. and Matikas, T. E. 2011. Acoustic emission for fatigue damage characterization in metal plates. *Mechanics Research Communications* 38(2), pp. 106-110.

Akaike, H. 1974. Markovian representation of stochastic processes and its application to the analysis of autoregressive moving average processes. *Annals of the Institute of Statistical Mathematics* 26(1), pp. 363-387.

Al-Jumaili, S. K., Eaton, M. J., Holford, K. M., Pearson, M. R., Crivelli, D. and Pullin, R. 2016a. Characterisation of Fatigue Damage in Composites Using an Acoustic Emission Parameter Correction Technique. *Composites Part B: Engineering* under review.

Al-Jumaili, S. K., Holford, K. M., Eaton, M. J. and Pullin, R. 2015. Parameter Correction Technique (PCT): A novel method for acoustic emission characterisation in large-scale composites. *Composites Part B: Engineering* 75, pp. 336-344.

Al-Jumaili, S. K., Holford, K. M., Pullin, R. and Eaton, M. J. 2014. A Parameter Correction Technique (PCT) for Acoustic Emission Characterisation in Large-Scale Composites. In: *31st Conference of the European Working Group on Acoustic Emission (EWGAE).* Dresden, Germany.

Al-Jumaili, S. K., Pearson, M., Holford, K. M., Eaton, M. J. and Pullin, R. 2016b. Fast and Reliable Acoustic Emission Source Location Technique in Complex Structures. In: *24th UK Conference of the Association for Computational Mechanics in Engineering (ACME-UK).* Cardiff, UK, 31 March - 1 April.

Al-Jumaili, S. K., Pearson, M. R., Holford, K. M., Eaton, M. J. and Pullin, R. 2016c. Acoustic emission source location in complex structures using full automatic delta T mapping technique. *Mechanical Systems and Signal Processing* 72–73, pp. 513-524.

Albouy, W. and Vieille, B. 2014. Determination of the damage threshold in woven-ply thermoplastic laminates at T > Tg : Acoustic emission and microscopic damage analysis. *Composites Part B: Engineering* 64, pp. 138-146.

Anderberg, M. R. 1973. Cluster analysis for applications. *Academic Press, New York*.

Arumugam, V., Kumar, C. S., Santulli, C., Sarasini, F. and Stanley, A. J. 2013. Identification of Failure Modes in Composites from Clustered Acoustic Emission Data Using Pattern Recognition and Wavelet Transformation. *Arabian Journal for Science and Engineering* 38(5), pp. 1087-1102.

Asamene, K., Hudson, L. and Sundaresan, M. 2015. Influence of attenuation on acoustic emission signals in carbon fiber reinforced polymer panels. *Ultrasonics* 59, pp. 86-93.

ASTM. 1982. Standard Definitions of Terms Relating to Acoustic Emission. *American Society for Testing and Materials*, E610-82.

ASTM. 1986. Standard Method for Primary Calibration of Acoustic Emission Senseors. *American Society for Testing and Materials*, E1106-86.

ASTM. 1994. A standard guide for determining the reproducibility of acoustic emission sensor response. *American Society for Testing and Materials*, E976.

ASTM. 1997. Standard Guide for Mounting Piezoelectric Acoustic Emission Sensors. *American Society for Testing and Materials*, E650-97.

Barré, S. and Benzeggagh, M. 1994. On the use of acoustic emission to investigate damage mechanisms in glass-fibre-reinforced polypropylene. *Composites Science and Technology* 52(3), pp. 369-376.

Baxter, M. 2007. *Damage assessment by Acoustic Emission (AE) during landing gear fatigue testing.* Cardiff University.

Baxter, M. G., Pullin, R., Holford, K. M. and Evans, S. L. 2007. Delta T Source Location for Acoustic Emission. *Mechanical Systems and Signal Processing* 21(3), pp. 1512-1520.

Ben Ammar, I., El Mahi, A., Karra, C., El Guerjouma, R. and Haddar, M. 2013. Mechanical behaviour and damage evaluation by acoustic emission of composite materials. *Multidiscipline Modeling in Materials and Structures* 9(1), pp. 100-115.

Ben Ammar, I., Karra, C., El Mahi, A., El Guerjouma, R. and Haddar, M. 2014. Mechanical behavior and acoustic emission technique for detecting damage in sandwich structures. *Applied Acoustics* 86, pp. 106-117.

Bohse, J. 2000. Acoustic emission characteristics of micro-failure processes in polymer blends and composites. *Composites Science and Technology* 60(8), pp. 1213-1226.

Boominathan, R., Arumugam, V., Santulli, C., Adhithya Plato Sidharth, A., Anand Sankar, R. and Sridhar, B. T. N. 2014. Acoustic emission characterization of the temperature effect on falling weight impact damage in carbon/epoxy laminates. *Composites Part B: Engineering* 56, pp. 591-598.

Bravo, A., Toubal, L., Koffi, D. and Erchiqui, F. 2013. Characterization of tensile damage for a short birch fiber-reinforced polyethylene composite with acoustic emission. *International Journal of Material Science* 3(3), pp. 79-89.

Bravo, A., Toubal, L., Koffi, D. and Erchiqui, F. 2015. Development of novel green and biocomposite materials: Tensile and flexural properties and damage analysis using acoustic emission. *Materials & Design* 66, pp. 16-28.

Carter, D. 2000. *Acoustic Emission Techniques for the Structural Integrity Monitoring of Steel Bridges*. Cardiff University.

Ciampa, F. and Meo, M. 2010. A new algorithm for acoustic emission localization and flexural group velocity determination in anisotropic structures. *Composites Part A: Applied Science and Manufacturing* 41(12), pp. 1777-1786.

Crivelli, D., Guagliano, M., Eaton, M., Pearson, M., Al-Jumaili, S., Holford, K. and Pullin, R. 2015. Localisation and identification of fatigue matrix cracking and delamination in a carbon fibre panel by acoustic emission. *Composites Part B: Engineering* 74, pp. 1-12.

Crivelli, D., Guagliano, M. and Monici, A. 2014. Development of an artificial neural network processing technique for the analysis of damage evolution in pultruded composites with acoustic emission. *Composites Part B: Engineering* 56, pp. 948-959.

David, L. D. and Donald, W. B. 1979. A Cluster Separation Measure. *Pattern Analysis and Machine Intelligence, IEEE Transactions on* 1(2), pp. 224-227.

de Groot, P., Wijnen, P. and Janssen, R. 1995. Real-Time Frequency Determination of Acoustic Emission for Different Fracture Mechanisms in Carbon/Epoxy Composites. *Composites Science and Technology* 55(4), pp. 405-412.

de Oliveira, R. and Marques, A. T. 2008. Health monitoring of FRP using acoustic emission and artificial neural networks. *Computers & Structures* 86(3), pp. 367-373.

Dudoit, S. and Fridlyand, J. 2002. A prediction-based resampling method for estimating the number of clusters in a dataset. *Genome Biology* 3(7), pp. 1-21.

Dzenis, Y. A. 2003. Cycle-based analysis of damage and failure in advanced composites under fatigue: 1. Experimental observation of damage development within loading cycles. *International Journal of Fatigue* 25(6), pp. 499-510.

Earle, P. S. and Shearer, P. M. 1994. Characterization of global seismograms using an automatic-picking algorithm. *Bulletin of the Seismological Society of America* 84(2), pp. 366-376.

Eaton, M., May, M., Featherston, C., Holford, K., Hallet, S. and Pullin, R. 2011a. Characterisation of Damage in Composite Structures using Acoustic Emission. In: *9th International Conference on Damage Assessment of Structures (DAMAS).* IOP Publishing,

Eaton, M., Pearson, M., Holford, K., Featherston, C. and Pullin, R. 2012a. Detection and Location of Impact Damage using Acoustic Emission. *Advanced Composite Materials and Technologies for Aerospace Applications*, p. 29.

Eaton, M. J. 2007a. *Acoustic Emission (AE) Monitoring of Buckling and Failure in Carbon Fibre Composite Structures.* Cardiff University.

Eaton, M. J., Holford, Karen Margaret, Featherston, Carol Ann and Pullin, Rhys. 2007b. Damage in Carbon Fibre Composites: The Discrimination of Acoustic Emission Signals Using Frequency. *Journal of Acoustic Emission* 25 pp. 140-148.

Eaton, M. J., Pullin, R., Hensman, J. J., Holford, K. M., Worden, K. and Evans, S. L. 2011b. Principal Component Analysis of Acoustic Emission Signals From Landing Gear Components: An Aid to Fatigue Fracture Detection. *Strain* 47, pp. 588-594.

Eaton, M. J., Pullin, R. and Holford, K. M. 2012b. Acoustic Emission Source Location in Composite Materials Using Delta T Mapping. *Composites Part A: Applied Science and Manufacturing* 43(6), pp. 856-863.

Featherston, C. A., Eaton, M., Pullin, R. and Holford, K. M. 2009. Structural health monitoring of buckling composite structures using acoustic emission. In: *ICCES: International Conference on Computational & Experimental Engineering and Sciences.* pp. 29-35.

Gathercole, N., Reiter, H., Adam, T. and Harris, B. 1994. Life prediction for fatigue of T800/5245 carbon-fibre composites: I. Constant-amplitude loading. *International Journal of Fatigue* 16(8), pp. 523-532.

Giordano, M., Calabro, A., Esposito, C., D'Amore, A. and Nicolais, L. 1998. An Acoustic-Emission Characterization of the Failure Modes in Polymer-Composite Materials. *Composites Science and Technology* 58(12), pp. 1923-1928.

Godin, N., Huguet, S. and Gaertner, R. 2005. Integration of the Kohonen's self-organising map and k-means algorithm for the segmentation of the AE data

collected during tensile tests on cross-ply composites. *NDT & E International* 38(4), pp. 299-309.

Godin, N., Huguet, S., Gaertner, R. and Salmon, L. 2004. Clustering of Acoustic Emission Signals Collected During Tensile Tests on Unidirectional Glass/Polyester Composite Using Supervised and Unsupervised Classifiers. *NDT & E International* 37(4), pp. 253-264.

Gorman, M. R. 1991. Plate wave acoustic emission. *The Journal of the Acoustical Society of America* 90(1), pp. 358-364.

Gorman, M. R. and Prosser, W. H. 1991. AE source orientation by plate wave analysis.

Gorman, M. R. and Ziola, S. M. 1991. Plate waves produced by transverse matrix cracking. *Ultrasonics* 29(3), pp. 245-251.

Grondel, S., Delebarre, C., Assaad, J., Dupuis, J. P. and Reithler, L. 2002. Fatigue crack monitoring of riveted aluminium strap joints by Lamb wave analysis and acoustic emission measurement techniques. *NDT & E International* 35(3), pp. 137-146.

Gutkin, R., Green, C. J., Vangrattanachai, S., Pinho, S. T., Robinson, P. and Curtis, P. T. 2011. On acoustic emission for failure investigation in CFRP: Pattern recognition and peak frequency analyses. *Mechanical Systems and Signal Processing* 25(4), pp. 1393-1407.

Hamstad, M., O'Gallagher, A. and Gary, J. 2002. A wavelet transform applied to acoustic emission. *Journal of acoustic emission* 20, pp. 39-61.

He, T., Pan, Q., Liu, Y., Liu, X. and Hu, D. 2012. Near-field beamforming analysis for acoustic emission source localization. *Ultrasonics* 52(5), pp. 587-592.

Hensman, J., Mills, R., Pierce, S. G., Worden, K. and Eaton, M. 2010. Locating Acoustic Emission Sources in Complex Structures Using Gaussian Processes. *Mechanical Systems and Signal Processing* 24(1), pp. 211-223.

Holford, K. M. and Carter, D. C. 1999. Acoustic emission source location. *Key Engineering Materials* 167, pp. 162-171.

Holland, S., Kosel, T., Weaver, R. and Sachse, W. 2000. Determination of plate source, detector separation from one signal. *Ultrasonics* 38(1), pp. 620-623.

Hsu, N. N. and Breckenridge, F. R. 1981. Characterization and Calibration of Acoustic Emission Sensors. *Materials Evaluation* 39(1), pp. 60-68.

Huang, M., Jiang, L., Liaw, P., Brooks, C., Seelev, R. and Klarstrom, D. 1998. Using Acoustic Emission in Fatigue and Fracture Materials Research. *JOM* 50(11), pp. 1-14.

Huguet, S., Godin, N., Gaertner, R., Salmon, L. and Villard, D. 2002. Use of Acoustic Emission to Identify Damage Modes in Glass Fibre Reinforced Polyester. *Composites Science and Technology* 62(10), pp. 1433-1444.

Jiao, J., He, C., Wu, B., Fei, R. and Wang, X. 2004. Application of wavelet transform on modal acoustic emission source location in thin plates with one sensor. *International Journal of Pressure Vessels and Piping* 81(5), pp. 427-431.

Johnson, M. 2002. Waveform Based Clustering and Classification of AE Transients in Composite Laminates Using Principal Component Analysis. *NDT & E International* 35(6), pp. 367-376.

Kim, S. T. and Lee, Y. T. 1997. Characteristics of damage and fracture process of carbon fiber reinforced plastic under loading-unloading test by using AE method. *Materials Science and Engineering: A* 234, pp. 322-326.

Kinjo, T., Suzuki, H., Saito, N., Takemoto, M. and Ono, K. 1997. Fracture-mode classification using wavelet-transformed AE signals from a composite. *Journal of acoustic emission* 15(1-4), pp. 19-32.

Kontsos, A., Loutas, T., Kostopoulos, V., Hazeli, K., Anasori, B. and Barsoum, M. W. 2011. Nanocrystalline Mg–MAX composites: Mechanical behavior characterization via acoustic emission monitoring. *Acta Materialia* 59(14), pp. 5716-5727.

Kostopoulos, V., Loutas, T. H., Kontsos, A., Sotiriadis, G. and Pappas, Y. Z. 2003. On the identification of the failure mechanisms in oxide/oxide composites using acoustic emission. *NDT & E International* 36(8), pp. 571-580.

Kostopoulos, V., Tsotra, P., Karapappas, P., Tsantzalis, S., Vavouliotis, A., Loutas, T. H., Paipetis, A., Friedrich, K. and Tanimoto, T. 2007. Mode I interlaminar fracture of CNF or/and PZT doped CFRPs via acoustic emission monitoring. *Composites Science and Technology* 67(5), pp. 822-828.

Kotsikos, G., Evans, J. T., Gibson, A. G. and Hale, J. 1999. Use of acoustic emission to characterize corrosion fatigue damage accumulation in glass fiber reinforced polyester laminates. *Polymer Composites* 20(5), pp. 689-696.

Kundu, T. 2014. Acoustic source localization. *Ultrasonics* 54(1), pp. 25-38.

Kundu, T., Nakatani, H. and Takeda, N. 2012. Acoustic source localization in anisotropic plates. *Ultrasonics* 52(6), pp. 740-746.

Kundu, T., Yang, X., Nakatani, H. and Takeda, N. 2015. A two-step hybrid technique for accurately localizing acoustic source in anisotropic structures without knowing their material properties. *Ultrasonics* 56, pp. 271-278.

Kurz, J. H., Grosse, C. U. and Reinhardt, H. W. 2005. Strategies for reliable automatic onset time picking of acoustic emissions and of ultrasound signals in concrete. *Ultrasonics* 43(7), pp. 538-546.

Li, D., Hu, Q. and Ou, J. 2012. Fatigue Damage Evolution and Monitoring of Carbon Fiber Reinforced Polymer Bridge Cable by Acoustic Emission Technique. *International Journal of Distributed Sensor Networks* 2012.

Li, L., Lomov, S. V. and Yan, X. 2015. Correlation of acoustic emission with optically observed damage in a glass/epoxy woven laminate under tensile loading. *Composite Structures* 123, pp. 45-53.

Li, L., Lomov, S. V., Yan, X. and Carvelli, V. 2014. Cluster analysis of acoustic emission signals for 2D and 3D woven glass/epoxy composites. *Composite Structures* 116, pp. 286-299.

Liu, P. F., Chu, J. K., Liu, Y. L. and Zheng, J. Y. 2012. A study on the failure mechanisms of carbon fiber/epoxy composite laminates using acoustic emission. *Materials & Design* 37, pp. 228-235.

Lokajíček, T. and Klima, K. 2006. A first arrival identification system of acoustic emission (AE) signals by means of a high-order statistics approach. *Measurement Science and Technology* 17(9), p. 2461.

Lopresto, V., Leone, C., Caprino, G. and De Iorio, I. eds. 2009. *Analysis of acoustic emission signals produced by different carbon fibre reinforced plastic laminates*. Proceedings of 17th international conference on composite materials-ICCM-17, Edinburgh–UK.

Loutas, T. H. and Kostopoulos, V. 2009. Health Monitoring of Carbon/Carbon, Woven Reinforced Composites. Damage Assessment by Using Advanced Signal Processing Techniques. Part I: Acoustic Emission Monitoring and Damage Mechanisms Evolution. *Composites Science and Technology* 69(2), pp. 265-272.

Loutas, T. H., Kostopoulos, V., Ramirez-Jimenez, C. and Pharaoh, M. 2006. Damage evolution in center-holed glass/polyester composites under quasi-static loading using time/frequency analysis of acoustic emission monitored waveforms. *Composites Science and Technology* 66(10), pp. 1366-1375.

Lu, C., Ding, P. and Chen, Z. 2011. Time-frequency Analysis of Acoustic Emission Signals Generated by Tension Damage in CFRP. *Procedia Engineering* 23, pp. 210-215.

MacQueen, J. 1967. Some Methods for Classification and Analysis of Multivariate Observations. In: *the fifth Berkeley symposium on mathematical statistics and probability.* pp. 281-297.

Mäder, E., Moos, E. and Karger-Kocsis, J. 2001. Role of film formers in glass fibre reinforced polypropylene — new insights and relation to mechanical properties. *Composites Part A: Applied Science and Manufacturing* 32(5), pp. 631-639.

Maeda, N. 1985. A method for reading and checking phase times in auto-processing system of seismic wave data. *Zisin= Jishin* 38(3), pp. 365-379.

Maillet, E., Godin, N., R'Mili, M., Reynaud, P., Fantozzi, G. and Lamon, J. 2014. Damage monitoring and identification in SiC/SiC minicomposites using combined acousto-ultrasonics and acoustic emission. *Composites Part A: Applied Science and Manufacturing* 57, pp. 8-15.

Maillet, E., Godin, N., R'Mili, M., Reynaud, P., Lamon, J. and Fantozzi, G. 2012. Analysis of Acoustic Emission energy release during static fatigue tests at intermediate temperatures on Ceramic Matrix Composites: Towards rupture time prediction. *Composites Science and Technology* 72(9), pp. 1001-1007.

Mal, A. 2002. Elastic waves from localized sources in composite laminates. *International Journal of Solids and Structures* 39(21), pp. 5481-5494.

Manson, G., Worden, K., Holford, K. and Pullin, R. 2001. Visualisation and Dimension Reduction of Acoustic Emission Data for Damage Detection. *Journal of Intelligent Material Systems and Structures* 12(8), pp. 529-536.

Mao, H. and Mahadevan, S. 2002. Fatigue damage modelling of composite materials. *Composite Structures* 58(4), pp. 405-410.

Marec, A., Thomas, J. H. and El Guerjouma, R. 2008. Damage Characterization of Polymer-Based Composite Materials: Multivariable Analysis and Wavelet Transform For Clustering Acoustic Emission Data. *Mechanical Systems and Signal Processing* 22(6), pp. 1441-1464.

Martínez-Jequier, J., Gallego, A., Suárez, E., Juanes, F. J. and Valea, Á. 2015. Real-time damage mechanisms assessment in CFRP samples via acoustic emission Lamb wave modal analysis. *Composites Part B: Engineering* 68, pp. 317-326.

Masmoudi, S., El Mahi, A. and El Guerjouma, R. 2014a. Mechanical behaviour and health monitoring by acoustic emission of sandwich composite integrated by piezoelectric implant. *Composites Part B: Engineering* 67, pp. 76-83.

Masmoudi, S., El Mahi, A., El Guerjouma, R. and Turki, S. 2014b. Mechanical behaviour and identification of damage by acoustic emission of smart composites. *Multidiscipline Modeling in Materials and Structures* 10(1), pp. 2-17.

Masmoudi, S., El Mahi, A. and Turki, S. 2015. Use of piezoelectric as acoustic emission sensor for in situ monitoring of composite structures. *Composites Part B: Engineering* 80, pp. 307-320.

Matt, H. M. and Di Scalea, F. L. 2007. Macro-fiber composite piezoelectric rosettes for acoustic source location in complex structures. *Smart Materials and Structures* 16(4), pp. 1489-1499.

McCrory, J., Al-Jumaili, S. K., Pearson, M., Eaton, M., Holford, K. and Pullin, R. 2014. Automated corrected MAR calculation for characterisation of AE signals. In: *31st Conference of the European Working Group on Acoustic Emission (EWGAE).* Dresden, Germany.

McLaskey, G. C., Glaser, S. D. and Grosse, C. U. 2010. Beamforming array techniques for acoustic emission monitoring of large concrete structures. *Journal of Sound and Vibration* 329(12), pp. 2384-2394.

Mehan, R. and Mullin, J. 1971. Analysis of Composite Failure Mechanisms Using Acoustic Emissions. *Journal of Composite Materials* 5(2), pp. 266-269.

Miller, K. R. and Hill, E. K. 2005. Nondestructive Testing Handbook, Third Edition: Volume 6, Acoustic Emission Testing. *American Society for Non-Destructive Testing*.

Moevus, M., Godin, N., R'Mili, M., Rouby, D., Reynaud, P., Fantozzi, G. and Farizy, G. 2008. Analysis of Damage Mechanisms and Associated Acoustic Emission in Two Sicf/[Si–B–C] Composites Exhibiting Different Tensile Behaviours. Part II: Unsupervised Acoustic Emission Data Clustering. *Composites Science and Technology* 68(6), pp. 1258-1265.

Mohd, S. 2013. *Acoustic emission for fatigue crack monitoring in nuclear piping system.* Cardiff University.

Momon, S., Godin, N., Reynaud, P., R'Mili, M. and Fantozzi, G. 2012. Unsupervised and Supervised Classification of AE Data Collected During Fatigue Test on CMC at High Temperature. *Composites Part A: Applied Science and Manufacturing* 43(2), pp. 254-260.

Momon, S., Moevus, M., Godin, N., R'Mili, M., Reynaud, P., Fantozzi, G. and Fayolle, G. 2010. Acoustic emission and lifetime prediction during static fatigue tests on ceramic-matrix-composite at high temperature under air. *Composites Part A: Applied Science and Manufacturing* 41(7), pp. 913-918.

Morscher, G. N. 1999. Modal acoustic emission of damage accumulation in a woven SiC/SiC composite. *Composites Science and Technology* 59(5), pp. 687-697.

Ni, Q. Q. and Iwamoto, M. 2002. Wavelet transform of acoustic emission signals in failure of model composites. *Engineering Fracture Mechanics* 69(6), pp. 717-728.

Nielsen, A. 1980. *Acoustic emission source based on pencil lead breaking*.

Niri, D. E., Farhidzadeh, A. and Salamone, S. 2014. Nonlinear Kalman Filtering for acoustic emission source localization in anisotropic panels. *Ultrasonics* 54(2), pp. 486-501.

Omkar, S. and Senthilnath, J. 2009. Artificial bee colony for classification of acoustic emission signal source. *International Journal of Aerospace Innovations* 1(3), pp. 129-143.

Omkar, S. N. and Karanth U, R. 2008. Rule extraction for classification of acoustic emission signals using Ant Colony Optimisation. *Engineering Applications of Artificial Intelligence* 21(8), pp. 1381-1388.

Oskouei, A. R. and Ahmadi, M. 2009. Fracture Strength Distribution in E-Glass Fiber Using Acoustic Emission. *Journal of Composite Materials*.

Oskouei, A. R. and Ahmadi, M. 2010. Acoustic Emission Characteristics of Mode I Delamination in Glass/Polyester Composites. *Journal of Composite Materials* 44(7), pp. 793-807.

Oskouei, A. R., Ahmadi, M. and Hajikhani, M. 2009. Wavelet-based acoustic emission characterization of damage mechanism in composite materials under

mode Idelamination at different interfaces. *eXPRESS Polymer Letters* 3(12), pp. 804-813.

Oskouei, A. R., Heidary, H., Ahmadi, M. and Farajpur, M. 2012. Unsupervised Acoustic Emission Data Clustering For the Analysis of Damage Mechanisms in Glass/Polyester Composites. *Materials & Design* 37, pp. 416-422.

PAC. 2003. WaveGen1410 Arbitrary Waveform Generator Subsystem User's Mannual Rev.2. Physical Acoustics Corporation, Princeton Junction, New Jersey, USA.

PAC. 2004. PCI-2 Based AE System User's Manual. Physical Acoustics Corporation, Princeton Junction, New Jersey, USA.

Pappas, Y. Z., Kontsos, A., Loutas, T. H. and Kostopoulos, V. 2004. On the Characterization of Continuous Fibres Fracture by Quantifying Acoustic Emission and Acousto-Ultrasonics Waveforms. *NDT & E International* 37(5), pp. 389-401.

Pappas, Y. Z., Markopoulos, Y. P. and Kostopoulos, V. 1998. Failure Mechanisms Analysis of 2D Carbon/Carbon Using Acoustic Emission Monitoring. *NDT & E International* 31(3), pp. 157-163.

Pearson, M. 2013. *Development of lightweight structural health monitoring systems for aerospace applications.* Cardiff University.

Pollock, A. 1986. Classical Wave Theory in Practical AE Testing. *Progress in Acoustic Emission III, Proceedings of the Eighth International Acoustic Emission Symposium, The Japanese Society for Nondestructive Testing*, pp. 708 - 721.

Prosser, W., Jackson, K., Kellas, S., Smith, B., McKeon, J. and Friedman, A. 1995. Advanced waveform-based acoustic emission detection of matrix cracking in composites. *Materials evaluation* 53(9), pp. 1052-1058.

Prosser, W. H. 1991. *The propagation characteristics of the plate modes of acoustic emission waves in thin aluminum plates and thin graphite/epoxy composite plates and tubes.* John Hopkins University.

Prosser, W. H. 1996. Advanced AE techniques in composite materials research. *Journal of Acoustic Emission* 14, pp. 1-11.

Pullin, R., Baxter, M., J., E. M., Holford, K. M. and Evans, S. L. 2007a. Novel Acoustic Emission Source Detection. *Journal of Acoustic Emission* 25 pp. 215-223.

Pullin, R., Holford, K. M. and Baxter, M. 2005. Modal analysis of acoustic emission signals from artificial and fatigue crack sources in aerospace grade steel. *Key Engineering Materials* 293, pp. 217-226.

Pullin, R., Holford, K. M., Evans, S. L., Baxter, M. and Hensman, J. J. 2007b. Advanced location and characterisation of damage in complex metallic structures using acoustic emission. In: *13th International Conference on Experimental Mechanics ICEM.* pp. 925-926.

Qi, G. 2000. Wavelet-Based AE Characterization of Composite Materials. *NDT & E International* 33(3), pp. 133-144.

Ramirez-Jimenez, C. R., Papadakis, N., Reynolds, N., Gan, T. H., Purnell, P. and Pharaoh, M. 2004. Identification of Failure Modes in Glass/Polypropylene Composites by Means of the Primary Frequency Content of the Acoustic Emission Event. *Composites Science and Technology* 64(12), pp. 1819-1827.

Rindorf, H. J. 1981. *Acoustic emission source location in theory and in practice*. Brüel & Kjær.

Rippengill, S., Worden, K., Holford, K. M. and Pullin, R. 2003. Automatic Classification of Acoustic Emission Patterns. *Strain* 39(1), pp. 31-41.

Rousseeuw, P. J. 1987. Silhouettes: A Graphical Aid to the Interpretation and Validation of Cluster Analysis. *Journal of Computational and Applied Mathematics* 20, pp. 53-65.

Sause, M. G. R., Hamstad, M. A. and Horn, S. 2013. Finite element modeling of lamb wave propagation in anisotropic hybrid materials. *Composites Part B: Engineering* 53, pp. 249-257.

Sause, M. G. R., Müller, T., Horoschenkoff, A. and Horn, S. 2012. Quantification of Failure Mechanisms in Mode-I Loading of Fiber Reinforced Plastics Utilizing Acoustic Emission Analysis. *Composites Science and Technology* 72(2), pp. 167-174.

Sawan, H. A., Walter, M. E. and Marquette, B. 2015. Unsupervised learning for classification of acoustic emission events from tensile and bending experiments with open-hole carbon fiber composite samples. *Composites Science and Technology* 107, pp. 89-97.

Scholey, J. J., Wilcox, P. D., Wisnom, M. R., Friswell, M. I., Pavier, M. and Aliha, M. R. 2009. A generic technique for acoustic emission source location. *Journal of Acoustic Emission* 27, pp. 291-298.

Sedlak, P., Hirose, Y., Khan, S. A., Enoki, M. and Sikula, J. 2009. New automatic localization technique of acoustic emission signals in thin metal plates. *Ultrasonics* 49(2), pp. 254-262.

Sharma, S. 1995. *Applied multivariate techniques*. John Wiley & Sons, Inc.

Sleeman, R. and van Eck, T. 1999. Robust automatic P-phase picking: an on-line implementation in the analysis of broadband seismogram recordings. *Physics of the earth and planetary interiors* 113(1), pp. 265-275.

Surgeon, M. and Wevers, M. 1999. Modal analysis of acoustic emission signals from CFRP laminates. *NDT & E International* 32(6), pp. 311-322.

Talreja, R. 1989. Damage development in composites: Mechanisms and modelling. *The Journal of Strain Analysis for Engineering Design* 24(4), pp. 215-222.

Theobald, P., Zeqiri, B. and Avison, J. 2008. Couplants and their influence on AE sensor sensitivity. *Journal of Acoustic Emission* 26, pp. 91-97.

Theobald, P. D. 2004. Towards traceable calibration of acoustic emission measurement systems: development of a reference source at the UK's National Physical Laboratory. In: *DGZfP-Proceedings BB.* pp. 683-690.

Toyama, N., Koo, J. H., Oishi, R., Enoki, M. and Kishi, T. 2001. Two-dimensional AE source location with two sensors in thin CFRP plates. *Journal of Materials Science Letters* 20(19), pp. 1823-1825.

Vallen. 2006. AMSY-5 User's Mannual, Vallen-Systeme GmbH, Schäftlarner Weg 26A, 82057 Icking, Germany.

Vallen, H. 2002. AE testing fundamentals, equipment, applications. *Journal of Nondestructive Testing(Germany)* 7(9), pp. 1-30.

Wang, J. and Teng, T.-L. 1995. Artificial neural network-based seismic detector. *Bulletin of the Seismological Society of America* 85(1), pp. 308-319.

Wang, X., Zhang, H. P. and Yan, X. 2011. Classification and identification of damage mechanisms in polyethylene self-reinforced laminates by acoustic emission technique. *Polymer Composites* 32(6), pp. 945-959.

Wevers, M. 1997. Listening to the Sound Of Materials: Acoustic Emission for the Analysis of Material Behaviour. *NDT & E International* 30(2), pp. 99-106.

Wise, B. M., Gallagher, N. B., Butler, S. W., White, D. D. and Barna, G. G. 1999. A Comparison of Principal Component Analysis, Multiway Principal Component Analysis, Trilinear Decomposition and Parallel Factor Analysis for Fault Detection in a Semiconductor Etch Process. *Journal of Chemometrics* 13(3-4), pp. 379-396.

Woo, S. C. and Choi, N. S. 2007. Analysis of Fracture Process in Single-Edge-Notched Laminated Composites Based on the High Amplitude Acoustic Emission Events. *Composites Science and Technology* 67(7), pp. 1451-1458.

Woo, S. C., Choi, N. S. and Cho, N. 2008. Characterization of the Fracture Process of Notched Glass Fiber/Aluminum Hybrid Laminates by Acoustic Emission. *Composites Science and Technology* 68(6), pp. 1521-1530.

Zhao, J., Wang, K. and Guo, Y. 2010. Acoustic emission signals classification based on support vector machine. In: *Computer Engineering and Technology (ICCET), 2010 2nd International Conference IEEE.* 16-18 April 2010. pp. 300-304.

Zhuang, X. and Yan, X. 2006. Investigation of Damage Mechanisms in Self-Reinforced Polyethylene Composites by Acoustic Emission. *Composites Science and Technology* 66(3), pp. 444-449.

Ziola, S. M. and Gorman, M. R. 1991. Source location in thin plates using cross-correlation. *The Journal of the Acoustical Society of America* 90(5), pp. 2551-2556.

APPENDIX

PUBLISHED PAPERS

Mechanical Systems and Signal Processing 72-73 (2016) 513–524

Contents lists available at ScienceDirect

Mechanical Systems and Signal Processing

journal homepage: www.elsevier.com/locate/ymssp

Acoustic emission source location in complex structures using full automatic delta T mapping technique

Safaa Kh. Al-Jumaili [a,b,*], Matthew R. Pearson [a], Karen M. Holford [a], Mark J. Eaton [a], Rhys Pullin [a]

[a] Cardiff School of Engineering, Cardiff University, Queen's Buildings, The Parade, Cardiff CF24 3AA, UK
[b] University of Basrah, Basrah, Iraq

ARTICLE INFO

Article history:
Received 18 September 2015
Received in revised form
10 November 2015
Accepted 19 November 2015
Available online 2 December 2015

Keywords:
Acoustic emission
Source location
Complex structure
Unsupervised clustering
Delta T mapping technique

ABSTRACT

An easy to use, fast to apply, cost-effective, and very accurate non-destructive testing (NDT) technique for damage localisation in complex structures is key for the uptake of structural health monitoring systems (SHM). Acoustic emission (AE) is a viable technique that can be used for SHM and one of the most attractive features is the ability to locate AE sources. The time of arrival (TOA) technique is traditionally used to locate AE sources, and relies on the assumption of constant wave speed within the material and uninterrupted propagation path between the source and the sensor. In complex structural geometries and complex materials such as composites, this assumption is no longer valid. *Delta T mapping* was developed in Cardiff in order to overcome these limitations; this technique uses artificial sources on an area of interest to create training maps. These are used to locate subsequent AE sources. However operator expertise is required to select the best data from the training maps and to choose the correct parameter to locate the sources, which can be a time consuming process.

This paper presents a new and improved fully automatic delta T mapping technique where a clustering algorithm is used to automatically identify and select the highly correlated events at each grid point whilst the "Minimum Difference" approach is used to determine the source location. This removes the requirement for operator expertise, saving time and preventing human errors. A thorough assessment is conducted to evaluate the performance and the robustness of the new technique. In the initial test, the results showed excellent reduction in running time as well as improved accuracy of locating AE sources, as a result of the automatic selection of the training data. Furthermore, because the process is performed automatically, this is now a very simple and reliable technique due to the prevention of the potential source of error related to manual manipulation.

1. Introduction

Acoustic emission (AE) is a non-destructive testing (NDT) technique concerned with the passive monitoring of ultrasonic stress waves emitted from a variety of sources in a structure [1]. There are a variety of sources that cause AE which include

* Corresponding author at: Cardiff School of Engineering, Cardiff University, Queen's Buildings, The Parade, Cardiff CF24 3AA, UK. Tel.: +4402920877297,fax: +442920874939.
E-mail addresses: Al-JumailiSK@cardiff.ac.uk (S. Kh. Al-Jumaili), PearsonMR@cardiff.ac.uk (M.R. Pearson), Holford@cardiff.ac.uk (K.M. Holford), EatonM@cardiff.ac.uk (M.J. Eaton), PullinR@cardiff.ac.uk (R. Pullin).

http://dx.doi.org/10.1016/j.ymssp.2015.11.026
0888-3270/

crack propagation, friction, fretting and impact damage. These events will generate acoustic waves which can be detected at the structure's surface using piezoelectric transducers. The use of AE is important for SHM as it offers the potential for the real time monitoring of the health of a structure. The ability to track the early onset of damage and hence determine the structure's integrity will enable the switch from periodic inspections to a more condition based approach, therefore enabling increased inspection intervals, reducing structure downtime and maintenance costs. SHM techniques can be utilised to monitor hard to access structures such as off-shore wind turbines. One of the most attractive features of AE is the capability of source location and it is considered an important step for SHM [2]. For large-scale structures it is very costly and time consuming to inspect every part of the structure using the traditional techniques, such as X-ray and active ultrasonic techniques. If the damage location is known in advance it would enable maintenance teams to focus on particular areas of concern when using other NDE techniques. In addition, knowledge of the damage location can improve damage characterisation, because damage mechanisms are often dependent upon particular geometric features and loading conditions.

The conventional AE source location technique, known as the time-of-arrival or TOA technique, is discussed in detail in the NDT handbook [1]. It has been widely used to locate AE sources in isotropic and homogenous structures and is based on detecting the arrival time of an AE signal at each of the sensors for the fastest propagating mode, which enables the source to be located using a simple triangulation technique. The TOA technique relies on the assumptions of a constant wave speed in all directions from the source to sensor and an uninterrupted propagation path between the source and the sensor. In realistic structures the wave speed is rarely constant due to thickness changes and anisotropy in composite materials, where the wave velocity is dependent on the propagation direction, for instance the wave velocity of the fastest propagating mode is considerably higher in the fibre direction. Geometric features such as holes, lugs and structural discontinuities will also considerably affect the propagation path and velocity [3,4]. These factors mean that the assumptions relied upon by the TOA technique are not valid and hence will introduce errors in the source location calculation. In addition, any errors in the determination of signal arrival times will result in a further loss of accuracy in the estimated source locations. The threshold crossing approach, used commercially to pick the time of arrival of the AE signal is not satisfactory, because using a high threshold level will lead to inaccurate time of arrival measurement, while a lower threshold value will increase the ability to pick the accurate waveform onset but also increases the risk of a false trigger. In order to improve arrival time estimation a number of approaches have been investigated. The STA/LTA method compares the average energy in a short term window (STA) with the average energy in a long term window (LTA) prior to a point I in a signal [5]. The change in ratio indicates the signal arrival, however, despite good performance in noisy data the use of averages makes accurate determination difficult and a threshold is still needed to detect the change. The cross-correlation technique [6] has been used to find the arrival of a particular frequency within a signal by cross-correlation a short, single frequency, Gaussian windowed pulse with the recorded signal. An expansion of this is the use of wavelet transforms which identify energy arrival across a range of frequency. However it has been shown that the accuracy of this approach is poor in complex structures where multiple reflections are present [7]. Lokajicek and Klima [8] took the sixth order statistical moment of a sliding short time window which changes with the presence of structured data points associated to the signal. Although the moment is sensitive the detection of the change still relies upon a threshold. The use of neural networks has been investigated [9] however, its computational complexity limits its application in practice. A more reliable approach for arrival time estimation of seismic and ultrasonic signals adopts the Akiake information criteria (AIC) [10]. The AIC was first adapted for use directly on transient seismic data by Maeda [11]. However, more recently it has been demonstrated for accurate determination of arrival time of AE and ultrasonic transient signals [4,12–14]. The AIC function compares the signal entropy before and after each point i in a signal and returns a minimum at the signal onset where the greatest difference is seen between the high entropy random noise seen prior to signal onset and the low entropy structured signal after onset.

Attempts to improve upon the triangulation approach used in the TOA algorithm have been widely reported. AE source location in isotropic materials without prior knowledge of the wave speed has been reported by many researchers as an improvement over the simple TOA approach. These include the beamforming method [15,16] which is based on the delay-and-sum algorithm from small sensor arrays and the strain rosette technique [17] where the source location was predicted from the principal strain directions using rosette arranged macro-fibre composite (MFC) sensors. The modal acoustic emission method [18,19], where the AE wave modes in thin isotropic plates are predicted from the dispersion characteristics has also been used. The wavelet transform theory has been utilised to determine the arrival times of the different modes for one-dimensional [20] and two-dimensional location [7,21] respectively. AE location in anisotropic materials is challenging due to anisotropic propagation velocities. A number of interesting approaches have been taken to solving this problem [22–24] and improvements in accuracy have been shown in simple laminate plates. Ciampa et al. [25] utilised a specific layout of sensors to locate impact events in anisotropic materials without prior knowledge of the plate properties. Solution of a system of nonlinear equations is required in this technique. Kundu et al. [22] successfully developed a technique based on a cluster of sensors which was demonstrated in anisotropic plates and avoids the need to solve a system of nonlinear equations. Niri et al. [23] used the nonlinear Kalman Filtering algorithms (Extended Kalman Filter (EKF) and Unscented Kalman Filter (UKF)) as a probabilistic localisation algorithms to estimate the location of AE sources in anisotropic panels. Kundu et al. [24] present a two-step hybrid technique to locate sources in anisotropic plates. Wave propagation in a straight line is assumed in the first step to find the initial source location and solving an optimisation problem is the second step to improve the initial location accuracy.

However none of these approaches account for structural complexities that may alter the wave propagation path and velocity, such as holes and thickness changes that may be present in reality. The development of the *Delta T Mapping (DTM) technique* accounts for these sources of error. The technique is a mapping approach whereby artificial sources are used to map a structure and thus allow high location accuracy on realistic complex structures. Originally developed for complex geometry metallic structures [26], the technique has also been shown to perform very well in anisotropic materials such as composites [27].

Although the DTM technique has shown the ability to locate with a high level of accuracy in complex structures, the collection and processing of training data can be very time consuming. It requires an operator with an AE background to select the optimal data to ensure the greatest possible accuracy. Furthermore, for locating AE sources a user must rely on experience and trial and error to determine processing parameters such as a suitable cluster diameter. Overcoming these problems will lead to a fully automatic process which would not relay on experience and would remove any human error whilst still maintaining or improving the accuracy of source location.

The objective of this paper is to extend the previous work on the DTM technique [26–29] and create a fully automatic technique which reduces human input and increases accuracy, reliability and the speed of the process.

The remainder of this paper is structured as follows: Section 2 will present the original *Delta T Mapping technique* in detail and describe the main limitations. The next section will present the main outline of the proposed methodology, followed by the experimental procedure for validation. The results are then presented and discussed and finally conclusions are drawn.

2. Original Delta-T Mapping technique methodology

According to Baxter [26] the main steps for the implementation of the DTM technique are outlined briefly below:

i. **Determine an area of interest and construct a grid system**: The DTM technique offers the ability for monitoring the complete structure or a part of it, which maybe of specific interest due to geometric features or known stress concentrations. A grid is constructed on the area of interest within which AE events will be located. A source which creates a broadband artificial AE source is preferable and different sensor types can be used to monitor the area of interest. Sensors can also be placed within the area of interest, as long as most of the sensors provide coverage with the area of interest within the sensor array.

ii. **Collect arrival time data from artificial sources at each grid node**: Hsu–Nielson (H–N) pencil lead fracture sources [30] are generated at each node position within the grid. The H–N source creates an artificial AE source which enables the determination of the TOA from source to sensors to be calculated for each sensor pair. Averaging the recorded TOAs of several events at each node of the grid is used to reduce source errors in the training data. Missing nodal data, as a result of holes, for example can be interpolated from the other surrounding nodes.

iii. **Calculate ΔT maps**: Once the TOA data for each node position has been collected the difference in arrival time (delta-T) for each sensor pair can be calculated, for example four sensors would results in six sensor pairs. Knowing the co-ordinates of each node results in the generation of average delta-T maps for each sensor pair. Contours of constant delta-T relative to all sensor pairs can be visualised as a resulting map.

iv. **Real AE data location**: Once real AE data has been collected, the delta-T for each sensor pair from a real AE event can be calculated. The resulting delta-Ts for each sensor pair can be represented by a line of constant delta-T which displays possible source locations. By overlaying these identified contours for each sensor pair a convergence point is identified, indicating the source location. As with the time of TOA technique, at least three sensors are required to provide a 2D source location. The confidence in source location estimation can be improved using additional sensors. Theoretically all lines should intersect at one location; however in reality, not all lines will cross at the same point. Therefore, to estimate the source location all convergence points are identified and a cluster analysis provides the most probable source location.

The traditional DTM technique used threshold crossing to determine the arrival times of the propagation waves at the sensors. The most recent version of DTM technique is known as the AIC DTM technique and was developed by [28,29] and overcame the limitation of arrival time calculation. Although the traditional DTM technique located successfully AE sources in different structural materials and complexity, the major disadvantage was the first threshold crossing approach which can generate erroneous locations when the actual signal onset is lower than the threshold level set. Pearson et al. [28,29] present a solution of this problem by exploiting the Akiake Information Criteria (AIC) [10] to determine the actual signal onset for both the training and the actual event data.

Although these iterations of the DTM approach have made improvements in location accuracy and reliability, there are still a number of limitations with this approach. Firstly, as mentioned above, several events are required to be generated at each node in the grid. Selection of the correct events and removing erroneous data is essential to constructing the training maps. Nominally this is conducted by recording times at which erroneous data occurred and by visual inspection by the operator, resulting in a lengthy process depending on the size of the grid. Secondly, only the convergence points inside a specific cluster diameter are used to calculate the probable AE source location (step 4). The optimum cluster diameter is

determined by the operator by collecting data from known random node positions and comparing the error between actual and estimated source locations before testing commences. The optimum cluster diameter might not be same for all positions.

These limitations have a direct effect on the performance of the technique and result in less accurate probable source locations. The inclusion of incorrect events in each grid point will affect the training map accuracy and/or selecting non-optimum cluster diameters will affect source location accuracy. Furthermore, the process of manual selection of optimum training data is time consuming. This paper presents a new approach which overcomes these limitations.

3. Improved Delta T mapping technique

In order to reduce the sources of error related to the traditional DTM technique a fully automatic new DTM approach is presented here. This approach can be divided into two parts; firstly, selecting the valid events at each grid point using an unsupervised clustering technique and secondly, calculating the AE source location using the Minimum Difference approach [1,31], to eliminate any human manipulation of the data. The main new features of the fully automatic DTM technique are presented in the flowchart (Fig. 1). This section will describe each part of the new approach.

3.1. Selection of correct events

3.1.1. Unsupervised clustering methodology of AE events

After collection of the training data by applying artificial sources on each node position in the grid the time of arrival to each sensor is obtained. There is no restriction to the number of artificial sources used at each position, typically five to 10 H–N sources gives good repeatability. The classification process is applied at each grid position to select AE events which are highly similar to each other, where the input data vector for the clustering process is the time difference between sensors pairs and will be used for the similarity criteria.

In previous versions of the DTM technique, front end amplitude filters were used on the acquisition systems to remove erroneous data from additional hits arising from reflections from the specimen boundary. This ensured the number of hits in an event corresponded to the total number of used sensors. The front end filters required user experience to be set correctly and in larger structures often required changing during collection of the training data, both of which slowed the process. Erroneous data was still collected when a set of hits less than the number of used sensors and hits from bad pencil lead breaks were recorded respectively. These sources of erroneous data required manual removal by the user, again adding additional time to the process. However in this work, for each point of the Delta T grid, the recorded hits were separated automatically to create AE events using a time based approach. In this work all the used sensors were required to register a hit within a certain time window in order for it to be considered as an event. Simultaneously, the incorrect erroneous data

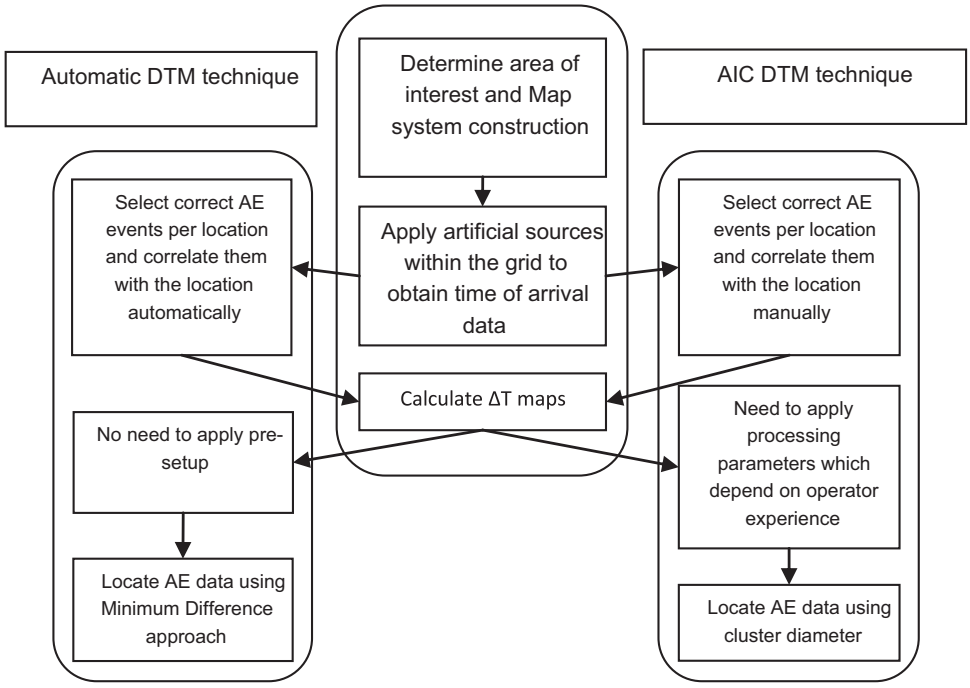

Fig. 1. Flow diagram representation of (a) automatic DTM technique and (b) AIC DTM technique.

caused from those conditions mentioned above were automatically removed. Then, the AE hits from each point within the delta grid are correlated with the point coordinates (x, y) automatically, using time stamps placed by the operator within the collected data. Where the time stamps are placed in the data following acquisition from each grid node and are then used to automatically identify which hits are associated with each grid node.

3.1.2. Apply the unsupervised clustering

For each grid point within the map, in order to select the correct events to construct the training maps, an unsupervised classification is performed and the highly correlated events (similar to each other) are selected. The events are treated as pattern vectors and used as input to the unsupervised clustering. Each event is identified by the calculated difference in time of arrival for each sensor pair (e.g. the case of four sensors creates six sensor pairs 1–2, 1–3, 1–4, 2–3, 2–4 and 3–4). The correlation between events refers to the similarity between the events arrival time difference of their sensor pairs. A complete link hierarchical clustering algorithm [32] is then used to group events based on their similarity, or correlation coefficient.

The complete link hierarchical clustering algorithm for data of N events is described by the following steps:

i Assign each event to its own cluster (for N events we have N clusters).
ii Compute the distances (similarities) between clusters, where the distance is equal to the largest distance from any member of one cluster to any member of the other cluster.
iii Reduce the number of clusters by one through merging of the most similar pair of clusters.
iv Repeat steps 2 and 3 until all items are clustered into a single cluster.

At a higher level of correlation coefficient a greater number of groups will exist because the events in each group must be very highly correlated and vice versa, at a low correlation coefficient fewer groups will exist because each group can contain lesser correlated difference in time of arrival for each sensor pair. In this work the 0.99 correlation coefficient level from the largest group was selected and all events in this group were used (correlation coefficient of 1 means total correlation); each group at this level or above is deemed to contain highly correlated events and used for onward analysis. Conversely the groups are deemed to be suitably less correlated at a correlation level lower than the highest level. So, they are ignored and not used for onwards analysis.

3.1.3. Calculate ΔT maps

The average values of the difference in time of arrival for each sensor pair is calculated for the selected highly correlated events at each grid point. Finer resolution grids were created using interpolation between training data points in order to provide high precision of the location calculation results. In this work a 0.5 mm resolution was selected to perform the calculations.

3.2. Calculate location of real AE data

In order to overcome the need to identify the cluster size for calculation of the real AE data location, a new approach is presented here; this will be known as the Minimum Difference approach. This is a numerical approach, which is dependent on finding the point at which the difference between the source data and the training map data is minimised. There are four steps associated with the Minimum Difference approach which are described below:

i. Calculate source time difference: for each source using its sensors data, the arrival time difference of each sensor pair is calculated at that source. This step applies after the arrival time has been corrected using the AIC approach.
ii. Find the difference between the source pairs and the training maps pairs: Subtract each sensor pair time difference from the same sensor pair time difference of the training map.
iii. Sum the differences of all source sensors pairs (n) using Eq. (1):

$$sum = \sum_{1}^{n} |T\ source - T\ training\ map| \tag{1}$$

Where *T source* is the time difference of the source, *T training map* is the time difference of the training map.

iv. Find the point within the grid at which the minimum difference with the source time difference occurs. This point is taken to be the source position.

Using this approach will avoid any human interaction with the calculation process and therefore reduce the error source, increase result reliability and reduce the running time of the whole process.

A comparison between the conventional TOA, AIC Delta T mapping and new Automatic Delta T mapping for located AE events in a number of specimens will be presented in the experimental section of this chapter.

4. Experimental procedure

In order to evaluate the performance of the improved DTM technique against the traditional TOA and the AIC DTM technique, two tests were conducted. The first was conducted on a simple geometry specimen made from 20 mm thick ASTM 516 gr 70 steel with overall dimensions of 90 mm × 2 m. At 17 mm from one end of the specimen a grid was constructed on the specimen with dimensions of 300 × 90 mm. Within this grid two geometric features were present; the first was 4.4 mm wide and 10 mm deep v-notch and the other was a 20 mm diameter half circle cut out as shown in Fig. 2. Six AE sensors were mounted to the specimen using silicone RTV adhesive (Loctite 595) to provide an acoustic coupling and a mechanical fixture (Fig. 2). Four MISTRAS Nano 30 sensors (sensors 1–4) and two MISTRAS WD sensors (sensors 5 and 6) were used and their relative positions are shown in Fig. 2. AE Data were recorded using a MISTRAS PCI-2 system with a 45 dB threshold and a 5 MHz sample rate. Prior to testing, Delta T Mapping training data was collected from the grid nodes at two resolutions, 10 mm resolution near the notch area (40 × 90 mm) and 20 mm resolution for the rest of the grid (Fig. 2). For the purpose of the training data 10 H–N sources were generated at each node on the grid. Ten arbitrary locations were selected within the grid and five H–N sources were performed at each position. The recorded signals, from all six sensors were used to calculate locations using the TOA, AIC DTM and the improved DTM. For the TOA technique an experimentally derived wave speed of 4600 m/s was used and the co-ordinates of the sensors were used as an input to the technique. The standard algorithm integrated in the AEwin software was used for the TOA location calculation. In practice, the standard approach involves the minimisation of the objective function X^2 in Eq. (2) [1], with respect to X_s and Y_s, the source position.

$$X^2 = \sum \left(\Delta t_{i,obs} - \Delta t_{i,calc}\right)^2 \tag{2}$$

where

$$\Delta t_{i,obs} = t_i - t_1$$

and

$$\Delta t_{i,calc} = \left[\sqrt{(X_i - X_s)^2 + (Y_i - Y_s)^2} - \sqrt{(X_1 - X_s)^2 + (Y_1 - Y_s)^2}\right] \times v^{-1}$$

t_1 and t_i are the arrival times at sensor 1 and the ith sensor in the array, v the wave speed in the given media, X_s, Y_s, X_1, Y_1, X_i and Y_i the x and y positions of the source, sensor 1 and the ith sensor respectively.

Furthermore, for the AIC DTM technique, visual inspection was used to remove erroneous events from each position in the training data grid.

To assess the performance of the improved DTM technique on a more complex geometry, a further test was conducted on an aerospace grade 2024-T3 aluminium plate, with dimensions of 370 × 200 mm with a thickness of 3.18 mm. The specimen contained a series of differing diameter circular holes as shown in Fig. 3. A MISTRAS PCI-2 system was used to record all AE data at 40 dB threshold and 2 MHz sampling rate. Four MISTRAS Nano-30s were adhered on the front face of the specimen (Fig. 3) using silicon RTV (Loctite 595). All transducers were connected to MISTRAS 0/2/4 pre-amps which had a frequency filter of 20 kHz to 1 MHz. The Delta T Mapping grid on the specimen covered an area of interest of 200 mm × 160 mm and had a resolution of 10 mm (Fig. 3). Five H–N sources were used at each node position within the grid. In order to assess the performance of the new Delta T mapping technique in a more complex structure, six arbitrary positions were selected within the Delta T grid and three H–N sources were conducted at each position. The average wave speed was calculated as 5400 m/s. Source locations were calculated using all four sensors for the three techniques.

Further investigation was conducted on the aluminium specimen using real AE sources. In order to generate AE from fatigue cracking a tension–tension fatigue test was conducted on the specimen until final failure. Load transfer was achieved using 20 mm loading pins with 5 mm steel plates connected either side of the specimen using seven M10 bolts at each end in order to distribute the load. The cyclic load regime was applied at 2 Hz in four batches. Initially a maximum load of 15 kN was applied for 7000 cycles followed by a maximum load of 20 kN for 18,000 cycles. Then the maximum load was increased to 22 kN and the test was run for 58,000 cycles. Finally the maximum load was increased to 24 kN and the test was run for 20,000 cycles before the final failure occurred. For the entire duration of the fatigue test the minimum load was fixed at 0.25 kN.

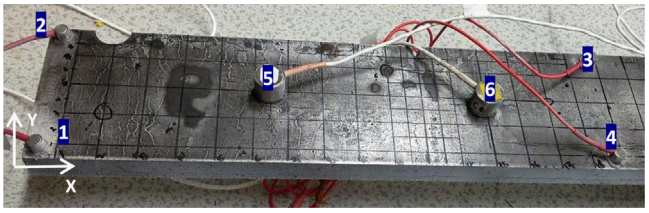

Fig. 2. Steel specimen configuration.

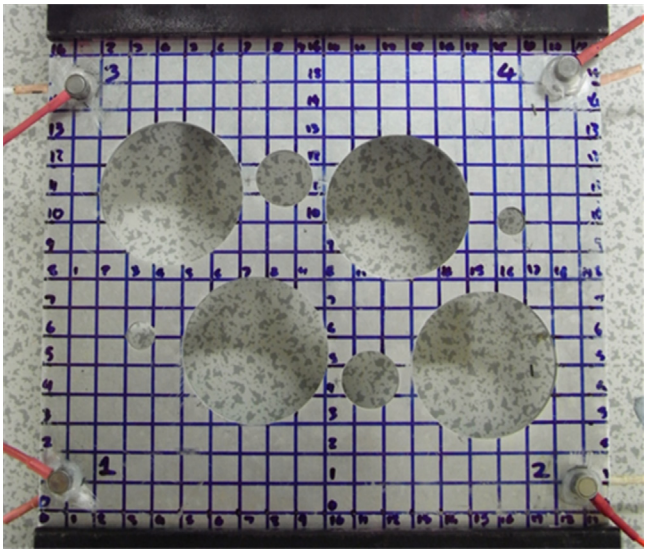

Fig. 3. Aluminium specimen configuration.

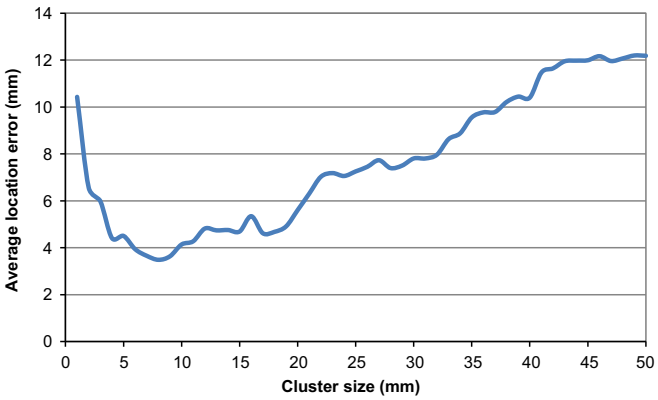

Fig. 4. Cluster size effect on the AIC Delta T accuracy.

5. Results and discussion

5.1. Validation testing on the simple steel specimen

For the AIC DTM location calculations, the optimal cluster size was calculated using a trial and error procedure, by assessing the accuracy of located AE events against the actual known positions. Fig. 4 shows the average location error (the Euclidian distance between the actual source position and the calculated source position) for the 50 sources versus the cluster diameter used in the AIC DTM algorithm. Basically, the optimal cluster size will refer to the lowest average error value and here in this work was selected to be 8 mm. But practically, the cluster diameter which gives the lowest average error for all source locations may not be the optimum diameter value for each source individually. Many source events will have the lowest location error at different cluster diameter values. As a result, choosing the optimum cluster diameter is a difficult process. It is clear that the cluster diameter has a significant effect on the location accuracy with the error ranging from less than 4 mm to over 12 mm depending on the diameter used. Selection the optimum cluster diameter is a time consuming process because it is nominally found using trial and error.

For the Automatic DTM source location calculations, the training maps are constructed by automatically removing the erroneous events for each grid positions using the unsupervised clustering procedure where only highly correlated events ($\geqslant$99%) are selected. The source locations are then calculated using the Minimum Difference approach. Finally, the TOA location results were exported directly from the MISTRAS AEwin software. The location results from H–N sources at 10 positions, calculated using the three location methods are presented in Fig. 5. It can be seen that there is marked improvement in source location accuracy using both of the DTM techniques over the traditional TOA technique due to the more accurate approach for the arrival time calculation. Furthermore, the Automatic DTM location accuracy slightly

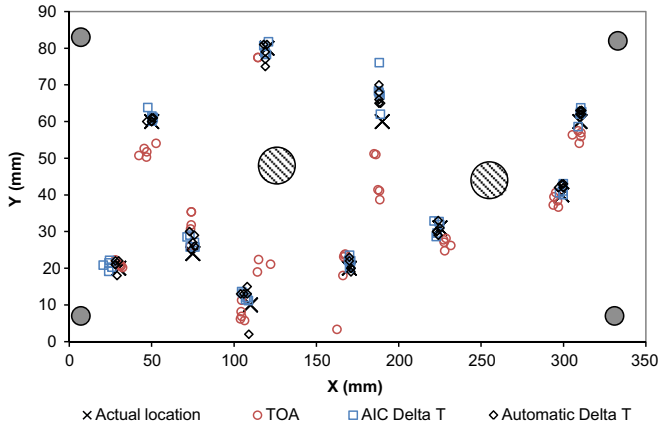

Fig. 5. Calculated source location by three techniques.

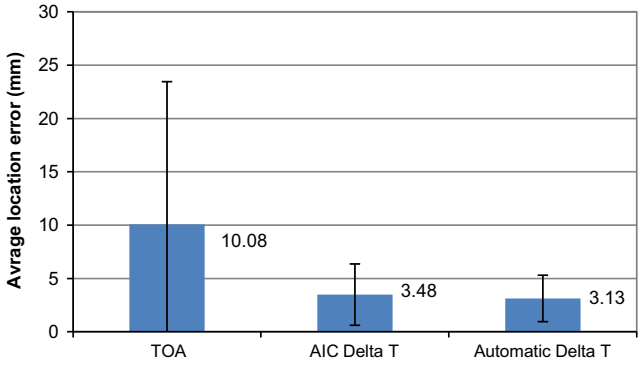

Fig. 6. Average location error for the three techniques result.

improves that of the AIC DTM due to using the new automatic selection of the correct events for constructing the training data and no longer requiring the use of the cluster diameter which prevents any human manipulation.

The average location error for the 50 sources, calculated as the Euclidian distance between the actual source position and the calculated source position, using the three location methods is presented in Fig. 6. The error bars in the figure represent one standard deviation above and below the average location error. It can be clearly seen that the average error is reduced significantly to 3.48 mm and 3.13 mm using the AIC and Automatic DTM techniques respectively compared with that of the TOA at 10.08 mm. These results are promising because the error is reduced to approximately 66% and 69% of the TOA error in this simple geometry, homogeneous specimen. Furthermore the Automatic DTM reduces the error by approximately 10% of the AIC DTM even though the process has been fully automatised and no longer requires an operator experience.

Further examination of the results reveals that the Automatic DTM not only improves the location accuracy but also speeds up the whole process and significantly reduces the time invested in implementing the technique. A comparison between the AIC and the Automatic DTM based on the time resources of the operator is provided in Table 1. From the table, the most time consuming step in the AIC DTM is represented by the selection and preparing of the AE data to construct the training maps, which was approximately 8 h for a small grid (similar to the one used in this work). On the other hand, the Automatic DTM is very fast and reduces the running time for constructing the training maps to approximately 18 s which is a significant improvement. Moreover, the new DTM does not require the trial and error process of determining the optimal cluster diameter when compared with the AIC DTM the cost is approximately 3.6 h.

These initial results are very promising findings, demonstrating the potential for the Automatic DTM technique to improve the location accuracy in comparison with the TOA and AIC DTM techniques. The automated technique is simpler to use, significantly reduces implementation time and simultaneously improves the reliability of location results.

5.2. Validation testing on the complex geometry aluminium specimen

The AIC DTM location calculations were determined using a 20 mm cluster diameter, which was concluded to be the optimum value using the trial and error procedure outlined earlier in this work. For the Automatic DTM location calculations the same procedure used for the steel specimen was implemented. Fig. 7 displays the located source from a series of H–N sources on the specimen for all three location techniques. The AIC and the Automatic DTM results show estimated sources

Table 1
Running time comparison.

Stage	AIC Delta T (s)	Automatic Delta T (s)
Prepare the AE data to construct the training maps	about 28,800 (8 h)	18.19
Calculate the optimal Cluster size (try from 1 to 50 mm)	13,089	0
Calculate the source location	261.78	60.35
Total time	42,150.78	78.55

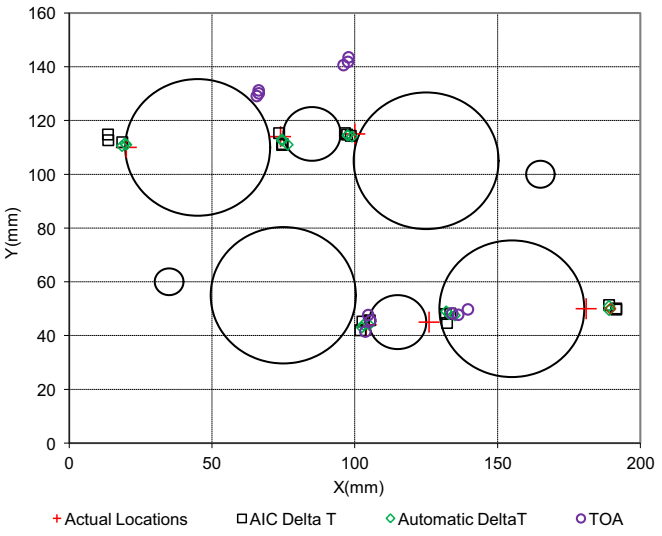

Fig. 7. Source locations on a complex specimen using three techniques.

very close to their actual location position. The TOA results show results distributed close to the actual position, far away from the position and outside the specimen boundary. This highlights the improved accuracy of both DTM techniques over traditional TOA approach to calculate source location in complex structure. The reasons for inaccurate results for the TOA technique are because the techniques relies on two assumptions, constant wave speed through the structure and a straight propagation line between the source and the sensor, both of which are difficult to achieve in real structures.

The average location error for all 18 sources (the Euclidian distance between the actual source position and the calculated source position) for all three techniques is presented in Fig. 8. The error bars represent plus and minus one standard deviation of the average. The average error of the DTM techniques is considerably lower than the TOA and offers an improvement in accuracy from 222 mm to approximately 5 mm. This figure presents two important points. Firstly, it highlights the fact that the TOA is not well suited to dealing with complex structures, as discussed previously. Secondly the new automatic DTM results show an improvement in accuracy over the AIC DTM results reducing the error from 4.96 mm to 3.88 mm

5.3. *Validation testing from fatigue testing*

The resulting fatigue crack after the specimen had been subjected to 96,000 fatigue cycles can be seen in Fig. 9. The location of the crack is in the high stress regions around the thin webbed section between the holes. The AE source location from the test was calculated using the three techniques, TOA and DTMs, using the same procedure as outlined earlier.

Due to the high quantity of recorded data from this test, the AE location results are presented in the form of spatially binned plots in order to ease representation of the data, these can be seen in Figs. 10–12. The area of interest was divided into 5×5 mm sub-sections with the cumulative events located in each bin presented in the figures. The location of the actual crack is highlighted by the red line in each figure. Fig. 10 shows the TOA source locations without any significant spatial bins with a high number of events. The highest sub-section contains about 20–60 events. This shows the inability of TOA to accurately locate AE sources in complex structures.

Fig. 11 and Fig. 12 show the AE source location calculations using the AIC and the Automatic DTM techniques, respectively. The figures show the significant area of events, 400 events for AIC DTM and 550 events of Automatic DTM, above the crack location. This area is located at around 15 mm from the location of the actual crack. These results show the high accuracy of the two mapping techniques in calculating the AE source location and significanctly lower resource requirement of the new technique.

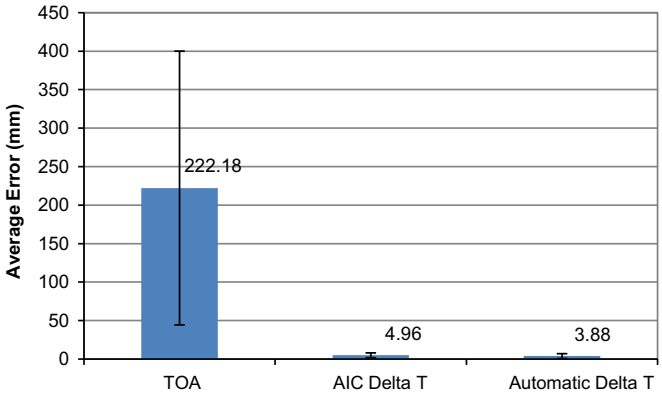

Fig. 8. Sources location error.

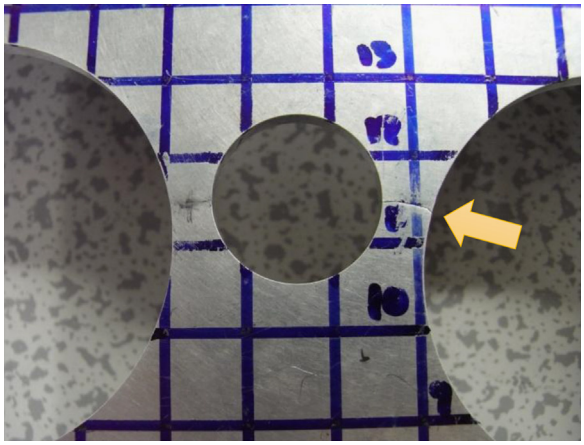

Fig. 9. Crack location after the final failure [28].

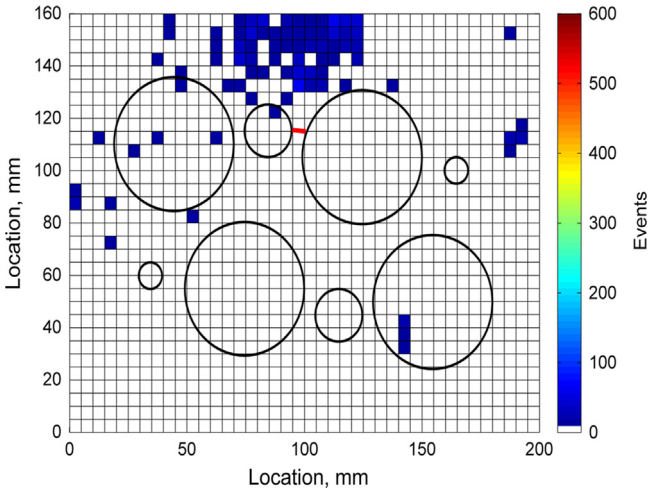

Fig. 10. TOA binned events locations. (For interpretation of the references to colour in this figure, the reader is referred to the web version of this article.)

Comparing the Automatic DTM with the TOA and the AIC DTM results highlights significant benefits such as the improvement in the accuracy and reliability of source location calculations. Experimental investigations on simple and complex structures have shown that the time consuming manual process has been replaced with a reliable automatic and less time consuming process which relies on a clustering algorithm.

Overall the new fullly Automatic DTM technique is a faster, easier to implement location technique which results in reducing testing downtime for set-up and requires less operator skill making it more compatible with commercial needs.

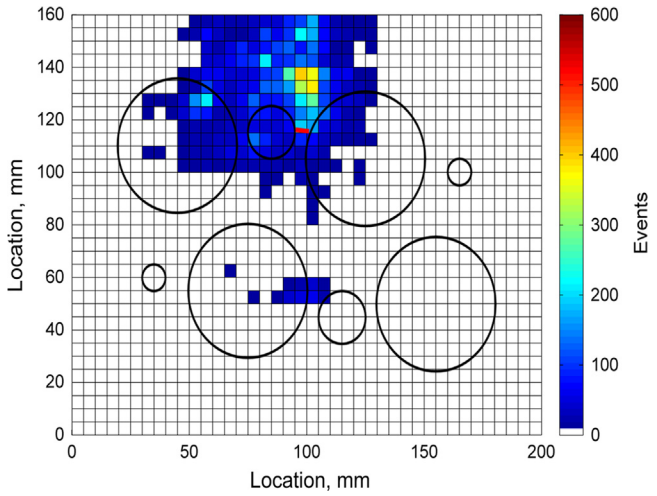

Fig. 11. AIC Delta T binned events locations. (For interpretation of the references to colour in this figure, the reader is referred to the web version of this article.)

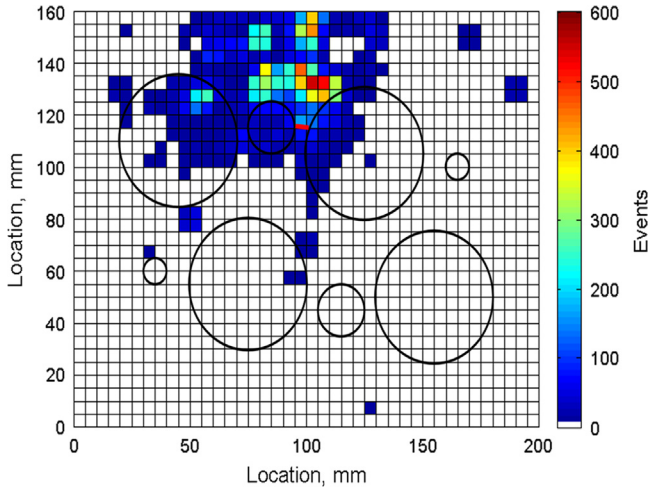

Fig. 12. Automatic Delta T binned events locations. (For interpretation of the references to colour in this figure, the reader is referred to the web version of this article.)

Having the automatic clustering technique for training data and the Minimum Difference approach for the AE source estimation reduces the potential for human error, the need for a skilled operators and manual process of selecting the optimal location cluster diameter.

6. Conclusions

A new fully Automatic DTM technique is introduced and verified experimentally using a variety of tests, in both simple and complex structures. The results obtained are excellent and demonstrate the success of the adopted methodology. The AIC DTM technique has been improved considerably as summarised below:

- Fast: The automatic selection and elimination of erroneous training data greatly decreases the process time from about 8 h to approximately 18 s.
- Increased reliability: Making the process fully automatic increases the reliability of the result and eliminates human error.
- Efficient: The process requires less resources in terms of time, operator skill and experience.
- More accurate: The technique was able to reproduce and even increase the accuracy of the already excellent accuracy of the AIC DTM technique, which was achieved in an automated and efficient way. It shows an increase in the accuracy for simple and complex geometry specimen. In simple geometry, the average location error is improved from 10 mm

(using TOA) and (3.48 mm) (using AIC DTM) to only 3.13 mm. In complex structure, the average location error is improved from 222 mm (using TOA) and 4.96 mm (using AIC DTM) to only 3.88 mm using the Automatic DTM.

- Increased simplicity: No need for highly skilled operators to perform the process.
- More capability to apply in large scale structures.

The results of this study highlight the potential for the use of AE monitoring as a tool of SHM for damage localisation tasks; a high simplicity, fast, reliable, cheap and accurate technique has been presented. If this technique is integrated with commercial AE monitoring systems, it will be a powerful tool to provide real time highly accurate source location within complex large-scale components.

Acknowledgements

The authors would like to thank the Iraqi Ministry of Higher Education and Scientific Research for supporting this research and the technical staff of Cardiff University School of Engineering for their kind assistance with the testing programme.

References

[1] K.R. Miller, E.K. Hill, Non-Destructive Testing Handbook, Acoustic Emission Testing, American Society for Non-Destructive Testing, 2005.
[2] T. Kundu, Acoustic source localization, Ultrasonics 54 (2014) 25–38.
[3] R. Pullin, M. Baxter, M.J. Eaton, K.M. Holford, S.L. Evans, Novel acoustic emission source detection, J. Acoust. Emiss. 25 (2007) 215–223. ISSN 0730-0050.
[4] J. Hensman, R. Mills, S.G. Pierce, K. Worden, M. Eaton, Locating acoustic emission sources in complex structures using gaussian processes, Mech. Syst. Signal Process. 24 (2010) 211–223.
[5] P.S. Earle, P.M. Shearer, Characterization of global seismograms using an automatic-picking algorithm, Bull. Seism. Soc. Am. 84 (1994) 366–376.
[6] S.M. Ziola, M.R. Gorman, Source location in thin plates using cross-correlation, J. Acoust. Soc. Am. 90 (1991) 2551–2556.
[7] M. Hamstad, A. O'Gallagher, J. Gary, A wavelet transform applied to acoustic emission, J. Acoust. Emiss. 20 (2002) 39–61.
[8] T. Lokajíček, K. Klima, A first arrival identification system of acoustic emission (AE) signals by means of a high-order statistics approach, Meas. Sci. Technol. 17 (2006) 2461.
[9] J. Wang, T.-L. Teng, Artificial neural network-based seismic detector, Bull. Seism. Soc. Am. 85 (1995) 308–319.
[10] H. Akaike, Markovian representation of stochastic processes and its application to the analysis of autoregressive moving average processes, Ann. Inst. Stat. Math. 26 (1974) 363–387.
[11] N. Maeda, A method for reading and checking phase times in auto-processing system of seismic wave data, Zisin=Jishin 38 (1985) 365–379.
[12] J.H. Kurz, C.U. Grosse, H.-W. Reinhardt, Strategies for reliable automatic onset time picking of acoustic emissions and of ultrasound signals in concrete, Ultrasonics 43 (2005) 538–546.
[13] P. Sedlak, Y. Hirose, S.A. Khan, M. Enoki, J. Sikula, New automatic localization technique of acoustic emission signals in thin metal plates, Ultrasonics 49 (2009) 254–262.
[14] R. Sleeman, T. van Eck, Robust automatic P-phase picking: an on-line implementation in the analysis of broadband seismogram recordings, Phys. Earth Planet. Inter. 113 (1999) 265–275.
[15] T. He, Q. Pan, Y. Liu, X. Liu, D. Hu, Near-field beamforming analysis for acoustic emission source localization, Ultrasonics 52 (2012) 587–592.
[16] G.C. McLaskey, S.D. Glaser, C.U. Grosse, Beamforming array techniques for acoustic emission monitoring of large concrete structures, J. Sound. Vib. 329 (2010) 2384–2394.
[17] H.M. Matt, F.L. Di Scalea, Macro-fiber composite piezoelectric rosettes for acoustic source location in complex structures, Smart Mater. Struct. 16 (2007) 1489–1499.
[18] K.M. Holford, D. Carter, Acoustic emission source location, Key Eng. Mater. Trans. Tech. Publ. (1999) 162–171.
[19] H. Yamada, Y. Mizutani, H. Nishino, M. Takemoto, K. Ono, Lamb wave source location of impact on anisotropic plates, J. Acoust. Emiss. 18 (2000) 51.
[20] J. Jiao, C. He, B. Wu, R. Fei, X. Wang, Application of wavelet transform on modal acoustic emission source location in thin plates with one sensor, Int. J. Press. Vessel. Pip. 81 (2004) 427–431.
[21] N. Toyama, J.H. Koo, R. Oishi, M. Enoki, T. Kishi, Two-dimensional AE source location with two sensors in thin CFRP plates, J. Mater. Sci. Lett. 20 (2001) 1823–1825.
[22] T. Kundu, H. Nakatani, N. Takeda, Acoustic source localization in anisotropic plates, Ultrasonics 52 (2012) 740–746.
[23] E. Dehghan Niri, A. Farhidzadeh, S. Salamone, Nonlinear Kalman Filtering for acoustic emission source localization in anisotropic panels, Ultrasonics 54 (2014) 486–501.
[24] T. Kundu, X. Yang, H. Nakatani, N. Takeda, A two-step hybrid technique for accurately localizing acoustic source in anisotropic structures without knowing their material properties, Ultrasonics 56 (2015) 271–278.
[25] F. Ciampa, M. Meo, A new algorithm for acoustic emission localization and flexural group velocity determination in anisotropic structures, Compos. Part A: Appl. Sci. Manuf. 41 (2010) 1777–1786.
[26] M.G. Baxter, R. Pullin, K.M. Holford, S.L. Evans, T. Delta, Source location for acoustic emission, Mech. Syst. Signal Process. 21 (2007) 1512–1520.
[27] M.J. Eaton, R. Pullin, K.M. Holford, Acoustic emission source location in composite materials using Delta T mapping, Compos. Part A: Appl. Sci. Manuf. 43 (2012) 856–863.
[28] M. Pearson, Development of lightweight structural health monitoring systems for aerospace applications (Ph.D. thesis), Cardiff School of Engineering, Cardiff University, UK, 2013.
[29] M.R. Pearson, M. Eaton, C.A. Featherston, R. Pullin, K. Holford, Improved acoustic emission damage source location during fatigue testing of complex structures, in: Proceedings of the 34th Conference and the 28th Symposium of the International Committee on Aeronautical Fatigue and Structural Integrity (ICAF2015), Helsinki, Finland, 2015.
[30] N.N. Hsu, F.R. Breckenridge, Characterization and calibration of acoustic emission sensors, Mater. Eval. 39 (1981) 60–68.
[31] J.W. Scholey, P.D. Wisnom, M.R. Friswell, M.I. Pavier, M.J. Alika, MR, A generic technique for acoustic emission source location, J. Acoust. Emiss. 27 (2009) 291–298.
[32] A.M.R. Cluster, Analysis for Applications, Academic Press, New York, 1973.

Composites Part B 75 (2015) 336–344

Contents lists available at ScienceDirect

Composites Part B

journal homepage: www.elsevier.com/locate/compositesb

Parameter Correction Technique (PCT): A novel method for acoustic emission characterisation in large-scale composites

Safaa Kh. Al-Jumaili [a, b, *], Karen M. Holford [a], Mark J. Eaton [a], Rhys Pullin [a]

[a] Cardiff School of Engineering, Cardiff University, Cardiff, UK
[b] University of Basrah, Basrah, Iraq

ARTICLE INFO

Article history:
Received 16 September 2014
Received in revised form
25 November 2014
Accepted 29 January 2015
Available online 10 February 2015

Keywords:
A. Carbon fibre
C. Statistical properties/methods
D. Acoustic emission
Structural health monitoring

ABSTRACT

In composite materials, accurate characterisation of damage using NDT techniques is vital. Techniques which are well developed in homogeneous materials do not translate easily to composites due to their complex and anisotropic properties. This is especially true in acoustic emission (AE) where propagation behaviour significantly affects the signal data. This paper describes a novel solution to enable AE parameters to be "corrected" to account for the material properties and the geometry of the structure. The "Parameter Correction Technique (PCT)" derives an empirical relationship between signal parameters and varying source amplitude from a number of locations, across a structure. This method does not require knowledge of the sensor location or wave velocity. A five-step description of the process is provided and practical results from an initial trial are presented. Results from the initial trial demonstrate a considerable improvement over the conventional parameters.

1. Introduction

Acoustic emission (AE) is widely used in research applications for the detection of micro failures in all kinds of materials [1]. AE in materials originates when a failure mechanism is activated and part of the total strain energy is dissipated as mechanical stress waves, which spread concentrically around the place of origin. This released energy can be detected with suitable sensors: the recorded mechanical information from the material is then converted into an electrical signal [2].

In recent years, composite materials have been increasingly used in industrial applications, with reinforced composite structures being widely used in large-scale and safety critical structures for infrastructure and transport, (aerospace, energy and marine), all of which require structural health monitoring (SHM) for continuous and global monitoring of the structure in order to increase safety and reduce the amount of inspection required. Acoustic emission (AE) has great potential for use in SHM systems: it is able to locate the AE source position within a structure, which is considered to be one of the most important and useful attributes of the technique. It can also provide information about the damage mechanisms from the received signals.

Until now, to associate every AE signature to a specific failure type has been considered as a non-trivial challenge even in small-scale homogenous material specimens in a controlled environment. The difficulty of characterization increased when AE sources are emitted at different distances from a sensor due to different signal propagation paths. In composite materials wave propagation and scattering phenomenon are complex, and this complexity increases further when AE propagation paths are interrupted by obstacles such as cracks, holes and thickness change. Furthermore, AE signal energy attenuation in large-scale composite materials or in complex geometry structures makes collecting all AE activity using one sensor difficult. Yet, the use of multiple sensors is unacceptable for source identification analysis due to the differences in transfer function from one sensor to another.

To date most studies carried out to discriminate damage mechanisms in composite materials under different loading regimes have been based on conventional AE analysis in which AE features are recorded directly using the AE acquisition systems. AE signal features are then used to cluster signals exhibiting similarities in groups. The traditional AE features extracted directly from the signal waveform include amplitude, count, duration, etc. [1]

* Corresponding author. Cardiff School of Engineering, Cardiff University, Queen's buildings, The Parade, Cardiff CF24 3AA, UK. Tel.: +44 02920877297; fax: +44 2920874939.
E-mail addresses: Al-JumailiSK@cardiff.ac.uk, safaa_kh@yahoo.com (S.Kh. Al-Jumaili), holford@cardiff.ac.uk (K.M. Holford), eatonm@cardiff.ac.uk (M.J. Eaton), pullinr@cardiff.ac.uk (R. Pullin).

http://dx.doi.org/10.1016/j.compositesb.2015.01.044
1359-8368/

and additional features are extracted from the waveform using special transformations such as frequency [3,4]. These analyses usually use the AE activity diagrams versus load or number of cycles, the correlation of some traditional AE features and also unsupervised and supervised classification techniques.

A modern approach is multidimensional classification analysis and it is considered to be a reliable and sufficient solution to classify AE signals into different clusters dependent upon their descriptors' values and to correlate different damage mechanisms with the AE data. Many multivariate classification approaches have been performed using different algorithms with the main consideration being the inclusion of a large number of AE features. However, all these previous approaches do not provide evidence of the validity of the clustering results after they classify the AE data. Most simply use a single parameter or correlation plot as evidence for labelling to validate the clustering results.

This paper describes a novel AE parameter correction methodology known as "Parameter Correction Technique (PCT)", applicable to two-dimensional plate-like structures. It is applied to a carbon fibre panel in order to recalculate the AE signal parameters that are recorded from a number of artificial sources at different locations. This technique was developed in order to correct the AE parameters in large-scale complex geometries and anisotropic composite structures. The performance of the technique is assessed by performing a thorough analysis using single parameter analysis and unsupervised clustering analysis results utilising the corrected parameters. Due to the novelty of this approach and the lack of relative studies in the field of AE parameter correction it is difficult to compare the result obtained with other techniques. Only a comparison with the traditional parameter values is made. The four fundamental parameters, amplitude, duration, count and energy were corrected in this work with high accuracy.

Up to now, traditional AE analysis uses single sensor data in order to avoid errors caused by the differing sensors transfer functions. AE propagates as a stress wave with geometric beam spreading and damping causes the signal amplitude to decrease with distance [1]. So in order to ensure all sources are recorded, the sensor must be kept within reasonable distance from the source. However, in a large-scale structure it is not practical to depend on a single sensor to collect all AE activity. The Parameters Correction Technique presents the advantage of using all sensors data to recalculate each signal parameter, ensuring there is no missing data due to long source-sensor distances. Furthermore, the inherent attributes of a mapping approach make it ideally suited for use in composite materials and structures with complex geometries and layups. In the presented analysis events are located using the *Delta T* technique, which was originally developed for complex geometry metallic structures [5], but has also been shown to perform very well in anisotropic materials such as composites [6].

The remainder of the paper is organized as follows. An outline of the proposed technique methodology is given in Section 2, followed by a description of the multivariate, classification and visualisation, techniques. Section 3 provides a description of the experimental setup and procedure. Section 4 presents the results and discussion. Finally, the parameters correction method results are concluded in Section 5.

2. Data processing

2.1. Parameters Correction Technique (PCT) methodology

The novel technique in this paper utilises an artificial source to record the relationship between acquired signal parameters and varying source amplitude from an array of locations, creating a multi-layer map of features for each sensor. Each layer represents one source amplitude and demonstrates the variation in parameters with source to sensor distance as shown in Fig. 1b. Then for each position within the map multiple layers (at different amplitudes) can be stacked up to construction the relationship between source amplitude and recorded parameters (Fig. 1d). Using these relationships, any previous, current or future AE data received from within the PCT map area can be corrected. This method does not require knowledge of the sensor location or wave velocity. The PCT methodology was first used in previous work [7] and a five-step description of the technique is provided below:

- **Determine area of interest**: The PCT method can provide complete coverage of an entire structure or part of a structure for time-saving purposes. It can be used as an improvement method to correct parameter values of AE emitted from important areas, which are predicted to have high stress levels using analysis methods such as finite element.
- **Map system Construction**: A grid is constructed on the area of interest within which AE events will be generated. It is important that sources and not the sensor should be referenced within the grid. Placing the sensors within the grid is unnecessary (Fig. 1a) and does not affect the result.
- **Apply artificial sources to obtain parameters value data set**: Artificial source with varying input amplitude are generated at each node of the grid to provide AE parameter readings at each sensor. An average result of the recorded AE data is achieved by repeating the same source amplitude several times at each node, reducing the error. Interpolation between node points allows for greater spatial resolution and accounts for missing node data as a result of holes, for example. The resulting data can be presented as a contour map (Fig. 1b) showing the parameter values recorded from each grid position using the same source amplitude.
- **Calculate PCT maps**: A contour map is generated for each source amplitude and then used to generate a multilayer map (Fig. 1c) that allows more accurate correction of AE parameters from sources with varying amplitude. For any (x, y) coordinate within the grid a relationship can now be formed between the source amplitude (in volts) and the recorded parameter value, by taking the parameter value from each map level (Fig. 1d).
- **Real AE data parameters re-calculation**: When real AE data are recorded from a test they can be corrected using the PCT maps in the following way:

I. Calculate source location: data are located using the Delta T Mapping algorithm to give an accurate estimate of their source position. Knowledge of the source position is essential to the operation of the PCT process.

II. Determine parameter vs source amplitude relationship: Using the estimated source position the relevant parameter vs source voltage relationship can be determined from the multi-layer map for each sensor. If the source position is not at a known grid position then data are interpolated to derive the required relationship.

III. Correct parameters: Using the parameter vs source amplitude relationship, the correct source amplitude can be determined from the recorded parameter. If the recorded parameter falls between amplitude levels used when training the map, then interpolation is used to ensure accurate correction. Furthermore if the recorded parameter falls outside the range of training amplitudes then extrapolation is used to determine the correct source voltage. The average of the corrected source parameters from all sensors is then taken as the final corrected value.

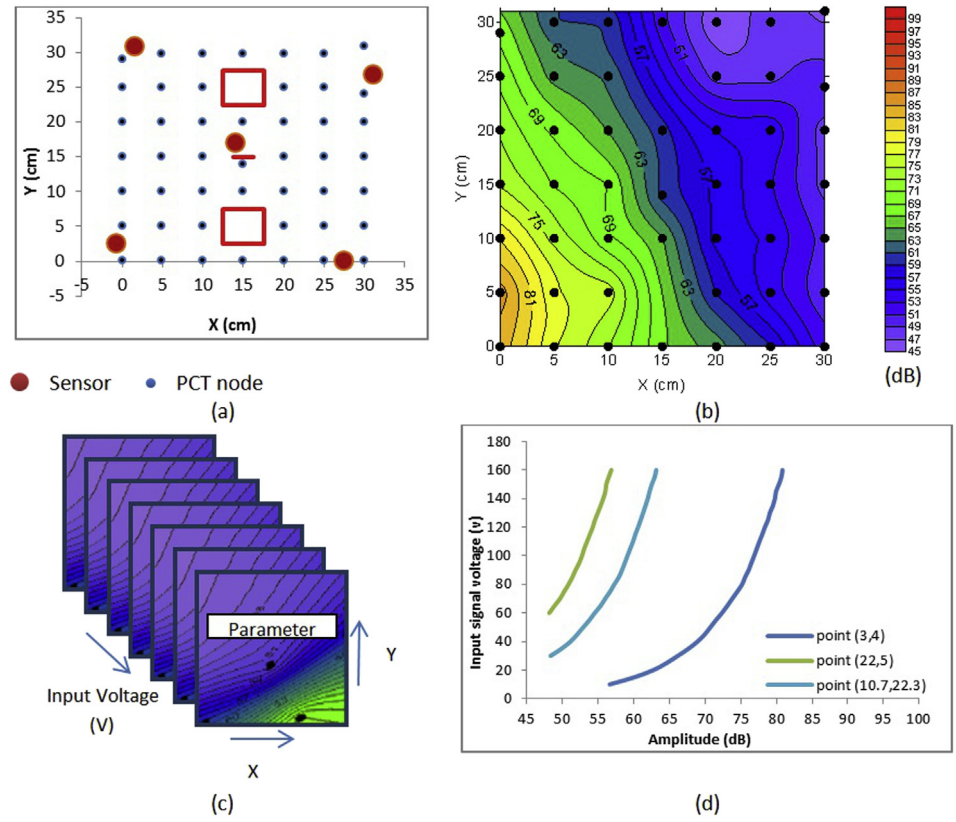

Fig. 1. (a) the PCT grid (b) Traditional amplitude values within the PCT grid (c) the structure of the PCT map for each parameter of each sensor (d) Different locations parameter-voltage relationships.

2.2. Unsupervised clustering methodology of AE signals

In this section the PCT's performance is assessed within a multi-parameter classification process to classifying different AE sources. This is achieved by using previously labelled signals as input vectors to the multi-dimensional process and then checking the correct assignment of the signals. Here, the AE signals are treated as a pattern vector described by a number of features. The same data is used twice as an input vector to the multivariate statistical techniques. In the first case the traditional signal parameters were used, while in the second case the same parameters are passed through an extra stage to correct them using the PCT. The classification results from both cases are presented for comparison. The main idea here is that the accuracy of classification is used as a criteria of classifier performance. Because the classifier is the same in both cases, the accuracy will reflect the PCT performance. The unsupervised clustering method and their performance were evaluated through two special mathematical criterions.

The clustering pattern involves the steps presented in Fig. 2. Each step will be described in this section (except assigning the results which will be discussed in Section 4).

In both cases, each AE signal is identified using four basic features, namely, amplitude, counts, energy and duration. In order to avoid biasing the classification towards the feature exhibiting the highest physical dimensions, the AE data was standardised [8,9]. It was applied only with the traditional parameters. In the second case the standardisation is not required because the corrected parameters have already received equal weighting from the PCT, which is considered an advantage that will reduce computing time.

The unsupervised clustering was performed using the k-means technique. The k-means clustering aims to partition n observations into k clusters, specified in advance, in which each observation belongs to a cluster [10]. Knowing in advance the number of desired classes is necessary to conduct the k-means process. The optimal number of classes was determined by evaluating the clustering results using validity criteria. Two widely-used clustering quality

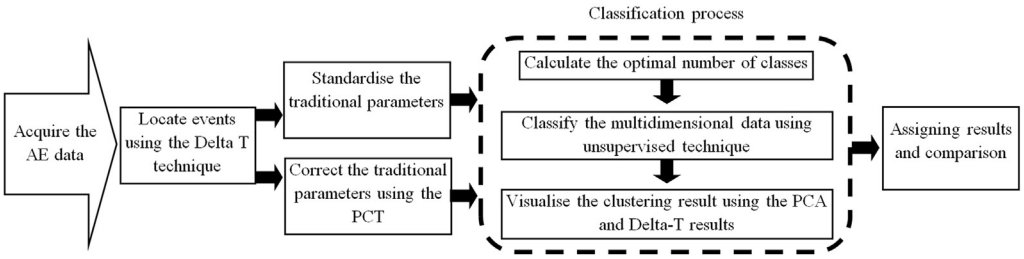

Fig. 2. The clustering pattern of the AE data.

criterions, the Silhouette [11] and Davies-Bouldin [12] indexes, were used as an indication of the compactness and the separation among the resulting classes. Higher cluster quality results in a maximum value of the Silhouette criterion and minimum value of Davies-Bouldin criterion.

Two-dimensional visualization for the clustering results was achieved using Principal Component Analysis (PCA) as a visualization and dimension reduction method. The technique provides a two-dimensional projection of the *n-dimensional* space, where *n* is the number of selected descriptors, four in this work, and using PCA will provide visualization of the separation of the clusters. The PCA is known as a classical method of multivariate statistics and its theory and use are well documented in textbooks from that field [13]. In this work the more basic techniques for classification and visualization were used, because the main objective of this study is not improving the multi-dimensional statistical techniques themselves but to improve the results by using reliable and correct input data. It is understood that using more complicated multi-dimensional algorithms with incorrect input data will definitely lead to greater processing time and will not improve the result accuracy. Also, it is important to bring to the attention of the reader that the simple techniques can be applied in the case of largely separable data and give accurate results if the correct input data is used.

3. Experimental procedure

3.1. Test specimen

This study was conducted on a 500 × 500 mm carbon fibre composite plate was manufactured in an autoclave from Hexcel Corporation M21/35%/UD268/T800S uni-directional pre-preg material. The final laminated consisted of 8 plies with a $((0, 90)_2)_s$ layup and a nominal thickness of 2.02 mm. The specimen is presented in Fig. 3a. The central area of interest of 300 mm × 300 mm was used in this study and all locations in the rest of this study will be measured in respect to this area. During the layup process an artificial crack was introduced in the centre of the specimen by cutting the inner layer's fibre in 0° direction with 25 mm using a fresh razor blade to initiate an artificial matrix crack. Four 5 mm thick aluminium tabs with 50 mm × 50 mm dimensions were bonded on the both sides of the panel along the 0° material direction using the resin ARALDITE 420 A/B (2 Component Epoxy Adhesive). To accelerate the gluing process the specimen with tabs were cured at 50 centigrade for 4 h. The specimen was drilled through the tabs to produce a 20 mm hole. Local delamination was produced by impacting the specimen using a low velocity impact by a polished hemispherical tup with a 20 mm diameter between the tabs. Ten repeated low velocity impacts were used, from 5 J to 14 J with various intervals. Following the final impact event, C-scan inspection of the panel was conducted in order to assess the delamination area. Fig. 3b shows the C-scan result of the specimen before and after impact.

3.2. Acoustic emission

AE monitoring was conducted during the test using a Vallen acquisition system at a sample rate of 5 MHz. The AE signals were monitored using five PAC WD wideband transducers with bandwidth of 100–1000 kHz and a resonant frequency at 650 kHz. The sensor locations are presented in Fig. 3a. Sensor outputs were pre-amplified by 34 dB using Vallen AEP3 amplifiers and in order to eliminate background noise during sampling the threshold level was set a 44.9 dB. Silicon adhesive (Loctite 595) was used to provide an acoustic couplant agent and a mechanical fixture between the plate and the sensors. A sensitivity test was conducted using a Hsu-Nielson (H–N) source [14] to ensure that all sensors were mounted correctly and have adequate coupling. It should be noted that the calibration of each sensor does not affect the proposed technique performance. An artificial AE source was used to generate test signals for the training map of the proposed technique. This was achieved by using a Physical Acoustics Ltd. arbitrary waveform generator (WaveGen1410) and an in-house manufactured broadband conical transducer provided by the National Physical Laboratory, UK. Multi-purpose grease was used as a couplant to provide good contact between the conical transducer and the specimen surface.

Fig. 3a also shows the Delta-T location grids. A 50 mm grid resolution, with 10 mm resolution near to the artificial crack, was applied to the central area of interested of 300 × 300 mm, for the purposes of training the Delta-T maps. At each grid point the training data from five Hsu-Nielsen pencil lead fractures was collected to estimate the average Δts. The Delta-T location maps were constructed before the test.

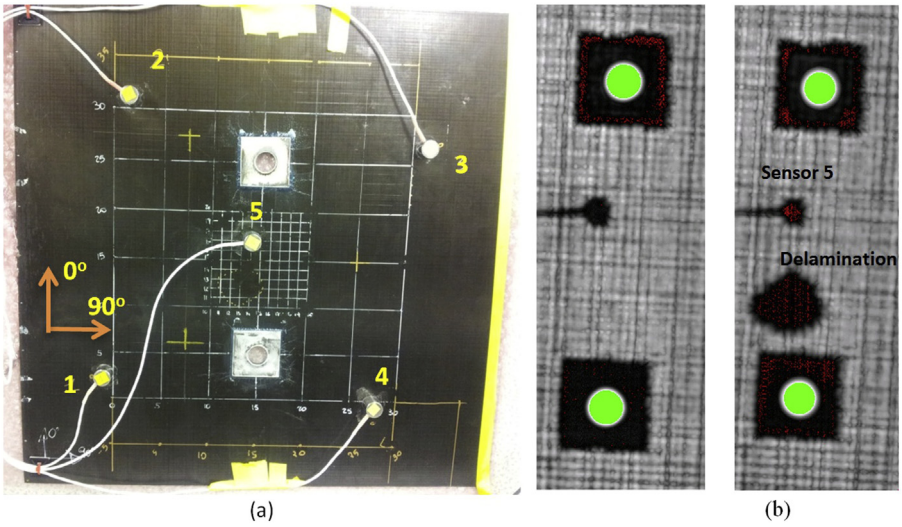

Fig. 3. (a) Test specimen configuration (b) C-scan images before and after impact.

4. Result and discussion

4.1. Initial PCT practical calculations

In this work, the training data for the PCT mapping was collected from an area of 300 × 300 mm, identical to the Delta-T map area, to allow the location of events with high accuracy. This area contains several components of geometry features such as holes, thickness change, fibre discontinuity and delamination. A PCT grid density of 50 mm was used, creating 47 nodes on the PCT mapping area as shown in Fig. 1a. Two nodes were not available to collect due to their location within the tabs holes. Because there is no restriction to the use of irregular nodes distribution, the nodes very close to the sensors positions were shifted by approximately 10–20 mm from the proposed node location. In order to excite the AE system the artificial excitation pulse (rectangular shape pulse of 10 μs width) was used at each node. Pulse amplitude started at 10 V and increased to 160 V with 5 V increments. At each position and increment the pulse was repeated 5 times to provide an average and avoid any erroneous results. Real-time recording of AE signal parameters using the five sensors was conducted. Fig. 1b shows the amplitude values within the PCT grid recorded using sensor 1 at the 160 V source amplitude, as an example. The other three parameters exhibited similar behaviour to that presented in this figure. Also, Fig. 1d shows the relationship between the amplitude values recorded by sensor 1 versus the pulse input voltage from three arbitrary source positions. It was noted that the relationships for both the amplitude and energy are smoother than that of the count and duration. This is because amplitude and energy are less dependent on the acquisition threshold level in comparison with counts and duration.

The PCT training maps highlight the problems related to using AE for classification in large-scale composite components and provides an important piece of information about the real signal attenuation within the structure. Fig. 1b shows how the recorded AE parameter values vary greatly with the propagation direction, Euclidian distance between the source and recording sensor and with propagation path features such as holes and thickness changes. This highlights the difficulty of AE sources identification in anisotropic materials and large components.

Most previous studies have been conducted using small-scale specimens without consideration for the effects of signal propagation direction or structural features on the recorded data, which is not the case here. The effect that the observed variation can have on the accuracy of any analytical solution is significant and as a result it is difficult to characterise AE signal generated from different locations within large-scale complex structures using AE data directly.

Clearly, if one could correct each recorded parameter according to the parameter distribution contours, as shown in Fig. 1b, then much of these problems would be negated. Unfortunately, in practice, there are many limitations. This is because each damage mechanism generates signals with different levels of energy, while the presented contour was generated from one energy level source. Furthermore, the final assessment relies mainly on the inspector's own experience and subjective decision-making, because the correction process will depend on the chosen sensor data and the specific correction distance from that sensor. Moreover, the difficulty will increase if the AE data was collected using more than one sensor, as is the situation in large-scale structures, because it will be difficult to find a comparable scale between the different sensors corrected data. The proposed PCT overcomes the dependency on the operator choice and obtaining the corrected results by using comparable scale. This is considered to be a significant improvement in the field of the acoustic emission. It makes it possible to compare with more confidence the AE collected from different source locations, different specimens, different materials and from different sensor types.

The relationships extracted from the PCT maps are used to correct the recorded AE parameters and obtain the corresponding voltage values.

4.2. Validation approach

In order to validate and assess the performance of the parameter correction methodology, a validation test was performed on different types of artificial sources. This used artificial signals with varying width and shape to represent different source types. The sources details are shown in Table 1. Six arbitrary positions were chosen to conduct this investigation and at each position each source type was repeated five times to reduce the error. The position of each testing point is labelled during the rest of this paper according to the information provided in Table 2.

For each generated source the AE signal parameters were recorded by the sensors. Furthermore, the source locations were located using the *Delta-T* technique. In order to assess the *Delta-T* technique result accuracy, the average location error (the Euclidian distance between the actual source position and the calculated source position for the six arbitrary source locations) of all the signals was calculated to be 6.6 mm and the standard deviation of the average location error was found to be 5.7 mm.

To assess the performance of the PCT, a comparison was made between the traditional and the corrected parameters for the three tests. For the traditional parameter values, sensor 1 was chosen arbitrarily to perform this comparison. The traditional amplitude and the corrected amplitude for the three tests are presented in Fig. 4. Similar performance was achieved for the remaining parameters (counts, energy and duration).

The graphs herald many significant and very promising findings. Firstly, there is great discernible difference between traditional amplitude values from the different sources locations. Secondly, it can be clearly seen that the PCT results provide a significant improvement in correcting the recorded amplitude value. The corrected amplitude is deemed to be more than acceptable as it eliminates all propagation effects on the recorded amplitude and presents each source at a stable level. The fluctuation in the PCT results is related to a number of sources of error. The largest error is considered to be due to the location accuracy and another potential source of error is that related to human manipulation (including accurate positioning of the artificial source and the level of coupling).

In addition to the substantial improvement that are achieved by correcting the AE parameters, it is worth highlighting another important advantage of the PCT. Due to use of data from all sensors, the PCT shows clear separation between different sources in the corrected parameters, whereas this separation is not always clear depending on the traditional parameters recorded by one sensor. For example, the amplitude values of the two sources at location

Table 1
Artificial sources details.

The source code	001	002	003	007	009	010
Pulse name (waveform)	Sine wave	Sine wave	Sine wave	Saw tooth	Saw tooth	Saw tooth
Wave envelop	Sine curve	Sine curve	Sine curve	Sine curve	Sine curve	Sine curve
Frequency (kHz)	300	300	300	300	200	100
Cycle	1	1	1	1	1	1
Amplitude (V)	50	100	150	100	100	100

Table 2
The point number and its location on the specimen.

Point number	X (mm)	Y (mm)
From 1 to 5	75	275
From 6 to 10	75	60
From 11 to 15	150	140
From 16 to 20	75	175
From 21 to 25	0	200
From 26 to 30	150	300

Table 3
Sensors response of the Code007 source signals from six locations.

Sensor no.	Number of signal hits the sensor	% Of located data
1	25	100
2	25	100
3	15	60
4	10	40
5	25	100
The PCT	25	100

(75, 275) mm have approximately the same value (55.8 dB and 54.3 dB for sine wave and saw tooth sources, respectively) as presented in Fig. 4a. On the other hand, clear separation was accomplished in the PCT results in Fig. 4b. The reason behind that, as noted earlier, is that the PCT calculates each event parameters value based on data from all sensors which recorded that event. So, it can be concluded that using data from only one sensor is more challenge in field of source discrimination and damage identification. While, with the proposed technique, using data from many sensors makes it possible to improve the accuracy.

Moreover, using data from all sensors in the correction process leads to all the located events being used in the final results and there are no missing AE events. This is seen as a substantial advance over the traditional AE. Usually in medium and large-scale structures, it is difficult to collect all AE activity using one sensor and the operator will chose the sensor with the highest AE quantity to perform the analysis. This means that there is potential to miss AE events in the final analysis if they are located far away from the used sensor. Further investigation was undertaken to highlight this benefit. For example, the code007 source was repeated five times in each position of the six different locations, so ideally there would be 30 events recorded by all sensors. In reality the *Delta-T* locates only 25 events as shown in Fig. 4a because some signals hit less than three sensors [5]. The number of signals hit at each sensor is provided in Table 3.

From Table 3 it can be seen that the variation in amount of recorded AE data by each sensor depends on the recorded sensor position from the source location. For example, if the traditional analysis was conducted using data from sensor 3 or sensor 4 that would mean losing 40% and 60% of the located AE activity,

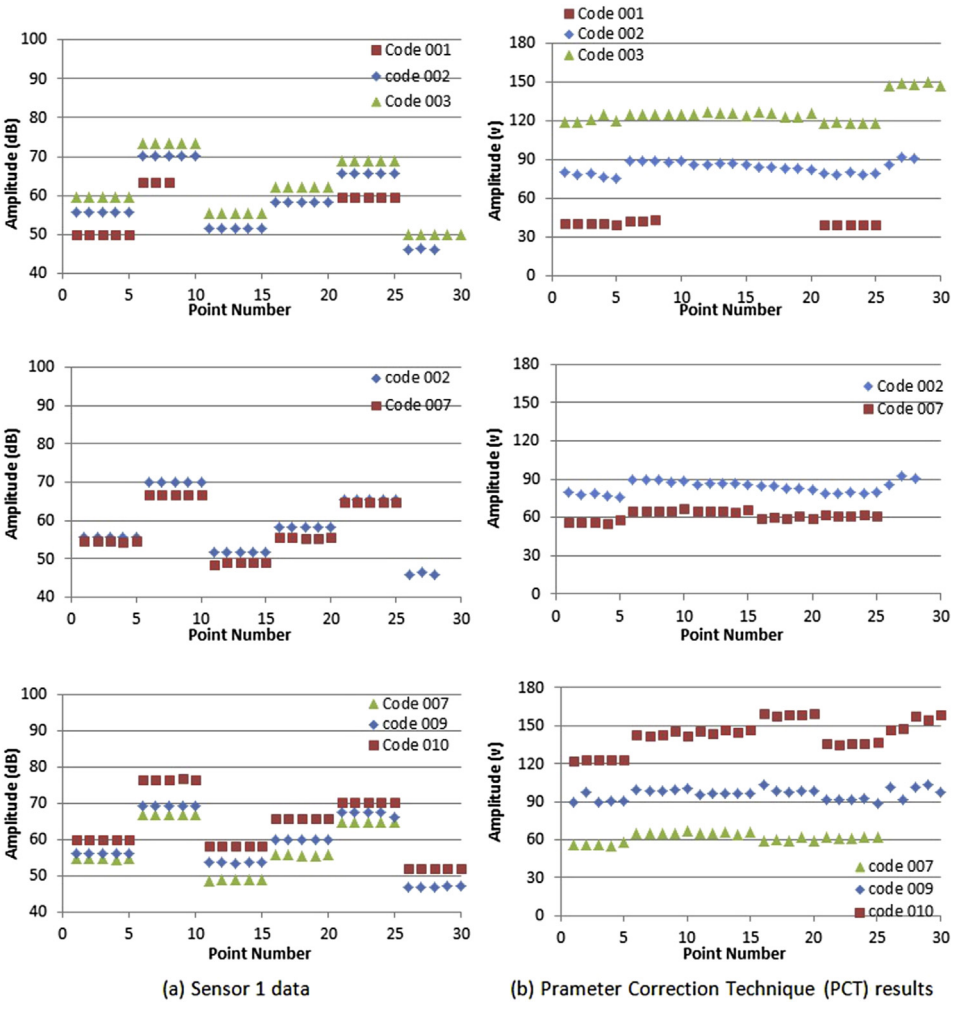

Fig. 4. Comparison between the sensor 1 amplitude values and the corrected amplitude using the PCT.

respectively. So, it can be concluded that using the traditional parameters of data from one sensor to analyse AE data is limited in large-scale structures. Whereas, the PCT is able to use data from all sensors, as listed in Table 3 to correct the parameters. So, there are no missing located AE events and that is considered as a significant improvement in this AE analytical approach.

4.3. Classification results

This part of the study investigates the performance of the PCT on the source identification process using multivariate statistical techniques for classification and visualization. Two cases were performed. The first (Case-1) was performed using traditional parameters, while the second (Case-2) was performed using the corrected parameters. In each case, a data set of 71 labelled signals recorded using sensor 1 was used as an input vector and consists of three different amplitude sources, namely, code001 (18.31% of signals), code002 (39.44% of signals) and code003 (42.25% of signals). All these sources are detailed in Table 1. According to the clustering quality criterion values, optimal class numbers for the Case-1 was calculated to be six and ten using the Silhouette criterion and Davies-Bouldin, respectively, demonstrating poor accuracy when using traditional AE features. For Case-2 the optimum cluster number was calculated to be three using both criterion, highlighting the improvement when using corrected parameters. However, because the number of sources is known to be three, the unsupervised clustering procedure was performed with three classes in both cases to ensure fair comparison of their classification performance. The signals were then clustered into the three classes using the k-means algorithm and identified as Class-1, Class-2 and Class-3 for the next stage of analysis.

Visualisation of class separation was achieved using PCA, performed using the same input data and Fig. 5 presents the signal distributions projected on score plots for the first principal component (PC1) versus the second principal component (PC2). In Fig. 5a and b classes are labelled by the classification process, for case-1 and case-2 respectively, and in Fig. 5c and d classes are labelled using their known prior labels, for case-1 and case-2 respectively. When the class are labelled by the classification process (Fig. 5a and b), three separate and non-overlapping clusters are observed in both cases. A user would now most likely assume the three clusters resulted from three different sources and aim to attribute them to observable (or expected) damage mechanism. However it is evident that the classes are differently distributed for case-1 and case-2, indicating that classification has not been performed in the same way for both cases. If we now consider the same data but with known prior labels (Fig. 5c and d) it can be seen that in case-1, using traditional features, very poor differentiation between sources was actually achieved, highlighting how misleading classification results can be if the effects of propagation are not considered. Whereas for case-2 there is no change in the observed classification is seen and demonstrating the correct classification of signals through application of the PCT approach. More details about each class elements for both cases are presented in Table 4.

Fig. 6a and b presents the signals with the classification derived labelling overlaid with the *Delta-T* location, for case-1 and case-2 respectively. The figure shows that accurate classification using the PCT is achieved, however using traditional parameters there are errors in classification due to the effects of signal propagation.

5. Conclusions

Parameters Correction Technique (PCT) provides a novel approach for overcoming the problems associated with AE parameters changing in large-scale composite components or complex geometry structures due to signal propagation path effects. In the present investigation, the new technique was examined using a variety of artificial sources on different locations on a carbon fibre composite specimen. A continual and significant improvement in overall performance/efficiency was achieved in the corrected

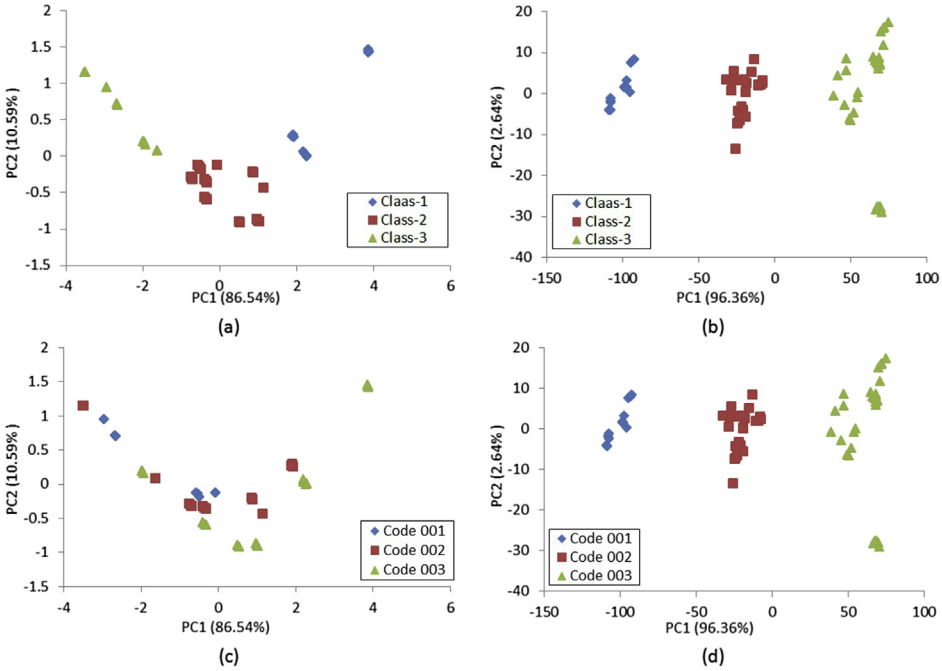

Fig. 5. The k-means clustering results presented using PCA (a) traditional parameters clustering with the class number label (b) corrected parameters clustering with the class number label (c) traditional parameters clustering with the source type label (d) corrected parameters clustering with the source type label.

Table 4
A summary of the clustering result with each class ingredients (a) Traditional parameters (b) Corrected parameters.

	(a)Traditional parameters (Case-1)			(b) Corrected parameters (Case-2)		
	Code 001 (%)	Code 002(%)	Code 003 (%)	Code 001 (%)	Code 002 (%)	Code 003 (%)
class-1	0	33.33	66.67	100	0	0
class-2	21.06	39.47	39.47	0	100	0
class-3	27.78	44.44	27.78	0	0	100

parameters generated from different amplitude, waveform and frequency sources at different locations. The performance of this technique was seen to be very good. Moreover, the robustness of the approach was assessed for commercial use.

A comparison with traditional parameters was conducted using single parameter analysis, correlation plots and multi-dimensional clustering analysis. The AE data was collected from different AE sources generated on different locations on unidirectional carbon fibre specimen. Results reveal that the traditional parameters are completely misleading for damage identification in large-scale components. Moreover, an excellent corrected result was obtained using the corrected parameters. The PCT shows the ability to use all sensors data to improve accuracy and avoid losing data. On the basis of this investigation we can state that the PCT gives an important benefit to the identification between different damage mechanisms. These findings show great potential for the use of AE monitoring in SHM of large-scale composite structures as found in aerospace structures and wind turbines.

Including all these factors in one algorithm and correcting the recorded AE data is difficult to achieve in practice and in an automatic and robust fashion. The proposed PCT technique overcomes all detrimental factors and corrects the recorded parameters with a high performance by using the actual path propagation of each signal.

Further studies with other signal characterization techniques are on-going and will help in validating signal separation. Selection of the correct features will reflect the source signature and enable full knowledge about the experimental conditions and all factors that effect the signals descriptors to obtaining the correct signal features.

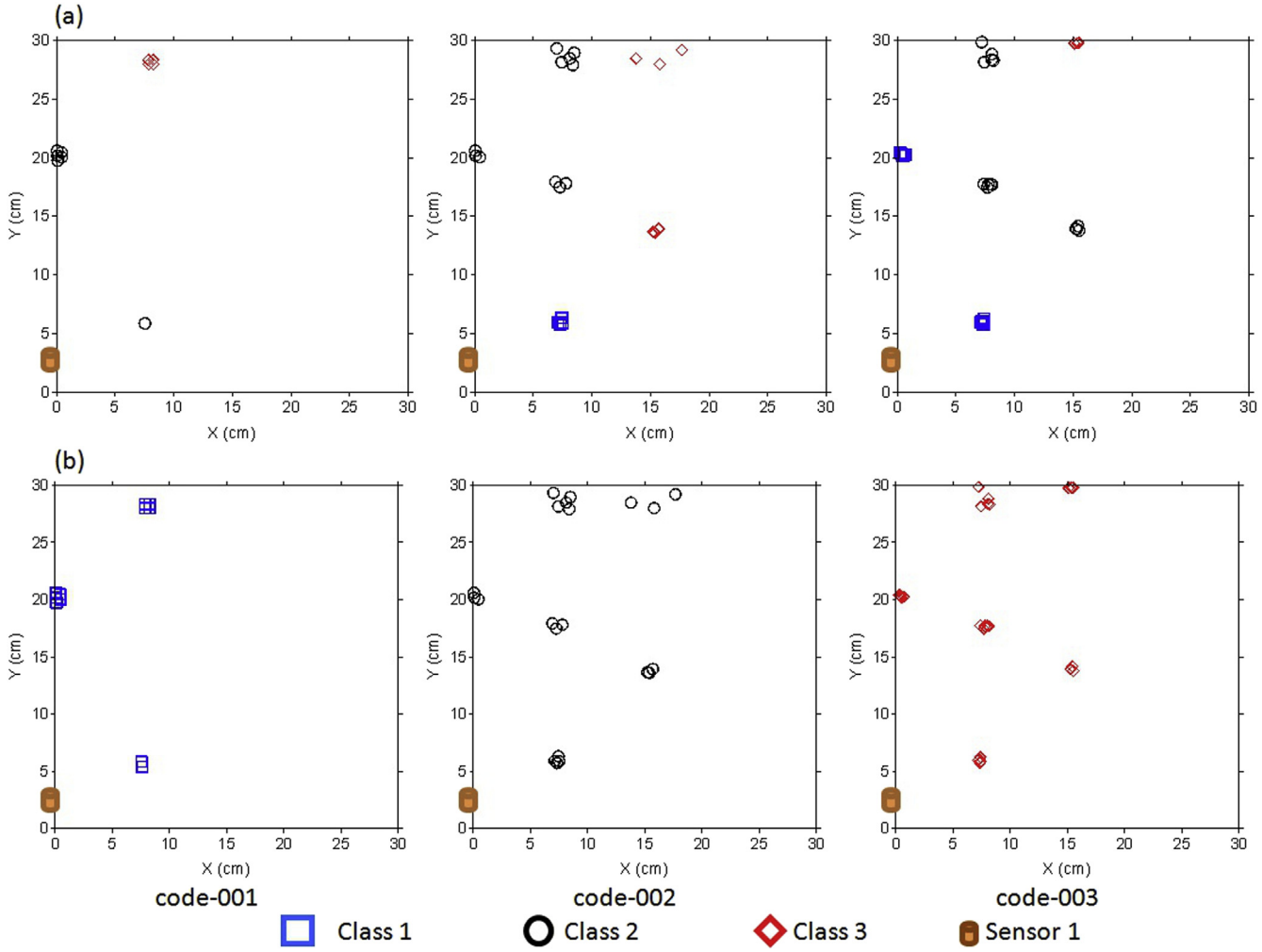

Fig. 6. The Delta-T location of each source type with the clustering result label (a) Case-1 (b) Case-2.

The PCT technique does have some limitations. Firstly, because the AE event location is essential to start the correction of its parameters, only located events can be corrected using the PCT. Secondly, this technique considers each structure as unique and thus it is necessary to generate a unique training map for each specimen or for each area of interest in the structure.

Acknowledgements

The authors would like to thank the Iraqi Ministry of Higher Education and Scientific Research for supporting this research, Dr. Davide Crivellia (Politecnico di Milano, Italy) for his assistance with manufacturing the test specimen, Dr. Matthew R. Pearson (Cardiff University, UK) for his assistance and the technical staff of Cardiff School of Engineering for their kind assistance with the testing programme.

References

[1] Miller KR, Hill EK. Non-destructive testing Handbook; acoustic emission testing. Am Soc Non Destructive Test 2005;6(3).
[2] Ramirez-Jimenez CR, Papadakis N, Reynolds N, Gan TH, Purnell P, Pharaoh M. Identification of failure Modes in glass/polypropylene composites by means of the primary frequency content of the acoustic emission event. Compos Sci Technol 2004;64(12):1819–27.
[3] Qi G. Wavelet-based AE characterization of composite materials. NDT E Int 2000;33(3):133–44.
[4] Lu C, Ding P, Chen Z. Time-frequency analysis of acoustic emission signals generated by Tension damage in CFRP. Procedia Eng 2011;23(0):210–5.
[5] Baxter MG, Pullin R, Holford KM, Evans SL. Delta T source location for acoustic emission. Mech Syst Signal Process 2007;21(3):1512–20.
[6] Eaton MJ, Pullin R, Holford KM. Acoustic emission source location in composite materials using Delta T mapping. Compos Part A Appl Sci Manuf 2012;43(6):856–63.
[7] Al-Jumaili SK, Holford KM, Pullin R, Eaton MJ. A parameter correction technique (PCT) for acoustic emission characterisation in large-scale composites. In: 31st conference of the European working Group on acoustic emission (EWGAE); 2014 [Accepted].
[8] Manson G, Worden K, Holford K, Pullin R. Visualisation and dimension reduction of acoustic emission data for damage detection. J Intelligent Material Syst Struct 2001;12.
[9] Rippengill S, Worden K, Holford KM, Pullin R. Automatic classification of acoustic emission patterns. Strain 2003;39(1):31–41.
[10] MacQueen J. Some methods for classification and analysis of multivariate observations. Proc Fifth Berkeley Symp Math Statist Prob, vol. 1. Univ of Calif Press; 1967. p. 281–97.
[11] Rousseeuw PJ. Silhouettes: a graphical aid to the interpretation and validation of cluster analysis. J Comput Appl Math 1987;20(0):53–65.
[12] David LD, Donald WB. A cluster separation measure. IEEE Trans Pattern Anal Mach Intell 1979;1(2):224–7.
[13] Subhash Sharma SM. Applied multivariate techniques. John Wiley & Sons Canada, Limited; 1996.
[14] Hsu NN, Breckenridge FR. Characterization and calibration of acoustic emission sensors. Mat Eval 1981;39(60).

Composites Part B 74 (2015) 1–12

Contents lists available at ScienceDirect

Composites Part B

journal homepage: www.elsevier.com/locate/compositesb

Localisation and identification of fatigue matrix cracking and delamination in a carbon fibre panel by acoustic emission

Davide Crivelli [a, *], Mario Guagliano [a], Mark Eaton [b], Matthew Pearson [b], Safaa Al-Jumaili [b], Karen Holford [b], Rhys Pullin [b]

[a] Politecnico di Milano, Department of Mechanical Engineering, via La Masa 1, 20156 Milano, Italy
[b] Cardiff School of Engineering, Cardiff University, Queen's Building, The Parade, Cardiff CF24 3AA, Wales, UK

ARTICLE INFO

Article history:
Received 9 April 2014
Received in revised form
6 November 2014
Accepted 30 December 2014
Available online 12 January 2015

Keywords:
A. Carbon fibre
A. Laminates
C. Damage mechanics
D. Acoustic emission
Artificial damage

ABSTRACT

Background: The use of Acoustic Emission (AE) as a Structural Health Monitoring (SHM) technique is very attractive thanks to its ability to detect not only damage sources in real-time but also to locate them.
Methods: To demonstrate the AE capabilities on known damage modes, a carbon fibre panel was manufactured with cut fibres in a central location and subjected to fatigue loading to promote matrix cracking. Subsequently, a delamination was created within the panel using an impact load, and the test was continued.
Results: AE signals were located within the crack area in the first part of the test. After impact, AE signals were detected from both areas under fatigue loading; signals from this area were located and used for further analysis with the neural network technique.
Conclusions: The application of an unsupervised neural network based classification technique successfully separated two damage mechanisms, related to matrix cracking and delamination. The results obtained allowed a more detailed understanding of such sources of AE in carbon fibre laminates.

1. Introduction

The growing use of composite materials is encouraged by those industrial sectors in search of lightweight materials, which guarantee the same safety levels and reliability as those in traditional metallic structures. A solution is to equip those structures with an on-board sensing technique, capable of detecting damage. This family of techniques goes under the name of Structural Health Monitoring (SHM), comprising all those systems that monitor, either continuously or at specific moments, the health status of a material, giving an indication to the user about damage developing, damage severity and eventually damage location [1].

Such SHM systems, if appropriately designed, will also allow a reduction in the downtime of assets. Planned, inspection-interval based maintenance will no longer be required in favour of an on-demand maintenance programme. Safety critical structures, such as off-shore wind turbines or aircrafts, will receive the most benefit from this approach to monitoring, since their maintenance downtime represents a large part of their operative cost.

Among the SHM techniques being investigated at the moment, Acoustic Emission (AE) is considered to be a good candidate [2]. AE is based on the observation that materials, when undergoing some type of damage, release energy in the form of short, transient elastic waves in the ultrasound band (100 kHz–1000 kHz). These waves propagate in the structure through the material's bulk and surface, and eventually dissipate due to various phenomena. These waves can be recorded by means of appropriate sensors, usually of the piezoelectric type [3].

AE is classified as a passive Non Destructive Technique (NDT): it does not require signals to be emitted (i.e. to introduce energy in the structure) to detect damage. Instead, it waits for signals to be recorded; those signals originate inside the material by some damage or energy release process. This is a major advantage of AE, as it does not require continuous scanning of the structure or the continuous recording of data in search of a potential defect. This is however also a downside, because it does not provide information about a structure when it is not loaded, unlike other NDTs (like radiography or ultrasound). In other words, the source must be active to be detected; unstressed flaws will not generate AE.

* Corresponding author. Tel.: +39 02 2399 8595; fax: +39 02 2399 8202.
E-mail addresses: davide.crivelli@polimi.it (D. Crivelli), mario.guagliano@polimi.it (M. Guagliano), eatonm@cardiff.ac.uk (M. Eaton), pearsonmr@cardiff.ac.uk (M. Pearson), al-jumailisk@cardiff.ac.uk (S. Al-Jumaili), holford@cardiff.ac.uk (K. Holford), pullinr@cardiff.ac.uk (R. Pullin).

http://dx.doi.org/10.1016/j.compositesb.2014.12.032
1359-8368/

There are several sources of AE. In metallic structures, AE can arise from crack propagation and plastic deformation [4], as well as from non-detrimental phenomena such as friction and bonding relative movement. Spurious noise sources from parts that are acoustically connected are also a concern. In composite structures, AE sources are associated with the main failure modes of those materials: fibre breakage, matrix cracking, fibre pull-out and delamination [5]. An in-depth analysis of these AE events can lead to source type identification based on waveform characteristics; this is the subject of current extensive research [6]. Especially in composite materials, AE has proved to offer interesting indications to researchers about the development of damage. Static tests, but also fatigue tests [7–9], crack propagation, bond strength tests [10], residual strength tests [11] and many others have benefited from AE monitoring.

For all these applications, the necessity to identify different AE sources emerges. The main concern is to learn how to assess whether and when a specific failure mode occurs in a material; such research is usually aimed at increasing the knowledge regarding failure modes of materials or structures and is directed towards the development of better damage models.

One of the advantages of AE is its ability to localise damage sources by using multiple sensors (three or more for localisation on a plane [3]). Common planar location algorithms usually consider a uniform velocity in the whole plane; then, based on the time of arrival (ToA) of the waveforms, they compute the position by intersection of hyperbolas between sensor pairs. This algorithm is robust for homogeneous materials, provided that the waveforms ToA is computed correctly and the velocity is known with an adequate precision. However, in anisotropic materials, such as Carbon Fibre Reinforced Polymers (CFRP), the wave velocity depends on the orientation of the wavepath with respect to the ply orientation. This makes the ToA technique prone to errors. Moreover, local features (such as material's local inhomogeneities and discontinuities) add uncertainty to the problem. To overcome this issue, a technique called Delta-T was developed [12,13]. Delta-T utilises user-generated maps of ToA differences between sensors, without defining a wave velocity but with the help of a calibration grid. A HSU-Nielsen source [14] is generated at each grid point; subsequently, for each sensor pair, a ToA difference map is computed. The location algorithm then, when receiving a waveform (or, more specifically, the sensor pairs ToA differences) looks up each Delta-T map and identifies the source location. This technique proved to be more accurate than the ToA method in a number of test cases [15].

Commercial AE systems already provide some sort of data compression, by encoding the information contained in each waveform into different parameters, such as peak amplitude, frequency content, duration, energy and some others. Moreover, these parameters are thought to be linked to the kind of damage source that originated the signal. For SHM based on AE, this feature would be helpful because it provides information not only on the event localisation, but also on the activity of specific damage modes.

In composite materials, AE can be generated in a number of ways; the main failure modes include matrix cracking, fibre-matrix debonding, fibre fracture and delaminations. There are differences in the nature of the AE signals due to the source type; this is mainly due to the in-plane or out-of-plane energy content. It is known that matrix cracking and fibre breakage initiate mostly in-plane phenomena and generate extensional waves of higher frequency, while delaminations are dominated by flexural waves of lower frequency [16].

In a delamination, the laminate separates at the interface between two layers, in some cases without indications on the surface (for example, some impacts, although not visible from the impacted surface, may hide large delaminations). Some authors suggest delaminations give rise to high amplitude signals [17], while others point out medium amplitude signals for a ±45° laminate [18]; authors generally agree on delamination signals having in general a long duration [19], but tend to include debonding within the same classification.

Matrix cracking generally occurs between fibres at the fibre-matrix interface, or as shear failures between plies. These types of matrix failures usually cause hackles, which are visible on the surface. Results have been found to be dependent on material and testing procedure, with some agreement on defining matrix cracking AE as mid-to-high amplitude and low frequency [20], but some studies report low amplitude [17,18,21] and medium frequency [22] fast decay [23] but also slow decay [24].

Finally during loading, some fibres fail in tension. The expected AE signature is an abrupt energy release mechanisms, with high amplitude and fast rise time [18], as it would happen in a brittle crack phenomenon.

As discussed, early approaches based the classification of damage mechanisms on a single AE parameter, typically peak amplitude or frequency content. When trying to overcome some issues, mainly related to signal attenuation as a function of distance, multiple parameters at once have been considered [21,25]. Due to the high amount of data to be processed and difficulties in identifying patterns with traditional statistical techniques, machine

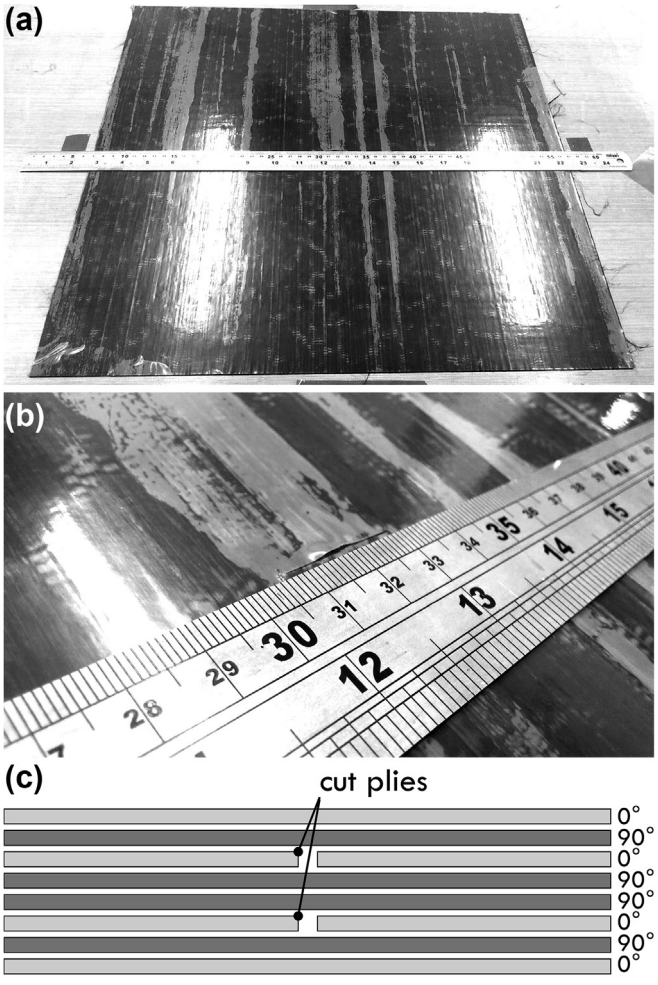

Fig. 1. CFRP panel during layup of the inner plies: entire panel (a), detail of the cut (b) and cut plies schematic (c).

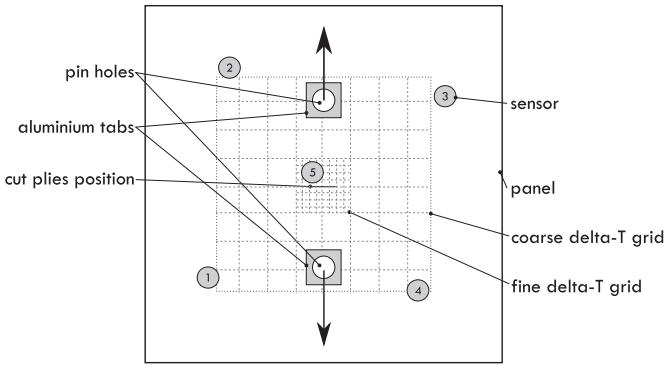

Fig. 2. Artificial crack panel after manufacturing.

learning algorithms, especially Artificial Neural Networks (ANN), have been increasingly used in this field [26–30]. Among these techniques, a previous paper by the authors [31] presented an unsupervised technique for the classification of AE signals, based on the Self Organizing Map (SOM) and the k-means clustering algorithm. The technique, for brevity referred to as *k-SOM*, also employs a number of clustering indexes to determine which is the optimal number of natural classes found in a dataset. In this way, no user input or tuning is required.

The aim of this experimental work is to obtain, analyse and identify AE signals from different damage sources. These sources should be generated in a way that they could be easily isolated from boundary effects (like edge reflections), while at the same time being in a known and distinct location. The positive identification of different damage sources by the *k-SOM* classification technique is key to separate the different contributions of the various AE modes in a real structure; for this reason, it is the intention of this work to provide a further validation of the technique.

2. Experimental plan

2.1. Panel

A 500 mm × 500 mm CFRP panel was manufactured from unidirectional pre-preg T800S carbon fibre (56.6% in volume) in epoxy resin (M21/35%/UD268/T800S, Hexcel Corporation). The final laminate consisted of eight layers, laid up as $[0/90]_{2s}$, giving a total thickness of 2.2 mm; this was in line with the indications of the manufacturer (a 2.1 mm thickness was expected).

To promote matrix cracking in the innermost 0° layers (3rd and 6th) a 25 mm crack was introduced by cutting the fibres with a knife. Particular attention was paid when manufacturing the final lay-up to ensure that the two cracked layers were aligned (Fig. 1). This would ensure matrix cracks are more likely to happen in this area as these plies are no longer supported by longitudinal fibres in the direct loading path.

The panel was then cured as per manufacturer specifications in an autoclave. The panel was subsequently C-scanned to make sure that no macroscopic defects or curing failures were present.

To allow the panel to be loaded in tension, two holes were drilled and reinforced with aluminium square tabs. This helped

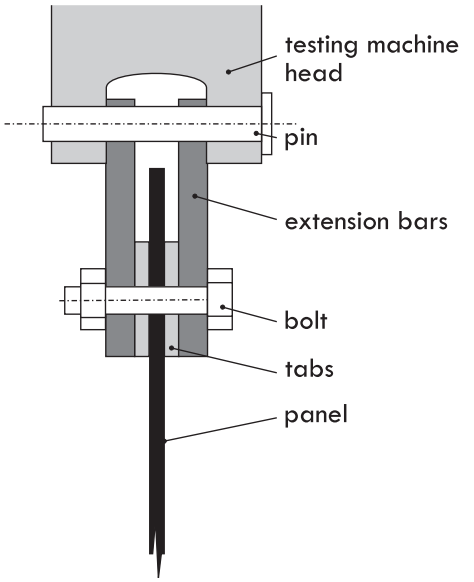

Fig. 3. Panel fitting in the tensile machine.

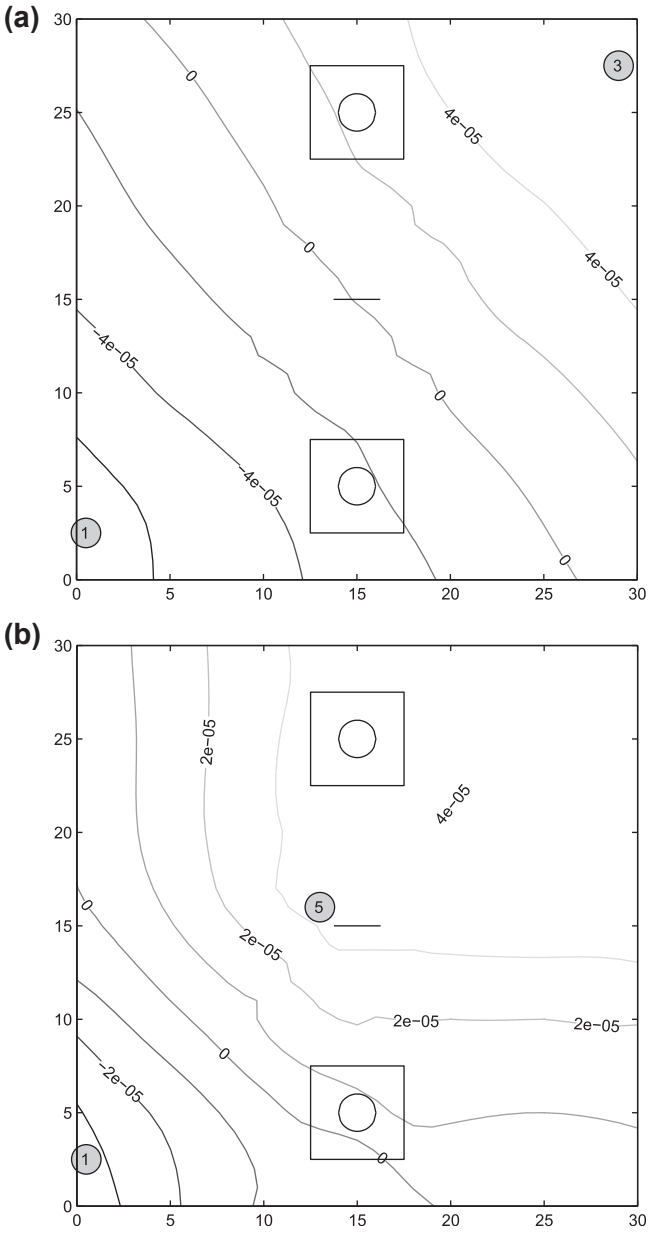

Fig. 4. Examples of Delta-T calibration maps for sensors 1–3 (a) and 1–5 (b).

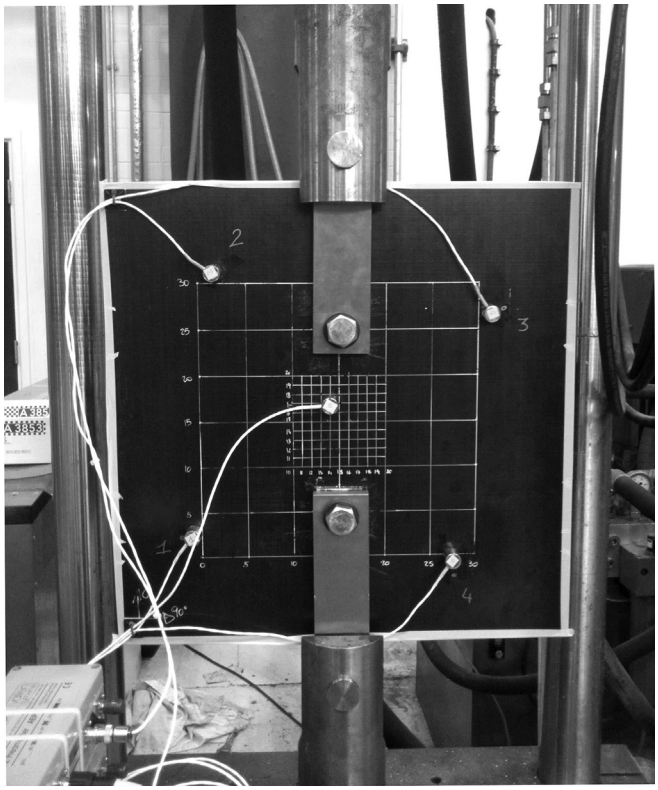

Fig. 5. Panel with sensors and fitted in the testing machine.

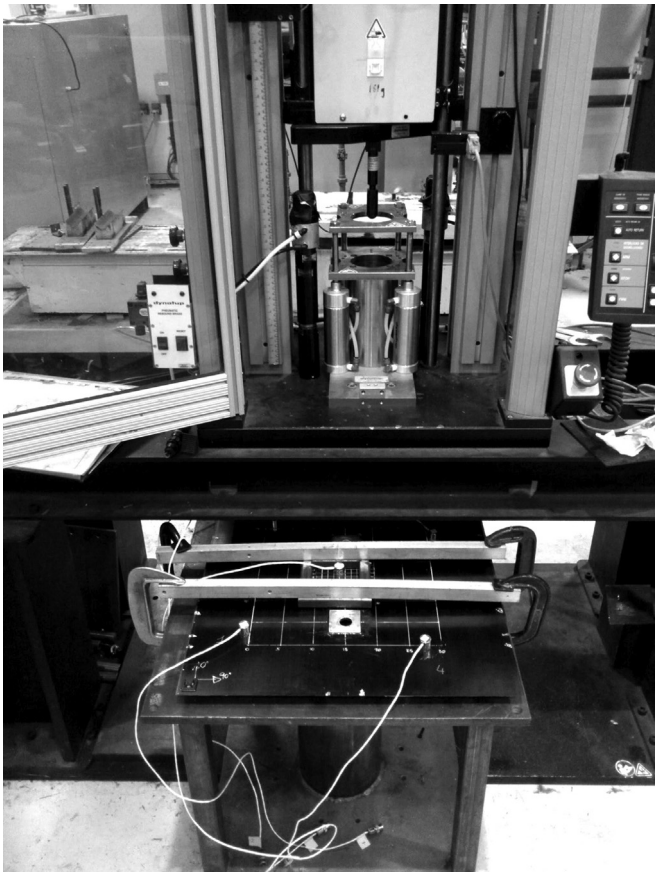

Fig. 6. Impact machine and panel fitting.

avoid damage deriving from the direct contact between the fixture and the panel surface.

The tabs were bonded before cutting the holes with araldite glue; the holes were then drilled through both aluminium and the material. Another C-scan was then performed to compare with the original scan to make sure that it was not damaged during this process. The final panel geometry is shown in Fig. 2.

A schematic drawing of the specimen in the tensile machine is shown in Fig. 3.

2.2. AE setup

For this test, a Vallen AMSY-4 system was used. Physical Acoustics Corporation WD (wideband) sensors were connected to Vallen AEP3 pre-amplifiers, with the gain set to 34 dB. A band-pass filter between 95 kHz and 1000 kHz was used. Sampling frequency for waveforms was set to 5 MHz with a set length of 4096 points, corresponding to a 819.2 μs wavelength. Noise threshold was set to 44.9 dB.

The panel was then prepared for the Delta-T location calibration. A square grid was drawn with two resolutions (Fig. 2): the bigger one, 300 mm × 300 mm wide, featured a 50 mm spacing; in the central region a finer grid was drawn, with a 10 mm spacing and a 100 mm × 100 mm size. The smaller grid is used to get a more accurate location of damage in the cut plies region.

Two examples of the Delta-T maps are shown in Fig. 4 (ten are created in total, one for each sensor pair). It is interesting to observe how the Delta-T technique allows for compensation of the disturbances of wave propagation around the tabs and local anisotropies in the wave velocity due to the material's layup.

2.3. Testing plan

After Delta-T calibration, the panel was fitted into the load test machine. A pin, running through each extension bar hole, connected the panel to the load test machine. The panel was then bolted into the extension bars (Figs. 3 and 5). The bolts were tightened before starting the test, thus using friction to improve the load transfer between the machine and the panel. Particular care was used in making sure that the extension bars were vertical at almost-zero load. The panel fitted in the testing machine can be seen in Fig. 5.

Table 1
Peak load levels for the pre-impact phase.

Batch nr.	Load (kN)	Batch nr.	Load (kN)	Batch nr.	Load (kN)
1	8	9–11	12	19	17
2	8	12–13	13	20–21	18
3–5	9	14–16	14	22	19
6–7	10	17	15	23–25	20
8	11	18	16	26	21

Table 2
Peak load levels for the post-impact phase.

Batch nr.	Load (kN)	Batch nr.	Load (kN)	Batch nr.	Load (kN)	Batch nr.	Load (kN)
1	14	6	20	15	24	21–22	28
2	16	7–8	21	16–17	25	23–24	29
3	18	9–11	22	18	26	25–30	30
4–5	19	12–14	23	19–20	27	31	31

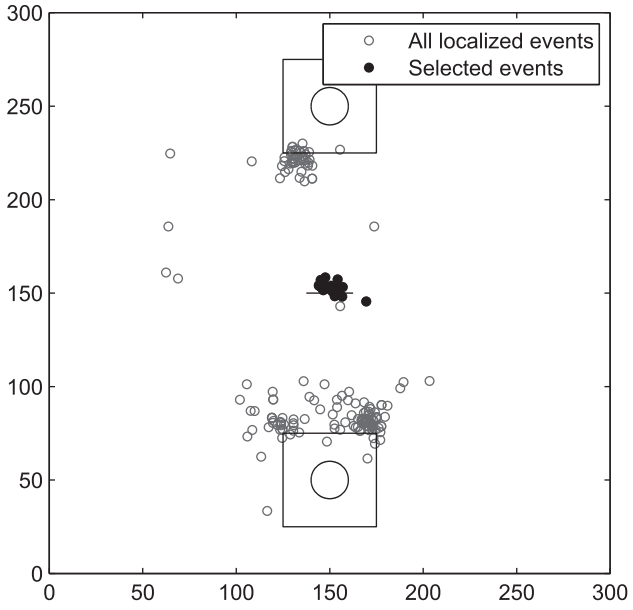

Fig. 7. Location of AE events from the crack propagation test.

The testing plan consisted in running fixed-amplitude batches of 5000 cycles, at 1 Hz; after each batch the panel was removed from the rig and C-scanned, monitoring the eventual damage growth in the panel. The load was increased after each batch if none or little AE was observed, otherwise another run was made at the

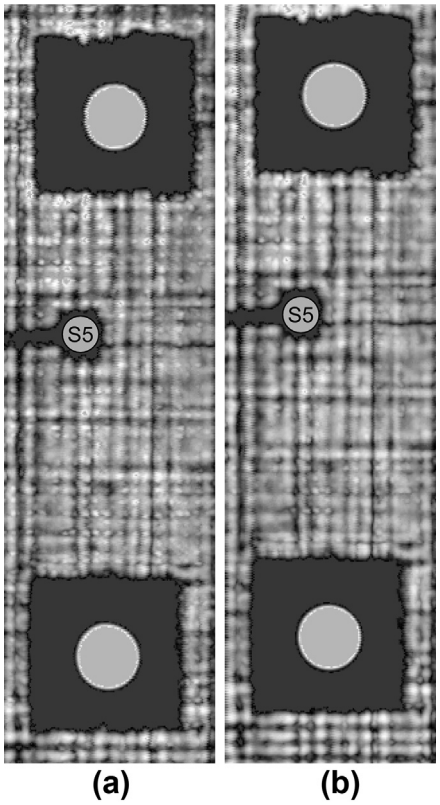

Fig. 9. C-scan images of the panel central region as manufactured (a) and before impact (b), also showing sensor location.

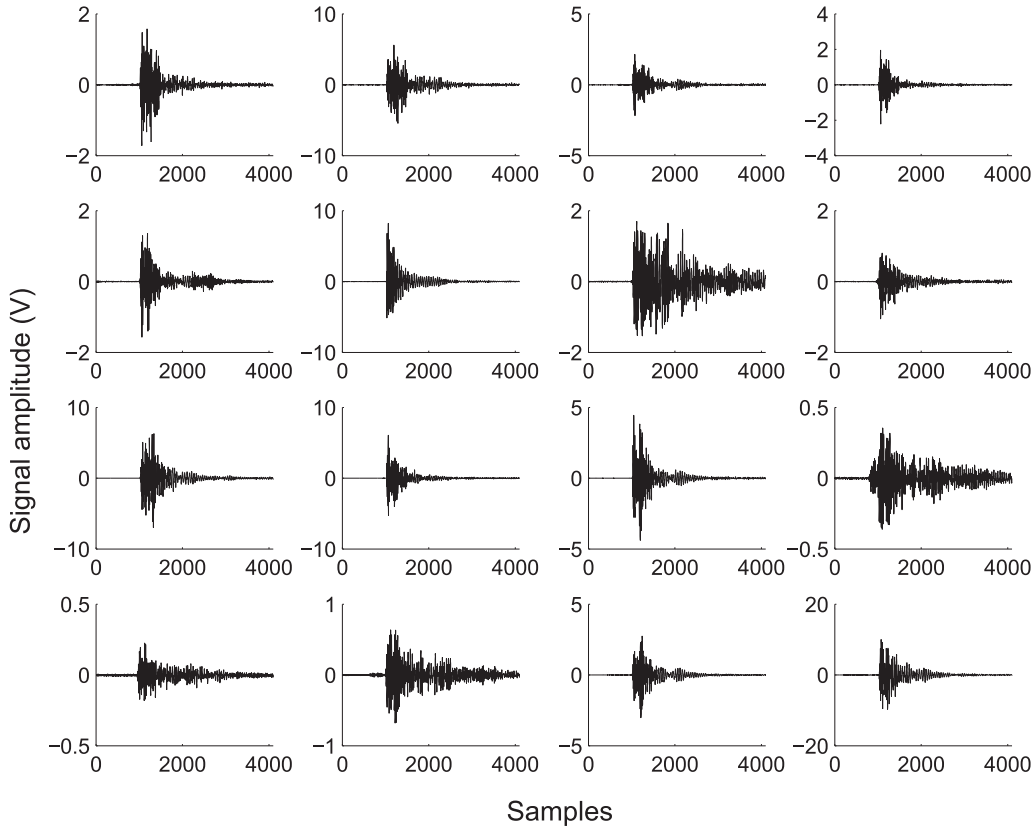

Fig. 8. AE events from crack region.

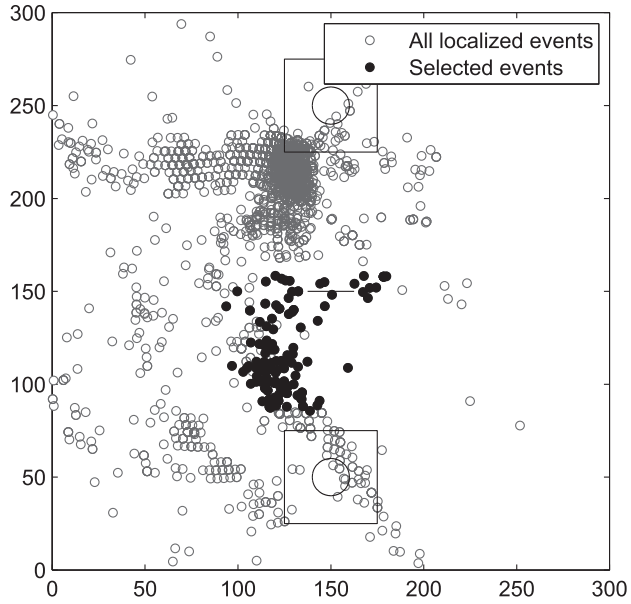

Fig. 10. AE events during the selected after impact batch.

same load level. Tests were run with an R ratio (min load/max load) of 0.1 to avoid compression loads and to obtain a sufficient preload in the fitting. The peak loads are summarised in Table 1.

After a sufficient number of AE signals from the artificial crack area were collected (to allow source characterisation), the panel was then impacted with an Instron Dynatup 9250HV impact

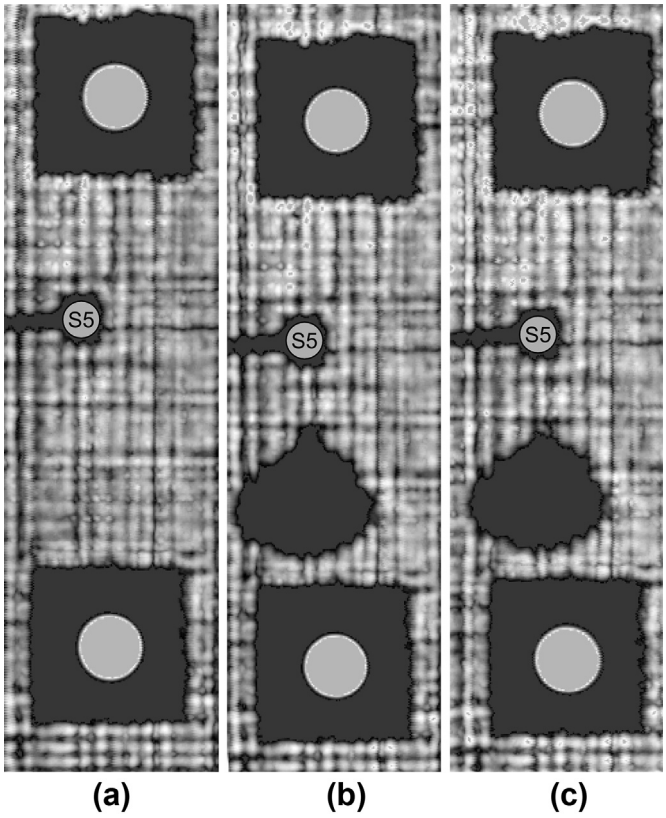

Fig. 12. C-scan images of the panel before impact (a), after impact (b) and end of test (c).

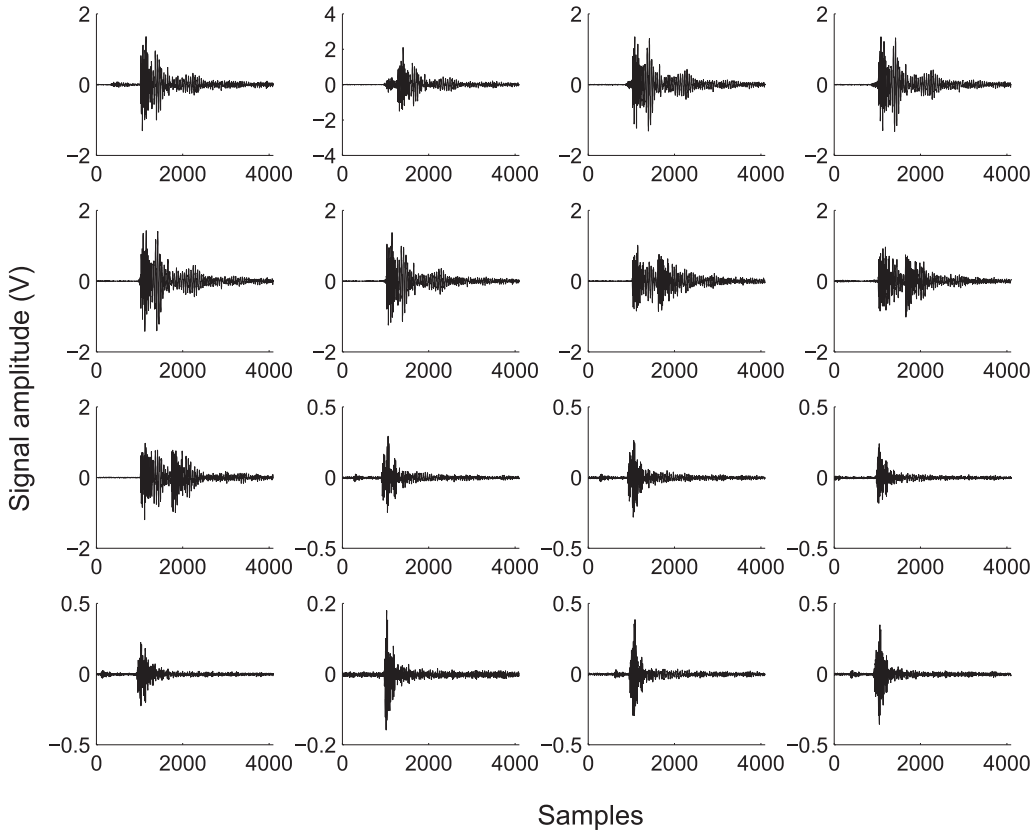

Fig. 11. AE events from delamination region.

machine at an energy of 14J, in a location far from the crack but still within the loading path of the test. The impact machine, with the panel frame fitting, can be seen in Fig. 6.

The purpose of the impact was to generate signals from both the crack and the delamination resulting from the impact. The panel was then tested again as previously, increasing the load and C-scanning after every batch of loading (Table 2).

3. Results

3.1. Pre impact

During the first phase of testing, about 40 AE signals were detected from the crack region, with a good location accuracy (Fig. 7). The regions around the bonded tabs also released AE signals, especially at the corners of the aluminium tabs; this was not unexpected since the stress field induced by the loading fixtures is likely to produce a concentration of stresses. Only signals from the crack region were used for this analysis as shown in Fig. 7.

For classification repeatability purposes, only signals recorded by sensor 5 were considered throughout the whole test. Therefore, there are a few signals (as visible in Fig. 7) that were located in the region of interest and were not recorded by sensor 5, although they are a small percentage (around 2% of the total). A sample of the selected waveforms are shown in Fig. 8.

The C-scans at the beginning and after the last batch without impact are shown in Fig. 9. The central sensor (number 5) is always visible in the C-scans as a dark spot with its attached cable running to the left.

C-scans confirm that no additional damage has been introduced during the test. No high attenuation (dark) areas are found; this confirms the absence of in-plane discontinuities, like delaminations. The crack region, below the sensor visible in the centre, appears to darken slightly, but no evidence of growth can be observed.

3.2. Post impact

After the impact, the AE activity of the panel increased significantly. Fig. 10 shows AE localised events for the last batch after impact (batch 31). The test was then interrupted since it showed significant sources from the impact region. The figure also shows the selected events from this set.

The location accuracy appears reduced, mainly due to the presence of the impact area, which alters the wave propagation path, while the original Delta-T calibration was still used. Nevertheless, it can be noticed that signals from the crack area have decreased in number, and moved toward the crack tips. This is a consequence of the crack region having reduced its stiffness: the stress field increases at the sides of the crack, and stress concentration areas are found around the crack tips. Therefore, those signals may indicate some damage mechanisms happening at or near the crack tip regions. A sample of the signals coming from the delamination region is shown in Fig. 11.

The delamination size after impact was determined by C-scanning the panel again, as visible in Fig. 12.

A final C-scan after all fatigue testing was completed indicated that the delamination had not grown significantly (Fig. 12c).

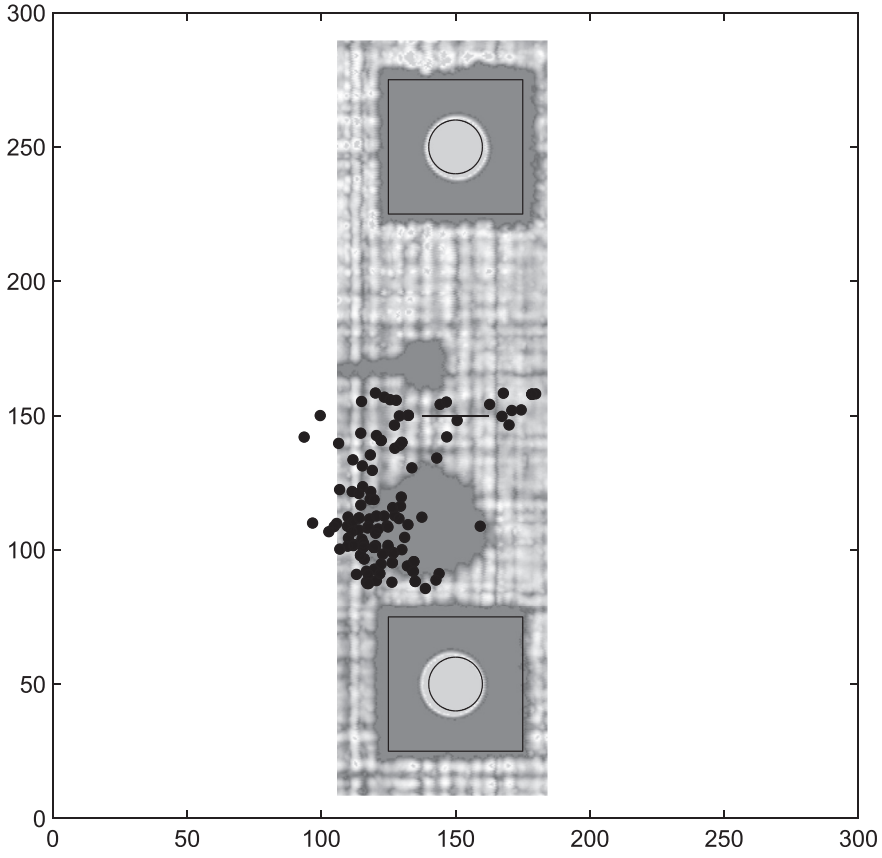

Fig. 13. AE selected events superimposed to the C-scan.

Superimposing AE data to the C-scan, it is clear that only the left border of the impacted area shows AE activity (Fig. 13).

A possible explanation for this, considering that the delamination has not grown, would be that the active areas in the delamination are the ones that experience some type of rubbing or frictional phenomena, in other words those areas that are experiencing a high stress gradient, due to the particular stress field the panel is exposed to.

3.3. Classification of AE signals

Classification of the dataset showed interesting results, with the identification of two classes of signals.

The parameters used for the classification are:

- Amplitude (A), in dB_{AE} (in logarithmic scale, with a reference voltage of 1 mV at the sensor output);

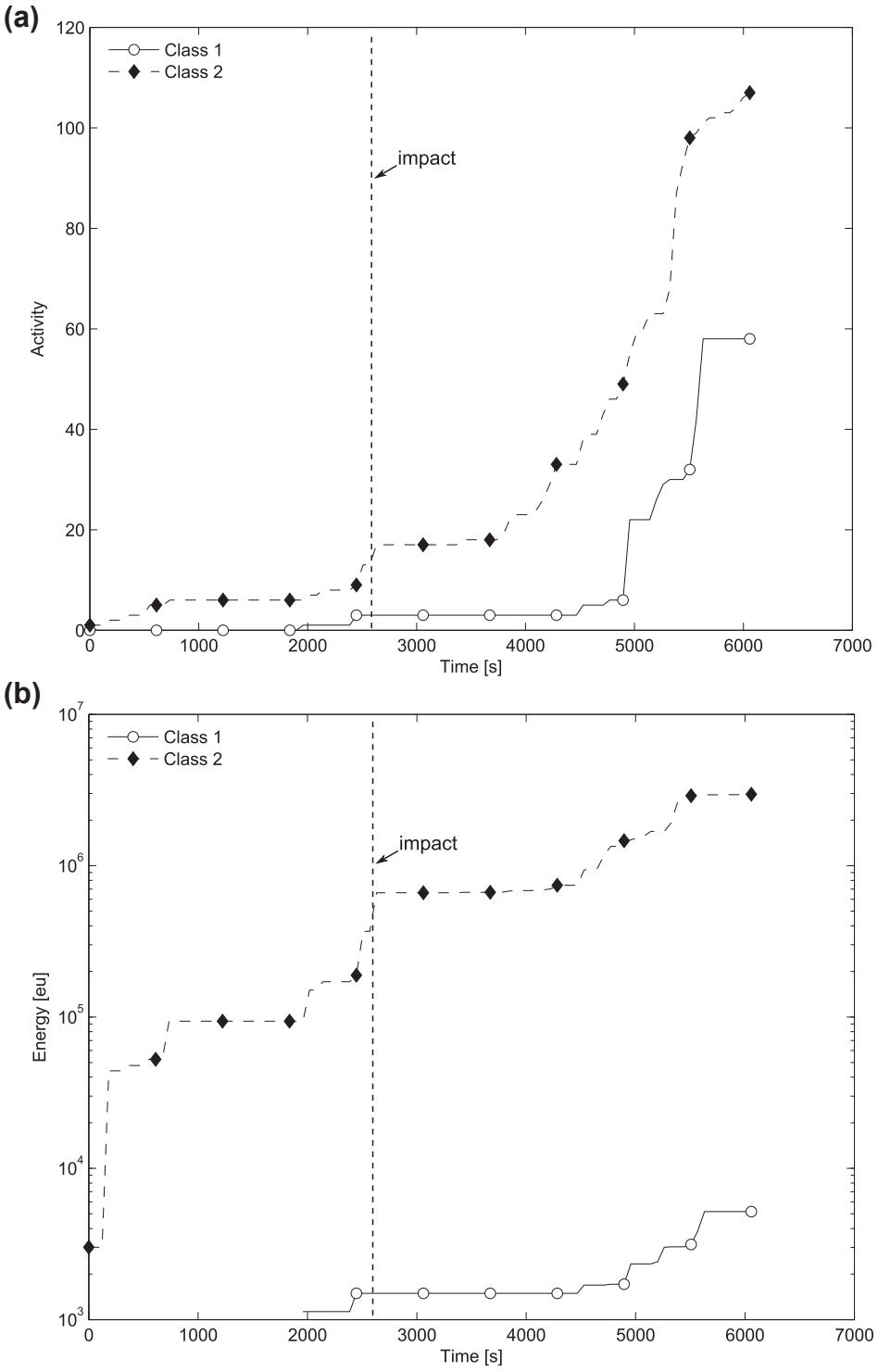

Fig. 14. AE activity (a) and energy (b) trends, after classification.

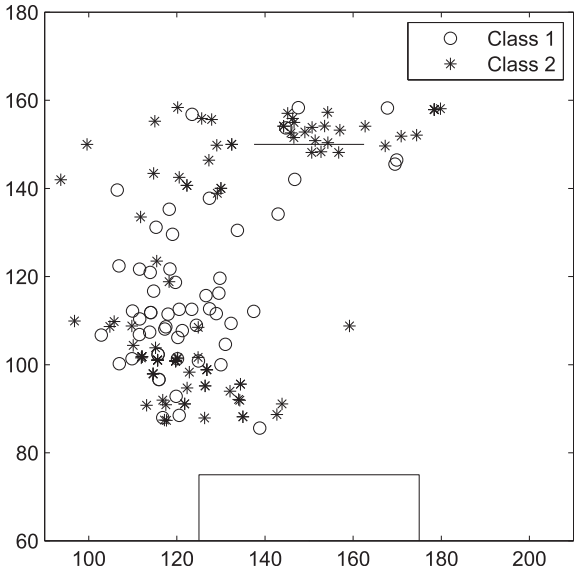

Fig. 15. Classified signals in the selected region.

- Duration (D), in μs;
- Risetime (R), in μs;
- Counts (CNTS), the number of signal zero-crossings;
- Energy (E), in eu (1eu = 10^{-14} V^2s), calculated measuring the area under the signal envelope;
- Frequency center-of-gravity (FCOG), the geometric center frequency of the signal's Fast Fourier Transform (FFT) in kHz;
- Peak Frequency (FMXA), the peak of the signal's FFT in kHz.

The classification technique, presented in detail in Refs. [31], uses a Self-Organizing Map which takes as input the waveform's parameters vector, and gives as output the Best-Matching Unit (BMU). In this way, the SOM maps the multidimensional input to a 2-dimensional space, which is then further mapped to a number of clusters, which themselves correspond to dataset classes. The optimal number of clusters in the dataset is chosen automatically considering a number of classification parameters.

For this dataset, the k-SOM classification technique identified two as the best number of natural classes. AE data has then been classified accordingly.

Global AE energy and activity trends (Fig. 14) show that the first part, before impact (0–2646 s), is dominated by Class 2, while Class 1 remains almost silent. Class 1 is observed at approximately 4500 s, with an increasing trend, which is followed by Class 2.

All classified localised signals for the two batches are shown in detail in Fig. 15.

From this preliminary observation, it can be noted that the crack region holds mainly Class 2 signals, while the impacted area shows a mixture of both classes, with Class 1 being evenly spread and Class 2 concentrating at the bottom boundary.

Energy and activity maps (Fig. 16) show that Class 1 has a lower energy than Class 2, and is concentrated, as previously observed, around the impacted area and at the crack tips. Class 2 is concentrated in the middle of the crack and at the tips, and at the bottom boundary of the impacted area.

Considering the aforementioned time blocks, the evolution of signals is shown in Fig. 17.

Here, the signal evolution indicates that, after impact (Fig. 17b), a number of Class 2 events appear in the damaged region; then, a mixture of Class 1 and Class 2 signals are emitted at a similar rate.

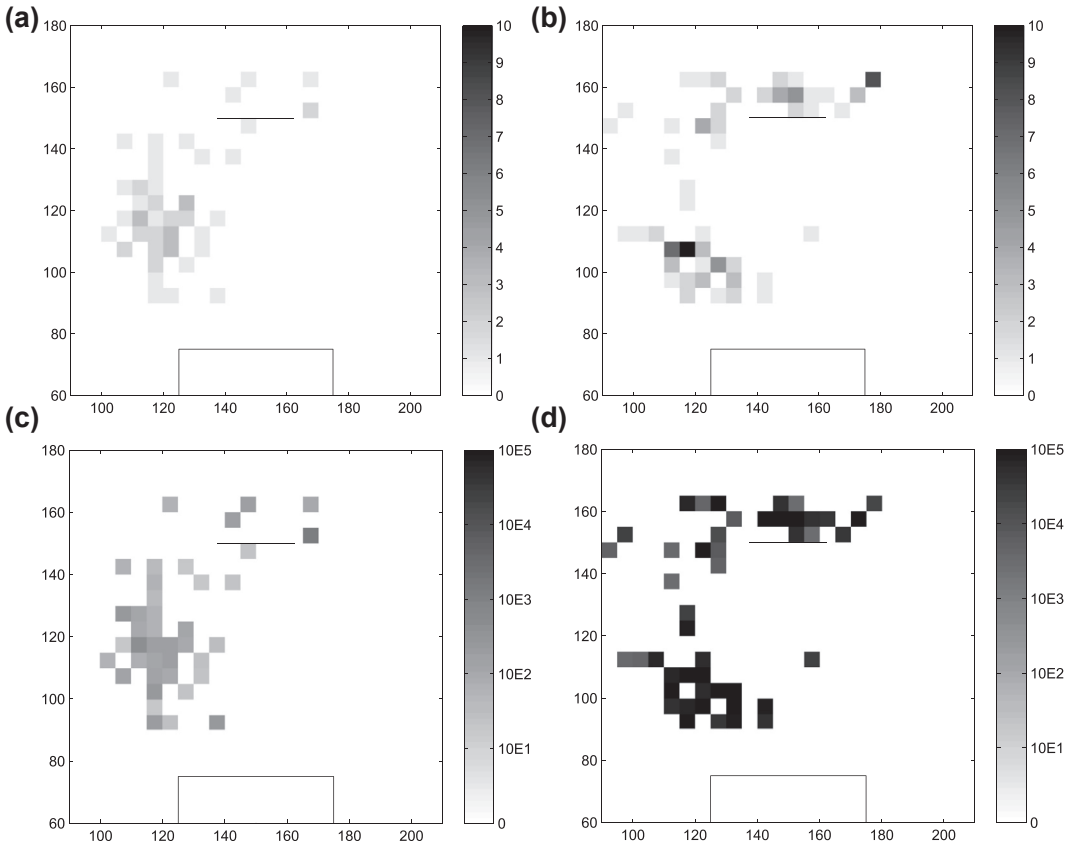

Fig. 16. AE energy and activity 2D maps, by class (a) activity, class 1 (b) activity, class 2 (c) energy, class 1 (d) energy, class 2.

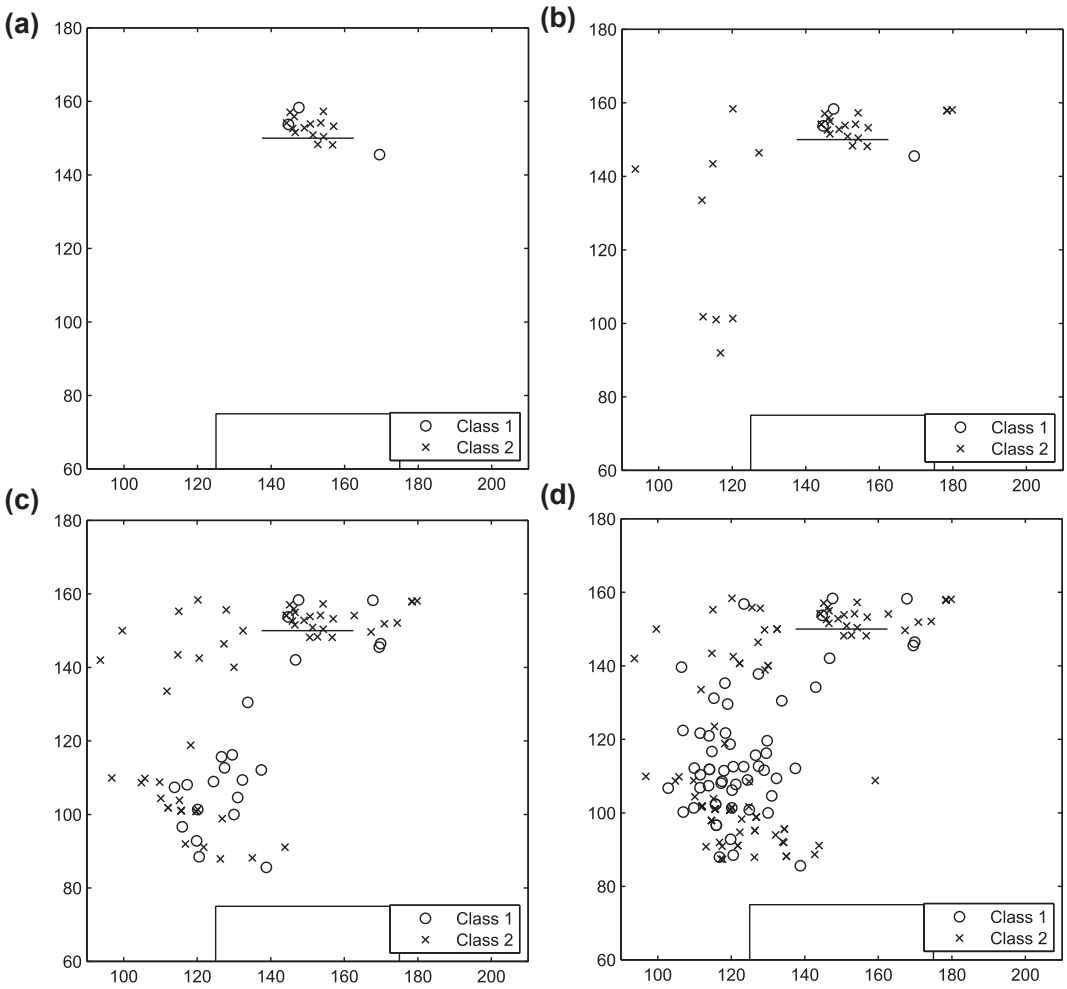

Fig. 17. AE events in time, classified (a) t = 0–2646 s (b) t = 0–4500 s (c) t = 0–5200 s (d) t = 0 to end.

An example of the waveforms from both classes is shown in Fig. 18. Here it is clear that the classification technique is capable of separating two distinct groups of waveform shapes. Also, average parameters for the two classes are reported in Table 3.

4. Discussion

The AE results presented in Section 3 provided some key information and confirmation regarding AE and damage detection in composites:

- Cutting the inner plies allowed the generation of an artificial flaw that favoured matrix cracking;
- The artificial crack area showed repeatable sources, as visible from the waveforms;
- A delamination induced by an impact becomes an active source of AE;
- The delamination source of this experiment contains two distinguishable classes of AE signals;
- The delamination source is active from the AE point of view even if the delamination does not grow.

When supported by ANN classification, the failure modes are correctly identified: the pre-impact phase shows only a single class of signals; when the panel is impacted, a second class appears. It is observed that in the impact region both delamination and crack signals are found.

The crack class signals seem to be more related to the region normal to the load path (matrix failing in tensile load); this is supported by the AE signals position relative to the delamination area observed in the C-scan and by the observation of almost only crack class signals in the cut ply region.

On the other hand, the delamination class signals are distributed in the delamination region, probably originated by debonded layer friction. Although this does not imply delamination growth, it provides a way to identify the delamination region, which may cause a significant reduction in structural compressive strength of the component.

It was also observed that the two classes show repeatable sources, with distinct waveforms and AE parameters. In particular, matrix cracking sources show higher amplitude and a relatively quicker decay, while delamination sources appear as a continuous-like source.

The augmentation of AE data with automatic classification information presented in this work represents an improvement for the use of AE as SHM system for carbon components. If a component is fitted with an AE sensor network and its signals are classified according to the procedure presented, the human discretion in interpreting AE trends and signals is significantly reduced, if not completely removed, when deciding if a component has developed a new damage mode.

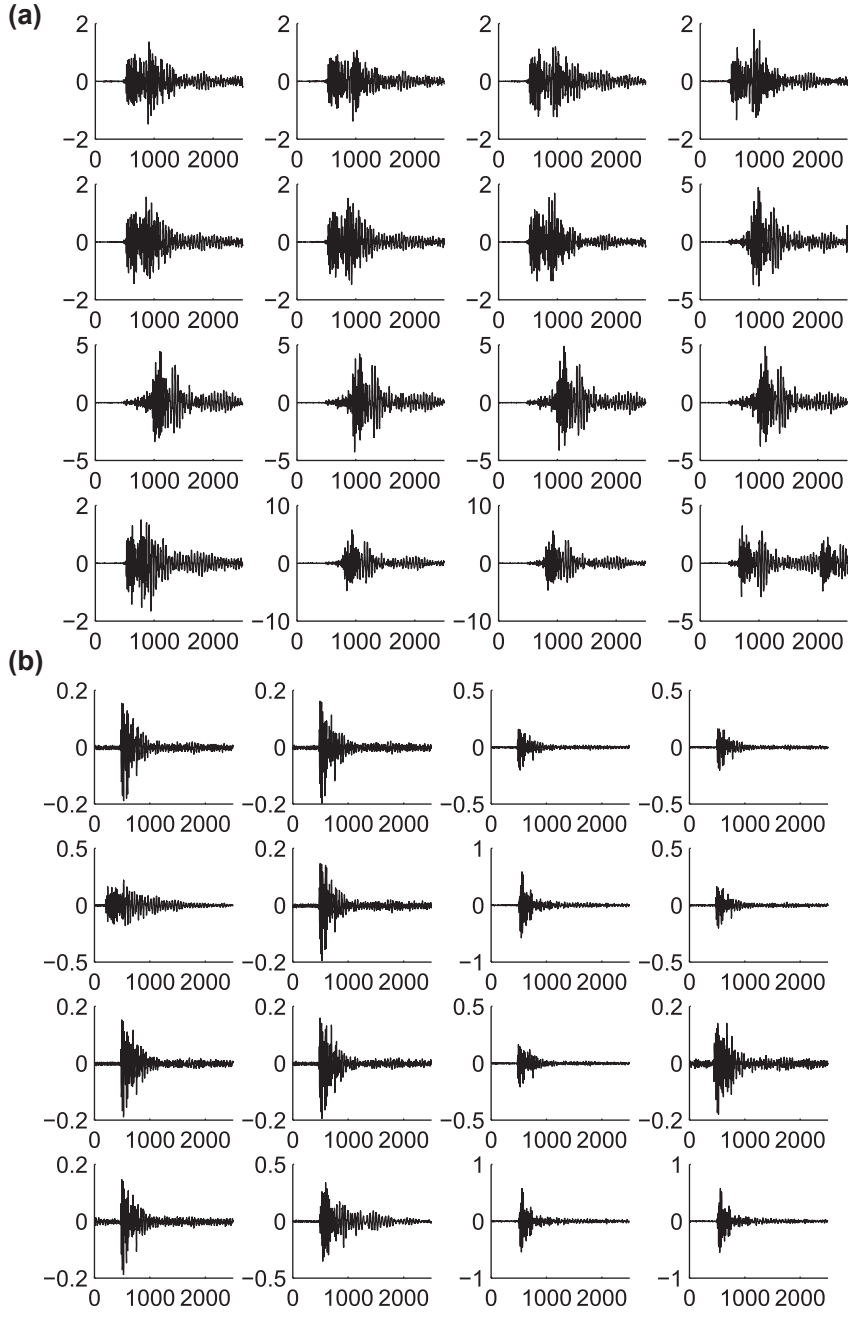

Fig. 18. Waveforms from class 1 (a) and class 2 (b).

An important feature to stress is, that if AE data is presented without classification data, it is not possible to discriminate whether a change in activity is related to a particular damage mode developing, or whether it is only a change in environmental conditions (e.g. noise). By coupling AE location data and classification information, it would be possible to separate the various contributions of the different classes, and monitor them separately both by location and in their time evolution.

This feature will be a benefit for real-time monitoring, maintenance and also laboratory component testing, since the use of AE may give precious indications to the system operator about damage characteristics, location and evolution, without involving direct human intervention or downtime for inspection. In the design phase of parts intended to be monitored, SHM will help limit both the weight

Table 3
Average parameters for the two classes.

	Class 1		Class 2	
	Average	Std. deviation	Average	Std. deviation
CNTS	3	4	85	41
A (dB)	49	3	69	6
E (eu)	89	151	27,680	28,732
R (μs)	8	20	94	126
D (μs)	25	33	810	504
FCOG (kHz)	263	38	266	59
FMXA (kHz)	224	57	174	77

of the structure and the involved safety factors. A SHM technique which provides precise information on each damage mode evolution reduces the uncertainties of the damage models themselves and consequently decrease inspection intervals. SHM alarms can therefore trigger direct, localized and focussed maintenance.

5. Conclusions

This experimental work presented a way of generating two distinct artificial AE signal sources in a CFRP plate, one related to matrix cracking phenomena and a second one related to impact-induced in-plane delamination. A neural network-based fully automated classification technique proved to be effective in identifying these two different sources and to correctly separate them. This was supported by visual observation and ultrasonic C-scanning.

The AE technique, supported both by advanced location algorithms (namely the Delta-T technique) and automatic classification methods (the k-SOM classifier), proved to be valid to monitor in real-time CFRP structures under fatigue load, and could be easily made capable of automatically identifying the onset of a novel damage mode in real-time.

Criteria for rejection or acceptance of parts (i.e. defining alarm levels and assessing false alarm probabilities) have yet to be investigated deeply. Also, the applicability of the classification technique to real-time AE data classification without having to consider the entire dataset is being evaluated at the moment.

Acknowledgements

The authors would like to acknowledge the support of Cardiff University – School of Engineering laboratories, facilities and staff for the support given during the experimental part of this work.

References

[1] Worden K, Farrar CR, Manson G, Park G. The fundamental axioms of structural health monitoring. Proc R Soc A Math Phys Eng Sci 2007;463:1639–64.
[2] Miller RK, McIntire P. NDT handbook, vol. 5. American Society for Nondestructive Testing; 1987. p. 652.
[3] Finlayson RD. Acoustic emission testing. In: Hellier C, editor. Handbook of nondestructive evaluation. McGraw-Hill Companies; 2003. 10.1–10.39.
[4] Huang M, Jiang L, Liaw PK, Brooks CR, Seeley R, Klarstrom DL. Using acoustic emission in fatigue and fracture materials research. J Oncol Manag 1998:50.
[5] Hamstad MA. Thirty years of advances and some remaining challenges in the application of acoustic emission to composite materials. In: Kishi T, Ohtsu M, Yuyama S, editors. Acoust. emiss. beyond Millenn. Oxford, UK: Elsevier; 2000. p. 77–91.
[6] Wang X, Zhang H-P, Yan X. Classification and identification of damage mechanisms in polyethylene self-reinforced laminates by acoustic emission technique. Polym Compos 2011;32:945–59.
[7] Caruso C, Lonetti P, Manna A. Dynamic crack propagation in fiber reinforced composites. In: Proc. COMSOL conf. 2009 Milan; 2009.
[8] Jessen SM, Plumtree A. Fatigue damage accumulation in pultruded glass/polyester rods. Composites 1999;20:559–67.
[9] Bourchak M, Farrow I, Bond I, Rowland C, Menan F. Acoustic emission energy as a fatigue damage parameter for CFRP composites. Int J Fatigue 2007;29(3):457–70.
[10] Ireman T, Ranvik T, Eriksson I. On damage development in mechanically fastened composite laminates. Compos Struct 2000;49:151–71.
[11] Caprino G, Teti R, de Iorio I. Predicting residual strength of pre-fatigued glass fibre-reinforced plastic laminates through acoustic emission monitoring. Compos Part B 2005;36:365–71.
[12] Baxter MG, Pullin R, Holford KM, Evans SL. Delta T source location for acoustic emission. Mech Syst Signal Process 2007;21:1512–20.
[13] Eaton MJ, Pullin R, Holford KM. Acoustic emission source location in composite materials using Delta T mapping. Compos Part A Appl Sci Manuf 2012;43:856–63.
[14] HSU NN. A mechanical AE simulator for system calibration and waveform analysis. In: 16th Meet. U.S. Acoust. Emiss. Work. Gr., Williamsburg, Va, United States; 1976.
[15] Holford KM, Pullin R, Baxter MG. Modal analysis of acoustic emission signals from artificial and fatigue crack sources in aerospace grade steel. Key Eng Mater 2005;293:217–24.
[16] Mal A. Elastic waves from localized sources in composite laminates. Int J Solids Struct 2002;39:5481–94.
[17] Huguet S, Godin N, Gaertner R, Salmon L, Villard D. Use of acoustic emission to identify damage modes in glass fibre reinforced polyester. Compos Sci Technol 2002;62:1433–44.
[18] Zhuang X, Yan X. Investigation of damage mechanisms in self-reinforced polyethylene composites by acoustic emission. Compos Sci Technol 2006;66:444–9.
[19] Ramirez-Jimenez CR, Papadakis N, Reynolds N, Gan TH, Purnell P, Pharaoh M. Identification of failure modes in glass/polypropylene composites by means of the primary frequency content of the acoustic emission event. Compos Sci Technol 2004;64:1819–27.
[20] Groot PJ De, Wijnen PAM, Janssen RBF. Real-time frequency determination of acoustic emission for different fracture mechanisms in carbon/epoxy composites. Compos Sci Technol 1995;55:405–12.
[21] Godin N, Gaertner SHR, Salmon L. Clustering of acoustic emission signals collected during tensile tests on unidirectional glass/polyester composite using supervised and unsupervised classifiers. NDT E Int 2004;37:253–64.
[22] Refahi Oskouei A, Ahmadi M. Acoustic emission characteristics of Mode I delamination in glass/polyester composites. J Compos Mater 2010;44:793–807.
[23] Laksimi A, Benmedakhene S, Bounouas L. Monitoring acoustic emission during tensile loading of thermoplastic composites materials. In: Proc. ICCM 12 Eur; 1999.
[24] Godin N, Huguet S, Gaertner R. Influence of hydrolytic ageing on the acoustic emission signatures of damage mechanisms occurring during tensile tests on a polyester composite: application of a Kohonen's map. Compos Struct 2006;72:79–85.
[25] Grosse C, Reinhardt H, Dahm T. Localization and classification of fracture types in concrete with quantitative acoustic emission measurement techniques. NDT E Int 1997;30:223–30.
[26] Leone C, Caprino G, de Iorio I. Interpreting acoustic emission signals by artificial neural networks to predict the residual strength of pre-fatigued GFRP laminates. Compos Sci Technol 2006;66:233–9.
[27] De Oliveira R, Marques AT. Health monitoring of FRP using acoustic emission and artificial neural networks. Comput Struct 2008;86:367–73.
[28] Bhat C, Bhat MR, Murthy CRL. Acoustic emission characterization of failure modes in composites with ANN. Compos Struct 2003;61:213–20.
[29] Doan DD, Ramasso E, Placet V, Boubakar L, Zerhouni N. An unsupervised pattern recognition approach for AE data originating from fatigue tests on polymer-composite materials. In: Proc EWSHM-7th European workshop on SHM Nantes, France; 2014.
[30] Sause MGR, Gribov A, Unwin AR, Horn S. Pattern recognition approach to identify natural clusters of acoustic emission signals. Pattern Recognit Lett 2012;33:17–23.
[31] Crivelli D, Guagliano M, Monici A. Development of an artificial neural network processing technique for the analysis of damage evolution in pultruded composites with acoustic emission. Compos Part B 2014;56:948–59.

A Parameter Correction Technique (PCT) for Acoustic Emission Characterisation in Large-Scale Composites

Safaa Kh. AL-JUMAILI [1,2], Mark EATON [1], Karen HOLFORD [1], Rhys PULLIN [1]
[1] Cardiff School of Engineering, Queen's buildings, The Parade, Cardiff, CF24 3AA, UK
[2] University of Basrah, Basrah, Iraq
E-mail addresses: Al-JumailiSK@cf.ac.uk (Safaa Kh. Al-Jumaili), Holford@cf.ac.uk (K.M. Holford), PullinR@cf.ac.uk (R. Pullin), EatonM@cf.ac.uk (Mark J. Eaton).

Abstract. Acoustic emission (AE) has been extensively used for over 40 years for non-destructive evaluation of damage in different types of materials and structures. Damage identification is considered as one of many attractive attributes of this technique. Most studies in this field have been conducted on small-scale specimens by analysing the AE parameters recorded using different commercial AE acquisition systems directly. However, these AE parameters are affected by attenuation, superposition, material properties and complex geometry which can lead to incorrect input data in the analysis process, thus making accurate characterisation challenging. Furthermore, using AE for the Structure Health Monitoring (SHM) is highly dependent on the recorded parameter values for decision making on the integrity of the structure.

This paper describes a novel solution to enable AE parameters to be "corrected" to account for the material properties and the geometry of the structure. The ''Parameter Correction Technique (PCT)'' utilises an artificial source; recording the relationship between the signal parameters and varying source amplitude from a number of locations, to create a multi-layer map to correct the recorded parameter value. A five-step description of the process is provided and practical results from an initial trial are presented. Initial trial results demonstrate a considerable improvement over the conventional parameters.

Various artificial sources were used to assess the performance of the Parameter Correction Technique in a composite panel. The technique is demonstrated on a single parameter analysis (namely amplitude) and the correlation plot. In order to demonstrate the advantage of the PCT, the traditional AE parameters are presented side-by-side for comparison, which reveals a substantial improvement in parameter value accuracy. The effects of attenuation, anisotropy etc. have been eliminated using the new method. Moreover, it is proven that AE signal propagation path seriously affects the recorded AE parameters and cannot be ignored. Thus, the PCT is an effective technique that may be used to overcome signal propagation effects and correct the recorded qualitative parameters to provide a better discrimination of different sources types in composite materials.

Introduction

Acoustic emission (AE) is a non-destructive testing technique which has been widely used in research applications for the detection of micro failures in a wide variety of materials [1]. The origin of the AE in materials is that when a failure mechanism is activated, part of the total strain energy is dissipated as mechanical stress waves, which are spread concentrically around the place of origin. The energy released in this way can be detected with suitable sensors: the recorded mechanical information from the material is then converted into an electrical signal [2]. During the last two decades, composite materials have found use in numerous industrial applications and nowadays, reinforced composite structures are widely used in large-scale and safety critical structures for infrastructure and transport, (aerospace, energy and marine). For large-scale metal or composite structures, acoustic emission (AE) has great potential for use in structural health monitoring (SHM), providing continuous and global monitoring of the structure, the ability to locate the AE source position within the structure and providing information about the damage mechanisms from the received signals.

To date most studies carried out for identification damage mechanisms in composite materials under different loading regimes have been based on conventional AE analysis using the recorded AE signal features directly from the acquisition system. Until now the association of each AE signature to a specific failure type is considered to be a non-trivial task in large-scale composite materials components. Due to the complex nature of the structure of a composite material the wave propagation and scattering phenomenon is highly complex. Also, the complexity increases as a result of signal transition interruption due to the presence of obstacles such as cracks, holes and thickness changes, in the propagation path. In addition, the AE signal energy degradation makes the collection of all the AE activity using one sensor difficult. On the other hand, the use of data collected from multiple sensors is highly problematic in terms of achieving accurate analysis due to the different transfer functions of each sensor.

This paper proposes a solution which will eliminate the effects of attenuation, anisotropy etc. on the recorded AE signals. A novel AE parameter correction methodology known as “Parameter Correction Technique (PCT)” is presented, which is applicable to two-dimensional plate-like structures. It is applied in order to correct the recorded AE parameters from artificial sources which are generated at different locations on a carbon fibre composite panel specimen. This technique has the ability to use the data recorded by all the sensors in an array to correct each signal’s parameters, improving reliability and confidence. Because of the novelty of this approach and the lack of relative studies in the field of AE parameter correction; only a comparison with the traditional parameters was made to assess the technique performance. The four fundamental parameters, amplitude, duration, count and energy were corrected in this work with high accuracy. In the presented analysis, events are located accurately using the Delta T technique. Originally developed for complex geometry metallic structures [3], the technique has also been shown to perform very well in anisotropic materials such as composites [4].

2. Experimental Procedure

2.1 Test specimen

The experiments were carried out on a carbon fibre composite panel manufactured from Hexcel Corporation material code is M21/35%/UD268/T800S. The final product is a layered structure specimen with 8 ply of uni-directional pre-preg using a $((0, 90)_2)_s$ with

dimensions of 500 x 500mm with nominal thickness of 2mm. During the layup process an artificial crack was introduced in the centre of the specimen by cutting the fibre in 0^o direction using a fresh razor blade to initiate an artificial matrix crack of 2.5mm length. Four aluminium plates with 5 x 50 x 50mm dimensions were glued on both sides of the panel using resin and a 20mm diameter hole drilled as shown in Figure 1a. Local delamination was produced using a low velocity impact of polished hemispherical tup with a 20mm diameter with different energy levels from 5 to 14 J on the specimen surface. Figure 1b shows the C-scan images of the specimen before and after impact with the delamination area.

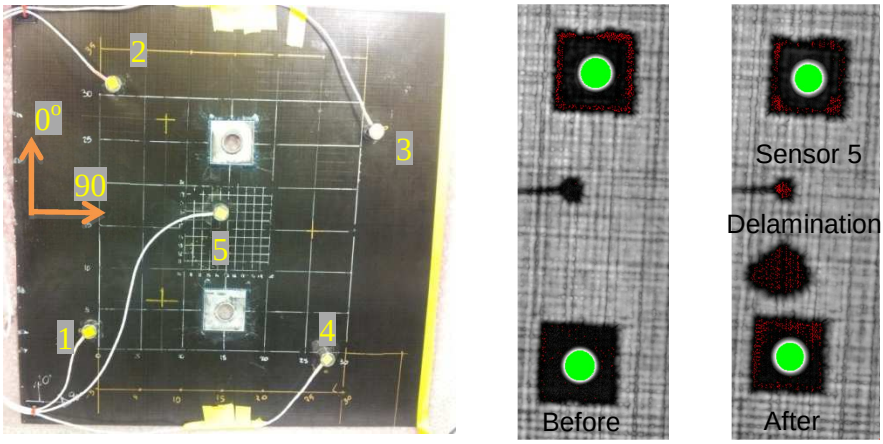

(a) (b)

Fig. 1. (a) Test specimen configuration (b) C-scan images before and after impact.

2.2 Acoustic emission:

AE activity was recorded using a Vallen acquisition system at a sample rate of 5 MHz. with five PAC WD wideband sensors of bandwidth 100-1000 kHz and a resonant frequency at 650 kHz as presented in Figure 1a. All sensors were pre-amplified using the Vallen AEP3 of 34 dB gain and a threshold level of 44.9 dB was set. The threshold level was selected to eliminate background noise. Silicon adhesive (595 Loctite) was used to provide both acoustic couplant and mechanical fixture between the specimen and the sensors. Installed sensor sensitivity was evaluated using a Hsu-Nielson (H-N) source [5]. Artificial sources were generated from a PAC wave generator and the signal transferred using a conical transducer. The multi purposes grease was used as a couplant to provide good contact between the conical transducer and the specimen surface. Figure 1a demonstrates the Delta T location grids. A 50mm grid resolution and with 10mm resolution near to the artificial crack was applied to the central area of interested of 300 x 300mm. The Delta T location maps was constructed before the test by record data from five pencil lead breaks, H-N sources, at each grid point.

3. Parameter Correction Technique (PCT) methodology

This technique utilises an artificial source, recording the relationship between the acquired signal parameters and varying source amplitude from a number of locations, to create a PCT multi-layer map for each sensor. This method does not require knowledge of the sensor location or wave velocity. A five-step description of the technique is provided.

- *Determine area of interest:* The PCT method can offer complete coverage of a structures. However PCT can be time consuming but it can also be applied to a small or critical component.

- *Map system Construction:* A grid is constructed on the area of interest within which AE events will be located. It is important that source position and not the sensor should be referenced to the grid. Placing the sensors within the grid is unnecessary and does not affect the final result.
- *Apply artificial sources to obtain the PCT data set: an* artificial source is generated at each node of the grid with different amplitudes (input voltage) and recorded at each sensor. At each amplitude the source is repeated several times and an average result of the parameter values is used to reduce the error. Data between nodes and for missing nodes as a result of holes for example can be interpolated from the other surrounding nodes. So, for each sensor, a distribution contour will define each parameter value within the grid, this is completed for each different input voltage.
- *Calculate PCT maps:* For each sensor, the parameter contours are arranged in ascending order depending on the source amplitude value. This allows construction of a multi-layer matrix (PCT map). At each location within the grid, the relationship between parameter value and the artificial source amplitude value is calculated.
- *Real AE data parameters re-calculation:* For each sensor, any previous, current or future located AE data received can then be overlaid on the relationships, and its source amplitude can be identified. Interpolation and extrapolation are utilised to obtain these values. The average from all sensors that record the same event is used to present the most accurate value.

3.1 Initial PCT practical calculations:

In this work, the training data for the PCT mapping was collected from an area of 300 x 300mm, identical to the Delta T map area. All dimensions will be referred to the left hand bottom corner of the Delta T map as the origin. A grid density of 50mm was used, creating 47 nodes on the PCT mapping area as shown in Figure 2a. Two nodes were in accessible due to their location within the tab holes (Figure 1a). The location of nodes next to the sensors was shifted by approximately 10 to 20mm to be able to use the conical transducer. An artificial pulse (the excitation pulse is rectangular shape of 10 µs width) was used at each node. Pulse amplitude started from 10 V to 160 V with 5 V increments. At each increment the pulse was repeated 5 times to provide an average and avoid any erroneous results. Real-time recording of AE signal parameters using the five sensors was obtained. Data at each node was used to interpolate across the entire grid.

Figure 2b shows the traditional amplitude values recorded by sensor 1 (Figure 1a) within the grid from a 160 V source amplitude. It can clearly be seen that the recorded parameter values vary strongly with the source location and its clear how the propagation distance, propagation direction and geometric properties affect the amplitude. As a result it is difficult to characterise between AE signals of different sources emitted from different locations using the traditional AE signal parameters. The multi-layers matrix of the PCT map is presented in Figure 2c.

It is worth to note that using the parameter distribution contour showed in Figure 2b to correct AE parameters has many limitations, because each damage mechanism generates signals with different levels of energy as well as amplitude. In addition, the final result of correction will depend on the operator decision to choose which sensor data to utilise and the distance from that sensor.

From Figure 2c it is possible to extract the parameter value in any position within the grid at each source voltage. Thus, for each sensor, the relationship between the parameter values and the source voltage at any location can be obtained. Figure 2d shows examples of these relationships between the traditional amplitude, recorded by sensor 1,

and the source voltage in three different arbitrary positions. The same process was conducted for the remaining parameters (count, energy and duration).

In this approach parameter values of the located AE events are overlaid on these relationships to identify the source amplitude. Thus the corrected traditional parameter will be referred to the next as the input voltage in volts.

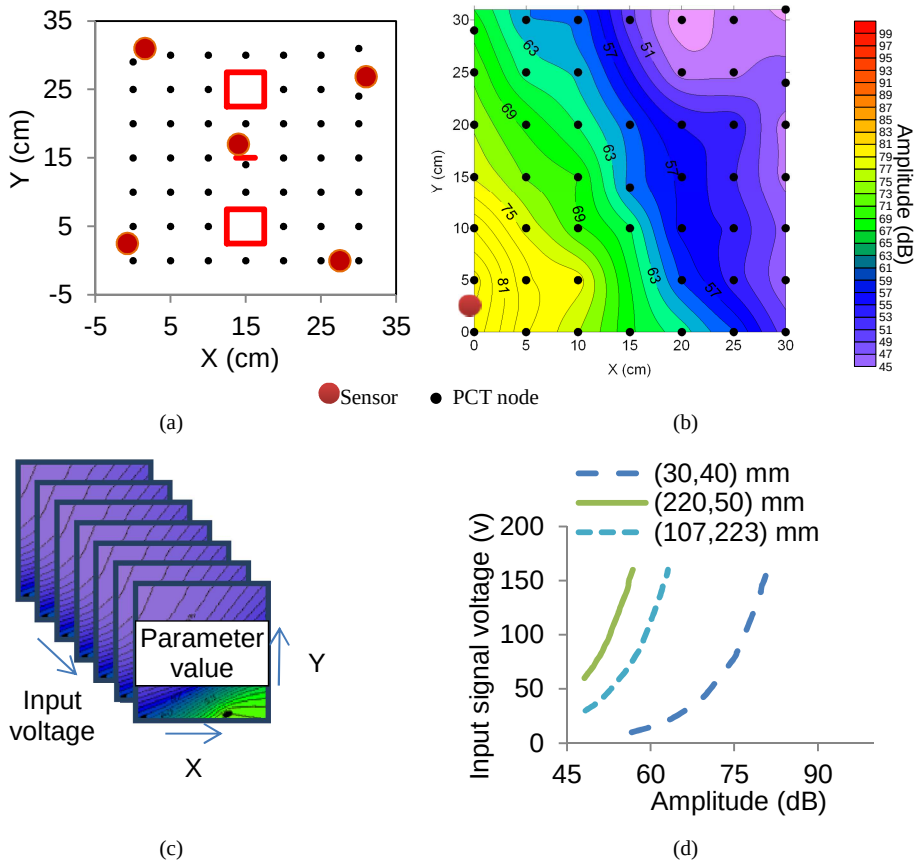

Fig. 2. (a) PCT grid (b) traditional amplitude recorded by sensor 1 (c) PCT map structure for one parameter from one sensor (d) traditional amplitude with the source amplitude relationship at different locations.

4. Validations Approach

In order to validate and assess the performance of the proposed technique, validation tests were performed using different artificial sources as a repeatable AE sources. Three tests were conducted; firstly using different sources amplitude (Codes 001, 002 and 003). Secondly, use different pulse shape sources (Codes 002 and 007). Thirdly, using different frequencies pulses (Codes 007, 009 and 010) (Further sources codes 004, 005, 006 were investigated but are not reported here). The sources details are listed in Table 1.
Six arbitrary positions were chosen to conduct this investigation and each source was repeated 5 times at each position. The positions will be labelled during the rest of this paper according to the information provided in Table 2.

The source position was located using the Delta T technique. The average location error between the actual and calculated locations of all sources was found to be 6.6 mm. A comparison between the traditional parameters of sensor 1 and the PCT result is presented in Figure 3. Only the amplitude comparison is presented here however the same results were achieved for the remaining parameters.

Table 1. Artificial sources details

Source code	001	002	003	007	009	010
Pulse name	Sine wave	Sine wave	Sine wave	Saw tooth	Saw tooth	Saw tooth
Wave envelop	Sine curve	Sine curve	Sine curve	Sine curve	Sine curve	Sine curve
Frequency (kHz)	300	300	300	300	200	100
Cycle	1	1	1	1	1	1
Amplitude (V)	50	100	150	100	100	100

Table 2. The location label and its location on the specimen

Point number	X (mm)	Y (mm)
From 1 to 5	75	275
From 6 to 10	75	60
From 11 to 15	150	140
From 16 to 20	75	175
From 21 to 25	0	200
From 26 to 30	150	300

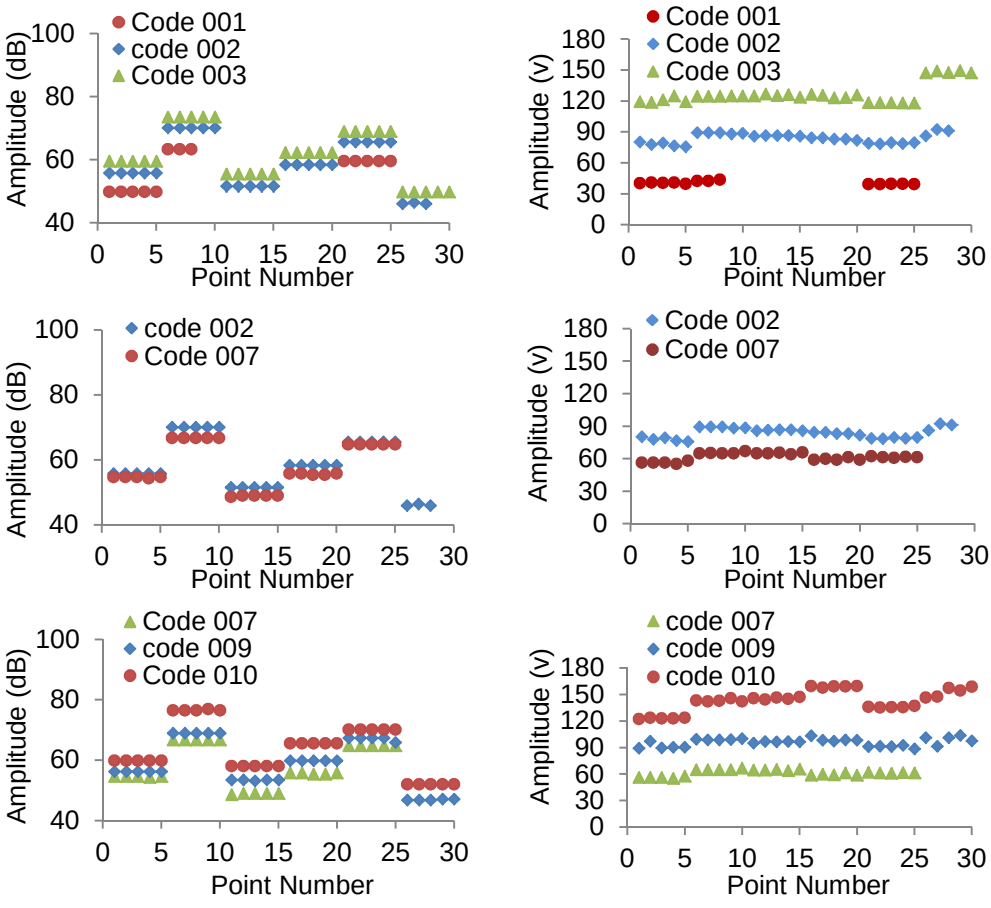

(a) Sensor 1 data (b) Prameter Correction Technique (PCT)

Fig. 3. Comparison between traditional and corrected amplitude.

As we can see the traditional amplitude was recorded with different value levels (Figure 3a) depending on the source location from the recording sensor. Demonstrating a challenge to use them for discrimination between different source types. While, the corrected amplitude value from all the six locations has a relatively stable level demonstrating that PCT eliminates the propagation effects on the recorded parameters. The fluctuation in the PCT results is related to the source location accuracy.

Furthermore, the ability of the PCT to use all sensor data has an advantage, that no missing AE data, and all the located events can be compared for the final analysis. Up to now, the traditional AE analysis suffers as only one sensor should be used to compare located sources, leading to in most cases missed data. This problem could be significant in large-scale components due to the attenuation. For example, in each position the source Code007 was repeated five times so ideally there are 30 located events. In reality the Delta T locates only 25 events as presented in Figure 3a because some source signals hit less than three sensors, the lowest number required to locate event in 2D [3]. Sensors response of this source is provided in Table 3:

Table 3. Sensors response of the source Code007

Sensor No.	Number of signals hitting the sensor	% of located data
1	25	100
2	25	100
3	15	60
4	10	40
5	25	100
The PCT	25	100

It can be seen clearly from Table 3 that if the traditional analysis is conducted using sensor 3 or sensor 4 mean 40% and 60% of the located AE activity is lost, respectively.
For the detection and potentially the characterisation of damage, correlation plots are used extensively in classic AE testing. One of the commonly used is the amplitude versus duration plot. It is hoped in an ideal case the plots would group the AE data points based on their mutual similarity.

A comparison between traditional and corrected parameters correlation plots of the three tests was performed and the result is presented in Figure 4. In the traditional parameters plots the different sources singles have random distribution as shown in Figure 4a. On the other hand, the corrected parameters in Figure 4b show significant improvement and each source is separated into a distinct cluster.

Conclusions

In the present investigation, a new technique was examined using a variety of artificial sources on different locations on the carbon fibre composite specimen. A continual significant improvement in overall performance/efficiency factors was achieved in correcting the traditional parameters value recorded from different amplitudes, waveform and frequency sources.

A comparison with traditional parameters was conducted using single parameter analysis and correlation plots. Results reveal that the traditional parameters are completely misleading if used for damage identification process in large-scale components. This technique has the ability to use all sensors which improves the results accuracy and avoids losing AE data. These findings show great potential for the use of AE monitoring in SHM of large-scale composite structures such as those found in the aircraft industry and in wind turbines.

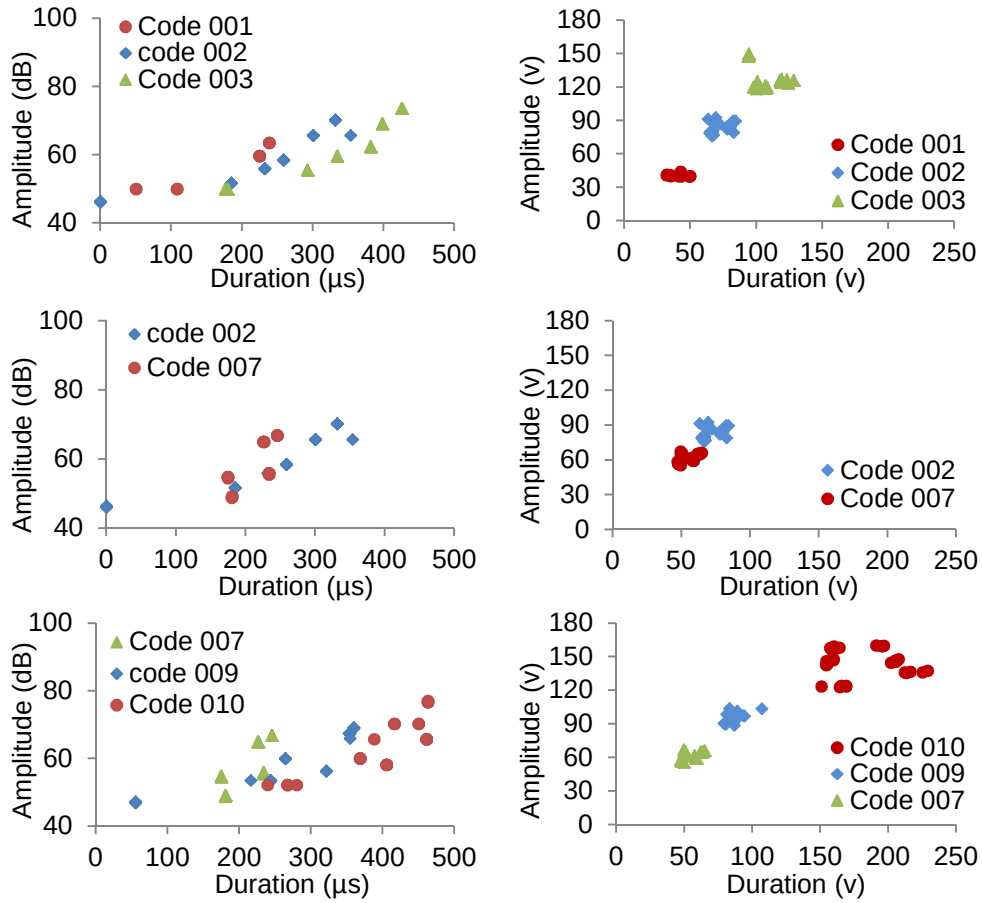

(a) Sensor (1) data (b) Corrected data

Fig. 4. The correlation plots using traditional parameters and the corrected parameters using PCT.

Acknowledgements

The authors would like to thank the Iraqi Ministry of Higher Education and Scientific Research for supporting this research, Dr. Davide Crivellia (Politecnico di Milano, Italy) for his assistance with manufacturing the test specimen, Dr. Matthew R. Pearson (Cardiff University, UK) for his assistance and the technical staff of Cardiff School of Engineering for their kind assistance with the testing programme.

References

[1] Miller, K.R. and E.K. Hill, *Non-Destructive Testing Handbook; Acoustic Emission Testing.* American Society for Non-Destructive Testing, 2005. **VoL 6**(3" ed).

[2] Ramirez-Jimenez, C.R., et al., *Identification of Failure Modes in Glass/Polypropylene Composites by Means of the Primary Frequency Content of the Acoustic Emission Event.* Composites Science and Technology, 2004. **64**(12): p. 1819-1827.

[3] Baxter, M.G., et al., *Delta T Source Location for Acoustic Emission.* Mechanical Systems and Signal Processing, 2007. **21**(3): p. 1512-1520.

[4] Eaton, M.J., R. Pullin, and K.M. Holford, *Acoustic Emission Source Location in Composite Materials Using Delta T Mapping.* Composites Part A: Applied Science and Manufacturing, 2012. **43**(6): p. 856-863.

[5] Hsu, N.N. and F.R. Breckenridge, *Characterization and Calibration of Acoustic Emission Sensors* Mat. Evaluation, 1981. **39**(60).

Proceedings of the 24th UK Conference of the
Association for Computational Mechanics in Engineering
31 March – 01 April 2016, Cardiff University, Cardiff

Fast and Reliable Acoustic Emission Source Location Technique in Complex Structures

***Safaa Al-Jumaili[1,2], Matthew Pearson[1], Karen Holford[1], Mark Eaton[1] and Rhys Pullin[1]**

[1]Cardiff School of Engineering, Cardiff University, Queen's buildings, The Parade, Cardiff, CF24 3AA, UK
[2]University of Basrah, Basrah, Iraq

*Al-JumailiSK@cardiff.ac.uk

ABSTRACT

Acoustic emission (AE) provides engineers with a powerful tool by allowing the location of damage sources as they occur. Damage localisation using traditional time of arrival approaches is inadequate in complex structure components. Cardiff University presented a novel approach known as Delta T mapping which overcame these limitations but it was considered as time consuming and an operator dependent approach. This paper presents new full automatic Delta T mapping technique overcomes these remaining limitations.

Keywords: *acoustic emission; source location; complex structure; unsupervised clustering; Delta T technique*

1. Introduction

Damage localisation in complex structures, such as those found in aerospace applications, is a difficult problem in the field of structural health monitoring (SHM). The development of an easy to use, fast to apply, cost-effective and very accurate technique is key for the uptake of SHM. The use of Acoustic Emission (AE) [1] is important for SHM as it offers the potential for the real time monitoring of the health of a structure. Acoustic emission (AE) arising from damage mechanisms and propagating through the structure in the form of Lamb waves can be detected using piezoelectric sensors mounted on the surface of the structure. The ability to track the early onset of damage and hence determine the structure's integrity will enable the switch from periodic inspections to a more condition based approach, therefore enabling increased inspection intervals, reducing structure downtime and maintenance costs.

The time of arrival (TOA) technique is traditionally used to locate these sources, and relies on the assumption of constant wave speed within the material and uninterrupted wave propagation path between the damage and the sensor. In reality, structural complexities such as holes and thickness changes that may be present, which alter the wave propagation path and velocity. In order to overcome these limitations, Cardiff University developed a technique (called Delta T Mapping [2]) to locate damage in complex structures with high accuracy [3-5] by using artificial sources on an area of interest to create training maps. These maps are used to locate subsequent AE events arising from damage events. However, this technique needs high operator expertise to deal with the training map data (e.g. selecting the correct data) which can be a time consuming process as well as it requires the cluster diameter value to be identified in advance to be able to calculate the source location (only the convergence points inside a specific cluster diameter are used to calculate the probable AE source location). The most recent version of Delta T technique is known as the AIC Delta T Mapping technique and was developed by Pearson et al [6, 7] and overcame the limitation of arrival time calculation, another source of error in the traditional approach.

In this paper, a new and improved fully automatic Delta T Mapping technique is present. Here the correct data in the training maps were identified and selected automatically using a clustering algorithm and a new approach (Minimum Difference approach) is used to determine the damage location. This paper reports experimental validation of the advantages of the new techniques achievements. The results showed excellent reduction in running time (from 7 hours to only 11 seconds) as well as improved accuracy (location error improved from 4.96mm to 3.88mm in a complex geometry).

2. Automatic Delta T mapping technique Methodology

This approach can be divided into two parts; firstly, selecting the valid events (to be used for creating the initial maps) at each grid point using an unsupervised clustering technique and secondly, calculating the AE source location using the Minimum Difference approach [1].
In the first part, after collection of the training data by applying H-N sources [8] (an artificial AE source) on each node position in the grid the time of arrival to each sensor is obtained using the AIC approach [9]. The classification process is applied at each grid position to select AE events which are highly similar to each other, where the input data vector for the clustering process is the time difference between sensors pairs and will be used for the similarity criteria by following these steps:

- In each point of the Delta T grid, the recorded hits were separated automatically to create AE events using a time based approach. Simultaneously, the incorrect erroneous data were automatically removed.
- The AE hits from each point within the delta grid are correlated with the point coordinates (x, y) automatically, using time stamps placed by the operator within the collected data. Where the time stamps are placed in the data following acquisition from each grid node and are then used to automatically identify which hits are associated with each grid node.
- Each event is identified by the calculated difference in time of arrival for each sensor pair (e.g. the case of four sensors creates six sensor pairs 1-2, 1-3, 1-4, 2-3, 2-4 and 3-4).
- A complete link hierarchical clustering algorithm [10] is then used to group events based on their similarity, or correlation coefficient. In this work the 0.99 correlation coefficient level from the largest group was selected and all events in this group were used (correlation coefficient of 1 means total correlation).
- Delta T maps from the average values of the difference in time of arrival for each sensor pair are calculated for the selected highly correlated events at each grid point.
- Calculate location of real AE data: the Minimum Difference approach is a numerical approach, which is dependent on finding the point at which the difference between the source data and the training map data is minimised.

3. Experimental Procedure

An aerospace grade 2024-T3 aluminium plate, with dimensions of 370 x 200mm with a thickness of 3.18mm was used to assess the performance of the new technique. The specimen contained a series of differing diameter circular holes as shown in Figure 1a. A MISTRAS PCI-2 system was used to record all AE data at 40 dB threshold and 2MHz sampling rate. Four MISTRAS Nano-30s were adhered on the front face of the specimen (Figure 1a) using silicon RTV (Loctite 595). All transducers were connected to MISTRAS 0/2/4 pre-amps which had a frequency filter of 20 kHz to 1MHz. The Delta T Mapping grid on the specimen covered an area of interest of 200mm x160mm and had a resolution of 10mm (Figure 1a). Five H-N sources were used at each node position within the grid. In order to assess the performance of the new Delta T mapping technique in a more complex structure, six arbitrary positions were selected within the Delta T grid and three H-N sources were conducted at each position. The average wave speed was calculated as 5400 m/s. Source locations were calculated using all four sensors using the traditional approach, Time of Arrival (TOA), AIC Delta T and the new Automatic Delta T for comparison.

4. Results and Discussion

Source location calculations using the AIC Delta T were conducted using 20mm cluster diameter (calculated using a trial and error procedure) and the training maps were filtered manually. For the Automatic Delta T source location calculations, the training maps are constructed automatically using the unsupervised clustering procedure. The source locations are then calculated using the Minimum Difference approach. Finally, the TOA location results were exported directly from the MISTRAS AEwin software. Figure 1b shows the source locations on the specimen from the three location methods.

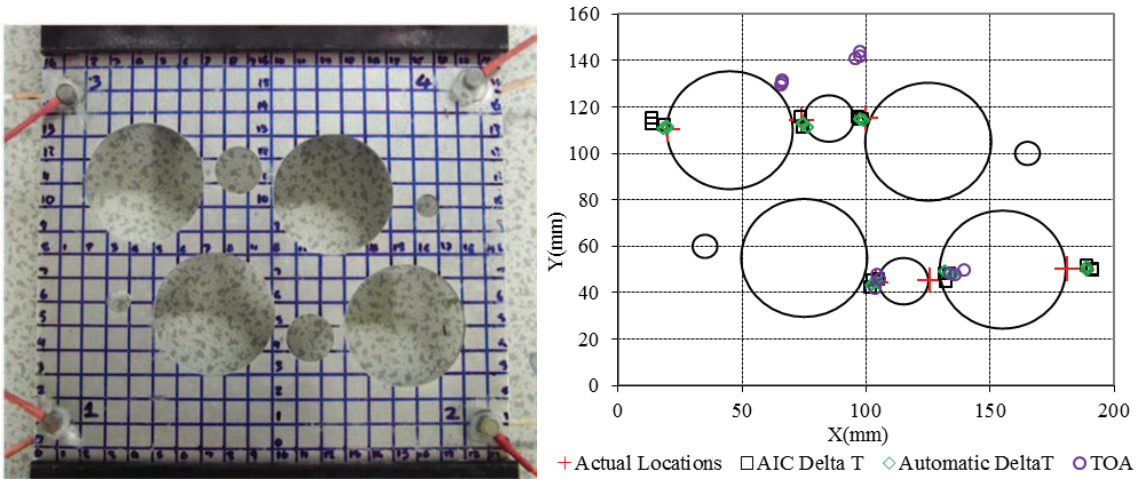

(a) (b)

Figure 1: (a) Specimen Configuration (b) Calculated source location by three techniques

A comparison between the three methods results are provided in Table 1. From the table it's clear that the average error of the Delta T techniques is considerably lower than the TOA and offers an improvement in accuracy from 222 mm to approximately 5mm. As well as the automatic Delta T shows an improvement in accuracy over the AIC Delta T results by reducing the error from 4.96mm to 3.88mm.

Furthermore, there is significantly reduces the time invested in implementing the technique. The most time consuming step in the AIC Delta T is represented by the selection and preparing of the AE data to construct the training maps which takes approximately 7 hours. On the other hand, the Automatic Delta T mapping is very fast and reduces the running time for constructing the training maps to approximately 11 seconds which is a significant improvement. Moreover, the new Delta T does not require the trial and error process of determining the optimal cluster diameter when compared with the AIC Delta T the cost is approximately 3.6 hours.

Table 1 Techniques performance comparison

	TOA	AIC Delta T	Automatic Delta T
Average location error	222.18mm	4.96mm	3.88mm
One standard deviation of the average	±177.75mm	±3.14mm	±3.19mm
Prepare the AE data to construct training maps	-	25200 sec (7 hours)	10.88 sec
Calculate the optimal Cluster size	-	13089	0

5. Conclusions

A new fully Automatic Delta T technique is introduced and verified experimentally using a complex structure. The results obtained are excellent and demonstrate the success of the adopted methodology. The AIC Delta T technique has been improved, with this approach, considerably and has increased in processing speed, increased reliability, efficiency, more accurate, increased simplicity and more capability to apply in large scale structures.

The results of this study highlight the potential for the use of AE monitoring as a tool of SHM for damage localisation tasks; a high simplicity, fast, reliable, cheap and accurate technique has been presented. If this technique is integrated with commercial AE monitoring systems, it will be a powerful tool to provide real time highly accurate source location within complex large-scale components.

Acknowledgements

The authors would like to thank the Iraqi Ministry of Higher Education and Scientific Research for supporting this research and the technical staff of Cardiff University School of Engineering for their kind assistance with the testing programme.

References

[1] K. R. Miller and E. K. Hill, *Non-Destructive Testing Handbook; Acoustic Emission Testing*, American Society for Non-Destructive Testing, VoL 6, 3rd Edition, 2005.

[2] M. G. Baxter, R. Pullin, K. M. Holford *et al.*, Delta T Source Location for Acoustic Emission, *Mechanical Systems and Signal Processing,* vol. 21, no. 3, pp. 1512-1520, 2007.

[3] S. K. Al-Jumaili, K. M. Holford, M. J. Eaton *et al.*, Classification of acoustic emission data from buckling test of carbon fibre panel using unsupervised clustering techniques, *Structural Health Monitoring*, vol. 14, no. 3, pp. 241-251, 2014.

[4] D. Crivelli, M. Guagliano, M. Eaton *et al.*, Localisation and identification of fatigue matrix cracking and delamination in a carbon fibre panel by acoustic emission, *Composites Part B: Engineering,* vol. 74, pp. 1-12, 2015.

[5] J. P. McCrory, S. K. Al-Jumaili, D. Crivelli *et al.*, Damage classification in carbon fibre composites using acoustic emission: A comparison of three techniques, *Composites Part B: Engineering,* vol. 68, pp. 424-430, 1, 2015.

[6] M. Pearson, Development of lightweight structural health monitoring systems for aerospace applications, *PhD Thesis,* Cardiff School of Engineering, Cardiff University, UK, 2013.

[7] M. R. Pearson, M. Eaton, C. A. Featherston *et al.*, Improved Acoustic Emission Damage Source Location During Fatigue Testing of Complex Structures, *Proceedings of the 34th Conference and the 28th Symposium of the International Committee on Aeronautical Fatigue and Structural Integrity (ICAF2015),* vol. Helsinki, Finland, no. ISBN 978-951-38-7442-1, 1st – 5th June, 2015.

[8] N. N. Hsu, and F. R. Breckenridge, Characterization and Calibration of Acoustic Emission Sensors. *Materials Evaluation,* vol. 39, no. 1, pp. 60-68, 1981.

[9] H. Akaike, Markovian representation of stochastic processes and its application to the analysis of autoregressive moving average processes, *Annals of the Institute of Statistical Mathematics,* vol. 26, no. 1, pp. 363-387, 1974.

[10] M. R. Anderberg, *Cluster analysis for applications*, Academic Press, New York, 1973.